PARACELSUS
MEDICAL
UNIVERSITY

ABSTRACTBAND 2022

virtual Science Get Together
Paracelsus Science Summer

www.pmu.ac.at/forschung-innovation

Vorwort

Der alljährliche „Paracelsus Science Get Together“ konnte auch 2022 durchgeführt werden – adaptiert an die neuen Gegebenheiten in Zeiten der Pandemie wechselten wir heuer zum dritten Mal auf die virtuelle Plattform #vSGT.

Forschende aus der Universität, den Universitätskliniken in Salzburg und Nürnberg sowie Kooperationspartnern aus Salzburg und Nürnberg folgten der Einladung und reichten insgesamt mehr als 77 internationale Poster (davon 9 Poster von Studierenden der Humanmedizin) ein. Sie stellten ihre aktuellen Forschungsarbeiten vor – virtuell und den ganzen Sommer über auch online verfügbar. Die gezeigten Arbeiten umfassen eine enorme thematische Bandbreite aus den verschiedensten Wissenschaftsbereichen, darunter Medizin, Natur- und Sozialwissenschaften, von Grundlagen- bis zu klinischer Forschung.

Rund 534 Besucherinnen und Besuchern konnte die medizinisch-wissenschaftliche Leistungsschau im bereits zwölften Jahr ihres Bestehens in neuem Format begeistern, wie auch die zahlreiche Teilnahme am neu eingeführten Publikumsvoting beweist. Mehr als 1094 Seitenaufrufe (!) wurden über den Sommer gezählt.

Herzliche Gratulation an alle Gewinnerinnen und Gewinner der Poster Awards. Das Publikum kürte das Poster von **Lukas Zell** mit dem Titel „Identification of novel dopamine D2 receptor ligands – a combined in silico / in vitro approach“ vom Institut für Pharmazie der Paracelsus Medizinischen Universität Salzburg zum besten Poster.

Die Fachjury entschied sich für **Viktoria Leb-Reichl** (Best Poster female) mit „Leveraging immune memory against measles virus as an anti-tumor strategy in a pre-clinical model of aggressive squamous cell carcinoma“ und **Rodolphe Poupardin** (Best Poster male) mit „Batch Effects during Human Bone Marrow Stromal Cell Propagation Prevail Donor Variation and Culture Duration: Impact on Genotype, Phenotype and Function“ (beide Salzburg). Zwei Best Student Poster gingen an **Nicole Schneider** mit „Analysis of Hv1 proton channel expression in acute leukemias and non-Hodgkin lymphomas compared to healthy control samples by qPCR“ und **Isabell Prothmann** mit „Verträglichkeit von Fortifiern aus gefriergetrockneter Frauenmilch zur Anreicherung der Ernährung von Frühgeborenen ab 31 Schwangerschaftswochen“ (beide Nürnberg).

Ein herzlicher Dank gilt unseren Organisatoren rund um Bruno Wöran, dem Leiter des Forschungsservice FMTT und Barbara Ruder, die am Standort Nürnberg für die Abwicklung verantwortlich war, sowie den zahlreichen Unterstützer*innen, die auch in diesem besonderen

Jahr die Durchführung des vSGT mitermöglicht haben. 9 internationale Sponsoren vertrauten auf das neue Format und ermöglichten das umfangreiche, internationale Netzwerken.

Wir freuen uns, Ihnen zum Abschluss des „Paracelsus virtual Science Get Together – Science Summer“ wie in jedem Jahr diesen Abstractband zum besseren Überblick und als Nachschlagewerk übermitteln zu dürfen, wiederum mit einer ISBN-Nummer versehen und damit zitierfähig. Für alle, die noch einen Blick auf die tatsächlichen Poster werfen möchten, die Ausstellung kann nach wie vor unter https://vsgt.pmu.ac.at/ besucht werden.

Der besondere Dank der Universität gilt neben den Mitarbeiterinnen und Mitarbeitern des Forschungsservices im FMTT der gesamten IT, die das neue Format zum Laufen brachten und jetzt bereits im dritten Jahr etablierten. So wurde der Netzwerkgedanke des vSGT nicht nur von den Teilnehmenden, sondern auch von der Organisation gelebt – ganz im Sinne des Leitbildes der Universität.

Es ist uns ein großes Anliegen, den Vernetzungsgedanken weiter zu verankern und auch gemeinsame Forschungsprojekte zwischen den beiden Universitäts-Standorten Salzburg und Nürnberg im Sinne eines Brückenschlages innerhalb der PMU weiter voranzutreiben und zu fördern.

Für 2023 laufen jetzt schon die Planungen: Es wird sowohl vor Ort als auch den ganzen Sommer über standortübergreifende virtuelle und hybride Veranstaltungen geben. Bleiben Sie gesund und neugierig und freuen Sie sich mit uns auf den „Science Get Together 2023“, in dem wir wieder großartige Leistungen präsentieren werden.

Es grüßen Sie herzlich

Univ.-Prof. Dr. Wolfgang Sperl
Rektor

Univ.-Prof. Dr. Ludwig Aigner
Vizerektor für Forschungsangelegenheiten

Inhaltsverzeichnis

Der Paracelsus virtual Science Get Together 2022 wurde mit freundlicher Unterstützung folgender Unternehmen ermöglicht:

Poster- & Abstractsammlung

Modulation of microglia function via omega-3 polyunsaturated fatty acid eicosapentaenoic acid (EPA) in Alzheimer's disease

Barbara Altendorfer[1,2], Iris Leister[1,2,3,4], Sophie Lefèvre-Arbogast[5], Claudine Manach[6], Dorrain Y Low[6], Mireia Urpi-Sarda[7], Cristina Andres-Lacueva[7], Raúl González-Domínguez[7], Thomas Felder[8], Julia Tevini[8], Diana Marisa Bessa de Sousa[1,2], Reinhold Schmidt [9], Paul J Lucassen[10], Silvie R Ruigrok[10], Chiara De Lucia[11], Andrea Du Preez[11], Catherine Helmer[5], Cécile Proust-Lima[5], Aniko Korosi[10], Cécilia Samieri[5], Sandrine Thuret[11,12] and Ludwig Aigner[1,2]

1, Institute of Molecular Regenerative Medicine, Paracelsus Medical University, Salzburg, Austria; 2, Spinal Cord Injury and Tissue Regeneration Center Salzburg (SCI-TReCS), Paracelsus Medical University, Salzburg, Austria; 3, ParaMove, SCI Research Unit, BG Trauma Center Murnau, Murnau, Germany, and Paracelsus Medical University, Salzburg, Austria; 4, Spinal Cord Injury Center, Clinical Research Unit, BG Trauma Center Murnau, Murnau, Germany; 5, University of Bordeaux, Inserm, Bordeaux Population Health Research Center, UMR 1219, 146 rue Léo-Saignat, Bordeaux 33076, France; 6, University of Clermont Auvergne, INRA, UMR1019, Human Nutrition Unit, Clermont Ferrand 63000, France; 7, Nutrition, Food Science and Gastronomy Department, Faculty of Pharmacy and Food Science, CIBER Fragilidad y Envejecimiento Saludable (CIBERFES), Instituto de Salud Carlos III, University of Barcelona, Barcelona 08028, Spain; 8, Department of Laboratory Medicine, Paracelsus Medical University, Salzburg, Austria; 9, Clinical department of general neurology, University Hospital of Neurology, Graz, Austria; 10, Brain Plasticity Group, Swammerdam Institute for Life Sciences, Center for Neuroscience, University of Amsterdam, Amsterdam 1098 XH, Netherlands; 11, Department of Basic and Clinical Neuroscience, Maurice Wohl Clinical Neuroscience Institute, Institute of Psychiatry, Psychology and Neuroscience, King's College London, London SE5 9NU, United Kingdom; 12, Department of Neurology, University Hospital Carl Gustav Carus, Technische Universität Dresden, Germany

Contact: barbara.altendorfer@pmu.ac.at

PARACELSUS MEDIZINISCHE PRIVATUNIVERSITÄT

Background: Genome-wide association studies identified several genes, implemented in microglia phagocytosis, which are associated with an increased risk for Alzheimer's disease (AD), offering microglia as potential therapeutic targets. Factors circulating in the blood, like food metabolites, might have effects on microglia function and thereby influence cognitive degeneration. Along this line, we investigated the effect of blood serum of AD patients and participants with cognitive decline on microglia by using an *in vitro* parabiosis system.

Methods: Microglia were incubated with human serum, encountered with pH-sensitive fluorescent particles and phagocytic particle uptake was measured by flow cytometry. The University Hospital Graz provided us with serum from AD patients and age-matched controls (n=30 per group). Another data set was obtained through a case-control study conducted by the EU D-CogPlast project, consisting not only out of blood samples taken before participants showed signs of cognitive deficit but also data on the metabolom (n=209 per group).

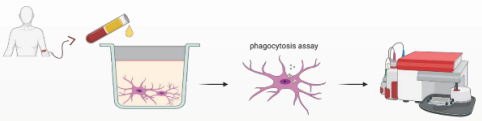

Results:

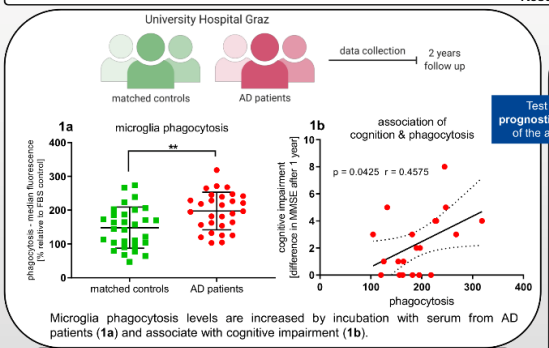

Microglia phagocytosis levels are increased by incubation with serum from AD patients (**1a**) and associate with cognitive impairment (**1b**).

Test of **prognostic** value of the assay

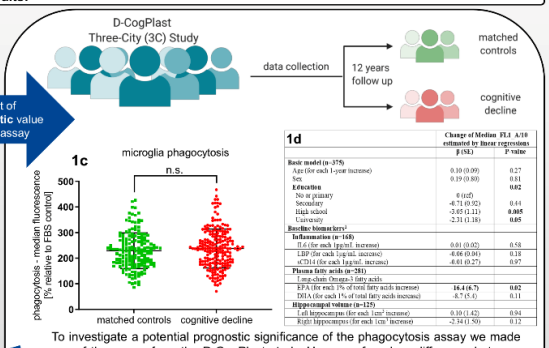

1d

	Change of Median FL1 A/10 estimated by linear regressions	
	β (SE)	P value
Basic model (n=375)		
Age (for each 1-year increase)	0.10 (0.09)	0.27
Sex	0.19 (0.80)	0.81
Education		**0.02**
No or primary	0 (ref)	
Secondary	-0.71 (0.92)	0.44
High school	-2.05 (1.11)	**0.005**
University	-2.31 (1.18)	**0.05**
Baseline biomarkers[2]		
Inflammation (n=168)		
IL6 (for each 1pg/mL increase)	0.01 (0.02)	0.58
LBP (for each 1µg/mL increase)	-0.06 (0.04)	0.18
sCD14 (for each 1µg/mL increase)	-0.01 (0.27)	0.97
Plasma fatty acids (n=281)		
Long-chain Omega-3 fatty acids		
EPA (for each 1% of total fatty acids increase)	**16.4 (6.7)**	**0.02**
DHA (for each 1% of total fatty acids increase)	-8.7 (5.4)	0.11
Hippocampal volume (n=125)		
Left hippocampus (for each 1cm³ increase)	0.10 (1.42)	0.94
Right hippocampus (for each 1cm³ increase)	-2.34 (1.50)	0.12

To investigate a potential prognostic significance of the phagocytosis assay we made use of the serum from the D-CogPlast study. Here, we found no difference between the groups (**1c**) and we had to reject the hypothesis of a prognostic value of the phagocytosis assay.
But we found that phagocytosis correlated negatively with the amount of eicosapentaenoic acid (EPA) (**1d**), one of the main omega-3 polyunsaturated fatty acids, in the blood.

Validation of association between phagocytosis and EPA

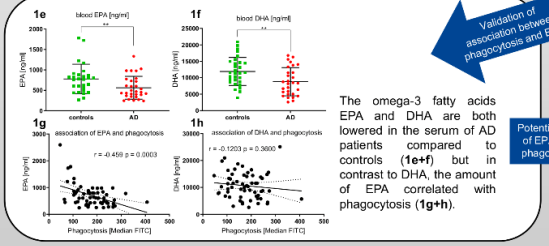

The omega-3 fatty acids EPA and DHA are both lowered in the serum of AD patients compared to controls (**1e+f**) but in contrast to DHA, the amount of EPA correlated with phagocytosis (**1g+h**).

Potential direct effects of EPA on microglia phagocytosis in vitro

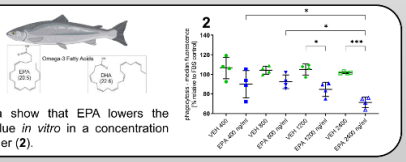

Preliminary data show that EPA lowers the phagocytosis value *in vitro* in a concentration dependent manner (**2**).

Conclusion: EPA likely has direct and/or indirect effects on microglial phagocytic activity, which would offer a potential attenuation of neurodegenerative diseases by influencing protein deposition and microglia driven neuroinflammation.

Outlook: *In vivo* experiment in a mouse model for Alzheimer's disease

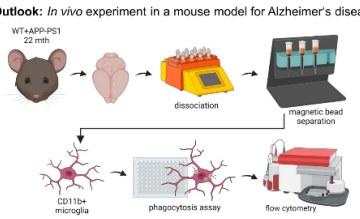

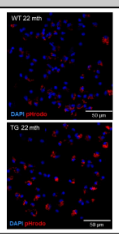

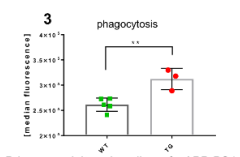

Primary adult microglia of APP-PS1 transgenic (TG) mice exhibited a higher phagocytosis value than microglia from their wildtype (WT) littermates (**3**).

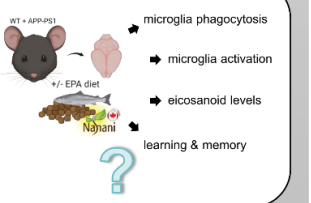

Acknowledgements: This project was part of the EU consortium DCogPlast 'Diet Cognition and Plasticity" funded by JPI-HDHL (Medical Research Council UK: MR/N030087/1; French National Research Agency ANR-15-HDHL-0002-05; PCIN-2015-229- MINECO; CiberFES- Cofund by FEDER Program from EU, 2017SGR1546 & ICREA 2018 Academia Award from the Generalitat de Catalunya), the BMWFW under BMWFW-10.420/0009-WF/V/3c/2015.
Graphics were created with BioRender.com

Modulation of microglia function via omega-3 polyunsaturated fatty acid eicosapentaenoic acid (EPA) in Alzheimer's disease

Barbara Altendorfer[1,2], Iris Leister[1,2,3,4], Sophie Lefèvre-Arbogast[5], Claudine Manach[6], Dorrain Y Low[6], Mireia Urpi-Sarda[7], Cristina Andres-Lacueva[7], Raúl González-Domínguez[7], Thomas Felder[8], Julia Tevini[8], Diana Marisa Bessa de Sousa[1,2], Reinhold Schmidt[9], Paul J Lucassen[10], Silvie R Ruigrok[10], Chiara De Lucia[11], Andrea Du Preez[11], Catherine Helmer[5], Cécile Proust-Lima[5], Aniko Korosi[10], Cécilia Samieri[5], Sandrine Thuret[11,12], Ludwig Aigner[1,2]

[1]Institute of Molecular Regenerative Medicine, Paracelsus Medical University, Salzburg, Austria; [2]Spinal Cord Injury and Tissue Regeneration Center Salzburg (SCI-TReCS), Paracelsus Medical University, Salzburg, Austria; [3]ParaMove, SCI Research Unit, BG Trauma Center Murnau, Murnau, Germany, and Paracelsus Medical University, Salzburg, Austria; [4]Spinal Cord Injury Center, Clinical Research Unit, BG Trauma Center Murnau, Murnau, Germany; [5]University of Bordeaux, Inserm, Bordeaux Population Health Research Center, UMR 1219, 146 rue Léo-Saignat, Bordeaux 33076, France; [6]University of Clermont Auvergne, INRA, UMR1019, Human Nutrition Unit, Clermont Ferrand 63000, France; [7]Nutrition, Food Science and Gastronomy Department, Faculty of Pharmacy and Food Science, CIBER Fragilidad y Envejecimiento Saludable (CIBERFES), Instituto de Salud Carlos III, University of Barcelona, Barcelona 08028, Spain; [8]Department of Laboratory Medicine, Paracelsus Medical University, Salzburg, Austria; [9]Clinical department of general neurology, University Hospital of Neurology, Graz, Austria; [10]Brain Plasticity Group, Swammerdam Institute for Life Sciences, Center for Neuroscience, University of Amsterdam, Amsterdam 1098 XH, Netherlands; [11]Department of Basic and Clinical Neuroscience, Maurice Wohl Clinical Neuroscience Institute, Institute of Psychiatry, Psychology and Neuroscience, King's College London, London SE5 9NU, United Kingdom; [12]Department of Neurology, University Hospital Carl Gustav Carus, Technische Universität Dresden, Germany; Contact: barbara.altendorfer@pmu.ac.at

Objective
Genome-wide association studies identified several genes, implemented in microglia phagocytosis, that are associated with an increased risk for Alzheimer's disease (AD), offering microglia as potential therapeutic targets. Factors circulating in the blood, like food metabolites, might have effects on microglia function and thereby influence cognitive degeneration. Along this line, we investigated the effect of blood serum of AD patients and participants with cognitive decline on microglia phagocytosis by using an in vitro parabiosis system.

Methods
A human microglia cell line was incubated with human serum, encountered with pH-sensitive fluorescent particles and subsequent phagocytic uptake was measured by flow cytometry. The University Hospital Graz provided us with serum from AD patients and age-matched controls (n = 30 per group). A different data set was obtained through a case-control study conducted by the EU D-CogPlast project, consisting not only out of blood samples taken before participants showed signs of cognitive deficit but also data on the metabolom (n = 209 per group).

Results
The serum of AD patients led to elevated phagocytosis levels, which were associated with cognitive impairment. To investigate a potential prognostic significance of the phagocytosis assay we made use of the serum from the D-CogPlast study. Here, we found no difference between the groups, but phagocytosis correlated negatively with the amount of eicosapentaenoic acid (EPA), one of the main omega-3 polyunsaturated fatty acids, in the blood. Testing of the single component EPA on microglia in vitro, revealed a concentration dependent decrease of phagocytic uptake, indicating an anti-inflammatory effect.

Conclusions
EPA likely has direct and/or indirect effects on microglial phagocytic activity, which would offer a potential attenuation of neurodegenerative diseases by influencing protein deposition and microglia driven neuroinflammation.

Development of a physiologically relevant, biomechanical test setup considering internal muscle forces for the investigation of complex pelvic ring fractures

Dirk Baumeister[1], [2], Jonas Mock[1], [3], Markus Greinwald[1], Martin Winkler[1], Peter Augat[1], [2]
[1] Institute for Biomechanics, BG Unfallklinik Murnau, Germany
[2] Institute for Biomechanics, Paracelsus Medical University, Salzburg, Austria
[3] Kempten University of Applied Sciences, Germany

BGU Murnau
Berufsgenossenschaftliche Unfallklinik Murnau

Introduction

The human pelvis is a ring-shaped bone structure, designed to transfer the load of the upper body to the lower extremities. Fractures of the pelvis can lead to disruptions of the ring-shaped structure which results in mechanical destabilization. Forces and moments can then no longer be transmitted by the pelvis. In order to address the existing instability, fractures of the pelvic ring require a mechanically stable osteosynthetic treatment, for which a variety of different methods are available. Previous biomechanical studies do not fully consider the complex loading situation at the pelvis, so that there is still a lack of knowledge about the mechanical stability of the different osteosynthetic treatments.

The aim of this project is to build a test setup able to determine the stability of different fixation methods for complex pelvic ring fractures under a loading situation simulating human gait: The weight of the upper body is alternately transferred to the legs via both hip joints. In addition, muscles at the pelvis counteract a tilting of the pelvis.

Test Setup

Two different types of forces are considered that act on the pelvis during human gait:

- **Force of the trunk**: Khoo et al. [1] developed a dynamic biomechanical model to determine loads at the lumbosacral joint-center during the stance phase of normal level walking. Their findings showed that the resultant loads at the lumbosacral joint-center were between 1.5 and 2 times body-weight. A force of this magnitude will be applied to the sacrum in vertical direction in the test setup.
- **Muscle forces:** Rajagopal et al. [2] built up a musculoskeletal model including bony geometry for the full body with 37 degrees of freedom to define joint kinematics, Hill-type muscle models of 80 muscle-tendon units and 17 ideal torque actuators driving the upper body. They also provide the simulation data of a 31 year old individual walking with a speed of 1.5 m/s. These data were used to determine the muscle forces that act on the pelvis during walking. For the purpose of experimentally realizing the muscle actions the individual muscles were combined into two muscle groups (anterior and posterior muscle group).

The mechanical test setup was constructed and built (Figure 1 shows a CAD-model). The vertical force of the trunk is applied on the sacrum via a hydraulic testing machine. In order to avoid uncontrollable shear forces between sacrum and testing machine, a linear bearing allows translational movement in the horizontal plane and a ball bearing mounted directly to the sacrum allows rotational movement around all three spatial axes.

A hip joint endoprosthesis with three rotational degrees of freedom is mounted to each acetabulum. The shafts of the endoprostheses are embedded to vertically slidable embedding pots.

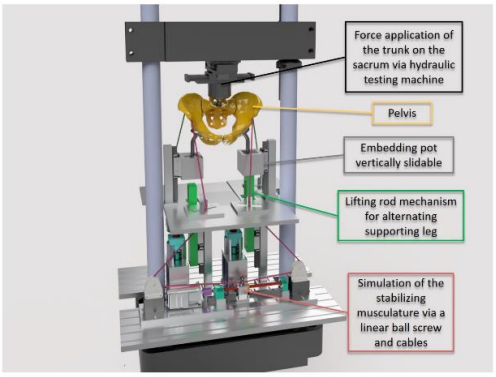

Figure 1: Rendering of the CAD-model of the test setup from the frontal perspective. The red cables represent the anterior muscle group, the green cables the posterior muscle groups. Not shown is the drive unit for the posterior muscle mechanism.

Test Sequence

To simulate the dynamic alternating load on the pelvis during walking, the load is alternately transferred via the two acetabula. The procedure for loading of the right side is described in detail as follows (see Figure 2):

A. When changing from left to right supporting leg, only small, negligible forces act on the sacrum and on the muscle pulls and all actuators move towards the initial positions. Both embedding pots are in contact with the lifting rods. To simulate the orientation of the pelvis when walking, the pelvis is tilted slightly to the right when standing on the right side. This is achieved by positioning the left lifting rod further up than the right.

B. The two muscle pulls (anterior and posterior) are tensioned with the same, low force ($F_{initial}$). Leverage results in a force on the sacrum.

C. To ensure that no force is transmitted via the non-supporting side (left), the left lifting rod is lowered and there is no longer contact between the embedding cup and the lifting rod (highlighted in Figure 2 C). The new lever ratios reduce the force on the sacrum.

D. In order to be able to increase the forces evenly during the actual loading phase, a specific preload (F_{pre}) must be set by the actuators.

E. During the actual loading phase, the forces are increased simultaneously until the final forces (F_{load}) are reached. A simultaneous increase in force at all force application points is important to prevent the pelvis from tilting forward/backward/to the side.

F. After the loading, the forces are reduced again and the same procedure is repeated for the left side. For the dynamic testing of osteosyntheses, this supporting leg change is repeated several thousand times with a cyclically increasing load.

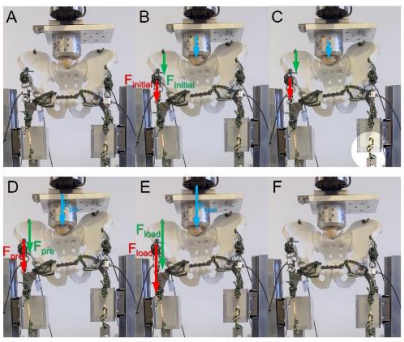

Figure 2: Detailed sequence of force increase on a synthetic pelvis during simulated right supporting leg phase. Red arrow: Force at the anterior muscle pull; Green arrow: Force at the posterior muscle pull; Blue arrow: Force at the sacrum

Discussion

In the current state of development, it was possible to demonstrate by means of a functional test that the simultaneous and alternating load application works. In the next step, the control system must be optimized to allow larger forces to be applied. A validation process is required to demonstrate that the loads applied to the pelvis in the test setup match the loads imposed in the requirements and that no constraint forces are generated. Many tests of osteosyntheses for pelvic ring fractures have been performed on previous single-leg test setups. In a further validation step, these tests will be reproduced on the new test setup (same synthetic model/fracture/osteosynthesis/etc.) and the new results will be compared with the previous results.

In summary, the newly designed test setup will be used to evaluate the fatigue strength of osteosyntheses used for complex pelvic ring fractures under loads that are similar to the loads that occur thousands of times between surgery and healing of the bone.

PARACELSUS MEDIZINISCHE PRIVATUNIVERSITÄT
20 JAHRE

Literature:
[1] Khoo, B., et al. (1995). Medical engineering & physics 17(1): 27-35.
[2] Rajagopal, A., et al. (2016).IEEE Transactions on Biomedical Engineering 63(10): 2068-2079.

Contact:
Dirk Baumeister, M.Sc.
E-mail: dirk.baumeister@bgu-murnau.de
Telephone: +49 8841 48-2536
Fax: +49 8841 48-4573

BG Klinikum Murnau,
Paracelsus Medical University
Prof.-Küntscher-Str. 8
82418 Murnau am Staffelsee
www.bg-kliniken.de/unfallklinik-murnau

Paracelsus virtual Science Get Together 2022

Development of a physiologically relevant, biomechanical test setup considering internal muscle forces for the investigation of complex pelvic ring fractures

Dirk Baumeister[1,2], Jonas Mock[1,3], Markus Greinwald[1], Martin Winkler[1], Peter Augat[1,2]

[1]Institute for Biomechanics, BG Unfallklinik Murnau, Germany; [2]Institute for Biomechanics, Paracelsus Medical University, Salzburg, Austria; [3]Kempten University of Applied Sciences, Germany; Contact: dirk.baumeister@bgu-murnau.de

Objective
Fractures of the human pelvis can lead to disruptions of the ring-shaped structure which results in mechanical destabilization of the pelvic ring. A variety of different methods for an osteosynthetic treatment are available, but there is still a lack of knowledge about the mechanical stability of these methods. The aim of this project is to build a test setup able to determine the stability of different fixation methods for complex pelvic ring fractures under a loading situation simulating human gait.

Methods
During gait, the human pelvis is loaded mainly by the weight of the trunk and muscle forces. Rajagopal et al. (1) built up a musculoskeletal model and provide simulation data of a 31-year old individual walking with a speed of 1.5 m/s. The muscle forces from this simulation were summarized into an anterior and a posterior muscle group.

Results
The vertical force of the trunk is applied on the sacrum via a hydraulic testing machine. Hip joint endoprostheses are mounted to the acetabuli of the specimen. The vertical movement of the hip joint endoprostheses can either be released (swing leg phase) or locked (stance leg phase). Muscle forces are applied with the help of ropes and their magnitude is determined with force sensors. By alternately loading the right and left acetabulum, gait cycles can be simulated.

Conclusions
To date, biomechanical experiments on pelvises have been performed primarily on single-leg stance or double-leg stance models. Because these do not fully take into account the complex loading situation during gait, the new test setup was developed. Simplifications were made to account for the applied loads, especially the muscle forces. The new test setup can be used to evaluate the fatigue strength of osteosynthetic constructs used for complex pelvic ring fractures.

References
1. Khoo, B., et al. (1995). Medical engineering & physics 17(1): 27-35.
2. Rajagopal, A., et al. (2016).IEEE Transactions on Biomedical Engineering 63(10): 2068-2079.

PARACELSUS MEDIZINISCHE PRIVATUNIVERSITÄT

Klinikum Nürnberg
Wir sind für Sie da!

Protein Metabolism in Preterm and Term Infants using a ^{15}N-Tracer and the Nitrogen Balance Method: A Pilot-Study

Sabrina Beck[1], Christoph Fusch[1,2], Jan Däbritz[3], Gerhard Fusch[2], Birgit Salewski[3], Klaus Wutzke[3], Niels Rochow[1,2,3]

[1]Pediatrics, Paracelsus Medical University, Nuremberg; [2]Pediatrics, McMaster University, Hamilton, Canada; [3]Pediatrics, University Medicine Rostock, Rostock

INTRODUCTION

- It is desired to provide preterm infants with nutrition that supports accrual of protein and fat-free mass.
- To maximize the utilization of protein building blocks, to optimize growth, excess protein oxidation and related urea production should be avoided.
- The composition of feedings determined by
  1) availability of macronutrients
  2) protein (gram) to energy ratio and
  3) carbs to fat ratio affects protein oxidation.

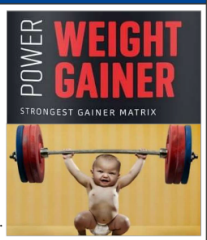

- Kinetic of urinary N excretion using ^{15}N-labeled amino acids (Tracer) can measure protein turnover, protein gain and urea production.
- This pilot study aims to establish a tracer method in preparation for a double-blind, randomized clinical trial (RCT) to identify a composition of fortified breast milk which maximizes protein accretion.

OBJECTIVES

- To analyze nitrogen balance, protein turnover and net protein gain using ^{15}N-labeled amino acid tracer in preterm infants.

METHODS

- Stable growing newborns with no gastrointestinal diseases which affect nutritional absorption were enrolled at McMaster Children's Hospital.
- Nitrogen kinetic was measured using a single shot (1mL/kg) ^{15}N-labeled amino acid mixture (ALGAL Amino Acid Mixture; 3.3 mg AA/mL).
- Urine was collected over a 36 hours period in 3 hours intervals.
- Urinary ^{15}N was measured using an elemental analyzer Solid Liquid (SL^{TM}, SerCon, CREWE, U.K.) and urea and creatinine were measured using standard clinical chemistry.
- Based on the three-compartment model (TCM), nitrogen balance, protein turnover and net protein gain were calculated (g/kg/d).

Three-Compartment Model (TCM)

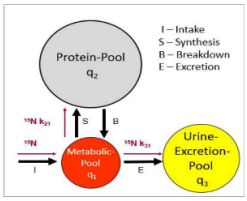

Nitrogen flux

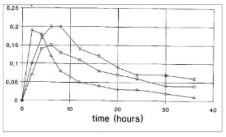

Example of urinary ^{15}N amino acid kinetic (Wutzke et al. 1992)

RESULTS

- 18 preterm male infants were enrolled (gestational age: 25 to 39 weeks, birth weight: 720 to 2770 g) and tracer were given between day of life 3 to 97.
- No adverse events were reported during the study.

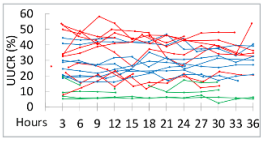

- Participants demonstrate individual starting levels of UUCR.
- Time course per participant seems to be stable with a constant intake.

Fig. 1: Urinary urea creatinine ratio (UUCR)
Colors represent the standard deviation (red: SD > 3.5%; blue: SD ≥ 1.6% to ≤ 3.5%; green: SD ≤ 1.5%).

RESULTS

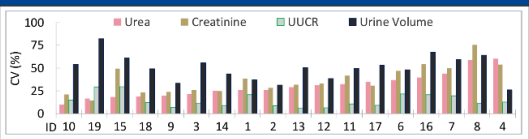

Fig. 2: Individual coefficient of variation (CV), 3 hours intervals

- The individual CV for urea ranges from 9.9 % to 60.3 %, for creatinine from 14.5 % to 75.6 %, for UUCR from 5.6 % to 29.6 % and for urine volume from 25.9 % to 82.3 %.
- Based on the CV of urea up to 60.3 %, spot urine does not seem sufficient in determining protein accretion.

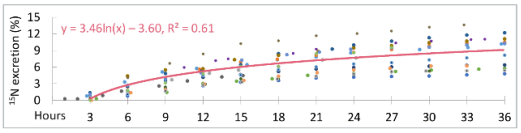

Fig. 3: Cumulative urinary ^{15}N-Tracer excretion (36 hour period)

- The cumulative urinary excretion dose from tracer varies between 4 % and 14 %.
- 86 % to 96 % of the tracer dose were stored in the body.
- Urinary ^{15}N kinetic curves plateaued at 36 hours.

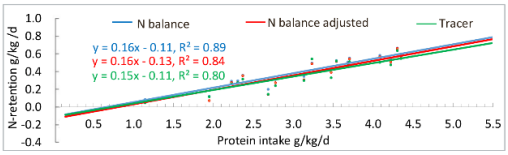

Fig. 4: Method comparison - Nitrogen retention per protein intake.
(N balance adjusted: N multiplied by factor 1.25 for other N containing components in urine)

- N balance, N balance adjusted and the tracer method yield similar slopes of regression lines.
- A linear relation is observed between nitrogen retention and protein intake from 1.25 to 5.5 g/kg/d.
- X-axis intercept at ~1.0 g protein /kg/d compares favorably with results of previous studies (Koletzko et al., 2014).

CONCLUSION

- A ^{15}N-Tracer has been established which is an useful and safe tool to analyze the protein metabolism. Additionally to common nitrogen balance studies, protein synthesis, protein breakdown, protein turnover and net protein gain can be calculated from urinary ^{15}N kinetics.
- The ^{15}N urinary measurements demonstrate a similar kinetic with a plateau at 36 hours which is comparable to data from the literature.
- The similarity of the results between tracer kinetic and balance method indicates the reliability of the ^{15}N-Tracer method.
- To optimize non-protein composition of fortified breast milk, protein synthesis will be studied in a double-blind RCT using ^{15}N-Tracer comparing low and high carbs nutrition with similar protein intake (table).

Group 1* Low Carbs/High Fat		Group 2* High Carbs/Low Fat	
Carbs	5.5	Carbs	11
Protein	3	Protein	3
Fat	5.5	Fat	3
Sum kcal	**86**	**Sum kcal**	**85.3**

*Values for 100 mL breast milk

Niels Rochow, MD, PhD, Pediatrics, Paracelsus Medical University, niels.rochow@klinikum-nuernberg.de

Protein Metabolism in Preterm and Term Infants using a 15N-Tracer and the Nitrogen Balance Method: A Pilot-Study

Sabrina Beck[1], Christoph Fusch[1,2], Jan Däbritz[3], Gerhard Fusch[2], Naghemeh Forghani[2], Birgit Salewski[3], Klaus Wutzke[3], Niels Rochow[1,2,3]

[1]Pediatrics, Paracelsus Medical University, Nuremberg; [2]Pediatrics, McMaster University, Hamilton, Canada; [3]University Medicine Rostock, Rostock; Contact: sabrina.beck@stud.pmu.ac.at

Objective
It is desired to provide preterm infants with nutrition that supports accrual of protein and fat-free mass. To maximize the utilization of protein building blocks, to optimize growth, excess protein oxidation and related urea production should be avoided. The composition of feedings determined by 1) availability of macronutrients, 2) protein (gram) to energy ratio and, 3) carbs to fat ratio affects protein oxidation. Kinetic of urinary N excretion using ^{15}N-labeled amino acids can measure protein turnover, protein gain and urea production. This study aims to establish a tracer method to measure protein turnover.

Methods
Stable growing newborns with no gastrointestinal diseases which affect nutritional absorption were enrolled in this observational study at McMaster Children's Hospital. Nitrogen kinetic was measured using a single shot (1mL/kg) ^{15}N-labeled amino acid mixture (ALGAL Amino Acid Mixture; 3.3 mg AA/mL).
Urine was collected over a 36 hours period in 2 to 4 hours intervals. Urinary ^{15}N was measured using an isotope mass spectroscopy and urea, creatinine and Urinary urea creatinine ratio (UUCR) were measured using clinical chemistry. Based on the three-compartment model, nitrogen balance, protein turnover and net protein gain were calculated.

Results
Eighteen male infants were enrolled (gestational age: 25 to 39 weeks, birth weight: 720 to 2770 g) and tracer were given between day of life 3 to 97. No adverse events were reported during the study.
The individual CV for urea ranges from 9.9 % to 60.3 %, for creatinine from 14.5 % to 75.6 %, for UUCR from 5.6 % to 29.6 % and for urine volume from 25.9 % to 82.3 %. Based on the CV of urea up to 60.3 %, spot urine does not seem sufficient in determining protein accretion. Further, infants demonstrated individual levels of UUCR. Time course per infant seemed to be stable with a constant intake.
The cumulative urinary excretion dose from tracer varied between 4 % and 14 %. 86 % to 96 % of the tracer dose were stored in the body. Urinary ^{15}N kinetic curves plateaued at 36 hours. N balance, N balance adjusted and the tracer method yield similar slopes of regression lines. A linear relation is observed between nitrogen retention and protein intake from 1.25 to 5.5 g/kg/d. X-axis intercept at ~1.0 g protein /kg/d compares favorably with results of previous studies.

Conclusions
A ^{15}N-Tracer has been established which is an useful and safe tool to analyze the protein metabolism. Additionally to common nitrogen balance studies, protein turnover can be calculated from urinary ^{15}N kinetics. The ^{15}N urinary measurements demonstrate a similar kinetic with a plateau at 36 hours which is comparable to data from the literature.
The similarity of the results between tracer kinetic and balance method indicates the reliability of the ^{15}N-Tracer method.

Inducing ferroptosis, a new approach to target biliary tract cancer?

Authors: Dino Bekric[1,4], Heidemarie Dobias[1,4], Marlena Beyreis[1], Martina Winklmayr[6], Daniel Neureiter[2], Markus Ritter[1,3], Tobias Kiesslich[1,5], Christian Mayr[1,5*]

[1] Center for Physiology, Pathophysiology and Biophysics – Salzburg and Auersperg, Institute for Physiology and Pathophysiology – Salzburg, 5020 Salzburg, Austria [2] Institute of Pathology, Paracelsus Medical University / Salzburger Landeskliniken (SALK), 5020 Salzburg, Austria [3] Kathmandu University School of Medical Sciences, Dhulikhel, Nepal [4] Gastein Research Institute, Paracelsus Medical University, 5020 Salzburg, Austria [5] Department of Internal Medicine I, Paracelsus Medical University/Salzburger Landeskliniken (SALK), 5020 Salzburg, Austria [6] Ludwig Boltzmann Institute for Arthritis and Rehabilitation, Paracelsus Medical University, 5020 Salzburg, Austria
*Correspondence: christian.mayr@pmu.ac.at

Objective:

Ferroptosis, a ROS and iron-dependent non-apoptotic form of regulated cell death, is characterized by excessive peroxidation of polyunsaturated fatty acids (PUFAs) which ultimately results in cell death. This novel form of cell death is distinct from other known types of cell death such as apoptosis, necroptosis and autophagy in a genetically, morphologically and mechanistically manner. The main mechanism how ferroptosis is triggered is the massive accumulation of iron and the generation of Lipid ROS, which leads to membrane rupture and therefore to cell death. Biliary tract cancer (BTC) is a deadly disease with a dismal overall survival rate, which is in part caused by limited therapeutic options. Therefore, the aim of this study is, to investigate, if ferroptosis can be induced in BTC and therefore might serve as a potential new therapeutic strategy.

Methods:

Investigation of potential cytotoxic effects were executed by the Resazurin assay and IC50 calculation, using a comprehensive BTC in vitro model (n=11 cell lines) and six substances that were described as ferroptosis-inducers (FINs) in other cancer entities (RSL-3, IKE, FINO2, FIN56, IFSP1, Brequinar). Additional rescue experiments using established ferroptosis, necroptosis and apoptosis inhibitors were performed to evaluate potential ferroptosis induction by these substances. Potential biomarkers of ferroptosis sensitivity were evaluated via Western Blot. To determine lipid ROS Liperfluo was used. Iron assay kit and and Glutathione assay kit will be used to investigate cellular ferrous iron levels and GPX4 protein activity as well as GSH/GSSG levels. To determine levels of NADP(H) in cells, Colorimetric NADP/NADPH Ratio Assay Kit will be used.

Conclusion & Outlook:

The current study reveals that BTC cell lines are affected by ferroptosis-inducing substances regarding cell viability and cell morphology. Furthermore, Lipid ROS levels are elevated in a cell-line and substance specific manner, if BTC cells are treated with ferroptosis inducer. Combination of ferroptosis-inducers with inhibitors of ferroptosis, necroptosis or apoptosis indicate ferroptotic events in the BTC cell lines CCC5, HUH-28 and KKU-055. Western Blot analysis of the ferroptosis-relevant proteins ACSL4, CD71, Ferritin Heavy Chain, GPX4 and System -xCT revealed a heterogeneous expression pattern. To further clarify the mode of death, accumulation of MDA levels and mitochondrial changes, will be evaluated. Additionally, potential biomarkers for ferroptosis sensitivity such as Fe^{2+} levels, GPX-4 activity and GSH/GSSG ratio will be investigated.

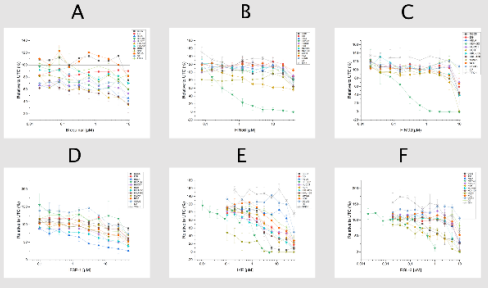

Results 1: BTC cell lines show heterogeneity towards different ferroptosis inducer

(A) BTC cells after 48h with Brequinar (B) Cell viability after 48h with FIN56 (C) Cell viability after 48h with FINO2 (D) BTC cells after IFSP-1 treatment for 48h (E) BTC cells treated with Imidazole Keton Erastin for 48h (F) Cell viability after RSL-3 treatment for 48h

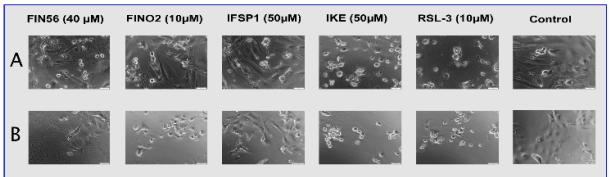

Results 2: Selected BTC cell lines show morphological changes after ferroptosis induction for 48h

(A) BTC cell line CCC5 (B) BTC cell line HuH-28

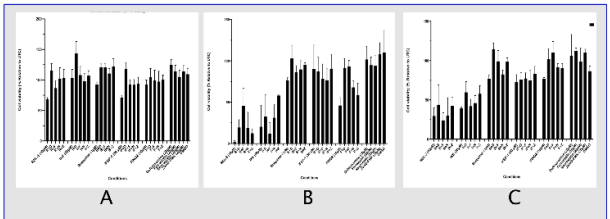

Results 3: BTC cell lines' decline of cell viability by FINs is rescued by ferroptosis inhibitors

(A) CCC5 (B) HuH-28 (C) KKU-055

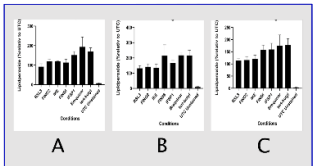

Results 4: Treatment with FINs causes Lipid ROS accumulation in selected BTC cell lines

(A) CCC5 (B) HuH-28 (C) KKU-055

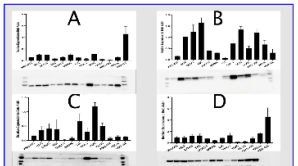

Results 5: BTC cell lines display heterogenous expression pattern of ferroptosis-relevant proteins

(A) ACSL4 (B) Ferritin Heavy Chain (C) GPX4 (C) System -xCT

In future studies, protein synthesis will be studied using ^{15}N-Tracer comparing low and high carbs nutrition with similar protein intake.
Inducing Ferroptosis, a new approach to target Biliary Tract Cancer?

Dino Bekric[1,4], Heidemarie Dobias[1,4], Marlena Beyreis[1], Martina Winklmayr[6], Markus Ritter[1,3,4,6], Daniel Neureiter[2], Tobias Kiesslich[1,5], Christian Mayr[1,5]

[1]Paracelsus Medical University , Center for Physiology, Pathophysiology and Biophysics -Institute for Physiology and Pathophysiology, Salzburg, Austria; [2]Paracelsus Medical University / Salzburger Landeskliniken (SALK), Institute of Pathology, Salzburg, Austria; [3]Kathmandu University School of Medical Sciences, Dhulikhel, Nepal; [4]Paracelsus Medical University , Gastein Research Institute, Salzburg, Austria; [5]Paracelsus Medical University/Salzburger Landeskliniken (SALK), Department of Internal Medicine I, Salzburg, Austria; [6]Paracelsus Medical University , Ludwig Boltzmann Institute for Arthritis and Rehabilitation, Salzburg, Austria; Contact: dino.bekric@pmu.ac.at

Objective
Ferroptosis, a ROS and iron-dependent non-apoptotic form of regulated cell death, is characterized by excessive peroxidation of polyunsaturated fatty acids (PUFAs) which ultimately results in cell death. Biliary tract cancer (BTC) is a deadly disease with a dismal overall survival rate, which is in part caused by limited therapeutic options. Therefore, the aim of this study is, to investigate, if ferroptosis can be induced in BTC and therefore might serve as a potential new therapeutic strategy.

Methods
Investigation of potential cytotoxic effects were executed by the Resazurin assay and IC50 calculation, using a comprehensive BTC in vitro model (n=11 cell lines) and six substances that were described as ferroptosis-inducers in other cancer entities (RSL-3, IKE, FINO2, FIN56, iFSP1, Brequinar). Additional rescue experiments using established ferroptosis, necroptosis and apoptosis inhibitors were performed to evaluate potential ferroptosis induction by these substances. Potential biomarkers of ferroptosis sensitivity were evaluated via Western Blot.

Results
Treatment of BTC cells with the mentioned ferroptosis-inducers resulted in a cell line- and time dependent reduction of cell viability, accompanied by changes in cell morphology. Interestingly, we identified BTC cell lines that were sensitive to most of the used substances as well as cell lines that showed general resistance. Combination of ferroptosis-inducers with inhibitors of ferroptosis, necroptosis or apoptosis indicate ferroptotic events in the BTC cell lines CCC5, HUH-28 and KKU-055. Western Blot analysis of the ferroptosis-relevant proteins ACSL4, CD71, Ferritin Heavy Chain, GPX4 and System -xCT revealed a heterogeneous expression pattern.

Conclusions
The current study reveals that BTC cell lines are affected by ferroptosis-inducing substances regarding cell viability and cell morphology. To further clarify the mode of death, lipid ROS accumulation as well as MDA levels and mitochondrial changes will be analysed. Additionally, potential biomarkers for ferroptosis sensitivity such as NADPH(H) and Fe2+ levels, GPX-4 activity and GSH/GSSG ratio will be investigated.

Acknowledgements
This research is funded by the PMU-FFF-stand-alone project (E-20/31/164-MAC).

The slow awakening of dormant neuronal precursors in the aging brain

Bruno Benedetti[1,2,3], Maximilian Reisinger[1,2,3], Lara Bieler[1,2,3], Gabriele Gabriele[1,2,3], Dominika Jakubecova[1,2,3], Ariane Benedetti[1,2,3], Rodolphe Poupardin[2,4] and Sébastien Couillard-Després[1,2,3]

[1]Institute of Experimental Neuroregeneration, Paracelsus Medical University, Salzburg, Austria; [2]Spinal Cord Injury and Tissue Regeneration Center Salzburg (SCI-TReCS); [3]Austrian Cluster for Tissue Regeneration, 1200 Vienna, Austria; [4] Institute of Experimental and Clinical Cell Therapy, Paracelsus Medical University, Salzburg, Austria

Introduction: Dormant neuronal precursors (dormant precursors) are a unique type of neuron, which exist in several areas of the brain of mammalian species. Dormant precursors are fundamentally different from neurogenic-niche progenitors, because they are generated during embryonic development, at which age they become postmitotic while their neuronal maturation is stalled. As consequence, dormant precursors retain latent immaturity and awaken only once the brain becomes adult. The awakening stimuli and the actual role of dormant precursors in the brain is yet unknown. Nevertheless, early work suggests that the integration of dormant precursors in the adult brain may be relevant for cognition and that dysfunctional maturation may associate to autism. Additionally, the extreme prolonged immaturity of some precursors (> 70 years in humans) could imply a functional role in the context of aging.

Goals and results: Pioneering research by the Institute of Experimental Neuroregeneration, PMU, Salzburg, allowed to discover and characterize the process of dormant precursor maturation in the adult brain and to determine that these cells become fully functional neurons. However, elderlyness may hinder maturation. Thus, precursor which maturation onset is delayed extremely may be disadvantaged in integrating into the aging brain network. We therefore questioned the capacity of dormant precursors to undergo maturation in the aging brain. Strikingly, despite prolonged immaturity late maturing precursors eventually become neurons. However, there are some peculiarities in the maturation process, partially caused by late maturation onset and partially by aging. However, we found that the functions of adult-matured precursors and neonatal-matured neurons in the aging brain are very similar. For improved analysis of synaptic integration of dormant precursors we are currently establishing innovative techniques, i.e. expansion microscopy. Moreover we are devising new strategies to control maturation pharmacologically *in vivo*, with the ultimate goal to resolve the role of dormant precursors in cognition, aging and pathology.

Can dormant precursors awaken in the aging brain?

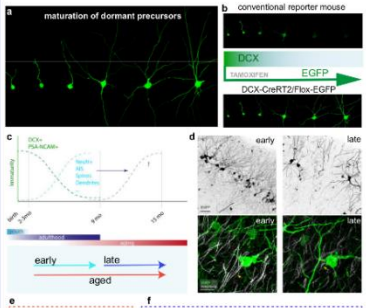

We discovered some unique cells, the "dormant precursors", which maintain a latent postmitotic immature state and can awaken in the adult brain to become neurons (a). We traced their maturation with transgenic (DCX-CreRT2/Flox-EGFP) mice, where precursors can be labelled permanently by tamoxifen administration (b), and we found that most precursors undergo maturation in the young-adult murine brain (3-9 months).

In this project we questioned whether precursor maturation can take place in the aging brain and whether late maturation leads to different outcomes in comparison to early maturation (c).

We found that precursors that remain dormant until old age (9 months) can eventually become mature neurons (d, scale bar = 15 µm). However, the morphology of late-maturing precursors is different from that of early maturing precursors (e, f): late maturation is associated with larger soma, shorter axon initial segment (AIS) and shorter dendrites.

Conversely, comparing early and aged precursors, we found that aging *per se* determines shrinkage of the soma, shortening of the AIS and shortening of the dendrites. Thus late maturation and aging have opposite effects in relation to cell soma morphology (red framed graphs) and similar effects in relation to AIS and dendrites (blue framed graphs).

Physiology: does late maturation equal neonatal maturation?

Dormant precursor mature in the adult brain. Conversely, most of the neighbouring principal neurons undergo maturation early after birth. Thus, we questioned whether the precursor awakening in the adult brain eventually leads to full functional maturation, comparable to that of early-postnatal matured neurons.

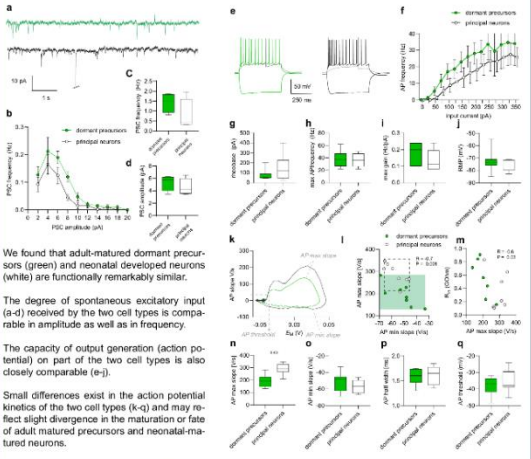

We found that adult-matured dormant precursors (green) and neonatal developed neurons (white) are functionally remarkably similar.

The degree of spontaneous excitatory input (a-d) received by the two cell types is comparable in amplitude as well as in frequency.

The capacity of output generation (action potential) on part of the two cell types is also closely comparable (e-j).

Small differences exist in the action potential kinetics of the two cell types (k-q) and may reflect slight divergence in the maturation or fate of adult matured precursors and neonatal-matured neurons.

Expansion microscopy: an innovative tool to resolve synaptic connectivity

Resolution of the synaptic connectivity was limited by the small size of synapses. Expansion microscopy is being established to improve the measurement and determine the extent of synaptic integration of mature dormant precursors (preliminary data).

Expansion microscopy relies on a process of polymer synthesis within the brain samples (a, b), followed by osmotic expansion (c). This allows to expand the brain (corpus callosum highlighted in yellow) by approximately fourfold. After expansion, histological, and cytological structures are fully preserved as highlighted by immunohistochemistry (d-f). Staining for EGFP (green) in DCX-CreRT2/-Flox-EGFP mice allowed to outline matured dormant precursors after expansion (d, e). Note the morphology of expanded nucleus (blue), soma (e, f), and dendrites (f). Expanded synaptic spines (f, white arrows) reached a length of up to 5 µm and were fully resolved by confocal microscopy.

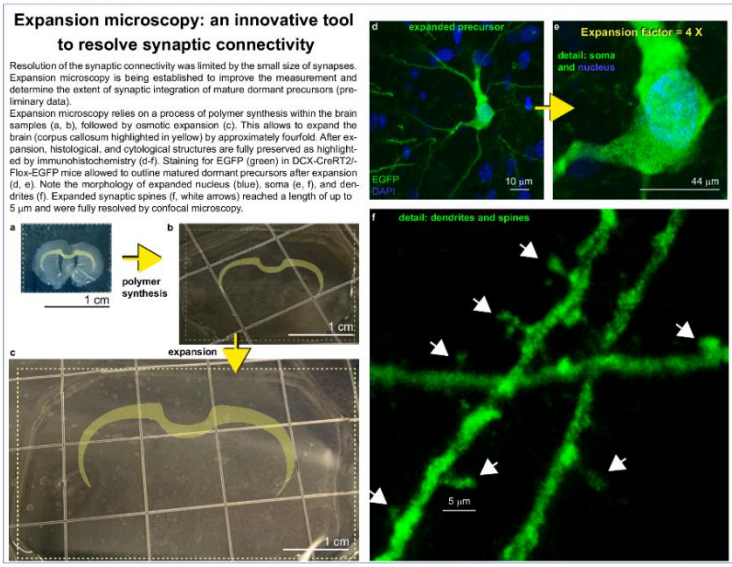

Outlook: how to control the mechanisms of dormant precursor maturation?

New strategies are being devised to control the rate of dormant precursor maturation (a), with the long term goal of deciphering their role in cognition, pathology and aging.

Preliminary experiments of single-cell transcriptomic analysis allowed to identify the monoaminergic receptors (Mor-X) that are selectively enriched in dormant precursors and best candidates to control maturation (b). Mor-X localization on dormant precursors was also confirmed on histological sections from adult brain (c).

Pharmacological tests in vivo will reveal the effects of Mor-X1 modulation for the maturation of dormant precursors.

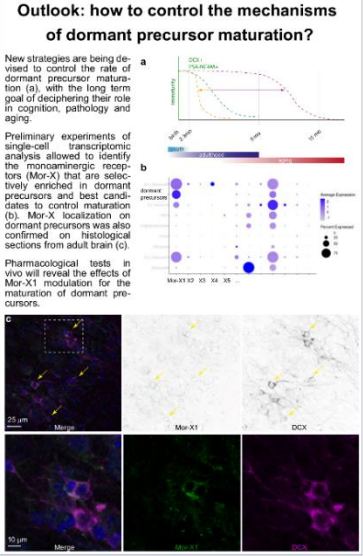

This project was possible thanks to the generous support of the Paracelsus Medical University of Salzburg, PMU-RIF: 2021-SEED-003-Benedetti.
Preliminary work was supported by PMU FFF: R-20/02/130-BEN and PMU-FFF: R-16/04/084-BEN, the German National Academic Foundation, the Spanish Ministry of Economy and Competitiveness, and Generalitat Valenciana.

We acknowledge the contributions of our collaborators: Prof. M. Engelhardt and her team at the Johannes Kepler University of Linz, Prof. L. Bonfanti at the University of Turin, Prof. J. Nacher and his team at the University of Valencia, and Dr. A. Fleischmann at the Brown University, RI, USA

The slow awakening of dormant neuronal precursors in the aging brain

Bruno Benedetti[1,2,3], Maximilian Reisinger[1,2,3], Lara Bieler[1,2,3], Gabriele Gabriele[1,2,3], Dominika Jakubecova[1,2,3], Ariane Benedetti[1,2,3], Rodolphe Poupardin[2,4], Sébastien Couillard-Despres[1,2,3]

[1]Institute of Experimental Neuroregeneration, Paracelsus Medical University; Salzburg, Austria; [2]Spinal Cord Injury and Tissue Regeneration Center Salzburg (SCI-TReCS); [3]Austrian Cluster for Tissue Regeneration, Vienna, Austria; [4]Institute of Experimental and Clinical Cell Therapy, Parecelsus Medical University, Salzburg, Austria; Contact: bruno.benedetti@pmu.ac.at

Objective
Pioneering research at the institute of Experimental Neuroregeneration, PMU, Salzburg, allowed to discover and characterize the maturation of a new type of dormant neuronal precursor in the adult brain and to determine that these cells can become fully functional neurons. However, elderliness may hinder maturation. As consequence, precursors which onset of maturation is delayed may be disadvantaged in integrating in old brain networks. Thus, this project questioned the capacity of dormant precursors to undergo maturation in the aging brain.

Methods
In transgenic mice (DCX-CreRT2/Flox-EGFP) the administration of tamoxifen allows to label immature dormant precursors permanently and to trace the course of maturation thereafter, throughout adulthood and elderliness.
Accordingly, the maturation of dormant precursors was analyzed in the adult and aging brain combining methods of expansion microscopy, immunohistochemistry, single-cell electrophysiology, and transcriptomic analysis. Some of these techniques are crucial for better resolution over the process of precursor synaptic integration and to devise new strategies for controlling pharmacologically the speed of precursor maturation *in vivo* (outlook).

Results
We found that, despite prolonged immaturity, late-maturing precursors become fully developed neurons. However, age appears relevant in relation to the outcome of the maturation process. Peculiarities in the products of late maturation involve different morphological traits that distinguish late-maturing precursors from those with earlier maturation onset. Some differences are caused by the late maturation onset itself, but others reflect the general aging of the brain. Nevertheless, the functional properties of adult-matured precursors and age-matched neonatal-matured neurons are very similar. While we establish innovative methods to resolve the finer details of precursor synaptic integration, we discovered that specific monoamine receptors are enriched in dormant precursors and suitable candidates to control their maturation.

Conclusions
Our work reveals that brain aging does not hinder and only partially affects the maturation of dormant precursors, so that even late maturation leads to full neuronal development. Thus, dormant precursors are exploitable to refine the elderly brain networks. To this end, our preliminary work suggest which mechanisms may accelerate or delay the maturation, allowing to decipher the impacts of dormant precursors on cognition, aging, and age-related pathology.

Acknowledgements
This project was possible thanks to the generous support of the Paracelsus Medical University, Salzburg, PMU-RIF: 2021-SEED-003-Benedetti

PARACELSUS MEDIZINISCHE PRIVATUNIVERSITÄT

Klikum Nürnberg
wir sind für Sie da!

Risk stratification of SARS-CoV-2 breakthrough infections based upon an outbreak at a students' festive event

Ralph Bertram[1*], Vanessa Bartsch[2], Johanna Sodmann[2], Luca Hennig[2], Engin Müjde[2], Jonathan Stock[2], Vivienne Ruedig[2], Philipp Sodmann[3], Daniel Todt[4,5], Eike Steinmann[4], Wolfgang Hitzl[6,7,8] and Joerg Steinmann[1]

[1] Institute of Clinical Hygiene, Medical Microbiology and Infectiology, Klinikum Nürnberg, [2] Paracelsus Medical University, study program in human medicine, Nuremberg, [3] Department of Internal Medicine II, University Hospital Würzburg, [4] Department of Molecular and Medical Virology, Ruhr-Universität Bochum, Bochum, [5] European Virus Bioinformatics Center (EVBC), Jena, [6] Department of Research and Innovation Management, biostatistics and publication of clinical trial studies, Paracelsus Medical University, Salzburg, [7] Paracelsus Medical University Salzburg, Department of Ophthalmology and Optometry, Salzburg, [8] Research Program Experimental Ophthalmology and Glaucoma Research, Paracelsus Medical University Salzburg

* Correspondence: ralph.bertram@klinikum-nuernberg.de , Tel.: +49 911 398 119131

The outbreak setting

Main room (Fig. 1) ~85 m², ~250 m³ of airspace. Arithmetic mean of the area per person: 0.85 m², personal radius of 0.52 m. Duration of the party: ~8h Poor ventilation, no masks, no social distancing.

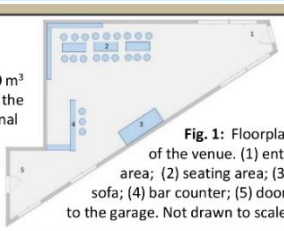

Fig. 1: Floorplan of the venue. (1) entry area; (2) seating area; (3) sofa; (4) bar counter; (5) door to the garage. Not drawn to scale.

Data of infected individuals

Individual*	Vax status#	Time since last vax (d)	Total nr. of contacts	Time at the party (min)	Contact to put. index	Day of 1st positive test	Rapid antigen test	PCR (CT)	Nr. of symptoms
1-2*	2xBNT	178	12	270	n/a	+1	pos	pos (24)	7
1-6	2xBNT	136	12	315	++	+4	pos	pos (29)	3
1-8	2xBNT	192	11	255	++	+5	neg	pos (32)	7
1-9	2xBNT	268	18	330	++	+2	pos	neg (36)	3
1-10	2xBNT	112	18	450	++	+5	-	pos (19)	1
1-11	2xBNT	154	33	360	++	+6	neg	pos (32)	7
1-12	1xJNJ	157	19	330	++	+6	neg	pos (32)	0
1-13	2xMOD	143	16	360	++	+5	neg	pos (27)	2
2-4	AZD+ 2xBNT	99	7	330	-	+4	pos	pos (20)	6
2-5	AZD+BNT	141	19	285	+	+6	neg	pos (30)	8
2-10	none	-	4	360	++	+6	neg	pos (24)	4
2-16	AZD+BNT	136	23	300	++	+4	pos	pos (24)	4
2-17	AZD+BNT	142	50	300	++	+4	pos	pos (20)	6
2-24	2xAZD	156	52	360	++	+3	pos	pos (18)	5
2-27	AZD+BNT	141	19	360	++	+5	neg	pos (unknown)	6
3-2	AZD+BNT	136	26	345	-	+5	-	pos (17)	7
3-11	2xAZD	165	20	330	-	+6	pos	pos (21)	3
3-22	AZD+BNT	157	38	510	-	+7	neg	pos (30)	0
3-26	AZD+BNT	127	16	210	-	+5	neg	pos (25)	5
3-27	AZD+BNT	141	11	240	-	+6	neg	pos (34)	6
3-28	AZD+BNT	141	8	240	-	+6	pos	pos (24)	2
3-30	AZD+BNT	141	33	435	-	+5	pos	-	5
3-33	AZD+BNT	141	28	390	-	+6	neg	pos (unknown)	7
3-34	AZD+BNT	148	25	450	-	+6	neg	pos (32)	5

*putative index person; #AZD, AstraZeneca; BNT, BioNTech/Pfizer; JNJ, Johnson&Johnson; MOD, Moderna; ++: closer than 1.5m and > 10 min; +: conversation shorter and/or more distant; -: no direct contact

Synopsis

A festive event in October 2021 in Northern Bavaria resulted in a SARS-CoV-2 delta outbreak. Interrogation and correlation analysis of a comprehensive set of data permitted to stratify risk factors for infection. Significant correlations to increased risk: Duration at the event, contact to putative index person and homologous vaccination scheme.

Demographic data

- 100 guests, 95 participants in the retrospective study
- 18-30 years of age, 53 males, 42 females
- 4 recovered from COVID-19 prior to the party
- 90 persons vaccinated with 1-3 jabs
- 24 persons positive after the event (all delta, B1.617.2)

Contact tracing

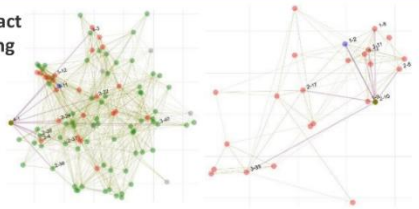

Fig. 2: Interactions between guests closer than 1.5 m and >10 min are shown. Individuals infected after the event are marked in red. Blue: putative index. **Left**: all contacts, **right**: only positive persons

Correlation analysis and risk stratification

- Duration of stay (Fig. 3). No one that stayed ≤ 210 min was positive.
- Conversation with the supposed index person. Risk of infection 36% vs. 17% w/o conversation
- Lower risk of infection w/ AZD + BNT (23%) vax vs. AZD + AZD (60%).

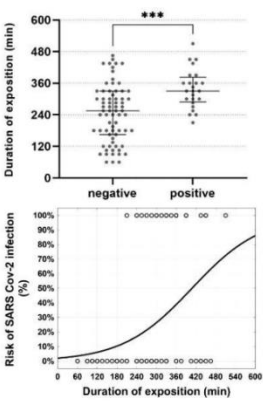

Fig. 3: Above: Scatter dot plot, **below**: Calculated risk of infection

We thank our collaborators of the study. Conflict of interest/Funding: none. For complete publication, please see doi.org/10.3390/vaccines10030432

Risk Stratification of SARS-CoV-2 Breakthrough Infections Based on an Outbreak at a Student Festive Event

Ralph Bertram[1], Vanessa Bartsch[2], Johanna Sodmann[2], Luca Hennig[2], Engin Müjde[2], Jonathan Stock[2], Vivienne Ruedig[2], Philipp Sodmann[3], Daniel Todt[4, 5], Eike Steinmann[4], Wolfgang Hitzl[6, 7, 8], Joerg Steinmann[1]

[1]Institute of Clinical Hygiene, Medical Microbiology and Infectiology, Klinikum Nürnberg, Paracelsus Medical University, Nuremberg; [2]Study Program in Human Medicine, Paracelsus Medical University, Nuremberg; [3]Department of Internal Medicine II, University Hospital Würzburg; [4]Department of Molecular and Medical Virology, Ruhr-Universität Bochum; [5]European Virus Bioinformatics Center (EVBC), Jena; [6]Department of Research and Innovation Management, Biostatistics and Publication of Clinical Trial Studies, Paracelsus Medical University, Salzburg; [7]Department of Ophthalmology and Optometry, Paracelsus Medical University, Salzburg; [8]Research Program Experimental Ophthalmology and Glaucoma Research, Paracelsus Medical University, Salzburg; Contact: ralph.bertram@klinikum-nuernberg.de

Objective
In early 2022, the Coronavirus disease 2019 (COVID-19) remains a global challenge. COVID-19 is caused by an increasing number of variants of the Severe Acute Respiratory Syndrome Coronavirus 2 (SARS-CoV-2). Here, we report an outbreak of SARS-CoV-2 breakthrough infections related to a student festive event with 100 mostly vaccinated guests, which took place in Northern Bavaria, Germany, in October 2021. Based upon a comprehensive set of data, we delineated ans stratified risk factors for infection.

Methods
We conducted standardized telephone interviews with participants of the festive event who had given written consent. Data were collected in pseudonymized form, with individuals arbitrarily assigned unique numbers as identifiers. The data were compiled in Excel and checked for consistency. Crosstabulation tables were analyzed using Pearson's Chi-Square test, Fisher's Exact test, and the Kruskal–Wallis test for singly ordered tables. The Mann–Whitney U test and Bootstrap t-tests were used to test continuously distributed variables. Logistic regression analysis was applied to test and illustrate the effect of various risk factors on the risk of infection. All reported tests were two-sided, and p-values below 0.05 were considered statistically significant. All statistical analyses in this report were performed with STATISTICA 13, PASW 24, or GraphPad Prism 9.3.1.

Results
95 students participated in the study, with 94 being fully vaccinated and 24 reporting infection by the delta variant. Correlation analyses among 15 examined variables revealed that time spent at the event, conversation with the supposed index person, and a homologous viral vector vaccination regime were significant risk factors for infection. Non-significant observations related to higher rates of infection included time since last vaccination, shared use of drinking vessels, and number of individual person-to-person contacts at the event.

Conclusions
Our data suggest that a high rate of breakthrough infections with the delta variant occurs if no preventive measures are practiced. To limit infection risk, high-quality testing of participants should be considered a mandatory measure at gatherings, irrespective of the participants' vaccination status.

Understanding the role of platelets in Alzheimer's disease

Diana M Bessa de Sousa[1,2], Michael Unger[1,2], Heike Mrowetz[1,2], Barbara Altendorfer[1,2], Arianne Benedetti[2,3], Rodolphe Poupardin[2,4], Thomas Fröhlich[5], Ludwig Aigner[1,2,6], Kathrin Kniewallner[1,2]

1: Institute of Molecular Regenerative Medicine, Paracelsus Medical University, Salzburg, Austria. 2: Spinal Cord Injury and Tissue Regeneration Center Salzburg (SCI-TReCS), Paracelsus Medical University, Salzburg, Austria. 3: Institute of Experimental Regeneration, Paracelsus Medical University, Salzburg, Austria. 4: Cell Therapy Institute, Paracelsus Medical University, Salzburg, Austria. 5: Laboratory of Functional Genome Analysis (LAFUGA), Gene Center, Ludwig Maximilian University of Munich, Germany. 6: Austrian Cluster for Tissue Regeneration, Vienna, Austria.

Contact: diana.bessa@pmu.ac.at

Introduction

In Alzheimer's disease (AD) platelets become dysfunctional contributing to vascular injury and neuroinflammation.

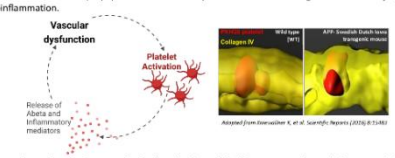

Adapted from Ewerlöv K, et al. Scientific Reports (2019); 8:15481

However, the molecular changes of platelets in AD and their impact on the pathology remain largely unexplored. Under the hypothesis, that platelets in AD are activated, have an aggressive phenotype and actively contribute to disease pathogenesis, we aim to better understand the role of platelets in AD using a transgenic AD mouse model (i.e., APP Swedish PS1 dE9, APP-PS1). (Created with BioRender.com)

Experimental setup

A. Molecular and cellular characterization of APP-PS1 mouse platelets

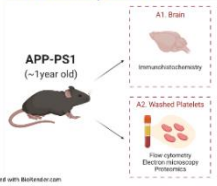

B. Immune-mediated platelet depletion in APP-PS1 mice

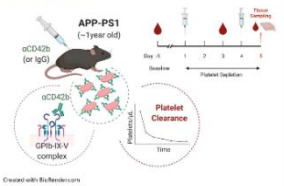

A1. Platelets in APP-PS1 mice are activated and invade the brain[1]

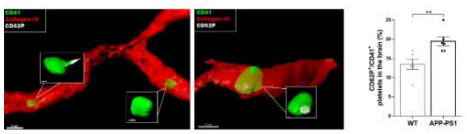

Figure 1. Immunohistochemical analysis of platelet activation status in APP-PS1 mice. An increased percentage of CD41+ platelets (green) expressing the activation marker CD62P (white) circulated within cerebral blood vessels (red) in APP-PS1 compared to age-matched WT. Statistical analysis: unpaired Student's t test (**p < 0.01; n=6/genotype). Scale: 5 µm and 1 µm (zoom in).

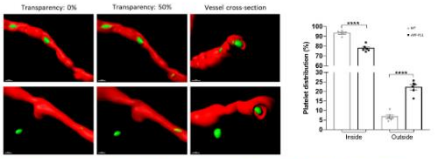

Figure 2. Immunohistochemical analysis of platelet distribution in the brain of APP-PS1 mice. CD41+ platelets were mainly located within the cerebral blood vessels (counted as inside); but in APP-PS1 mice, platelets were frequently seen in the brain parenchyma or at the blood vessel wall, suggesting extravasation (counted as outside, arrows). Statistical analysis was performed by two-way ANOVA with Tukey's multiple comparison test (****p < 0.0001; n=6/genotype). Scale: 3 µm.

A2. Characterization of peripheral blood platelets

Figure 3. Activation status and ultrastructure analysis of peripheral blood platelets in APP-PS1 mice.[1] The percentage of activated platelets (CD62P+/CD41+) was not significantly different between APP-PS1 and WT mice. However, APP-PS1 platelets showed morphological features of activation: membrane protrusions (arrows), microparticle (MP,*) formation, and a 30% smaller area. Statistical analysis: unpaired Student's t test (n=7/genotype). Scale: 250nm.

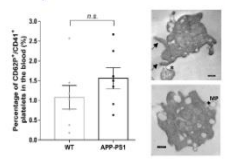

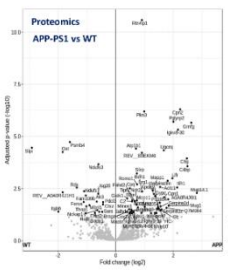

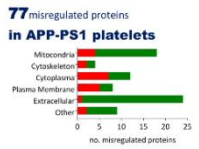

Figure 4. Proteomic analysis of peripheral blood platelets in APP-PS1 mice. Volcano plot of significantly differentially expressed proteins and their respective fold changes (n=3/genotype). GO term analysis of dysregulated proteins related to their cellular components in APP-PS1 mouse platelets (**red:** downregulation; **green:** upregulation).

B1. Immune-mediated platelet depletion in APP-PS1 mice

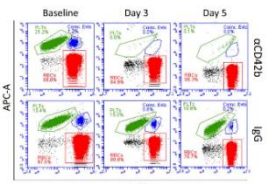

Figure 5. Anti-CD42b antibody intraperitoneal injections induced platelet depletion with up to 99% efficacy. Platelet counts were monitored by flow cytometry. (n=9-10 mice/group; antibody dose: 2µg/g of body weight). Statistics: mixed effects model analysis with Sidak's multiple comparisons test (****p < 0.0001; n=9-11/group).

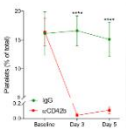

B2. Platelet depletion shifts amyloid plaque size distribution in APP-PS1 females

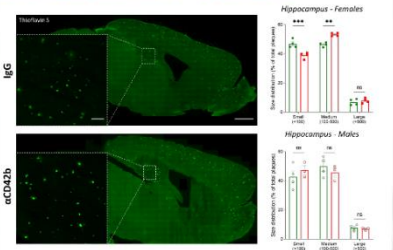

Figure 6. Immunohistochemical analysis of amyloid plaque load. Platelet depleted and control mice showed similar hippocampal and cortical amyloid plaque loads (n=9-10 animals/group). The proportion of small (30-100 µm²) and medium (100-500 µm²) plaques in the hippocampus of platelet depleted females differed from control animals. Statistical analysis was performed by two-way ANOVA with Tukey's multiple comparison test (*p < 0.05; **p<0.01; n=4-5/group). Scale: 250 µm.

B3. Platelet depletion increases neuritic dystrophy in APP-PS1 females

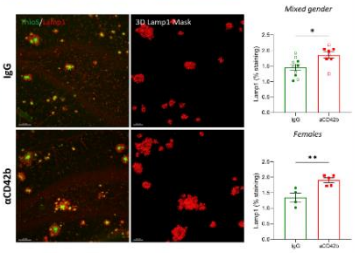

Figure 7. Immunohistochemical analysis of neuritic dystrophy around amyloid plaques. Upon platelet depletion, female APP-PS1 mice showed increased volume of Lamp1+ clusters around amyloid plaques in the hippocampus. Statistics: Mann-Whitney test (*p<0.05; n=8-10/treatment; 3-6/gender). Scale: 80µm merged image; 50µm 3D mask.

B4. Platelet depletion impairs microglia phagocytosis in APP-PS1 females

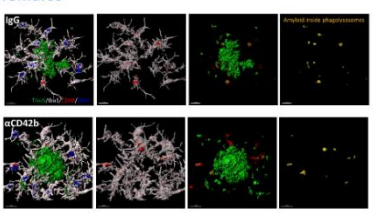

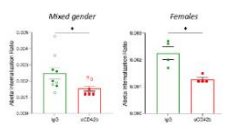

Figure 8. 3D in silico modelling of amyloid beta phagocytosis by microglia. Upon platelet depletion, microglia of APP-PS1 females showed reduced levels of amyloid beta uptake. Statistical analysis: Mann-Whitney test or unpaired Student's t test (*p < 0.05; n= 7-9/group). Scale: 10 µm.

B5. Platelet depletion affects amyloid plaque coverage by astrocytic processes

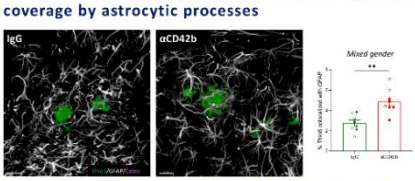

Figure 9. Immunohistochemical analysis of fibrillary amyloid plaque coverage by astrocytes. Platelet-depleted mice showed higher coverage of Thioflavin S+ (ThioS) amyloid plaques by astrocytic processes in the hippocampus. Statistical analysis: unpaired Student's t test (**p < 0.01; n= 8/group). Scale: 20µm.

Acknowledgments: The authors thank the microscopy core facility of SCI-TReCS (Spinal Cord Injury and Tissue Regeneration Center Salzburg). This study was supported by the Austrian Science Funds (P24734-B24), the PMU Rise Project (PMU-FFF) (R17/04/097-KNI) and the PMU postgraduate students support program DISCITE! (D-19/01/008-BES).

[1] Kniewallner KM, et al. Front Neurosci. 2020; 14:129 doi:10.3389/fnins.2020.00129

Understanding the role of platelets in Alzheimer's disease

Diana Marisa Bessa de Sousa[1,2], Michael Stephan Unger[1,2], Heike Mrowetz[1,2], Barbara Altendorfer[1,2], Ariane Benedetti[2,3], Rodolphe Poupardin[2,4], Thomas Fröhlich[5], Ludwig Aigner[1,2,6]

[1]Institute of Molecular Regenerative Medicine, Paracelsus Medical University, Salzburg, Austria; [2]Spinal Cord Injury and Tissue Regeneration Center Salzburg (SCI-TReCS), Paracelsus Medical University, Salzburg, Austria; [3]Institute of Experimental Regeneration, Paracelsus Medical University, Salzburg, Austria; [4]Cell Therapy Institute, Paracelsus Medical University, Salzburg, Austria; [5]Laboratory of Functional Genome Analysis (LAFUGA), Gene Center, Ludwig Maximilian University of Munich, Germany; [6]Austrian Cluster for Tissue Regeneration, Vienna, Austria; Contact: diana.bessa@pmu.ac.at

Objective
In Alzheimer's disease (AD), platelets become dysfunctional. However, it remains unclear whether platelet dysfunction in AD is a consequence of the ongoing pathological events or a driver of the disease. To investigate platelets' contribution to AD pathology, we used an AD transgenic mouse model (i.e. APP Swedish PS1 dE9, APP-PS1) for cellular and molecular characterization of platelets and immune-mediated platelet depletion.

Methods
We assessed the activation status (CD62P expression), ultrastructure and the proteome of blood isolated platelets in 14 months old APP-PS1 mice and wild type (WT) age-matched controls. Further, we induced short-term immune-mediated platelet depletion in APP-PS1 mice (12-13 months old) by intraperitoneal injections of an anti-CD42b antibody. Injection of non-immune rat immunoglobulins (IgG) served as control.

Results
APP-PS1 mice showed significantly higher percentages of activated platelets in the brain but only a slight, non-significant, higher platelet activation in the bloodstream. Nevertheless, preliminary proteomics data revealed 77 differentially expressed proteins in APP-PS1 blood isolated platelets compared to WT mice. Interestingly, in the APP-PS1 mouse brain, about 20% of the platelets were located extravascularly. Anti-CD42b antibody injections successfully induced thrombocytopenia (>99%) in APP-PS1 mice for five days. Platelet depleted APP-PS1 females showed significant shifts in amyloid plaque size distribution, presenting fewer small plaques (30-100 µm2) and more medium size plaques (100-500 µm2) compared with IgG treated females. Changes in amyloid plaque size were accompanied by an increase in neuritic dystrophy, reduction of microglial phagocytosis and an increase in the number of plaque-associated microglia cells in APP-PS1 females.

Conclusions
Platelets might present an altered cellular and molecular profile in AD, with implications for cerebral processes such as neuroinflammation. Even though the mechanisms underlying platelets' influence on the brain remain unknown, these findings provide a base for future developments.

Acknowledgements
This study was supported by the Austrian Science Funds (P24734-B24), the PMU Rise Project (PMU-FFF) (R17/04/097-KNI) and the PMU postgraduate students support program DISCITE! (D-19/01/008-BES).

Batch Effects during Human Bone Marrow Stromal Cell Propagation Prevail Donor Variation and Culture Duration: Impact on Genotype, Phenotype and Function

Brachtl G[1*], Poupardin R[1*], Hochmann S[1], Raninger A[1], Jürchott K[2], Streitz M[2,3], Schlickeiser S[2], Oeller M[4], Wolf M[1], Schallmoser K[4], Volk HD[2,5,6], Geissler S[2,5], Strunk D[1]

rodolphe.poupardin@pmu.ac.at * Equal contribution

[1] Experimental and Clinical Cell Therapy Institute, Spinal Cord Injury and Tissue Regeneration Center Salzburg (SCI-TReCS), Paracelsus Medical University, Salzburg, Austria
[2] Center for Regenerative Therapies (BCRT), Berlin Institute of Health (BIH) at Charité - Universitätsmedizin Berlin, Berlin, Germany
[3] Friedrich-Loeffler-Institut, Federal Research Institute for Animal Health, Greifswald, Insel Riems, Germany
[4] Department of Transfusion Medicine and SCI-TReCS, PMU, 5020 Salzburg, Austria
[5] Berlin Center for Advanced Therapies (BeCAT), Charité Universitätsmedizin Berlin, Berlin, Germany
[6] Institut für Medizinische Immunologie, Charité - Universitätsmedizin, Berlin, Germany

BACKGROUND

The culture of mesenchymal stromal cells (MSCs) relies mainly on the use of human platelet lysate (**hPL**) or foetal bovine serum (**FBS**) media. However, as a xenogeneic product, FBS may induce unwanted immunologic reactions or potentially transmit prions or viruses. Moreover, the use of bovine foetuses for FBS production raises serious ethical and animal welfare concerns. HPL has been introduced as an attractive alternative for replacing FBS as a cell culture supplement [1-4]. Several studies have demonstrated that proliferation and cellular morphology may be differently affected by these supplements in addition to donor variability and culture duration. FBS batch effects can also result in selection of different cell types in therapeutic placental cell bulk cultures.

In this context, we wanted to investigate the impact of FBS vs. HPL-supplemented culture medium, culture duration and donor variability at the transcriptome and epigenome levels.

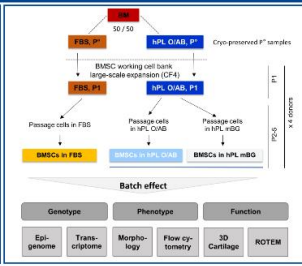

METHODS

Here we tested the influence of hPL vs. FBS on BMSC transcriptome & epigenome, cell surface proteomics and function (Figure 1).

Bone-Marrow derived mesenchymal stromal cells (BM-MSCs) were generated from BM samples in media supplemented either with FBS or pHPL (pooled human platelet lysate) O/AB and further expanded in cell factories (CF4) (group 1: FBS p1, group 3: pHPL 0/AB, p1). Cells were further cultured until passage 4 or 5 in media containing FBS (group 2: FBS p4/p5), or cells from pHPL 0/AB in media containing pHPL 0/AB (group 4: pHPL 0/AB p4/p5) or in media containing pHPL mBG (group 5: pHPL mBG p4/p5).

Organoid-like cartilage disk formation was tested as a surrogate for osteo-chondral regenerative competence. The procoagulant activity of short vs. long-term cultured BMSCs, under the aegis of FBS vs. two types of hPL, respectively, was analyzed in addition by ROTEM as a marker of cell therapy hemocompatibility.

← **Figure 1. Experimental approach**

RESULTS

Genotype — Culture conditions prevail donor variation & culture duration effect

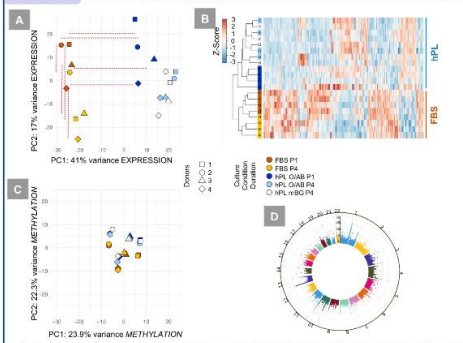

↑ **Figure 2 Batch effects on culture-expanded BMSC transcriptomics ((A) + (B)) and methylomics ((C) + (D)): (A) Principal component analysis (PCA)** showing the spatial clustering of the different samples (FBS, ocher shades; hPL, blue shades; P1, darker color; P4, lighter colors; hPL mBG open symbols) and different donors (symbols as indicated; color code and symbol legend for a–c). The culture conditions (hPL-vs. FBS-supplemented) explained most of the variance in the dataset (PC1, 41%). Horizontal red dotted lines highlight the distance of samples from the same donor cultured with FBS (left) vs. hPL (right). PC2 separated samples due to culture duration and donor variation. Vertical dotted lines highlight distance between P1 and P4, regardless of donor variation. **(B) Heatmap with expression values of top 100 most variable genes.** Samples in rows as indicated and genes in columns; different batch-defining serum supplements and passages in the general color code. Gene expression values were column Z-score normalized; lower expression blue and higher expression red color as shown in the legend. **(C) PCA of differentially methylated regions** with PC1 covering 23.9% and PC2 22.3% of differences. Color and symbol code as indicated. **(D) Differentially methylated regions were depicted as dots on the Manhattan plot** for all autosomal chromosomes. The dot height corresponds to the level of significance with higher dots indicating higher significance, i.e., lower *p*-value (-Log10 adjusted *p*-values).

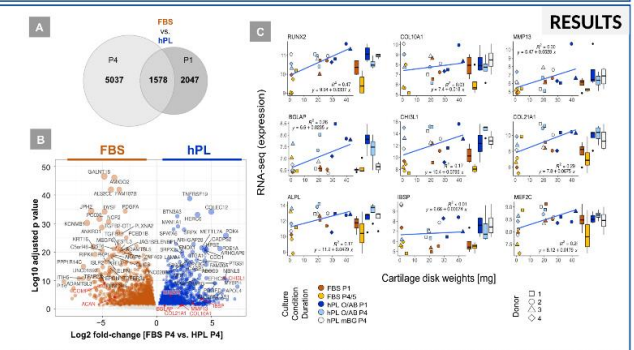

↑ **Figure 3 (A) Venn diagram showing the number of differentially expressed genes** in cells obtained by hPL- vs. FBS-driven culture for P4 and hPL vs. FBS for P1 (adjusted *p*-value < 0.05). **(B) Volcano plot showing most significantly expressed genes in FBS- (left) and hPL-driven cultures (right)**. Red dots marking genes significantly differentially expressed (adjusted *p*-value < 0.05); black dots, not significant. Most significantly differentially expressed genes indicated by gene ID. Red IDs show the key chondrogenic markers differentially expressed. **(C) Correlation analysis between RNA-seq gene expression and cartilage disk weight for selected genes linked to chondrogenesis.** For each gene, a dual plot shows, on the left side, the correlation analysis between RNA-seq expression on the *Y*-axis and cartilage disk weights on the *X*-axis, and on the right side, box plots depicting the RNA-seq signal in the different culture condition. Different donors are depicted by different symbols and culture conditions by different colors, as indicated. A blue linear-regression line is shown together with the regression equation and R2 value.

Morphology — Distinct immune-related phenotypic changes

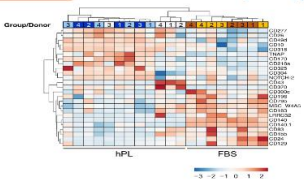

↑ **Figure 4. Hierarchical clustering heatmap of cell surface markers** that exhibited significant median differences of at least 10% between BMSCs in hPL O/AB and FBS.

We identified numerous **immunity-related marker molecules** to be differentially expressed by hPL O/AB- vs. FBS-expanded BMSCs further supporting the hypothesis that batch effects precipitate culture-related gene expression trajectories

Function — BMSCs cultured in hPL show a stronger chondrogenic potential

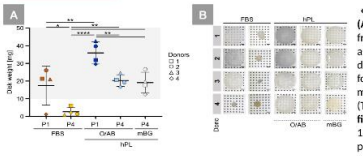

← **Figure 5. Organoid-like 3D cartilage disk formation. (A) Weight of 3D cartilage disks** generated in triplicates from BMSCs of four donors (1–4, depicted with symbols as indicated), pre-expanded in different media, and differentiated after P1 or P4 as indicated. Proper disk formation resulted in disks > 10 mg (grey area). Repeated measures, one-way ANOVA with multiple comparisons (Tukey). **(B) Representative pictures of corresponding fixated 3D cartilage disks created from BMSCs** of donors 1–4 after hPL- or FBS-expanded early (P1) and late passage (P4) cultures as indicated. Scale bar 1 mm; *n* = 4.

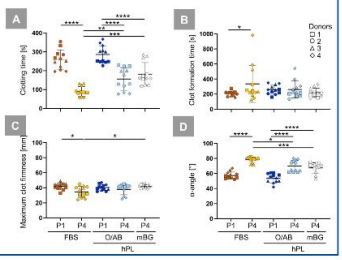

Figure 6. Coagulation activity of early (P1) and late passage (P4) BMSCs. (A) Significantly shortened clotting time values after 4 passages in FBS, more than hPL O/AB and hPL mBG, compared to passage 1, respectively. Repeated measures, one-way ANOVA with multiple comparisons (Tukey). **(B) The clot formation time and (C) maximum clot firmness showing limited donor dependent differences.** Clot formation time: Friedman test with multiple comparisons (Dunn); maximum clot firmness ANOVA as in (a). **(S) Significantly increased α-angles resulting from higher procoagulant activity of all late (P4) BMSCs, compared to early (P1) BMSCs**; statistics as in (b). Results of 4 donors analyzed in triplicate, symbols as indicated;

This work is published:

Brachtl G, Poupardin R, et al. Batch Effects during Human Bone Marrow Stromal Cell Propagation Prevail Donor Variation and Culture Duration: Impact on Genotype, Phenotype and Function. Cells. **2022**; 11(6):946. https://doi.org/10.3390/cells11060946

SUMMARY & OUTLOOK:

In the course of this study, we observed an unexpectedly distinctive serum-related batch effect resulting in pronounced differences in gene expression and phenotype as well as corresponding differences in BMSC chondrogenic function. We showed that hPL provides a better environment for BMSCs regarding cartilage formation. The distinct immune-related phenotypic changes may help to select most potent manufacturing conditions for immunomodulatory stromal cells. Marker profiling as indicated in this study and corresponding functional assays will allow the development of predictive potency assays for cell-based therapeutics. Finally, hPL mBG and hPL O/AB showed little differences regarding gene expression and function.

Batch Effects during Human Bone Marrow Stromal Cell Propagation Prevail Donor Variation and Culture Duration: Impact on Genotype, Phenotype and Function

Gabriele Brachtl[1], Rodolphe Poupardin[1], Sarah Hochmann[1], Anna Raninger[1], Karsten Jürchott[2], Mathias Streitz[2,3], Stephan Schlickeiser[2], Michaela Oeller[4], Martin Wolf[1], Katharina Schallmoser[4], Hans-Dieter Volk[2,5,6], Sven Geissler[2,5], Dirk Strunk[1]

[1]Spinal Cord Injury and Tissue Regeneration Center Salzburg (SCI-TReCS), Cell Therapy Institute, Paracelsus Medical University (PMU), 5020 Salzburg, Austria; [2]Center for Regenerative Therapies (BCRT), Berlin Institute of Health (BIH) at Charité–Universitätsmedizin Berlin, Berlin, Germany; [3]Friedrich-Loeffler-Institut, Federal Research Institute for Animal Health, Greifswald, Insel Riems, Germany; [4]Department of Transfusion Medicine and SCI-TReCS, PMU, 5020 Salzburg, Austria; [5]Berlin Center for Advanced Therapies (BeCAT), Charité Universitätsmedizin Berlin, Berlin, Germany; [6]Institute of Medical Immunology, Charité Universitätsmedizin Berlin, Berlin, Germany; Contact: rodolphe.poupardin@pmu.ac.at

Objective
Donor variation is a prominent critical issue limiting the applicability of cell-based therapies. We hypothesized that batch effects during propagation of bone marrow stromal cells (BMSCs) in human platelet lysate (hPL), replacing fetal bovine serum (FBS), can affect phenotypic and functional variability.

Methods
We therefore investigated the impact of donor variation, hPL- vs. FBS-driven propagation and exhaustive proliferation, on BMSC epigenome, transcriptome, phenotype, coagulation risk and osteochondral regenerative function.

Results
Notably, propagation in hPL significantly increased BMSC proliferation, created significantly different gene expression trajectories and distinct surface marker signatures, already after just one passage. We confirmed significantly declining proliferative potential in FBS-expanded BMSC after proliferative challenge. Flow cytometry verified the canonical fibroblastic phenotype in culture-expanded BMSCs. We observed limited effects on DNA methylation, preferentially in FBS-driven cultures, irrespective of culture duration. The clotting risk increased over culture time. Moreover, expansion in xenogenic serum resulted in significant loss of function during 3D cartilage disk formation and significantly increased clotting risk. Superior chondrogenic function under hPL-conditions was maintained over culture. The platelet blood group and isoagglutinins had minor impact on BMSC function.

Conclusions
These data demonstrate pronounced batch effects on BMSC transcriptome, phenotype and function due to serum factors, partly outcompeting donor variation after just one culture passage.

Cellular localization of the cysteinyl leukotriene system in the human, rat and mouse eye

Susanne M. Brunner, Andreas Koller, Julia Preishuber-Pflügl, Anja-Maria Ladek, Herbert A. Reitsamer & Andrea Trost.

Research Program for Experimental Ophthalmology, Department of Ophthalmology and Optometry, University Hospital of the Paracelsus Medical University

Objective

The cysteinyl leukotriene (CysLT) system assumes important functions in the regulation of inflammation and cellular stress. Blocking the CysLT receptors (CysLTRs) with specific antagonists is associated with a reduced development of retinopathies (e.g. diabetic retinopathy, wet AMD). However, the exact cellular localization of the CysLTRs and their ligands in the eye has not yet been clearly elucidated. It is also not known whether the expression patterns differ between humans, rats and mice.

Methods

Untreated Sprague Dawley rats (n=5, 8-13 weeks) and CD1 mice (n=8, 8 weeks) were euthanized and the eyes enucleated. Human eyes (n=5, 61.8±14 years) were provided by the corneal bank of the University Clinic for Ophthalmology, Salzburg. The eyes were fixed in 4% PFA. Cryosections (12 µm) were fluorescence-labeled with specific antibodies against CysLTR1 and CysLTR2. Expression patterns were evaluated using a confocal fluorescence microscope (LSM710, Zeiss).

Results

In rats and mice, CysLTR1-immunoreactivity (IR) was predominantly observed in the photoreceptor outer segments (OS), the outer plexiform layer (OPL) and in single cells of the inner nuclear layer (INL; Fig. 1A, E). Weak CysLTR1-IR was detected in cells of the ganglion cell layer (GCL; Fig. 1A, E), the retinal pigment epithelium (RPE; Fig. 1B, F) and in retinal vessels (Fig. 1C, G). In the human retina, CysLTR1-IR was absent in the OPL (Fig.1I) but cells of the outer nuclear layer (ONL) and INL revealed CysLTR1-IR (Fig. 1I). Like in rodents, we detected CysLTR1-IR in human photoreceptor OS, cells of the GCL (Fig. 1J) and retinal vessels (Fig. 1K).

Expression of CysLTR2 was very similar across all species (Fig. 2). Strong CysLTR2-IR was observed in the inner plexiform layer (IPL), the OPL and in single cells of the INL and GCL (Fig. 2A, D, G). The RPE revealed weak CysLTR2-IR (Fig. 2B, E). Vessels were absent for CysLTR2-IR (Fig. 2C, F, I). In the human retina, cone OS revealed CysLTR2-IR (Fig. 2G); in rats, photoreceptor inner segments (IS) showed weak CysLTR2-IR (Fig. 2B) and in mice, weak CysLTR2-IR was detected in photoreceptor OS (Fig. 2E).

Conclusions

The elucidation of the cellular localization of the CysLT system in the eye supports conclusions about the functions of the system. As CysLTR1 and CysLTR2 are distinctly expressed in the human and rodent retina, it can be assumed that both receptors exhibit different functions in this ocular tissue. In the current study, other sections of the eye are being examined in addition to the retina.

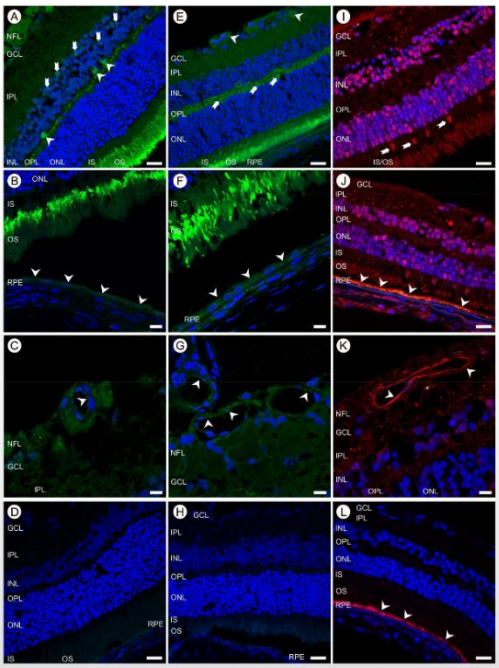

Figure 1. CysLTR1 in the rat (A-D), mouse (E-H) and human (I-L) retina. CysLTR1-IR is visualized in green in rodents (A-H) and in red in humans (I-L). Corresponding negative controls of retinal cross-sections (D, H, L). NFL=nerve fibre layer; GCL=ganglion cell layer; IPL=inner plexiform layer; INL=inner nuclear nlayer; OPL=outer plexiform layer; IS=photoreceptor inner segments; OS=photoreceptor outer segments; RPE=retinal pigment epithelium;

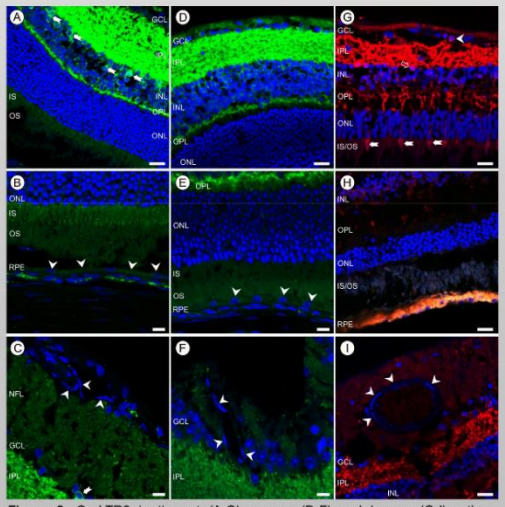

Figure 2. CysLTR2 in the rat (A-C), mouse (D-F) and human (G-I) retina. CysLTR2-IR is visualized in green in rodents (A-F) and in red in humans (G-I).

Cellular localization of the cysteinyl leukotriene system in the human, rat and mouse eye

Susanne M. Brunner[1], Andreas Koller[1], Julia Preishuber-Pflügl[1], Anja-Maria Ladek[1], Herbert A. Reitsamer[1], Andrea Trost[1]

[1]Research Program for Experimental Ophthalmology, Department of Ophthalmology and Optometry, University Hospital of the Paracelsus Medical University, Salzburg, Austria; Contact: su.brunner@salk.at

Objective
The cysteinyl leukotriene (CysLT) system assumes important functions in the regulation of inflammation and cellular stress. Blocking the CysLT receptors (CysLTRs) with specific antagonists is associated with a reduced development of retinopathies (e.g. diabetic retinopathy, wet AMD). However, the exact cellular localization of the CysLTRs and their ligands in the eye has not yet been clearly elucidated. It is also not known whether the expression patterns differ between humans, rats and mice.

Methods
Untreated Sprague Dawley rats (n=5, 8-13 weeks, 3 males/2 females) and CD1 mice (n=8, 8 weeks, 4 males/4 females) were euthanized and the eyes enucleated. Human eyes (n=5, 61.8±14 years, 4 males/1 female) were provided by the corneal bank of the University Clinic for Ophthalmology, Salzburg. The eyes were fixed in 4% paraformaldehyde. Cryosections (12 µm) were labeled by immunofluorescence with specific antibodies against CysLTR1 and CysLTR2. Expression patterns were evaluated using a confocal fluorescence microscope (LSM710, Zeiss).

Results
In the retina, expression patterns of CysLTR1 and CysLTR2 are very distinct.
In rats and mice, CysLTR1-immunoreactivity (IR) was predominantly observed in the photoreceptor outer segments (OS), the outer plexiform layer (OPL) and in single cells of the inner nuclear layer (INL). Weak CysLTR1-IR was detected in cells of the ganglion cell layer (GCL), the retinal pigment epithelium (RPE) and in retinal vessels. In contrast, in the human retina, CysLTR1-IR was absent in the OPL but many cells of the outer nuclear layer (ONL) and INL revealed CysLTR1-IR. Like in rodents, photoreceptor OS, cells of the GCL and retinal vessels showed CysLTR1-IR.
Expression of CysLTR2 was very similar across all species. Strong CysLTR2-IR was observed in the inner plexiform layer (IPL), the OPL and in single cells of the INL and GCL. The RPE revealed weak CysLTR2-IR. Vessels were absent for CysLTR2-IR. In the human retina, cone OS revealed CysLTR2-IR; in rats, photoreceptor inner segments (IS) showed weak CysLTR2-IR and in mice, weak CysLTR2-IR was detected in photoreceptor OS.

Conclusions
The elucidation of the cellular localization of the CysLT system in the eye supports conclusions about the functions of the system. As CysLTR1 and CysLTR2 are distinctly expressed in the human and rodent retina, it can be assumed that both receptors exhibit different functions in this ocular tissue. In the current study, further sections of the eye are under examination in addition to the retina.

Towards a characterization of CD cell surface antigen expression in the human spinal cord

Sofia Capito[1*], Elizaveta Rogova[1*], Max Schäbinger[1*], Marco Birke[2], Nicole Schider[2], Jan Pruszak[2#]

[1] Paracelsus Medical University (PMU), Salzburg, Austria, * equal contribution

[2] Institute of Anatomy and Cell Biology, Paracelsus Medical University (PMU), Salzburg, Austria

correspondence: jan.pruszak@pmu.ac.at

Background & Objective

Recent single cell-based phenotypic analyses have yielded critical novel insights into cellular hierarchies and functional relationships in a variety of human tissues including the human brain. Comparably fewer cellular analyses have so far been conducted in the human spinal cord (**Fig. 1**). Surface molecules have commonly been used to identify distinct cell populations and play major roles in cellular interactions in immunology, tumor biology and infectious disease. A systematic profile of cluster-of-differentiation (CD) surface antigens might serve to further characterize functional network relationships and to refine the anatomical cartography of the spinal cord. **We aim to comprehensively characterize the expression pattern of a broad array of CD surface antigens in the human spinal cord.**

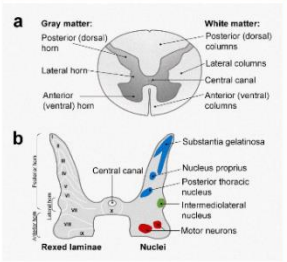

Figure 1 – Schematic representation of established spinal cord micro-anatomy. (**a**) Overview of gray vs. white matter. (**b**) Rexed laminae and nuclei commonly used to define gray matter subset regions [see Rexed B., *J Comp Neurol.* 1952].

Material & Methods

Immunofluorescence (IF) analysis was performed on 8 to 10 µm thick frozen human spinal cord specimens (cervical region; obtained from *Amsbio* [UK]). In brief, sections were air-dried (1h), fixed (2 min in 4% paraformaldehyde) followed by permeabilization/blocking (1h) in fish-gelatin solution containing 1% bovine serum albumin (BSA) and 0.1% Tween®20 in TBS. Primary antibodies at 1:50 dilution in 1% BSA/TBS were incubated overnight at 4°C. After washing, sections were incubated with the corresponding secondary antibodies [Invitrogen] for 7h at 4°C. Whole specimen IF images were taken using an Olympus VS120 slide scanner at 20x magnification.

Results

A select panel of >30 CD surface antigens has been analyzed to date. Besides some anticipated expression patterns, as e.g. for the integrin family member CD49b (**Fig. 2a**), other CD antigens showed specific and not previously described distribution. CD15 (Lewis-X, **Fig. 2b,g**) staining was exclusively discernable at the ependymal layer of the central canal, whereas the heat-stable antigen, CD24 (**Fig. 2c,h**), showed a pronounced expression around the central canal as well as in Rexed lamina II. CD90 (Thy-1, **Fig. 2d**) was predominantly expressed throughout the gray matter, yet sparing Rexed lamina X. In contrast, MIC2 or single-chain type-1 glycoprotein CD99 within the gray matter appeared to be confined to lamina X (**Fig. 2e**), whereas CD200 (OX-2, a glycoprotein involved in neuroprotection) was expressed in the entire gray matter including the region around the central canal (**Fig. 2f**).

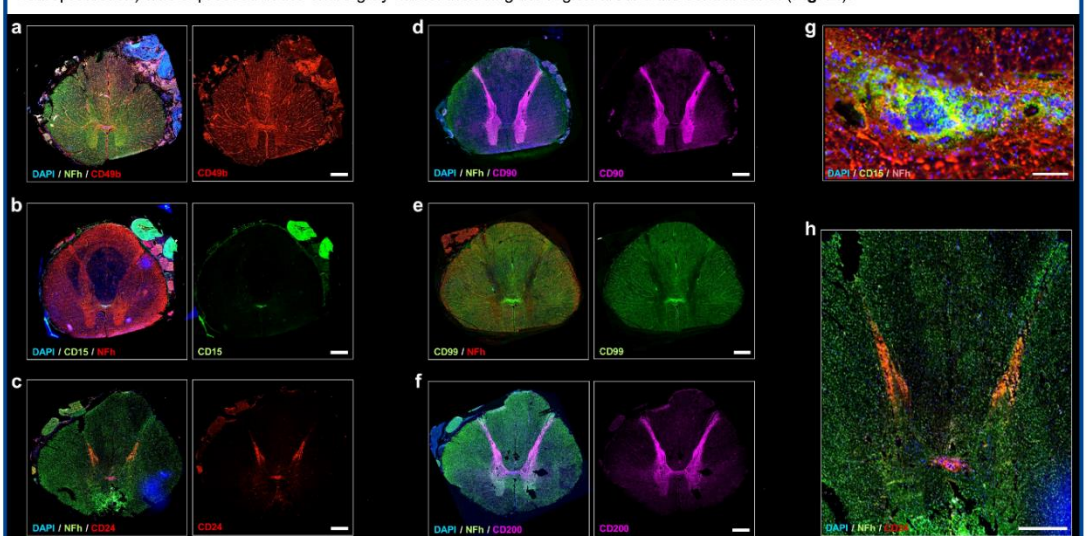

Figure 2 – Regionally confined expression of selected CD antigens in the human spinal cord. Tissue sections were subjected to IF analysis using the indicated antibodies (from *Fisher Scientific*). CD24 and CD49b (a+c+h) are shown in red, CD90 and CD200 (d+f) in magenta, and CD15 and CD99 (b+e+g) in green. Nuclear counterstaining was performed using DAPI (blue). Staining of neurofilament heavy chain (NFh, from *Merck*) served as an internal procedural control. (g,h) Enlarged panels show high magnification view of CD15 and CD24 patterns, respectively. Shown are representative stainings from duplicate spinal cord tissue sample sections. Scale Bars (a-f; h) ~1 mm; (g) 100 µm.

Acknowledgements

This project is supported by the PMU Research Fund (RISE 2020.0113). We thank Matthias Gatterbauer for technical support with image acquisition.

References

Rexed B., J Comp Neurol. 1952

Menon V. *et al.*, Sci Rep. 2019

Outlook

Prospectively, the ongoing expression screen for >200 CD antigens will elucidate the cellular cartography of the human spinal cord and may aid in identifying novel biomarkers for spinal cord pathophysiological processes and cellular therapeutics.

Towards a characterization of CD cell surface antigen expression in the human spinal cord

Sofia Capito[1*], Elizaveta Rogova[1*], Max Schäbinger[1*], Marco Birke[2], Nicole Schider[2], Jan Pruszak[2]

[1]Paracelsus Medical University (PMU), Salzburg, Austria, *equal contribution; [2]Institute of Anatomy and Cell Biology, Paracelsus Medical University (PMU), Salzburg, Austria; Contact: jan.pruszak@pmu.ac.at

Objective
Recent single cell-based phenotypic analyses have yielded critical novel insights into cellular hierarchies and functional relationships in a variety of human tissues including the human brain. Comparably fewer cellular analyses have so far been conducted in the human spinal cord. Surface molecules have commonly been used to identify distinct cell populations and play major roles in cellular interactions in immunology, tumor biology and infectious disease. A systematic profile of cluster-of-differentiation (CD) surface antigens might serve to further characterize functional network relationships and to refine the anatomical cartography of the spinal cord.
We aim to comprehensively characterize the expression pattern of a broad array of CD surface antigens in the human spinal cord.

Methods
Immunofluorescence (IF) analysis was performed on 8-10 mm thick frozen human spinal cord specimens (cervical region; obtained from Amsbio [UK]). In brief, sections were air-dried (1h), fixed (2 min in 4% paraformaldehyde) followed by permeabilization/blocking (1h) in fish-gelatin solution containing 1% bovine serum albumin (BSA) and 0.1% Tween®20 in TBS. Primary antibodies at 1:50 dilution in 1% BSA/TBS were incubated overnight at 4°C. After washing, sections were incubated with the corresponding secondary antibodies [Invitrogen] for 7h at 4°C. Whole specimen IF images were taken using an Olympus VS120 slide scanner at 20x magnification.

Results
A select panel of >30 CD surface antigens has been analyzed to date. Besides some anticipated expression patterns, as e.g. for the integrin family member CD49b, other CD antigens showed specific and not previously described distribution. CD15 (Lewis-X) staining was exclusively discernable at the ependymal layer of the central canal, whereas the heat-stable antigen, CD24, showed a pronounced expression around the central canal as well as in Rexed lamina II. CD90 (Thy-1) was predominantly expressed throughout the gray matter, yet sparing Rexed lamina X. In contrast, MIC2 or single-chain type-1 glycoprotein CD99 within the gray matter appeared to be confined to lamina X, whereas CD200 (OX-2, a glycoprotein involved in neuroprotection) was expressed in the entire gray matter including the region around the central canal.

Conclusions
Prospectively, the ongoing expression screen for >200 CD antigens will elucidate the cellular cartography of the human spinal cord and may aid in identifying novel biomarkers for spinal cord pathophysiological processes and cellular therapeutics.

Acknowledgements
Funding: PMU-FFF, RISE 2020.0113 [JP].

PARACELSUS MEDIZINISCHE PRIVATUNIVERSITÄT

Klinikum Nürnberg
Wir sind für Sie da!

Hidden pitfalls? Risk of atrioventricular block following surgical aortic valve replacement: a computed tomographic analysis of baseline characteristics

Marie Claes[1, 2]

1. Paracelsus Medical University, Nuremberg, Germany; 2. Cardiac Surgery, Paracelsus Medical University – Klinikum Nürnberg, Nuremberg, Germany;
Contact: marie.claes@stud.pmu.ac.at

INTRODUCTION

It is estimated that about 12.4% of the population older than 75 years suffer from aortic valve (AV) stenosis, 3.4% of them having a severe stenosis with the indication for either surgical (SAVR or suAVR) or transcatheter valve replacement.[1] One remaining Achilles heel of SAVR and even more suAVR prostheses are postoperative conduction disturbances such as an atrioventricular block III (AVB III) resulting in the implantation of a permanent pacemaker (PPI): 2.7 – 10.5%.[2] Apart from other risk factors, calcifications in different regions of the native valve and a smaller membranous interventricular septum (MIS) are promising candidates as they might favour mechanical stress to the Bundle of His.[3,4]

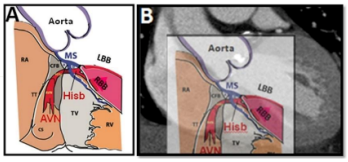

Figure 1. Schematic presentation of the conduction system's anatomy and topography (A) in combination with CT anatomy (B). [3]

OBJECTIVE

This study aimed to identify the impact of anatomical baseline characteristics and calcium load and distribution of the native aortic valve on postoperative third degree AVB in SAVR and suAVR. We hypothesized, that

1. the shorter the membranous interventricular septum the greater the risk to develop a postoperative third degree AVB and
2. the calcium load in the LVOT (left ventricular outflow tract) and on the native aortic valve apparatus may be another significant risk factor.

METHODS

- Retrospective single-centre study on patients with severe aortic valve stenosis who underwent SAVR with a stented biological prosthesis or suAVR (06/2016-12/2019)
- *Recorded data*: baseline (clinical, ECG, computed tomographic (membranous interventricular septum length calcifications of native valve), echocardiographic) and operative characteristics, in-hospital mortality, vascular complications, paravalvular leak (PVL), bleedings, acute kidney injury, stroke, conduction disturbances, permanent pacemaker implantation and length of stay, follow-up survival and cardiac morbidity
- *Analysis*:
  - I. Mann-Whitney U test to compare the study groups (AVB vs. nonAVB)
  - II. Two-tailed point biserial correlation was conducted to analyse possible associations
  - III. Binary logistic regression to detect the risk factors for each outcome in each group (AVB, nonAVB);
  - IV. Kaplan Meyer survival statistics to analyse the impact of calcium and anatomic variables on follow-up survival and conduction disturbances.

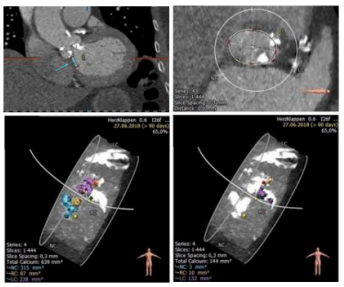

Figure 2. Measurement of membranous interventricular septum ( ), aortic valve area, calcifications in the aortic valve and the LVOT (MDCT scans).

RESULTS

A total of 155 (38% female) patients, mean age 71.2 ± 6 years were enrolled in our study: SAVR: N=109, suAVR: N=56

→ Study groups:

- **nonAVB** (N=144, 39% female)
- **AVB** (N=11, 27% female)

} Significant group differences in following calcium variables and membranous interventricular septum length:

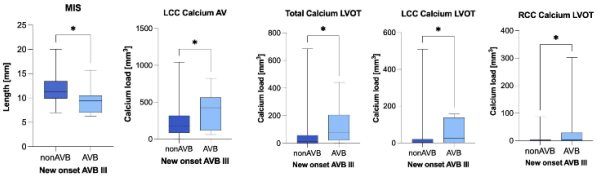

Figure 3. Mann Whitney-U test on MDCT data (MIS length and calcium load of the native aortic valve). The depicted variables differed signifcantly (*) between groups.

	nonAVB	AVB	p-value (2-tailed)
MIS length (mm)	11.7 (2.6)	9.6 (3.3)	0.014
LCC calcium AV (mm³)	229.1 (192.7)	386.2 (263.2)	0.044
Total calcium LVOT (mm³)	66.0 (120.8)	122.5 (129.8)	0.020
LCC calcium LVOT (mm³)	33.5 (82.4)	58.1 (62.2)	0.048
RCC calcium LVOT (mm³)	6.2 (14.5)	36.8 (89.3)	0.039

Table 1. Mann Whitney-U test on MDCT data. Values are presented as mean (± standard deviation). P-values < 0.05 are significant.

	Correlation coefficient r	p-value (2-tailed)	N	95% CI
MIS length [mm]	-0.202	**0.013**	150	-0.351-0.044
LCC calcium AV (mm³)	0.201	**0.012**	155	0.045-0.347
RCC calcium LVOT (mm³)	0.283	**<0.001**	155	0.131-0.422

Table 2. Point biserial correlation of new onset AVB III and MDCT data (MIS length and calcium load of the native aortic valve). LCC: left coronary cusp, RCC: right coronary cusp. P-values < 0.05 are significant.

CONCLUSION

We were able to show a significant impact of the length of the membranous interventricular septum: **Patients with postoperative new onset of AVB III had significantly shorter MIS. Patients of the AVB group had also significantly greater amounts of calcifications in the LCC of the aortic valve, the total LVOT and the LCC and RCC of the LVOT.**

We can state that patients with shorter MIS were more likely to experience an AVB III and greater calcifications in the LCC of the aortic valve and the RCC of the LVOT were positively correlated with such a conduction disturbance. Thus, we are one step closer to the identification of further risk factors that are able to predict postprocedural conduction disturbances such as AVB III.
This is aim and difficulty at the same time: select the best possible prosthesis and technique for aortic valve replacement for each patient. On our way to customized medicine, and not a "one fits all approach", the first step, to identify risk factors that are inherent in some patients is done.

We recommend including a MDCT in preoperative diagnostic testing for all patients undergoing SAVR or suAVR for further risk stratification, selection of prosthesis type, and surgical technique.

REFERENCES

1. Osnabrugge RLJ, Mylotte D, Head SJ, et al. Aortic stenosis in the elderly: Disease prevalence and number of candidates for transcatheter aortic valve replacement: A meta-analysis and modeling study. *Journal of the American College of Cardiology*. 2013;62(11):1002-1012. doi:10.1016/j.jacc.2013.05.015
2. Bagur R, Rodés-Cabau J, Gurvitch R, et al. Need for permanent pacemaker as a complication of transcatheter aortic valve implantation and surgical aortic valve replacement in elderly patients with severe aortic stenosis and similar baseline electrocardiographic findings. *JACC: Cardiovascular Interventions*. 2012;5(5):540-551. doi:10.1016/j.jcin.2012.03.004
3. Pollari F, Großmann I, Vogt F, et al. Risk factors for atrioventricular block after transcatheter aortic valve implantation: a single-centre analysis including assessment of aortic calcifications and follow-up. Europace. 2019 Jan 9. doi: 10.1093/europace/euy316.
4. Hamdan A, Guetta V, Klempfner R, et al. Inverse Relationship Between Membranous Septal Length and the Risk of Atrioventricular Block in Patients Undergoing Transcatheter Aortic Valve Implantation. *JACC: Cardiovascular Interventions*. Published online 2015. doi:http://dx.doi.org/10.1016/j.jcin.2015.05.010

ACKNOWLEDEGEMENT

At this point, I would like to thank Prof. Theodor Fischlein and Prof. Francesco Pollari for their trust in my abilities, support and the opportunities they offered me.

Hidden pitfalls? Risk of atrioventricular block following surgical aortic valve replacement: a computed tomographic analysis of baseline characteristics

Marie Claes[1, 2]

[1]Paracelsus Medical University, Nuremberg, Germany; Contact: marie.claes@stud.pmu.ac.at

Objective
Postoperative atrioventricular block III (AVBIII) and permanent pacemaker implantation (PPI) are still a noteworthy complication of surgical AVR. (1) Thus, the identification of preoperative risk factors is inevitable. We aimed to evaluate the impact of membranous interventricular septum length (MIS) and calcifications of the native valve, via preoperative multidetector computed tomography (MDCT) scan, on this outcome.

Methods
We analysed preoperative clinical characteristics, echo- and electrocardiograms, contrast-enhanced MDCT scans and procedural strategies of patients affected by aortic valve stenosis who underwent surgical AVR at our centre (06/2016-12/2019). The study population was divided into two groups (AVB, nonAVB) and variables were compared with a Mann-Whitney-U-test or X^2 test. Data were further analysed using point-biserial correlation, logistic regression, and Kaplan Meier.

Results
A total of 155 (38% female) patients, mean age 71.2±6 years were enrolled in our study: conventional stented bioprosthesis (N=109), sutureless prosthesis (N=56). A postoperative AVBIII was observed in 11 patients (7.1%). AVB patients had significant greater calcifications in LCC AV (nonAVB=229.1mm3±192.7 vs AVB=386.2mm3±263.2, p=0.044), LCC LVOT (nonAVB=33.5mm3±82.4 vs AVB=58.18mm³±62.2, p=0.048), RCC LVOT (nonAVB=6.2mm³±14.5 vs AVB=36.8mm3±89.3, p=0.039) and consequently in Total LVOT (total calcium LVOT: nonAVB=66.0mm³±120.8 vs AVB=122.5mm³±129.8, p=0.02) while their MIS was significantly shorter than in nonAVB patients (nonAVB=11.7±2.6 vs AVB=9.6±3.3 mm; p=0.014). Partially, these group differences correlated positively (LCC AV, r=0.201, p=0.012; RCC LVOT, r=0.283, p=<0.001) or negatively (MIS length, r=-0.202, p=0.008) with new-onset AVB III.

Conclusions
We recommend including a MDCT in preoperative diagnostic testing for all patients undergoing surgical SAVR for further risk stratification, selection of prosthesis type, and surgical technique.

References
1. Bagur R, Rodés-Cabau J, Gurvitch R, et al. Need for permanent pacemaker as a complication of transcatheter aortic valve implantation and surgical aortic valve replacement in elderly patients with severe aortic stenosis and similar baseline electrocardiographic findings. JACC: Cardiovascular Interventions. 2012;5(5):540-551. doi:10.1016/j.jcin.2012.03.004

Scalable production of hypoxic extracellular vesicles derived from pluripotent stem cells with angiogenesis potential

André Cronemberger Andrade [1], Martin Wolf [1], Heide-Marie Binder [1], Fausto Gueths Gomes [2], Felix Manstein[3], Patricia Ebner Peking [1], Rodolphe Poupardin [1], Robert Zweigerdt[3], Katharina Schallmoser [2] and Dirk Strunk [1]

[1] Experimental and Clinical Cell Therapy Institute (ExCT), Spinal Cord Injury and Tissue Regeneration Center, Paracelsus Medical University, Salzburg, Austria
[2] Department of Transfusion Medicine, Paracelsus Medical University, Salzburg, Austria
[3] Department of Cardiac, Thoracic, Transplantation and Vascular Surgery, Leibniz Research Laboratories for Biotechnology and Artificial Organs (LEBAO), Hannover Medical School, Hannover, Germany

andre.cronemberger@pmu.ac.at

INTRODUCTION

Stem cells secrete paracrine factors including EVs that are important in cellular communication and can support the regeneration of injured tissues. Reduced oxygen conditions (hypoxia) are crucial for proliferation and self-renewal of stem cells. Hypoxia is a key regulator in regeneration, and it may also be an important factor influencing cellular communication via EVs. There is evidence that, depending on the method of vesicle isolation, there is an impact on EV function. Therefore, we investigated whether hypoxic pre-conditioning could impact iPSC-EV quantity, quality and function.

GRAPHICAL ABSTRACT

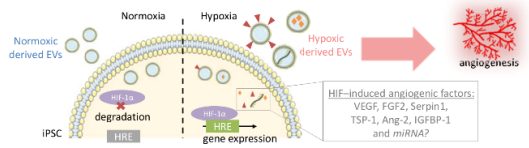

Figure 1. In this study we established a purification strategy for EV produced from a large-scale expansion of iPSC in hypoxic conditions. Upon hypoxia an accumulation of HIF-1a leads to binding of HIF complex to the hypoxia-response element (HRE) in the promoter of target genes. HIFs regulate the expression of several angiogenic genes. Angiogenic molecules can associate with EVs and serve as carriers for target cells boosting the angiogenesis potential.

METHODOLOGY FOR EV PRODUCTION AND PURIFICATION

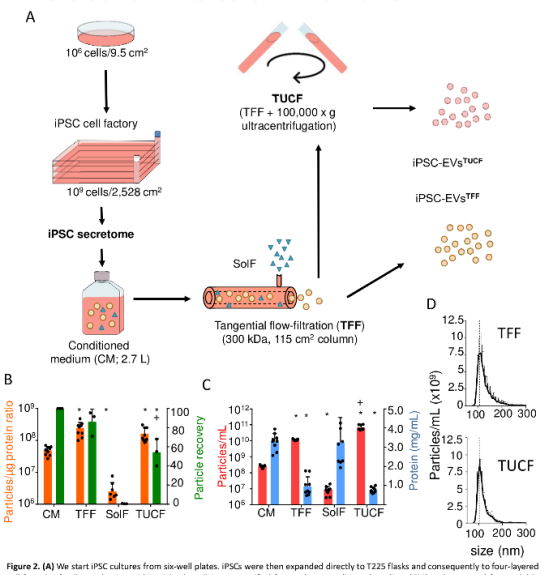

Figure 2. (A) We start iPSC cultures from six-well plates. iPSCs were then expanded directly to T225 flasks and consequently to four-layered cell factories for EV production within eight days. EVs were purified from culture-conditioned medium (CM) and separated from soluble factors (SolF) by tangential flow filtration (TFF) and further concentrated by ultracentrifugation (TUCF). **(B)** We monitored the EV purification by TRPS for measuring the particle concentration/size and by Bradford for protein quantification. The purity was accessed by particle/protein ratio and we observed an increase after TFF and TUCF. **(C)** After TFF, we obtained an enrichment in particles and a depletion in protein amount, the subsequent enrichment by ultracentrifugation further increased particles and depleted proteins. Efficiency of TFF is higher compared to TUCF. **(D)** Particle-size distribution for TFF and TUCF revealed a mode of diameter 109 and 103 nm respectively (dotted lines).

LARGE-EXPANSION OF iPSC AND EV PRODUTION USING BIOREACTORS

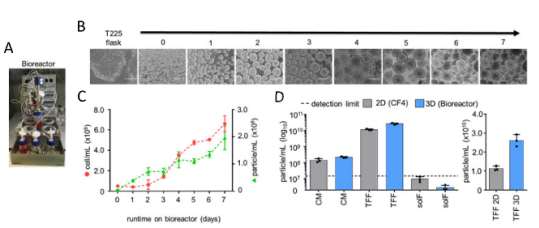

Figure 3. (A) Bioreactor Dasgip. **(B)** Aggregates formation and growth of iPSC on Bioreactor for 7 days. **(C)** Particle and cell count during expansion of cells on Bioreactor. **(D)** Comparison of purifications after using 2D cultures (CF4) and 3D cultures (Bioreactor).

CHARACTERIZATION OF HUMAN iPSC-EVs

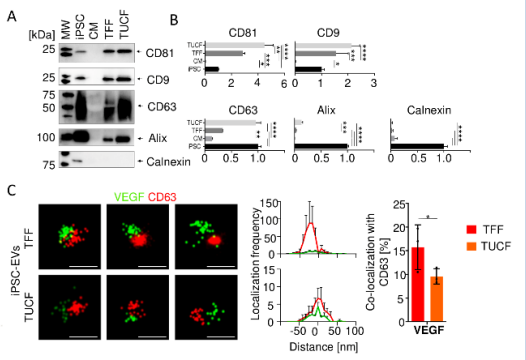

Figure 4. (A) (B) EV identity was determined by immunoblotting and we could observe an enrichment for tetraspanins (CD9, CD63 and CD81) and Alix after TFF and TUCF. As expected the EV samples were negative for Calnexin. **(C)** Using super-resolution direct stochastic optical microscopy (dSTORM), we detected the presence of CD63 and VEGF on the EVs. Scale bar 100nm. Co-localization signal of VEGF with CD63 was higher in TFF samples compared with TUCF.

HYPOXIC CONDITIONS OF HUMAN iPSC CULTURES

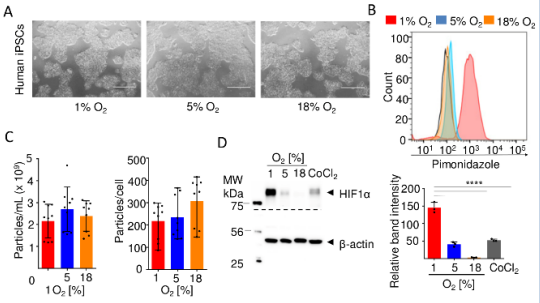

Figure 5. (A) iPSCs cultured under 1%, 5% and 18% oxygen conditions showing typical morphology **(B)** Using the hypoxiprobe pimonidazole we observed a higher signal after 1% oxygen culture. **(C)** After culturing iPSCs under different oxygen conditions the particle number and particles/cell displayed no alterations. **(D)** Immunoblotting for HIF-1α expression confirms higher levels of HIF-1α at 1% oxygen conditions.

ANGIOGENIC POTENTIAL OF HUMAN iPSC-EVs

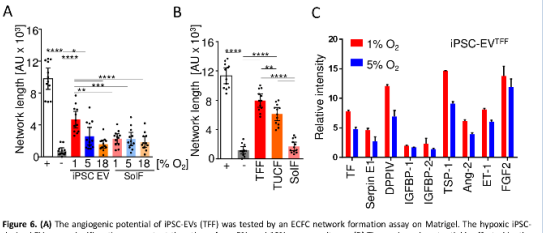

Figure 6. (A) The angiogenic potential of iPSC-EVs (TFF) was tested by an ECFC network formation assay on Matrigel. The hypoxic iPSC-derived EVs were significantly more potent than those from 5% and 18% oxygen cultures. **(B)** The angiogenic potential is affected by the method of choice when comparing TFF with TUCF EVs from iPSC 1% cultures. **(C)** We also compared the angiogenic protein profile of iPSC-EVs from 1% and 5% oxygen cultures where proteins related to angiogenesis showed higher expression levels in the iPSC-EVs (TFF).

SUMMARY/OUTLOOK

- We produced iPSC-EVs from large-scale iPSC cultures by tangential flow filtration and further concentrated these by ultracentrifugation, giving a good particle enrichment/quality.
- iPSC-EVs (TFF) from hypoxic condition cultures have a greater pro-angiogenic effect compared with iPSC-EVs derived from 5% and 18% conditions and soluble factors.
- An extended purification method to further concentrate the EVs by ultracentrifugation (TUCF) after TFF reduced the pro-angiogenic effect and showed a reduced amount of growth factor (VEGF) on the EVs.

ACKNOWLEDGEMENTS

This work was funded by the European Union's Horizon 2020; Cancer Cluster Salzburg—Smart Specialization Center (CCS); Transfer Center for Extracellular Vesicles Theralytic Technologies (EVTT); European Union H2020 project TECHNOBEAT; PACE.

Scalable production of hypoxic extracellular vesicles derived from pluripotent stem cells with angiogenesis potential

André Cronemberger Andrade[1], Martin Wolf[1], Heide-Marie Binder[1], Fausto Gueths Gomes, Felix Manstein[3], Patricia Ebner-Peking[1], Rodolphe Poupardin[1], Robert Zweigerdt[3], Katharina Schallmoser[2], Dirk Strunk[1]

[1]Cell Therapy Institute, Spinal Cord Injury and Tissue Regeneration Center Salzburg (SCI-TReCS), Paracelsus Medical University (PMU), Salzburg, Austria; [2]Department of Transfusion Medicine and SCI-TReCS, Paracelsus Medical University (PMU), Salzburg, Austria; [3]Department of Cardiac, Thoracic, Transplantation and Vascular Surgery, Leibniz Research Laboratories for Biotechnology and Artificial Organs (LEBAO), Hannover Medical School, Hannover, Germany; Contact: andre.cronemberger@pmu.ac.at

Objective
Improvement of protocols and methods using bioreactors for extracellular vesicles isolation is essential to produce vesicles with good quality and quantity. We choose to obtain vesicles from stem cells that secrete several paracrine factors including EVs that are important in cellular communication and can support the regeneration of injured tissues. A strategy to improve the function of the EVs derived from steam cells was preconditioning them using reduced oxygen conditions (hypoxia). As hypoxia is a key regulator in development and regeneration it may be an important factor influencing cellular communication via EVs. Here we investigated whether hypoxic pre-conditioning and cultivation in bioreactors can influence iPSC-EV EV quantity, quality and, EV-based angiogenic potential.

Methods
We cultivated iPSC in bioreactor or cell factories to produce iPSC EVs isolating using tangential flow filtration (TFF) from iPSC conditioned media from different oxygen level conditions, with further subsequent concentration by ultracentrifugation (TUCF). We quantified EVs by tunable resistive pulse sensing (TRPS). We characterized the EVs by immunoblotting for EV markers and using super-resolution microscopy (dSTORM). To check the functionality of the EVs derived from different oxygen conditions we performed an ECFC network formation assay on matrigel.

Results
EV quantity did not differ significantly at different oxygen conditions, but we also observed a higher yield of EVs when the cells were cultivated in bioreactors. In immunoblots, we found enrichment of the tetraspanins and Alix for the Ev purifications and not for Calnexin. We observed an elevated angiogenic potential on iPSC-EVs derived from 1% oxygen culture by TFF compared with iPSC-EVs from 5% and 18% conditions and soluble factors. An extended purification method to further concentrate the EVs by ultracentrifugation (TUCF) after TFF reduced the pro-angiogenic effect and showed a reduced amount of growth factor (VEGF) on the EVs.

Conclusions
We conclude that selecting a good strategy together with an improved protocol method can increase the production and function of iPSC-EVs from large-scale iPSC cultures (bioreactor) by TFF and concentrated by TUCF.

Developing a 3D brain model as an online learning tool for health profession students

Isolde Deleyto Rösner [1*], Victoria Gsenger[1*], Christian Platzl[2], Felix Eckstein[2], David Fürst[2], Martin Hudelmaier[2], Jan Pruszak[2#]

[1] Paracelsus Medical University (PMU), Salzburg, Austria * equal contribution

[2] Institute of Anatomy and Cell Biology, Paracelsus Medical University (PMU), Salzburg, Austria

[#] correspondence: jan.pruszak@pmu.ac.at

Introduction

Studying the complex morphology of the brain remains challenging for medical and other health professions students across the world. In order to enable an improved spatial understanding of the anatomical structures of the brain, a virtual 3D brain model was created based on a publically available open-access data set of an *ex vivo* human brain specimen imaged on a 7Tesla MRI scanner (Edlow *et al.*, 2019).

Material & Methods

The following steps were performed to construct the 3D model:

- Anatomically demanding and functionally relevant structures were chosen.
- The open-source medical image analysis software ITK-SNAP Version 3.6 was used for segmentation (*itksnap.org*; **Fig. 1 and 2**)
- Repair and smoothening of the exported 3D mesh with Autodesk Meshmixer Version 3.5 (*Autodesk Inc., CA*; **Fig. 3**)
- Importing the finalized 3D components into Unity to create an interactive 3D model (*Unity Technologies, CA*; **Fig. 4**)

Results

Anatomical structures segmented and visualized to date:

- Cerebral cortex
- Ventricular system
- Corpus striatum & Globus pallidus
- Cerebellum with Ncl. dentatus
- Limbic system
  - Hypothalamus
  - Amygdala
  - Hippocampus
  - Gyrus cinguli
  - Corpus callosum
  - Gyrus dentatus
  - Subthalamic nucleus

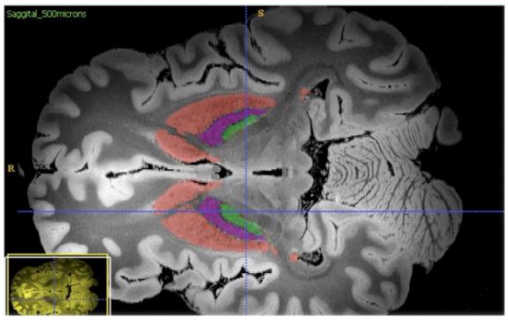

Figure 1 – Segmentation. Based on open-source MRI brain imaging data (see Edlow et al., 2019; ex vivo brain of a female human donor; 7T *Siemens Healthineers* Magnetom MRI scanner), the Corpus striatum (i.e., caudate nucleus and putamen; red), lateral (purple) and medial (green) segment of the globus palldus are highlighted after segmentation in *ITK-SNAP*.

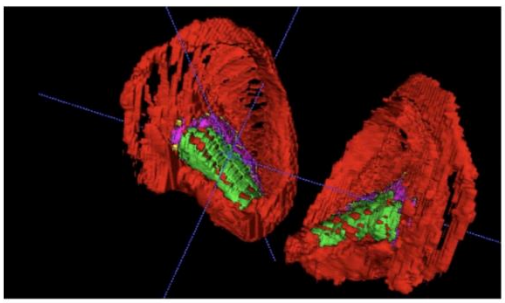

Figure 2 – 3D reconstruction. Visualized with ITK-SNAP, here the corpus striatum and palldium with *ITK-SNAP* Color code as above (see **Fig. 1**).

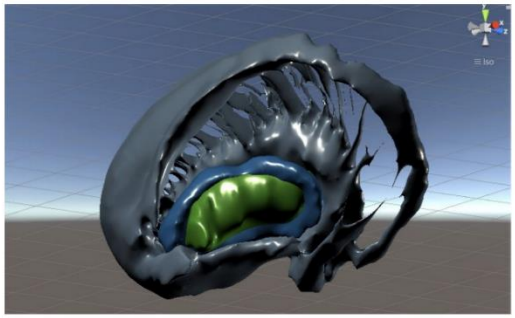

Figure 3 – Smoothened 3D-model. Corpus striatum (caudate nucleus and putamen in gray), lateral (blue) and medial (green) segment of the globus pallidus shown after smoothening with *Autodesk Meshmixer*.

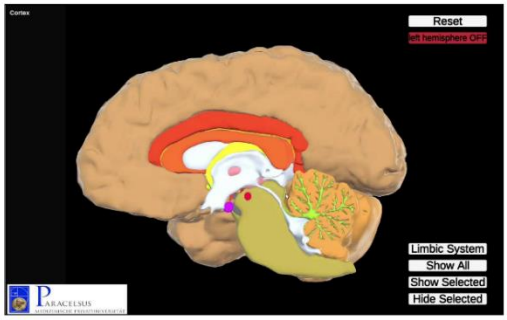

Figure 4 – Interactive 3D human brain model ("Click me" image). The resulting online tool provides a spatial visual representation of the brain, see-through, turning and sectioning features as well as labeling options.

Reference

Edlow BL *et al.* (2019). 7 Tesla MRI of the ex vivo human brain at 100 micron resolution. Sci Data. 6:244.

Conclusion

The final 3D-model can be freely accessed via the PMU website (pmu.ac.at/anatomie) to help students of the health professions and the neurosciences to better visualize neuroanatomical structures. We envision that this virtual brain model will allow an improved educational understanding of human brain anatomy.

Developing a 3D brain model as an online learning tool for health profession students

Isolde Deleyto Rösner[1,3], Victoria Gsenger[1,3], Christian Platzl[2], Felix Eckstein[2], David Fürst[2], Martin Hudelmaier[2], Jan Pruszak[2]

[1]Paracelsus Medical University, Salzburg, Austria; [2]Institute of Anatomy and Cell Biology, Paracelsus Medical University, Salzburg, Austria; [3]equal contribution; Contact: jan.pruszak@pmu.ac.at

Objective
Studying the morphology of the brain is challenging for medical students across the world. In order to create a better understanding of the multiple structures of the brain, a virtual 3D-brain model was created based on a free available ultra-high resolution 7 Tesla MRI dataset of an ex-vivo human brain specimen.

Methods
The dataset was part of the study "7 Tesla MRI of the ex-vivo human brain at 100 micron resolution" published October 2019 in Nature (1). Over a year our team from the Paracelsus Medical University (PMU) has been working on an innovative and original interactive 3D-model of the human brain. Specific structures were segmented in brain images using the open-source medical image analysis software ITK-SNAP. Repairing and smoothing the 3D-mesh was performed via Autodesk Meshmixer (Autodesk Inc., CA). The finalized mesh was imported into Unity (Unity Technologies, CA) to create the 3D-model.

Results
The completed interactive brain model will be accessible royalty free on the PMU website (https://www.pmu.ac.at/anatomie) to provide help for medical students to visualize and memorize challenging neurological brain anatomy like the corpus striatum, ventricular system, limbic system and cerebellum.

Conclusions
We envision that this brain model will allow a solid understanding of human brain anatomy in conjunction with other already existing 3D application and virtual learning tools.

References
1. Edlow BL et al. (2019). 7 Tesla MRI of the ex vivo human brain at 100 micron resolution. Sci Data. 6:244.

PARACELSUS MEDIZINISCHE PRIVATUNIVERSITÄT

Klinikum Nürnberg
Wir sind für Sie da.

Improvement of the antitumor activity of γδ T cells by combination of therapeutic antibodies

Karin Dootz[1], Anna Bold[1], Elisabeth Holzmann[1], Martin Wilhelm[1] und Stefan Knop[1]
[1]Clinic of Hematology and Oncology, Paracelsus Medical University, General Hospital Nuremberg
karin.dootz@klinikum-nuernberg.de

Background:
γδ T cells, which make up from 0.5 to 10% of human T cells, offer strong cytotoxic and pro-inflammatory activity towards malignant cells and tumors.[1-3] Therefore, γδ T cells are suitable candidates for cancer immunotherapy. Despite of successful transplantation of γδ T cells in Phase I studies, the clinical breakthrough could not be reached yet and mechanisms need to be found to improve this therapy.[1,4] The combination of γδ T cell immunotherapy with the administration of certain monoclonal antibodies improves the cytotoxicity of γδ T cells in vitro.[5,6,7] The underlying mechanism of this process is called antibody-dependent cellular cytotoxicity (ADCC), in which the antibody acts as a link between target and effector cell. As soon as the effector cells are activated, target cell death is induced leading to inhibition of tumour growth.[8,9]

ADCC of γδ T cells utilizing combinations of several monoclonal antibodies and a bispecific antibody

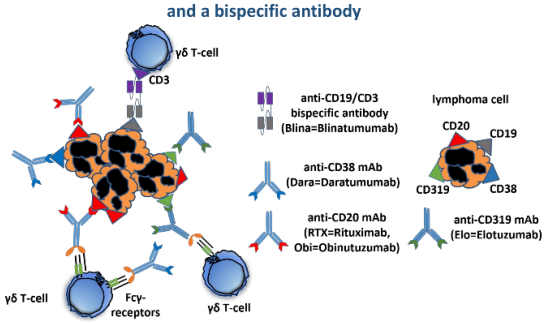

Objective:
The downregulation of antigens on cancer cells caused by a monoclonal antibody monotherapy represents a major obstacle, which is very common for the treatment with anti-CD19 and anti-CD20 antibodies.[1,10] The combination of several antibodies may prevent this resistance mechanism. Therefore, our aim was to investigate whether the combination of two therapeutic antibodies leads to an increased ADCC of γδ T cells compared to single antibody therapy or whether a steric hindrance arises between the antibodies, so that an inhibition of ADCC occurs. For this purpose, the anti-CD20-antibodies rituximab (RTX) and obinutuzumab (Obi), anti-CD38-antibody daratumumab (Dara) and anti-CD319-antibody elotuzumab (Elo) as well as the bispecific antibody blinatumumab (anti-CD3/CD19) were chosen. Even though Obi and RTX target the same antigen, they are directed towards different epitopes on the target cell surface.

Results:
Mononuclear cells were isolated from peripheral blood of healthy donors and stimulated with zoledronate and Interleukin-2 over 9 to 10 days, resulting in a cell population with more than 90% γδ T cells. For the cytotoxicity assay, these effector cells were co-incubated with target cells in different effector to target ratios and the therapeutic antibodies or their unspecific isotype control antibody. If not indicated differently, all antibodies were used in a mass concentration of 1 µg/ml. Lysis of target cells was then measured by flow cytometry. In most of our experiments, the specific lysis achieved by combining two therapeutic antibodies is comparable or even higher to the lysis that can be achieved with only one antibody. Apart from that, elotuzumab alone did hardly exhibit any effect on the ADCC of γδ T cells.

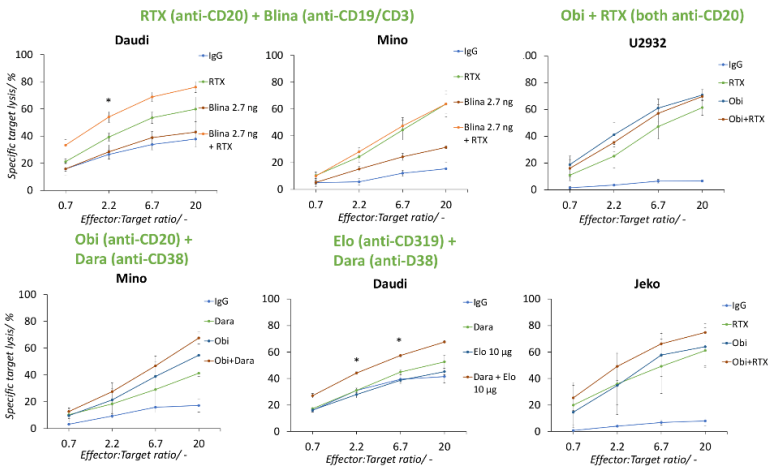

*P<0.05 comparing rituximab or daratumumab treatment with the combination of two antibodies. Data is presented as SEM of 3 independent experiments.

Conclusion:
The combination of two therapeutic antibodies leads to comparable or even increased ADCC of γδ T cells against B cell lymphoma cell lines. Therefore, the immunotherapy with γδ T cells combined with two therapeutic antibodies is a suitable approach for cancer therapy. Whether this can prevent antigen loss on cancer cells needs to be proven in future clinical studies.

References: (1) Hoeres, T. S., M.; Pretscher, D.; Wilhelm, M. . Improving the Efficiency of Vγ9Vδ2 T-Cell Immunotherapy in Cancer. *Front. Immunol.* **2018**, *9*. (2) Pauza, C. D.; Liou, M.-L.; Lahusen, T.; Xiao, L.; Lapidus, R. G.; Cairo, C.; Li, H. Gamma Delta T Cell Therapy for Cancer: It Is Good to be Local. *Frontiers in Immunology* **2018**, *9*. (3) Fisher, J. P.; Heuijerjans, J.; Yan, M.; Gustafsson, K.; Anderson, J. γδ T cells for cancer immuno-therapy: A systematic review of clinical trials. *Oncoimmunology* **2014**, *3*, e27572. (4) Nicol, A. J.; Tokuyama, H.; Mattarollo, S. R.; Hagi, T.; Suzuki, K.; Yokokawa, K.; Nieda, M. Clinical evaluation of autologous gamma delta T cell-based immunotherapy for metastatic solid tumours. *British Journal of Cancer* **2011**, *105*, 778-786. (5) Tokuyama, H.; Hagi, T.; Mattarollo, S. R.; Morley, J.; Wang, Q.; So, H. F.; Moriyasu, F.; Nieda, M.; Nicol, A. J. V gamma 9 V delta 2 T cell cytotoxicity against tumor cells is enhanced by monoclonal antibody drugs--rituximab and trastuzumab. *International journal of cancer* **2008**, *122*, 2526-2534. (6) Capietto, A. H.; Martinet, L.; Fournié, J. J. Stimulated γδ T cells increase the in vivo efficacy of trastuzumab in HER-2+ breast cancer. *Journal of immunology (Baltimore, Md. : 1950)* **2011**, *187*, 1031-1038. (7) Hoeres T, P. D. Improving Immunotherapy Against B-Cell Malignancies Using gd T-Cell-specific Stimulation and Therapeutic Monoclonal Antibodies. J Immunother, **2019**, 331-344. (8) Zahavi, D.; AlDeghaither, D.; O'Connell, A.; Weiner, L. M. Enhancing antibody-dependent cell-mediated cytotoxicity: a strategy for improving antibody-based immunotherapy. *Antibody Therapeutics* **2018**, *1*, 7-12. (9) Pennington, D. J.; Vermijlen, D.; Wise, E. L.; Clarke, S. L.; Tigelaar, R. E.; Hayday, A. C. The integration of conventional and unconventional T cells that characterizes cell-mediated responses. *Advances in immunology* **2005**, *87*, 27-59. (10) Vyas, M.; Müller, R.; Pogge von Strandmann, E. Antigen Loss Variants: Catching Hold of Escaping Foes. *Frontiers in Immunology* **2017**, *8*.

Improvement of the antitumor activity of γδ T cells by combination of therapeutic antibodies

Karin Dootz[1], Anna Bold[1], Elisabeth Holzmann[1], Martin Wilhelm[1], Stefan Knop[1]

[1]Clinic of Hematology and Oncology, Paracelus Medical University, General Hospital Nuremberg; Contact: karin.dootz@klinikum-nuernberg.de

Objective

γδ T cells, which make up from 0.5 to 10% of human T cells, offer strong cytotoxic and pro-inflammatory activity towards malignant cells and tumors.(1) Therefore, γδ T cells are suitable candidates for cancer immunotherapy. Despite of successful transplantation of γδ T cells in Phase I studies, the clinical breakthrough could not be reached yet and mechanisms need to be found to improve this therapy.(1,2) The combination of γδ T cell immunotherapy with the administration of certain monoclonal antibodies improves the cytotoxicity of γδ T cells in vitro.(3-5) The underlying mechanism of this process is called antibody-dependent cellular cytotoxicity (ADCC).(6,7) The downregulation of antigens on cancer cells caused by a monoclonal antibody monotherapy represents a major obstacle, which is very common for the treatment with anti-CD19 and anti-CD20 antibodies.(1,8) The combination of several antibodies may prevent this resistance mechanism. Therefore, our aim was to investigate whether the combination of two therapeutic antibodies leads to an increase or an inhibition of ADCC of γδ T cells compared to single antibody therapy. For this purpose, the antibodies rituximab and obinutuzumab, daratumumab and elotuzumab as well as blinatumumab were chosen.

Methods

Mononuclear cells were isolated from peripheral blood of healthy donors and stimulated with zoledronate and Interleukin-2 over 9 to 10 days, resulting in a cell population with more than 90% γδ T cells. For the cytotoxicity assay, these effector cells were co-incubated with target cells in different effector to target ratios and the therapeutic antibodies or their unspecific isotype control antibody. Lysis of target cells was then measured by flow cytometry.

Results

In most of our experiments, the specific lysis achieved by combining two therapeutic antibodies is comparable or even higher to the lysis that can be achieved with only one antibody. Apart from that, elotuzumab alone did hardly exhibit any effect on the ADCC of γδ T cells.

Conclusions

The combination of two therapeutic antibodies leads to comparable or even increased ADCC of γδ T cells against B cell lymphoma cell lines. Therefore, the immunotherapy with γδ T cells combined with two therapeutic antibodies is a suitable approach for cancer therapy. Whether this can prevent antigen loss on cancer cells needs to be proven in future clinical studies.

References

1. Hoeres, T. S., M.; Pretscher, D.; Wilhelm, M. Front. Immunol. 2018, 9
2. Nicol, A. J. et al. British Journal of Cancer 2011, 105, 778-786.
3. Tokuyama, H. et al. International journal of cancer 2008, 122, 2526-2534.
4. Capietto, A. H.; Martinet, L.; Fournié, J. J. (Baltimore, Md.: 1950) 2011, 187, 1031-1038.
5. Hoeres T, P. D. J Immunother, 2019, 331-344.
6. Zahavi, D.; AlDeghaither, D.; O'Connell, A.; Weiner, L. M. Antibody Therapeutics 2018, 1, 7-12.
7. Pennington, D. J. et al. Advances in immunology 2005, 87, 27-59.
8. Vyas, M.; Müller, R.; Pogge von Strandmann, E. Frontiers in Immunology 2017, 8.

Differentiated progenitor cells self-organize into skin organoids and vascularized human skin

Patricia Ebner[1], Linda Krisch[1,2], Martin Wolf[1], Sarah Hochmann[1], Anna Hoog[1], Balázs Vári[1], Katharina Muigg[1], Rodolphe Poupardin[1], Cornelia Scharler[1], Sabine Schmidhuber[3], Elisabeth Russe[4], Harald Stachelscheid[5], Achim Schneeberger[3], Katharina Schallmoser[2], Dirk Strunk[1]

[1]Cell Therapy Institute, Spinal Cord Injury and Tissue Regeneration Center Salzburg (SCI-TReCS), Paracelsus Medical University, Salzburg, Austria; [2]Department of Transfusion Medicine, Paracelsus Medical University, Salzburg, Austria; [3]Accanis Biotech, Biocenter Vienna, Austria; [4]Department of Plastic, Aesthetic and Reconstructive Surgery, Hospital Barmherzige Brueder, Salzburg, Austria; [5]Stem Cell Core Facility, Charité, Berlin Institute of Health; Berlin, Germany.

1) Introduction

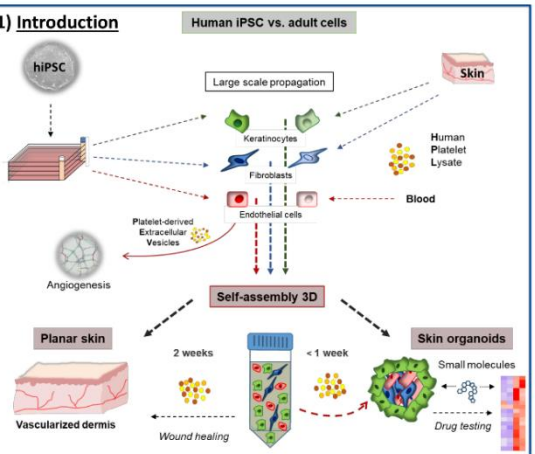

Self-assembly of adult and hiPSC-derived keratinocytes, fibroblasts and endothelial cells was promoted by platelet-derived growth factors, creating novel skin organoids within 6 days. Human skin organoids were properly characterized expressing markers of all skin layers and were used for high-content screening. We also established a humanized skin regeneration mouse model, based on self-assembly of adult as compared to iPSC-derived skin cell lineages under xeno-free conditions resulting in neo-vascularized human skin.

2) Platelet growth factors (HPL) support 3D organoid assembly

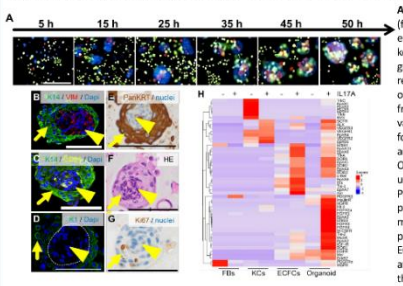

A: Nanoparticle labelling (fibroblasts (FBs) blue, endothelial cells (ECs)= red, keratinocytes (KCs) = green) and live cell imaging revealed sequential organoid assembly starting from initial stromal-vascular aggregation and followed by the superficial anchorage of adult KC. **B-G:** Organoid characterization using skin (VIM, K14, PanKRT), vessel (CD31) and proliferation (Ki67) markers. **H:** Proteome profiling of single FBs, ECFCs, KCs and organoids after 12 h stimulation in the absence (HCL control) or presence of IL17A. Z-scores.

3) Human iPSC-derived cell characterization

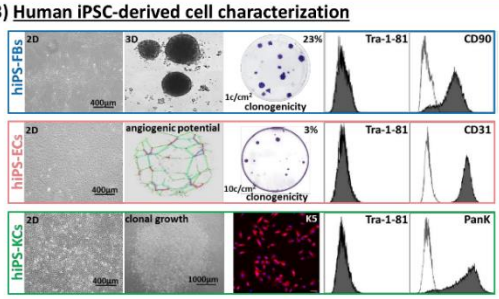

Cell characterization of hiPS-FBs, hiPS-ECs and hiPS-KCs revealed the cell type-specific morphology and marker expression. Tra-1-81 negative cell populations confirmed the lack of pluripotency in all three cell types. The angiogenic potential of iPS-EC was shown in a tube-like structure formation assay and iPS-FB and iPS-KC revealed clonogenic potential. Data from iPSC derived cells of two independent donors, repeated 2-6 times.

4) HPL supports rapid layered human skin organization *in vivo*

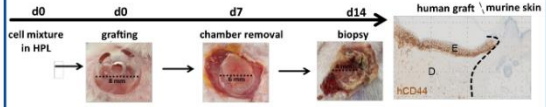

Schema of the skin cell transplantation model, where cells in animal serum-free 10% HPL or 10% FBS (Wang et al. 2000, JID) were transplanted. Anti-human CD44 (hCD44) staining of two weeks old skin grafts showed human cell organization into epidermis [E] and dermis [D] and the border between the human graft and the murine skin (dotted line).

5) Improved neo-vascularized skin in the presence of HPL

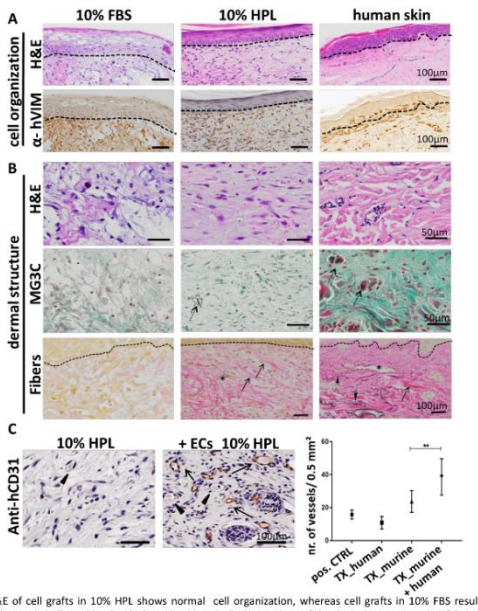

A: H&E of cell grafts in 10% HPL shows normal cell organization, whereas cell grafts in 10% FBS result in hyperkeratosis indicated by the thickened epidermis. **B:** Comparison of the dermal structures via H&E, MG3C and collagen fiber staining confirms the increased quality of 10% HPL by a regular fibroblast organization, blood vessels (dotted arrow), ground substance (asterisk) and collagen fiber production (arrow). **C:** Anti-human CD31 staining showed the formation of human blood vessels within the human skin upon co-transplantation of ECs. Quantification showed significantly increased vessel numbers upon co-transplantation of EC. Data from 3 biological and 3 technical replicates. Scale bar = 100 µm.

6) Successful iPSC-based self-organized skin regeneration

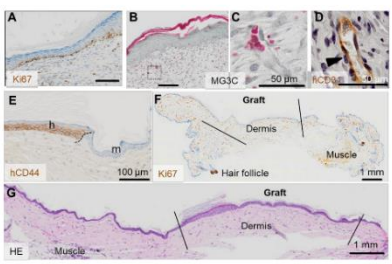

Human iPSC grafts, two weeks (**A-D**) and 3 months (**E-G**) after transplantation. **A:** Ki67 staining showed proliferation at the basal epidermal layer (brown). **B-C:** MG3C staining showed a vascularized dermis, (**C**) higher magnification, day 14. **D:** hCD31⁺ human vessel. **E:** hCD44 staining showed border between human graft and murine skin, 3 mo. **F-G:** Ki67 and HE staining showed the absence of tumorigenic structures in serial full section scans three months after grafting. 2 animals per condition.

7) Conclusion

Skin organoids permit novel rapid 3D skin-related pharmaceutical high-content testing opportunities. Multi-cell transplant self-organization facilitates development of iPSC-based organ regeneration strategies using cell suspension transplantation supported by human platelet factors.

Funding: European Union's Horizon 2020; grant agreement №668724 – TECHNOBEAT.

Cell Therapy Institute, PMU Salzburg
✉Dr. Patricia Ebner, patricia.ebner@pmu.ac.at

Referenz: Ebner-Peking et al. 2021. Theranostics. 11(17):8430-8447

Differentiated progenitor cells self-organize into skin organoids and vascularized human skin

Patricia Ebner[1], Linda Krisch[1,2], Martin Wolf[1], Sarah Hochmann[1], Anna Hoog[1], Balázs Vári[1], Katharina Muigg[1], Rodolphe Poupardin[1], Cornelia Scharler[1], Sabine Schmidhuber[3], Elisabeth Russe[4], Harald Stachelscheid[5], Achim Schneeberger[3], Katharina Schallmoser[2], Dirk Strunk[1]

[1]Cell Therapy Institute, Spinal Cord Injury and Tissue Regeneration Center Salzburg (SCI-TReCS), Paracelsus Medical University, Salzburg, Austria; [2]Department of Transfusion Medicine, Paracelsus Medical University, Salzburg, Austria; [3]Accanis Biotech, Biocenter Vienna, Austria; [4]Department of Plastic, Aesthetic and Reconstructive Surgery, Hospital Barmherzige Brueder, Salzburg, Austria; [5]Stem Cell Core Facility, Charité, Berlin Institute of Health; Berlin, Germany; Contact: patricia.ebner@pmu.ac.at

Objective

Stem/progenitor cells can self-organize into micro-sized organ units, termed organoids, partially modelling tissue function and regeneration. Here we demonstrated 3D self-assembly of adult and induced pluripotent stem cell (iPSC)-derived fibroblasts, keratinocytes and endothelial progenitors into both, planar human skin in vivo and human skin organoids in vitro, under the aegis of human platelet lysate (1).

Methods

Primary endothelial colony forming cells (ECFCs), skin fibroblasts (FBs) and keratinocytes (KCs) were isolated from human tissues and propagated under 2D xeno-free conditions. Human tissue-derived iPSCs were differentiated into endothelial cells (hiPSC-ECs), fibroblasts (hiPSC-FBs) and keratinocytes (hiPSC-KCs) according to efficiency-optimized protocols. Triple cell type skin organoid formation was promoted by human platelet-derived growth factors, using nanoparticle cell labelling for monitoring the organization process. Planar human skin regeneration was assessed in full-thickness wounds of immune-deficient mice upon transplantation of hiPSC-derived single cell suspensions.

Results

Organoids displayed a distinct architecture with surface-anchored keratinocytes surrounding a stromal core, and specific signaling patterns in response to inflammatory stimuli. Stratified human skin self-assembled within two weeks after either adult- or iPSC-derived skin cell-suspension liquid-transplantation, healing deep wounds of immune-deficient mice. No tumorigenesis was induced upon in vivo grafting of iPSC-derived progenitors, indicating the purity and lineage restriction of mature iPSC-derived cells. De-novo formed human blood vessels in the transplanted dermis were connected with the murine vasculature, proven by vessel perfusion with mouse blood. The quality of the skin was significantly increased upon engraftment in human platelet lysate compared to standard bovine serum, identified via following parameters: fiber/ground substance production/distribution, fibroblast density, dermal blood vessel content and epidermal stratification.

Conclusions

Skin organoids permit novel rapid 3D skin-related pharmaceutical high-content testing opportunities. Multi-cell transplant self-organization facilitates development of iPSC-based organ regeneration strategies using cell suspension transplantation supported by human platelet factors.

References

1. Ebner-Peking et al. 2021. Theranostics. 11(17):8430-8447

PARACELSUS MEDIZINISCHE PRIVATUNIVERSITÄT

Klinikum Nürnberg
wir sind für Sie da!

Clinical factors influencing stimulation parameters in navigated transcranial magnetic stimulation in patients with cerebral tumors

Thomas Eibl M.D.[1] Michael Schrey M.D.[1], Jens Weigel M.D.[1], Rüdiger Lange M. D.[2], Adrian Liebert M.D. [1], Markus Holtmannspoetter M.D.[3], Hans-Herbert Steiner M.D.[1]

1 Department of Neurosurgery, Paracelsus Medical University, Nuremberg, Germany
2 Department of Neurology, Paracelsus Medical University, Nuremberg, Germany
3 Department of Radiology, Section Neuroradiology, Paracelsus Medical University, Nuremberg, Germany
Correspondence to: thomas.eibl@klinikum-nuernberg.de

Objective: Navigated transcranial magnetic stimulation (nTMS) is highly valuable to create patient-individual data with motor-eloquent areas visible for the operating surgeon during the resection of cerebral pathologies. To obtain reliable and reproducible results in navigated transcranial stimulation brain mapping, nTMS-examinations are conducted in a standardized way. Factors influencing stimulation parameters and results of nTMS-examinations are not completely investigated yet. The objective was to determine factors which influence nTMS-stimulation parameters and the quality of nTMS-data for neurosurgical procedures.

Materials and Methods: Patient records, imaging and nTMS-data from examinations of the upper extremity muscles were retrospectively reviewed. Outcome measures were the resting motor threshold (rMT) and the feasibility of mapping the upper extremity muscles. For the assessment of the feasibility of mapping the upper extremity muscles, the ratio of positive muscle responses to all stimulations was calculated.

	n (%)	mean (SD)
Patient characteristics		
Age		59.95 (12.6)
Female	23 (39.3)	
Motor deficit	32 (49.2)	
Seizures	27 (41.5)	
Tumor characteristics		
Glioma	38 (58.5)	
Metastasis	20 (30.8)	
Meningioma	7 (10.8)	
Recurrent tumor	12 (18.5)	
Vicinity to primary motor area	24 (36.9)	
Tumor volume (cm^3)		23.7 (20.6)
nTMS examinations		
Resting Motor Threshold (% stimulator output)		32.7 (10.4)
Muscle for rMT-determination		
Abductor pollicis brevis (APB)	36 (55.4)	
Abductor digiti minimi (ADM)	18 (27.7)	
First dorsal interosseus (FDI)	7 (10.8)	
Others	4 (6.2)	

1

Table 1: summary of the patient cohort

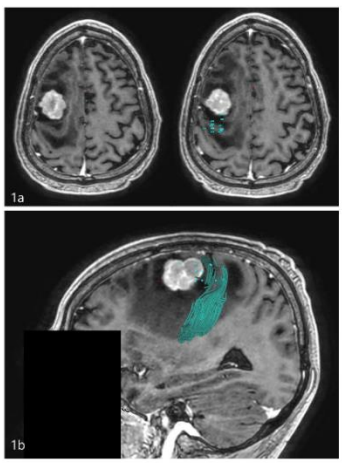

Figure 1a: adding information on motor function (nTMS-positive spots highlighted in turquoise) to MR-images
Figure 1b: combining nTMS-data with tractography

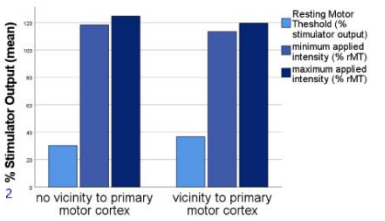

2

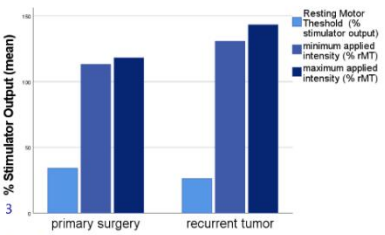

3

Figure 2: different rMT-values if the tumor infiltrated the primary motor cortex ($p<0.05$), relative stimulation intensities did not differ ($p>0.05$)
Figure 3: different rMT-values in patients with recurrent tumors ($p<0.05$), relative stimulation intensities did not differ ($p>0.05$)

Results: 65 nTMS-examinations in 61 patients (39.3% female) aged 59.95 years were evaluated. Resting motor threshold (rMT) was higher in patients with tumors in direct vicinity of the precentral gyrus ($p<0.05$), non-recurrent tumors ($p=0.024$) and in patients with motor deficits ($p=0.049$). Monitoring of more than two upper extremity muscles allowed mapping the upper extremity at lower intensities ($p=0.015$). Mapping conditions did not differ in patients with different tumor entities (all $p>0.2$). nTMS-mapping quality was user-independent. Applied stimulations and positive stimulations correlated significantly ($r_s=0.66$, $p<0.001$) . The ratio of positive stimulations and stimulation intensity (minimum applied stimulator output: $r_s=-0.14$, $p=0.26$, maximum applied stimulator output: $r_s=-0.15$, $p=0.25$) showed no correlation. Patients with arterial hypertension had lower ratios of positive stimulations ($p<0.05$). We did not observe differences in the ratio of positive stimulations among different tumor entities ($p>0.5$), vicinity to the primary motor cortex ($p=0.4$) or motoric deficits ($p>0.5$). Higher ratios of positive muscle responses were associated with no postoperative deterioration in patients with highly motor-eloquent tumors ($p<0.05$).

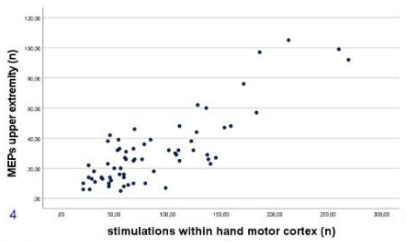

4

Figure 4: correlation of positive with all upper extremity responses ($r_s=0.66$, $p<0.001$)

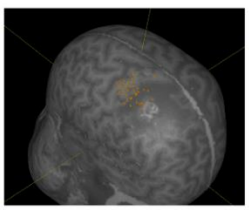

5

Figure 5: motor-map generated by nTMS: positive muscle responses colored in orange

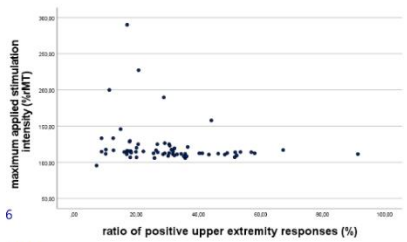

6

Figure 6: ratio of upper extremity MEPs and maximum applied stimulation intensity show no correlation ($r_s=-0.15$, $p=0.25$)

Conclusion: nTMS-examinations are influenced by different conditions. Most of these conditions are patient-specific or can be derived from imaging studies. Nonetheless, stimulation intensity should be kept as low as possible during nTMS-motor-mapping.

Clinical factors influencing stimulation parameters in navigated transcranial magnetic stimulation in patients with cerebral tumors

Thomas Eibl[1], Michael Schrey[1], Jens Weigel[1], Rüdiger Lange[2], Adrian Liebert[1], Markus Holtmannspötter[3], Hans-Herbert Steiner[1]

[1]Department of Neurosurgery, Paracelsus Medical University, Breslauer Str. 201, 90471 Nuremberg, GERMANY; [2]Department of Neurology, Paracelsus Medical University, Breslauer Str. 201, 90471 Nuremberg, GERMANY; [3]Department of Radiology, Section Neuroradiology, Paracelsus Medical University, Breslauer Str. 201, 90471 Nuremberg, GERMANY; Contact: thomas.eibl@stud.pmu.ac.at

Objective
Navigated transcranial magnetic stimulation (nTMS) is highly valuable to create patient-individual data with motor-eloquent areas visible for the operating surgeon during the resection of cerebral pathologies. To obtain reliable and reproducible results in navigated transcranial stimulation brain mapping, nTMS-examinations are conducted in a standardized way. Factors influencing stimulation parameters and results of nTMS-examinations are not completely investigated yet. The objective was to determine factors which influence nTMS-stimulation parameters and the quality of nTMS-data for neurosurgical procedures.

Methods
Patient records, imaging and nTMS-data from examinations of the upper extremity muscles were retrospectively reviewed. Outcome measures were the resting motor threshold (rMT) and the feasibility of mapping the upper extremity muscles. For the assessment of the feasibility of mapping the upper extremity muscles, the ratio of positive muscle responses to all stimulations was calculated.

Results
65 nTMS-examinations in 61 patients (39.3% female) aged 59.95 years were evaluated. Resting motor threshold (rMT) was higher in patients with tumors in direct vicinity of the precentral gyrus ($p=0.031$), non-recurrent tumors ($p=0.024$) and in patients with motor deficits ($p=0.049$). Monitoring of more than two upper extremity muscles allowed mapping the upper extremity at lower intensities ($p=0.015$). Mapping conditions did not differ in patients with different tumor entities (all $p>0.2$). nTMS-mapping quality was user-independent. Applied stimulations and positive stimulations correlated significantly ($rs=0.66$, $p<0.001$) . The ratio of positive stimulations and stimulation intensity (minimum applied stimulator output: $rs=-0.14$, $p=0.26$, maximum applied stimulator output: $rs=-0.15$, $p=0.25$) showed no correlation. Patients with arterial hypertension had lower ratios of positive stimulations ($p=0.045$). We did not observe differences in the ratio of positive stimulations among different tumor entities ($p=0.54$), vicinity to the primary motor cortex ($p=0.47$) or motoric deficits ($p=0.56$). Higher ratios of positive muscle responses with no postoperative deterioration in patients with highly motor-eloquent tumors ($p<0.05$).

Conclusions
nTMS-examinations are influenced by different conditions. Most of these conditions are patient-specific or can be derived from imaging studies. Nonetheless, stimulation intensity should be kept as low as possible during nTMS motor mapping.

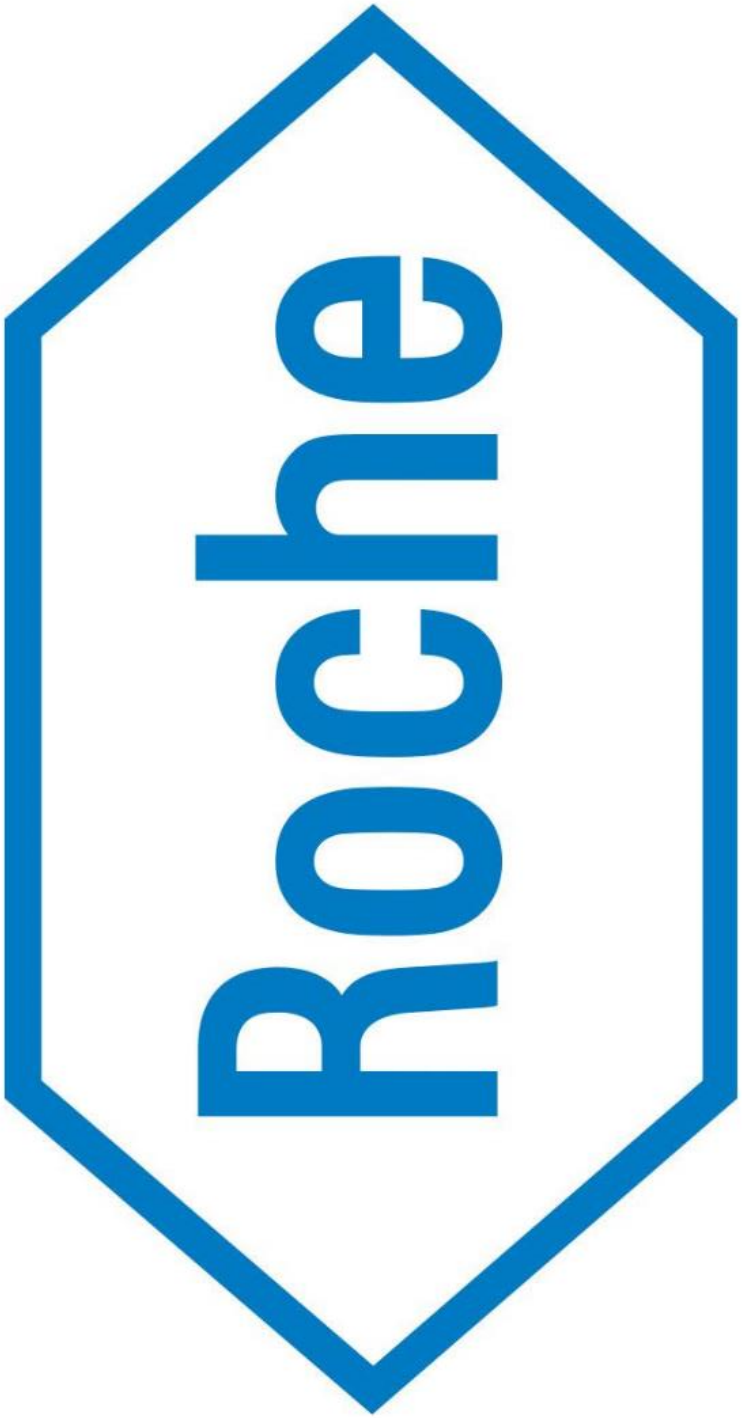
Roche


BIOMÉRIEUX
BE A GAME CHANGER
You can make a difference
with the right diagnostic tests that give you the power to fight infectious diseases—and save lives.
PIONEERING DIAGNOSTICS
A world leader in *in vitro* diagnostics, bioMérieux provides solutions that determine the origin of a disease. World leader in microbiology, specialized in immunoassays and leading pioneer in the syndromic molecular approach, we are committed on major public health issues, such as antimicrobial resistance, sepsis and respiratory infections.

PARACELSUS MEDIZINISCHE PRIVATUNIVERSITÄT

Klinikum Nürnberg
Wir sind für Sie da!

Resection of motor-eloquent gliomas using navigated transcranial magnetic stimulation in a multimodal approach

Thomas Eibl M.D.[1] Michael Schrey M.D.[1], Jens Weigel M.D.[1], Rüdiger Lange M. D.[2], Adrian Liebert M.D. [1], Markus Holtmannspoetter M.D.[3], Hans-Herbert Steiner M.D.[1]

1 Department of Neurosurgery, Paracelsus Medical University, Nuremberg, Germany
2 Department of Neurology, Paracelsus Medical University, Nuremberg, Germany
3 Department of Radiology, Section Neuroradiology, Paracelsus Medical University, Nuremberg, Germany
Correspondence to: thomas.eibl@klinikum-nuernberg.de

Objective: The resection of motor-eloquent gliomas remains challenging even the era of functional imaging and intraoperative monitoring. Preoperative mapping with navigated transcranial magnetic stimulation (nTMS) increases patients' safety during the resection of motor-eloquent gliomas. We investigated the combination of nTMS-based navigation, intraoperative monitoring (IOM) and navigated ultrasound (IUS) compared to solely nTMS-based navigation.

Materials and Methods: This is a retrospective study of glioma patients who underwent resection between April 2016 and September 2020. The cohort was divided into four groups: nTMS-based navigation (nTMS), nTMS and IOM, nTMS and IUS, nTMS and IOM plus IUS.

Item	Mean (SD)	N (%)
Age	58.1 (12.4)	
Female		
Motor deficit		13 (50%)
Seizure		12 (46.2%)
Tumor entity		
Glioblastoma CNS WHO grade 4		22 (84.6)
Astrocytoma CNS WHO grade 3		3 (11.5%)
Oligodendroglioma CNS WHO grade 3		1 (3.8%)
Tumor recurrence		6 (23.1)
Tumor location		
Frontal		3 (11.5%)
Parietal		7 (26.9%)
Temporal		2 (7.7%)
Gyrus precentralis		9 (34.6%)
Gyrus postcentralis		5 (19.2%)
Left-hemispheric		11 (42.3%)
Tumor volume (cm^3)	26.6 (25.1)	
Duration of surgery (mins)	263 (83)	
Resting Motor Threshold (% stimulator output)	32.4 (13.1)	
1 Tumor infiltration to primary motor cortex		12 (46.2%)

Table 1: Overview of the patient cohort

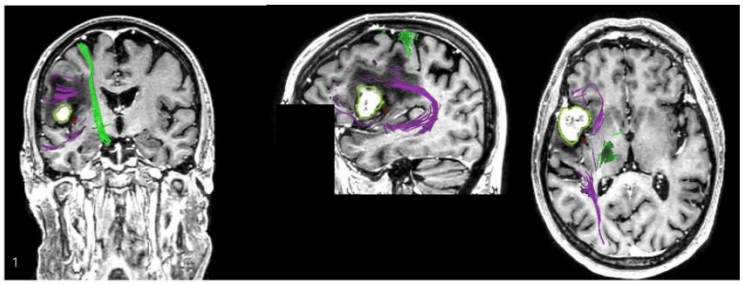

Figure 1: Implementation of motor (green) and language (purple) pathways into the neuronavigation MRI

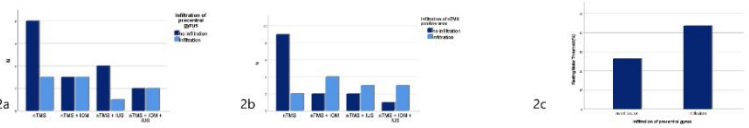

Figure 2a, b: Indication for IOM based upon anatomical criteria or nTMS-data (infiltration of primary motor cortex), p>0.05
Figure 2c: different rMT-values in patients with infiltration of the primary motor cortex (p<0.05)

Results: 26 patients (34.6% female) with motor-eloquent gliomas (22 Glioblastomas CNS WHO grade 4, 3 Astrocytomas CNS WHO grade 3, 1 Oligodendroglioma CNS WHO grade 3) were included. nTMS-motor-mapping was performed in all patients, 23 (88.5%) surgeries were performed with nTMS-based DTI-fibertracking. nTMS positive spots at tumor margins confirmed infiltration of the motor cortex based on anatomic criteria (p<0.01) serving as an indication for IOM. IOM with direct electric stimulation was used in 6 (23.1%) cases, IUS was used in 5 patients (19.2%). Both IOM and IUS were used in 4 procedures (15.4%). IUS was helpful in 8 surgeries (88.9%). Surgical time did not differ within the subgroups (p>0.8). The mean reduction in tumor volume was 93±7.5%. Extent of resection or neurologic outcome did not differ within the subgroups (p>0.6). 3 (11.5%) patients had a new motor deficit. Preoperative deficits aggravated postoperatively in 8 (30.8%), surgery-related deficits improved in 5 patients (45.5%). Positive nTMS-spots at the tumor margin were associated with transient (p=0.012) but not permanent deficits (p>0.5).

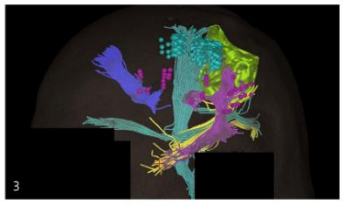

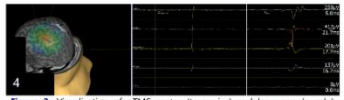

Figure 3: Visualization of nTMS motor (turquoise) and language (purple) positive spots, DTI-fibertracking of motor (turquoise cranio-caudal) and language (purple, yellow, blue, turquoise in a-p direction) pathways. Tumor is highlighted in green
Figure 4: creating the motor map with nTMS

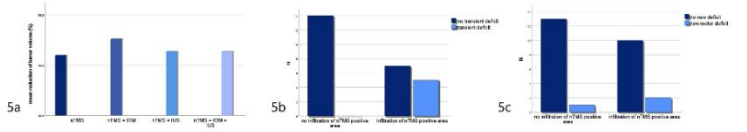

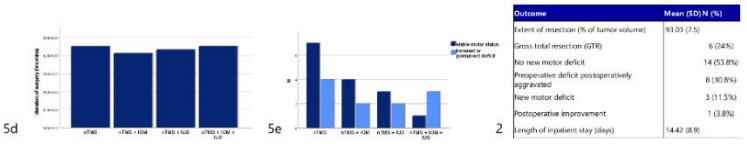

Figure 5a: Reduction of tumor volume (p>0.05)
Figure 5b: transient deficits associated with infiltration to the nTMS motor map (p<0.05)
Figure 5c: no association of permanent deficits with nTMS motor map (p>0.05)
Figure 5d: duration of surgery (p>0.05)
Figure 5e: postoperative functional outcome showed no difference among the subgroups

Outcome	Mean (SD) N (%)
Extent of resection (% of tumor volume)	93.03 (7.5)
Gross total resection (GTR)	6 (24%)
No new motor deficit	14 (53.8%)
Preoperative deficit postoperatively aggravated	8 (30.8%)
New motor deficit	3 (11.5%)
Postoperative improvement	1 (3.8%)
Length of inpatient stay (days)	14.42 (8.9)

Table 2: Overview over main outcome data

Conclusion: The multimodal approach represents a possible solution for a safe resection of highly motor-eloquent gliomas and nTMS is a perfect tool for risk stratification. IUS is a precious tool during tumor resection which can be easily implemented into surgical workflow.

Resection of motor-eloquent gliomas using navigated transcranial magnetic stimulation in a multimodal approach

Thomas Eibl[1], Michael Schrey[1], Jens Weigel[1], Adrian Liebert[1], Rüdiger Lange[2], Markus Holtmannspötter[3], Hans-Herbert Steiner[1]

[1]Department of Neurosurgery, Paracelsus Medical University, Breslauer Str. 201, 90471 Nuremberg, GERMANY; [2]Department of Neurology, Paracelsus Medical University, Breslauer Str. 201, 90471 Nuremberg, GERMANY; [3]Department of Radiology, Section Neuroradiology, Paracelsus Medical University, Breslauer Str. 201, 90471 Nuremberg, GERMANY; Contact: thomas.eibl@stud.pmu.ac.at

Objective
The resection of motor-eloquent gliomas remains challenging even the era of functional imaging and intraoperative monitoring. Preoperative mapping with navigated transcranial magnetic stimulation (nTMS) increases patients' safety during the resection of motor-eloquent gliomas. We investigated the combination of nTMS-based navigation, intraoperative monitoring (IOM) and navigated ultrasound (IUS) compared to solely nTMS-based navigation.

Methods
This is a retrospective study of glioma patients who underwent resection between April 2016 and September 2020. The cohort was divided into four groups: nTMS-based navigation (nTMS), nTMS and IOM, nTMS and IUS, nTMS and IOM plus IUS.

Results
26 patients (34.6% female) with motor-eloquent gliomas (22 Glioblastomas CNS WHO grade 4, 3 Astrocytomas CNS WHO grade 3, 1 Oligodendroglioma CNS WHO grade 3) were included. nTMS-motor-mapping was performed in all patients, 23 (88.5%) surgeries were performed with nTMS-based DTI-fibertracking. nTMS positive spots at tumor margins confirmed infiltration of the motor cortex based on anatomic criteria ($p<0.01$) serving as an indication for IOM. IOM with direct electric stimulation was used in 6 (23.1%) cases, IUS was used in 5 patients (19.2%). Both IOM and IUS were used in 4 procedures (15.4%). IUS was helpful in 8 surgeries (88.9%). Surgical time did not differ within the subgroups ($p>0.8$). The mean reduction in tumor volume was 93±7.5%. Extent of resection or neurologic outcome did not differ within the subgroups ($p>0.6$). 3 (11.5%) patients had a new motor deficit. Preoperative deficits aggravated postoperatively in 8 (30.8%), surgery-related deficits improved in 5 patients (45.5%). Positive nTMS-spots at the tumor margin were associated with transient ($p=0.012$) but not permanent deficits ($p>0.5$).

Conclusions
The multimodal approach represents a possible solution for a safe resection of highly motor-eloquent gliomas and nTMS is a perfect tool for risk stratification. IUS is a precious tool during tumor resection which can be easily implemented into surgical workflow.

Sideritis – a traditionally used plant to fight neurodegenerative disease?

Harald Fischill[1*], Joshua Hettig[1*], Ekaterina-Michaela Tomou[2,3,4], Helen Skaltsa[2], Corinna Urmann[3,4], Sébastien Couillard-Després[1] and Lara Bieler[1]

[1] Institute of Experimental Neuroregeneration and Spinal Cord Injury and Tissue Regeneration Center Salzburg, Paracelsus Medical University, Salzburg, Austria
[2] Faculty of Pharmacy, National and Kapodistrian University of Athens, Athens, Greece
[3] Weihenstephan-Triesdorf University of Applied Sciences, Organic-analytical Chemistry, Straubing, Germany
[4] TUM Campus Straubing for Biotechnology and Sustainability, Technical University of Munich, Straubing, Germany
[*] Authors contributed equally

lara.bieler@pmu.ac.at

1 BACKGROUND


S. perfoliata(3)

As a reason of a high living standard and continuous development in medical care, the live expectancy in our society increases steadily. With the growing number of elderly in the population, the occurrence of age-associated diseases rapidly took in importance. Neurodegenerative disorders are a significant group of age-associated diseases. Neurodegenerative disorders are characterized by a progressive neuronal and functional loss. Unfortunately, no cure for neurodegenerative disorders is available to date and progression of the diseases can rarely be slowed down or stopped.

Sideritis LL., better known as greek mountain tea, is a widely used plant for tea preparation first for its good taste and second for its implications as a traditional medicine, especially for the treatment of digestive problems or flu-like symptoms. However, in the last years, studies suggested an improvement in memory of people suffering from different forms of dementia (1). Therefore, we screened more than 60 extracts of various Sideritis subspecies and extraction methods for their neurogenic potential.

To determine the neurogenic potential of the different extracts a dual luciferase assay, based on the expression of doublecortin (DCX) as well as the expression of a constitutive promotor, was chosen. Doublecortin (DCX) is a microtubule – associated protein and known as an early marker of neuronal differentiation (2).

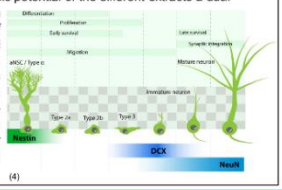

(4)

2 DUAL LUCIFERASE ASSAY

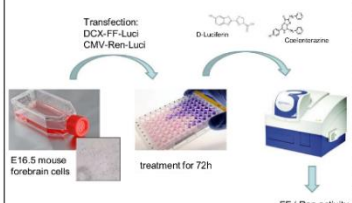

To analyse the neurogenic potential of Sideritis extracts, mouse embryonic forebrain cells (E16.5) were used in passage 2. In a first step, cells were transfected with plasmids encoding the firefly-luciferase under the control of the DCX-promotor and the renilla-luciferase under the control of the constitutive promoter CMV. After 24h, cells were treated with a variety of Sideritis extracts and concentrations. Neuronal induction was analysed 72h after the treatment by measuring the light emissions of the luciferases in a multi-well reader.

3 SCREENING

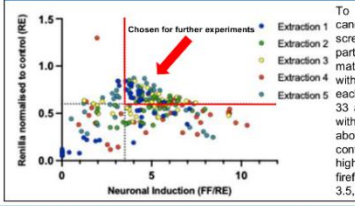

To identify the most promising candidates for further experiments, a screening with extracts from the aerial parts of 10 subspecies and root material from 4 subspecies extracted with 5 different extraction methods, each in 3 different concentrations (100, 33 and 11 µg/mL) was done. Extracts with a low toxicity, i.e. renilla signal above 0.6 normalized to the negative control (medium + 1% DMSO), and a high neuronal induction, i.e. ratio of firefly signal and renilla signal above 3.5, were further evaluated.

4 RESULTS

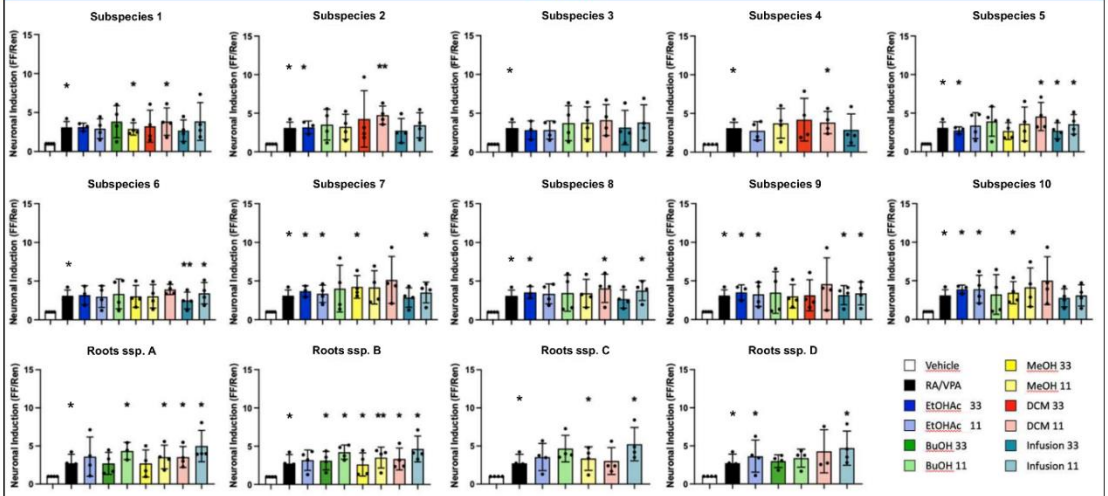

Graphs represent the neuronal induction capacity, i.e. ratio of firefly (DCX) signal and renilla (constitutive) signal, of one Sideritis subspecies extracted with the different indicated solvents (n=3-4). Data were normalized to the negative control (medium + 1% DMSO), a combination of 10 µM retinoic acid and 50 µM valproic acid served as positive control. Statistical significance was determined with a one-sample t-test against a hypothetical value of 1 (negative control) and was indicated in the graphs using asterisks (* $p < 0.05$; ** $p < 0.01$).

5 DISCUSSION

Multiple Sideritis extracts significantly induced neuronal differentiation in our testing system. Especially the infusions and dichlormethane extracts, indicated in the graphs in petrol-blue and red, respectively, seem to have a high potential to induce differentiation throughout the different subspecies and parts of the plant. In some cases, mainly butanol, methanol and ethylacetate extracts, we observed a reduction of activity with each consecutive repetition, which can likely be attributed to compounds with low stability being responsible for the mechanism of action. However, further *in vitro* studies are needed to confirm the findings of our testing system.


(5)

6 OUTLOOK

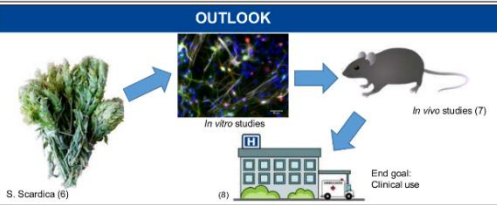

REFERENCES

1. Hofrichter et al.; Sideritis spp. Extracts Enhance Memory and Learning in Alzheimer's β-Amyloidosis Mouse Models and Aged C57Bl/6 Mice; J of Alzheimer Dis. 2016
2. Couillard-Despres, et al.; Human *in vitro* reporter model of neuronal development and early differentiation processes, BMC Neuroscience, 2008
3. https://commons.wikimedia.org/wiki/File:Sideritis_perfoliata_2.JPG (modified by H. Fischill)
4. Cassé, Richetin, Toni; Astrocytes' Contribution to Adult Neurogenesis in Physiology and Alzheimer's Disease; 2018 (modified by H. Fischill)
5. https://commons.wikimedia.org/wiki/File:Greekmountaintea.jpg
6. https://commons.wikimedia.org/wiki/File:Sideritis_scardica_IMG_4653.jpg
7. https://commons.wikimedia.org/wiki/File:201108_mouse.png
8. https://freesvg.org/hospital

Sideritis – a traditionally used plant to fight neurodegenerative disease?

Harald Fischill[1], Joshua Hettig[1], Ekaterina-Michaela Tomou[2,3,4], Helen Skaltsa[3], Corinna Urmann[3,4], Sébastien Couillard-Després[1], Lara Bieler[1]

[1]Institute of Experimental Neuroregeneration and Spinal Cord Injury and Tissue Regeneration Center Salzburg, Paracelsus Medical University, Salzburg, Austria; [2]Faculty of Pharmacy, National and Kapodistrian University of Athens, Athens, Greece; [3]Weihenstephan-Triesdorf University of Applied Sciences, Organic-analytical Chemistry, Straubing, Germany; [4]TUM Campus Straubing for Biotechnology and Sustainability, Technical University of Munich, Straubing, Germany; Contact: harald.fischill@stud.pmu.ac.at

Objective
High living standards and continuous development in medical care steadily increase the life expectancy in our society, which made age associated diseases rapidly take in importance. Neurodegenerative disorders are a significant group of age associated diseases, and unfortunately no cure is available to date. Sideritis LL. better known as greek mountain tea, is a widely used plant for tea preparations for good taste as well as for its implications as a traditional medicine, especially for the treatment of digestive problems or flu like symptoms. Recently however, improvement of different forms of dementia was suggested by studies. Therefore, we screened more than 60 extracts of various Sideritis subspecies and extraction methods for their neurogenic potential in vitro.

Methods
To determine the neurogenic potential of the different extracts a dual luciferase assay based on the expression of doublecortin (DCX) as well as the expression of a constitutive promotor was chosen. After transfection, mouse embryonic forebrain cells (E16.5) were treated with a variety of Sideritis extracts and concentrations. Neuronal induction was analysed 72h after the treatment by measuring the light emissions of the luciferases.

Results
Based on a first screening with 210 different treatment conditions, we excluded the conditions with signs of cellular toxicity. However, in our further experiments all subspecies were included, because at least one concentration of each exceeded our cut-off parameters. Multiple extracts significantly induced neuronal differentiation in our testing system. Especially the infusions and dichloromethane extracts. Both of them show high induction values throughout all of the different subspecies and concentrations. For some extracts, we recognized a high neurogenic potential in the first screening, which steadily decreased with each consecutive repetition.

Conclusions
In general, Sideritis extracts have a very high potential to induce neuronal differentiation in our testing system. The decline of neurogenic potential of certain extracts could be explained by low stability of the compounds responsible for the effect. In the next steps, we will employ further in vitro testing methods to confirm our results, to be able to go further in the direction of in vivo studies.

PARACELSUS MEDIZINISCHE PRIVATUNIVERSITÄT

FRIEDRICH-ALEXANDER UNIVERSITÄT ERLANGEN-NÜRNBERG
Chair of Health Psychology
Institute for Psychology

Biological and psychological stress responses after miscarriage: Cross-sectional results from the MALT randomized controlled trial (preliminary data)

Gerber, L[1,2], Braun, A[1], Müller, MM[1], Rohleder, N[2], Stein, B[1], Radermacher, P[3], Waller, C[1]

[1]Paracelsus Medical University, General Hospital Nuremberg, Department of Psychosomatic Medicine and Psychotherapy;
Contact: Luis.Gerber@klinikum-nuernberg.de
[2]Department of Psychology, Chair of Health Psychology, Friedrich-Alexander Universität Erlangen-Nürnberg
[3]Anesthesiological Pathophysiology and Process Engineering, Ulm University Hospital

Introduction

- Trauma and traumatic events can lead to a variance of somatic reactions/symptoms and disorders related to inflammation.[1]
- Women are more prone to traumatic events[2] and miscarriage might be a major event leading to Posttraumatic Stress Disease (PTSD).[3,4]
- The development of PTSD in women is not yet fully understood, not much information about the biological reactions AFTER the traumatic event and BEFORE the development of PTSD exists.
- We tried to somewhat assess this gap in the following study.

Study

Sample:
- Miscarriage (N=23) age: *M*= 27.25 *SD*= 7.41;
- Control (N=28); age: *M* = 34.00 *SD* = 4.76

Design:
Women were invited to a three hour assessment around the Socially Evaluated Cold Pressor Test (SECPT) during which blood and saliva was extracted at specific timeslots and a number psychological assessments were conducted in between.

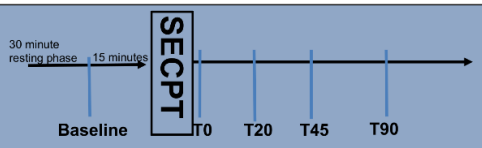

Results(preliminary)

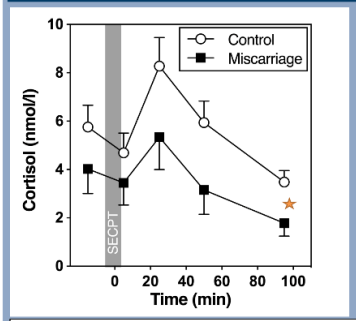

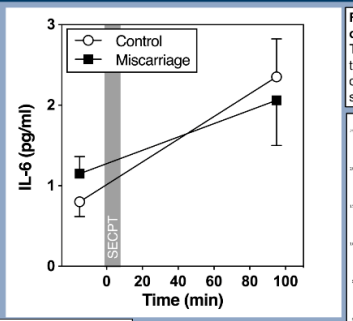

Figure 1: Differences in Cortisol reactivity control vs. miscarriage controlled by age
There is a highly significant time effect (F = 5.365 p = 0.01) in the entire sample. Controlled by age there is a non significant difference in overall cortisol between the groups (F = 3.49 p = .068)
There is no significant interaction between group variable and time (p = .829)
But comparing the individual time points a significant difference in the recovery rate of cortisol can be seen:
p(Baseline) = .28; p(T0) = .25; p(T20) = .10; **p(T45) = .05; p(T90) = .02**

Figure 2: Differences in Interleukin-6 reactions control vs. miscarriage
There was a strong and significant reaction related to the SECPT (F = 27.86 p < 0.001) but no significant differences between the groups (p = .77) and no significant interaction (p = .21)

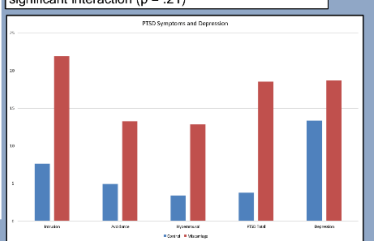

Figure 3: Differences in PTSD and Depression symptoms control vs. miscarriage
Women after miscarriage showed significant higher traumatization on Impact Of Event Scale (F = 22.66; p < 0.001) and on the Posttraumatic Diagnostic Scale (F = 52.73; p < 0.001. Depression symptoms also differ significantly between the groups (F = 36.13; p < 0.001).

Summary & Conclusions

- Controlled for age (Figure 1) there is no overarching difference in cortisol reactivity but the recovery rate differs between the two groups. A IL-6 reaction (Figure 2) can be observed but the two groups show a similar course. As we measured at 90 minutes after the SECPT we do not know if there might have been differences at later stages.
- Women that experienced a miscarriage suffer from many PTSD related symptoms (Figure 3)
- The SECPT functions as a less invasive method to induce a acute stress response in women and thus might make studies with traumatized patients easier for both patients and researchers.
- This difference in recovery rate might be an early biological indicator of PTSD related symptoms.

References

1 Afari, N., Ahumada, S. M., Wright, L. J., Mostoufi, S., Golnari, G., Reis, V., & Cuneo, J. G. (2014). Psychological trauma and functional somatic syndromes: a systematic review and meta-analysis. Psychosomatic medicine, 76(1), 2.
2 Kornfield, S. L., Hantsoo, L., & Epperson, C. N. (2018). What does sex have to do with it? The role of sex as a biological variable in the development of posttraumatic stress disorder. Current psychiatry reports, 20(8), 1-8.
3 Farren, J., Jalmbrant, M., Falconieri, N., Mitchell-Jones, N., Bobdiwala, S., Al-Memar, M., ... & Bourne, T. (2020). Posttraumatic stress, anxiety and depression following miscarriage and ectopic pregnancy: a multicentre, prospective, cohort study. American journal of obstetrics and gynecology, 222(4), 367-e1.
4 Sumner, J. A., Kubzansky, L. D., Elkind, M. S., Roberts, A. L., Agnew-Blais, J., Chen, Q., ... & Koenen, K. C. (2015). Trauma exposure and posttraumatic stress disorder symptoms predict onset of cardiovascular events in women. Circulation, 132(4), 251-259.

Acknowledgements

This research project is made possible by the contributions and commitment of all participating parties.

Funding is provided by Staedler Stiftung

The authors declare that there are no conflicts of interest.

MALT

STAEDTLER STIFTUNG

Biological and psychological stress responses after miscarriage: Cross-sectional results from the MALT randomized controlled trial.

Luis Gerber[1,2], Alexandra Braun[1], Markus Müller[1], Nicolas Rohleder[2], Barbara Stein[1], Peter Radermacher[3], Christiane Waller[1]

[1]Paracelsus Medical University, General Hospital Nuremberg, Department of Psychosomatic Medicine and Psychotherapy; [2]Department of Psychology, Chair of Health Psychology, Friedrich-Alexander Universität Erlangen-Nürnberg; [3]Anesthesiological Pathophysiology and Process Engineering, Ulm University Hospital; Contact: luisgerber@live.de

Objective
Traumatic life events have a great impact on the individuals' lives and their mental and physical health. However, few studies target early interventions for the prevention of post-traumatic stress disorder (PTSD) and their psychological and biological impact. The aim of this study is to help understand the difference in psychological and biological stress responses associated with traumatic symptoms between traumatized women and healthy controls.

Methods
Women (N = 23, 18 to 50 years old) who experienced a miscarriage (< 3 months before study inclusion) were recruited via cooperating clinics and counseling centers in Nuremberg. Prior to and after eight individual art therapy sessions, they were exposed to the socially evaluated cold-pressor test (SECPT). We measured biological and psychological stress repsonses and various mental health constructs and compared the results to a healthy control cohort (N = 28) that did not experience any recent traumatic events.

Results
Recently traumatized women scored significantly higher on psychological symptoms, including traumatization, stress and depression. In all biological measurements a significant stress response was observed (time effects: sAmylase: F= 3,961 p= 0,014; Cortisol: F= 17,935 p> 0,001Interleukin 6: F=30,246 p=0,001.) Both groups had a similar stress reactivity in all three measures (n.s.). Traumatized women showed lower overall cortisol (Group effect: F= 333,549 p= 0,031)

Conclusions
The study shows the effect of recent traumatic experiences on biological and psychological stress markers shortly after the traumatizing event. In addition, it highlights that the SECPT is an option to induce a stress response in a clinical setting. Further research is needed to assess the early development of PTSD symptoms and the influence of stress reactivity on the development of these symptoms.

Statistical challenges in clinical trials for rare diseases and how to overcome some of them

Geroldinger M [a, b], Thiel KE [a, b], Laimer M [c], Bauer JW [c], Zimmermann G [a, b]

[a] Team Biostatistics and Big Medical Data, IDA Lab Salzburg, Paracelsus Medical University, Salzburg, Austria
[b] Department of Research and Innovation, Paracelsus Medical University, Salzburg, Austria
[c] Department of Dermatology and Allergology, Paracelsus Medical University, Salzburg, Austria

What is EBStatMax?

A particular dataset from *Epidermolysis Bullosa* (EB) research forms the basis of the so-called *EBStatMax* project, aiming to reanalyze the data using various state-of-the-art methodologies, design recommendations for future trials, devise computational tools for practitioners, and provide educational material.

Statistical Methods for Ordinal Outcomes

Ordinal outcomes, such as *visual analogue scales* or *quality of life* questionnaires, are frequently used in clinical research. From a statistical perspective, these purely ordinal outcomes do not meet the assumptions of classical parametric methods and, hence, should be analyzed using non-parametric methods instead. Moreover, for more complex longitudinal designs (e.g cross-over) , which may include between- as well as within-subject factors, appropriate statistical methods for analyzing purely ordinal outcomes are scarce. In the *EBStatMax* Project several nonparametric approaches were compared neutrally. Especially the ANOVA-type test that is implemented in the R package *nparLD* and *generalized pairwise comparison (GPC) variants* might be promising approaches.

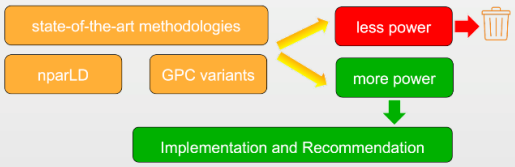

Methods

Various simulation studies were performed, aiming to evaluate which statistical methods should be used for data analysis. Secondly, to facilitate understanding of these non-traditional statistical methods, especially for non-statisticians, one of the main goals was to develop educational materials and a user-friendly application for implementing appropriate methods.

Results

Based on our simulations, various methods could be considered as alternatives to conventional methods. The results reveal that there is not one single best method, since a trade-off between achieving high power, accounting for cross-over period effects, and missing data should be made, but nonparametric approaches perform better with the small sample sizes than traditional methods.

How to educate a heterogenous group about statistical methods?

To better communicate the simulation results to non-statisticians, the educational materials were designed in a modular structure, and using a blended learning concept. Thereby, both biostatistical basics and statistical methods for rare diseases can be presented in a didactically meaningful way.

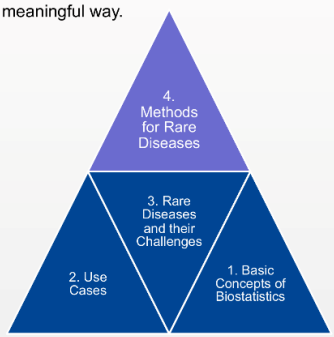

Basically, the aim was to design workshops for a heterogeneous audience as individually and learning-centered as possible. Due to the difference of knowledge in the field of biostatistics, various preliminary considerations were carried out, so that used cases as well as technical sequences are emphasized for statisticians, while biostatistical basics are provided for non-statisticians. This can be implemented effectively using blended learning. In addition, the goal was to construct a joint module in which the methods analyzed in the project for rare diseases in longitudinal study designs would be presented. The advantage of such a structure is that all learners, despite heterogeneity, can be brought to the same level of knowledge through the individualization possibilities, so that they have the required knowledge for the methods module (4).

A User-Friendly Application

For the benefit of the broader scientific community, we aim to spread knowledge gained in the EBStatMax project and make it easily usable in future research on rare diseases. Hence, we develop the *Rare Disease Analyser* (RDA), a web application that implements the statistical methods we examined before. The RDA provides users with recommendations and instructions on which statistical method to choose depending on the study data. Finally, users can perform visual analysis and statistical inference with their study data directly in the RDA.

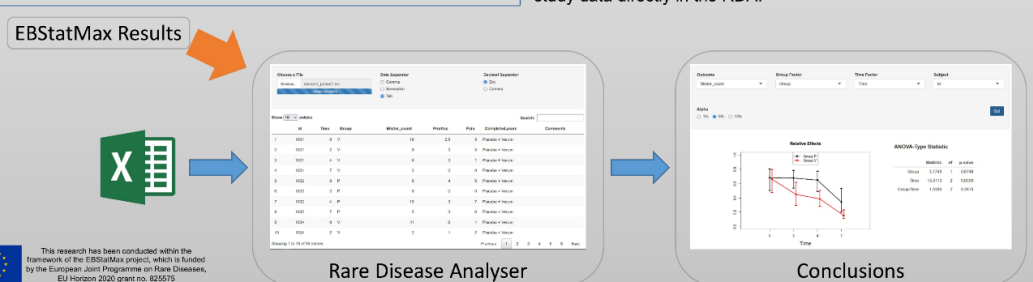

This research has been conducted within the framework of the EBStatMax project, which is funded by the European Joint Programme on Rare Diseases, EU Horizon 2020 grant no. 825575

for further questions: martin.geroldinger@pmu.ac.at

Statistical challenges in clinical trials for rare diseases and how to overcome some of them

Martin Geroldinger[1,2], Konstantin Emil Thiel[1,2], Martin Laimer[3], Johann W Bauer[3], Georg Zimmermann[1,2]

[1]Team Biostatistics and Big Medical Data, IDA Lab Salzburg, Paracelsus Medical University, Salzburg, Austria; [2]Department of Research and Innovation, Paracelsus Medical University, Salzburg, Austria; [3]Department of Dermatology and Allergology, Paracelsus Medical University, Salzburg, Austria; Contact: martin.geroldinger@pmu.ac.at

Objective
Small sample sizes represent a major challenge in drawing conclusions from rare disease trials. A particular dataset from Epidermolysis Bullosa research forms the basis of the so-called EBStatMax project, aiming to reanalyze the data using various state-of-the-art methodologies, design recommendations for future trials, devise computational tools for practitioners, and provide educational material.

Methods
Various simulation studies were performed to assess the impact of statistical methods on data analysis. Secondly, concepts for educational materials and a user-friendly application were developed to improve the understanding of these non-traditional statistical methods especially for non-statisticians and to facilitate their appropriate implementation. In this context, a survey among statisticians and non-statisticians (mainly clinicians and patients) was conducted to address their feedback in the conceptual workflow.

Results
Based on the simulation studies, various methods may be considered as alternatives to conventional methods. The results indicate that there is not one single best method, since a trade-off between achieving high power, accounting for period effects, and missing data must be made. However, nonparametric approaches perform better with the small sample sizes than traditional methods. To better communicate these results to non-statisticians, modularly structured educational materials were designed using a blended learning concept. Thereby, both biostatistical basics and statistical methods for rare diseases can be presented in a didactically meaningful way.

Conclusions
In simulation studies nonparametric statistical approaches yielded good power even in small sample sizes. Provision of web-applications as well as the creation of educational material and guidance papers in collaboration with key stakeholders are intended to boost their implementation.

THE ENHANCER LANDSCAPE PREDETERMINES SKELETAL REGENERATION CAPACITY OF BONE MARROW STROMAL CELLS

Sarah Hochmann[1,§], Kristy Ou[2,§], Rodolphe Poupardin[1§], Michaela Mittermeir[1], Martin Textor[2,3], Salaheddine Ali[2,4,5], Agnes Ellinghaus[2,3], Dorit Jacobi[2,3], Juri A. J. Elmiger[2,3], Samantha Donsante[6], Mara Riminucci[6], Richard Schäfer[7,8], Uwe Kornak[2,4,5,9], Katharina Schmidt-Bleek[2,3], Georg N. Duda[2,3,10], Julia K. Polansky[2,11,12], Sven Geissler[2,3,12,#*] and Dirk Strunk[1,#,*]

[1]Cell Therapy Institute, Spinal Cord Injury and Tissue Regeneration Center Salzburg (SCI-TReCS), Paracelsus Medical University (PMU), 5020 Salzburg, Austria ; [2]BIH Center for Regenerative Therapies (BCRT), Berlin Institute of Health at Charité – Universitätsmedizin Berlin, Charitéplatz 1, 10117, Berlin, Germany; [3]Julius Wolff Institute (JWI), Berlin Institute of Health at Charité – Universitätsmedizin Berlin, Berlin, Germany; [4]Institute for Medical Genetics and Human Genetics, Charité – Universitätsmedizin Berlin, Berlin, Germany; [5] Max Planck Institute for Molecular Genetics, Berlin, Germany; [6]Department of Molecular Medicine, Sapienza University of Rome, Italy; [7]Institute for Transfusion Medicine and Immunohematology, Goethe University Hospital, German Red Cross Blood Service Baden-Württemberg—Hessen gGmbH, Frankfurt am Main; [8]Institute for Transfusion Medicine and Gene Therapy, Medical Center – University of Freiburg, Germany; [9]Institute of Human Genetics, University Medical Center Göttingen, Göttingen, Germany; [10]Wyss Institute for Biologically Inspired Engineering, Harvard, Boston, USA; [11]German Rheumatism Research Centre (DRFZ), Berlin, Germany; [12]Berlin Center for Advanced Therapies (BCAT), Charité Universitätsmedizin Berlin, Berlin, Germany

sarah.hochmann@pmu.ac.at

Multipotent stromal cells are considered an attractive source for cell therapy and tissue engineering. Despite a multitude of experimental and clinical studies, broad application of stromal cell therapeutics is not yet emerging. A major challenge appears to be the functional diversity of available cell sources. Here, we investigated clinically relevant human stromal cells from bone marrow (BMC), white adipose tissue, and umbilical cord compared to mature chondrocytes (CH) and skin fibroblasts, regarding their regenerative potential. We used critical size bone defects as a model system to investigate the endochondral ossification potential and identify differences in multipotency depending on the cell source in vivo and in vitro. Although all stromal cell types express transcription factors related to the regenerative model process of endochondral ossification, only BMCs formed organoid-like cartilage discs in vitro that fully regenerated critical-sized femoral defects after transplantation in vivo. Apparently, a unique cell type-specific epigenetic landscape is the underlying molecular mechanism that controls transcriptional networks of stromal differentiation. Binding sites for common transcription factors in enhancer and promoter regions of ossification-related genes, including Runt and bZIP families, were accessible only in BMC but not in the extra-skeletal stromal cells. Our results suggest an epigenetically predetermined differentiation potential depending on the cell origin that allows common transcription factors to trigger distinct transcriptional programs. Quantification of such epigenetic enhancer signatures would enable a rationale selection of appropriate cell sources for distinct tissue regeneration – as shown here for endochondral processes and thereby help to advance "developmental" regeneration towards precision medicine.

Graphical Abstract

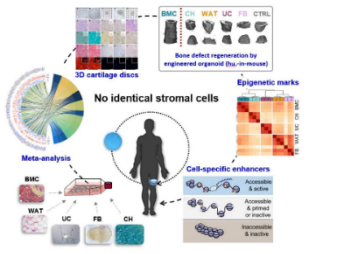

Graphical Abstract: **No identical stromal cells.** Direct comparison of stromal cells combined with stringent molecular, functional and morphological analysis substantiate the selection of chondro-/osteo-competent stromal progenitors for actual skeletal regeneration. Clinically relevant cell sources of MSC were compared for their skeletal gene expression signature in silico and for their chondrogenic competence in a 3 D cartilage organoid assay. Further, complete regeneration of critical size femur defects in NSG mice was only observed with prebuild human BM-derived scaffold-free cartilage organoid transplants after four weeks in vivo, despite maintained presence of human cells in all transplants.

Global Footprint of Stromal Identities

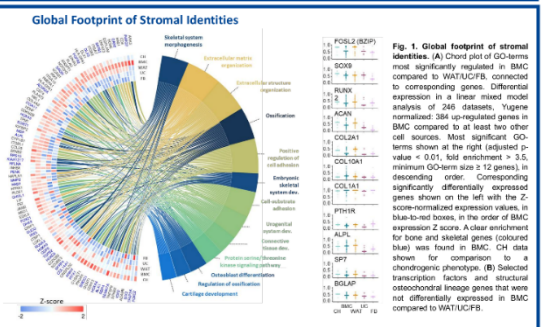

Fig. 1. Global footprint of stromal identities. (**A**) Chord plot of GO-terms most significantly regulated in BMC compared to WAT/UC/FB, connected to corresponding genes. Differential expression in a linear mixed model analysis of 246 datasets, Yugene normalized: 384 up-regulated genes in BMC compared to at least two other cell sources. Most significant GO-terms shown at the right (adjusted p-value < 0.01, fold enrichment > 3.5, minimum GO-term size ≥ 12 genes), in descending order. Corresponding significantly differentially expressed genes shown on the left with the Z-score-normalized expression values, in blue-to-red boxes, in the order of BMC expression Z score. A clear enrichment for bone and skeletal genes (coloured blue) was found in BMC. CH data shown for comparison to a chondrogenic phenotype. (**B**) Selected transcription factors and structural osteochondral lineage genes that were not differentially expressed in BMC compared to WAT/UC/FB.

Histological Examination

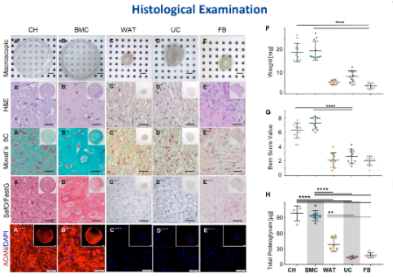

Fig. 2. Cartilage organoid-like disc formation by 3D chondrogenesis. (**A-B**) Macroscopic picture of cartilage discs and (**C-E**) contracted spheroids. (**A´-E´**) Haematoxylin and eosin (H&E) staining. (**A´´-E´´**) Movat's pentachrome (5C) staining showing proteoglycan in blue as stained by the Alcian blue component. (**A´´´-E´´´**) Safranin O/Fast Green (SafO/FastG) matrix staining, also used to determine the Bern score value of the tissue engineered cartilage samples. (**A´´´´-E´´´´**) Aggrecan (ACAN; red) reactivity and DAPI (blue) nuclear staining. (**A-E**) Scale bar 1 mm; all other scale bars 50 µm. (**F**) Weight, (**G**) Bern score values and (**H**) proteoglycan content of day 28 skeletal origin cartilage discs differed significantly from other stromal cell sources. One-way ANOVA, ****p < 0.0001, **p < 0.005; n ≥ 4.

Examination of Bone Transplants

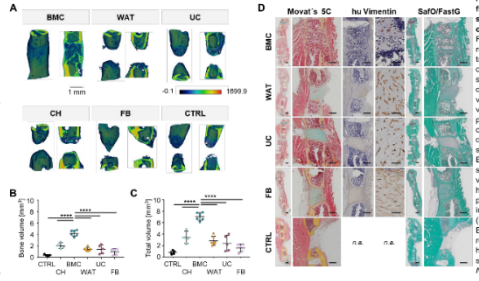

Fig. 3. Murine critical-size femur fracture 28 days after human stromal cell-derived cartilage organoid transplantation. (**A**) Representative 3D micro-CT reconstructions from animals treated as indicated, vs. empty control (CTRL), four weeks after surgery. (**BC**) Quantitative results of micro-CT-measured bone volume (BV) and total tissue volume (TV). (**D**) Movat's pentachrome (5C) staining confirming structural regeneration of femur fracture and marrow space in animals receiving human BMC-derived grafts. (CH grafts shown in Fig.S7). Anti-human (hu) vimentin reactivity confirmed human transplant origin and persistence of morphologically intact cells. Safranin O/Fast Green (SafO/FastG) staining revealed BMC-derived grafts fully remodelled to bone bearing haematopoiesis, four weeks after surgery. N = 4-6; ****p < 0.0001. *Not analysed (n.a.).*

Differences in Active Regulatory Regions

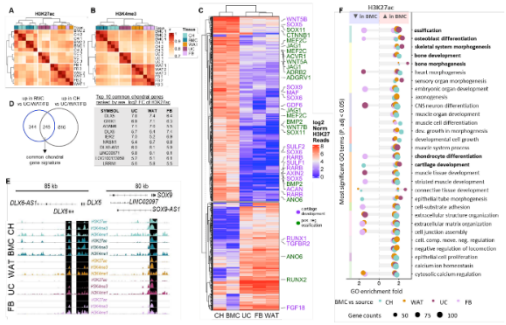

Fig. 4. Global analysis revealed differences in active regulatory regions, which predispose bone marrow stromal cells to superior bone formation. (**A**, **B**) Pearson's correlation plot of log2 RPKM values of (**A**) H3K27ac and (**B**) H3K4me3 peaks. (**C**) Significantly differentially enriched peaks (absolute log2 FC ≥ 2, FDR < 0.05) in BMC vs UC/WAT/FB, and in CH vs UC/FB/WAT. Genes involved in cartilage development and positive regulation of ossification are color-coded. (**D**) Comparison of chondral signatures in BMC and CH compared to UC/WAT/FB (log2 fold-change of H3K27ac ≥ 2, FDR < 0.05). Top 10 chondrogenic genes, ranked by mean log2 fold-change of H3K27ac in BMC vs UC/FB/WAT. (**E**) Genome browser view of H3K27ac, H3K4me1, H3K4me3 histone mark enrichment on *DLX5* and *SOX9* loci. (**F**) GO-term enrichment analysis of H3K27ac differentially significantly decreased ("down" ▼) or increased ("up" ▲) in BMC vs. other sources as color-coded. Peaks "up" in BMC mapped to skeletal genes, suggesting transcriptional activity in undifferentiated BMC compared to other cell types

Selectively Accessible Enhancers for Ossification and Osteoblast Differentiation

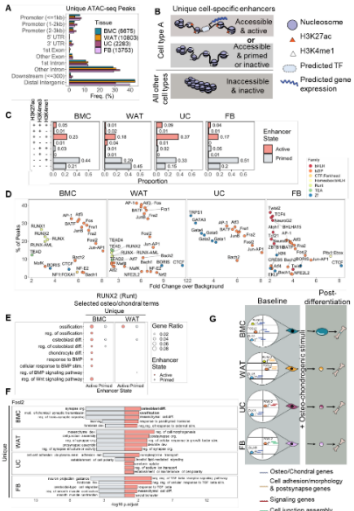

Fig. 5. Selectively accessible enhancers in undifferentiated BMC are important for ossification and osteoblast differentiation. (**A**) Unique tissue-specific peaks obtained by assay for transposase-accessible chromatin sequencing (ATAC-seq), considered as enhancers, primarily mapped to intergenic and intronic regions. (**B**) Schematic depiction of unique cell-specific enhancers. (**C**) Unique ATAC-seq peaks primarily overlapping with enhancer mark H3K4me1. (**D**) Unbiased motif enrichment analysis identified tissue-specific transcription factor motifs in unique ATAC-seq peaks: *GATA* for UC, *bHLH*-family for FB and common *bZIP* family colour-coded as indicated. (**E**) BMC-specific enhancers, mostly active, containing the RUNX2 motif, mapped to genes important for endochondral ossification. WAT-specific RUNX2 enhancers were mostly inactive. (**F**) Top 5 GO-terms for cell-type specific enhancers containing Fos2 motif, stratified by presence (red bars) or absence (grey bars) of overlapping H3K27ac peaks (overlap = active enhancer state). (**G**) Proposed molecular mechanism explaining the propensity of BMC to differentiate into bone-forming cartilage while the other stromal cells do not. Underlying cell type-specific epigenetic features favour basal transcription of osteogenic genes, e.g., by RUNX2 and FOSL2. The same transcription factors have access only to other organotypic enhancers, predicted to drive genes not involved in bone formation.

Here we demonstrate that BMSC harbour a unique capacity to regenerate bone via endochondral ossification, pre-determined at molecular level by the epigenetic landscape. Active enhancers of genes driving osteochondral differentiation were identified to be selectively accessible only in BMSC, but not in other stromal cells tested.

The authors declare no conflict of interest.

THE ENHANCER LANDSCAPE PREDETERMINES SKELETAL REGENERATION CAPACITY OF BONE MARROW STROMAL CELLS

Sarah Hochmann[1], Kristy Ou[2], Rodolphe Poupardin[1], Michaela Mittermeir[1], Martin Textor[2,3], Salaheddine Ali[2,4,5], Agnes Ellinghaus[2,3], Dorit Jacobi[2,3], Juri A. J. Elmiger[2,3], Samantha Donsante[6], Mara Riminucci[6], Richard Schäfer[7,8], Uwe Kornak[2,4,5,9], Katharina Schmidt-Bleek[2,3], Georg N. Duda[2,3,10], Julia K. Polansky[2,11,12], Sven Geissler[2,3,12], Dirk Strunk[1]

[1]Cell Therapy Institute, Spinal Cord Injury and Tissue Regeneration Center Salzburg (SCI-TReCS), Paracelsus Medical University (PMU), 5020 Salzburg, Austria; [2]BIH Center for Regenerative Therapies (BCRT), Berlin Institute of Health at Charité – Universitätsmedizin Berlin, Charitéplatz 1, 10117, Berlin, Germany; [3]Julius Wolff Institute (JWI), Berlin Institute of Health at Charité – Universitätsmedizin Berlin, Berlin, Germany; [4]Institute for Medical Genetics and Human Genetics, Charité – Universitätsmedizin Berlin, Berlin, Germany; [5]Max Planck Institute for Molecular Genetics, Berlin, Germany; [6]Department of Molecular Medicine, Sapienza University of Rome, Italy; [7]Institute for Transfusion Medicine and Immunohematology, Goethe University Hospital, German Red Cross Blood Service Baden-Württemberg—Hessen gGmbH, Frankfurt am Main; [8]Institute for Transfusion Medicine and Gene Therapy, Medical Center – University of Freiburg, Germany; [9]Institute of Human Genetics, University Medical Center Göttingen, Göttingen, Germany; [10]Wyss Institute for Biologically Inspired Engineering, Harvard, Boston, USA; [11]German Rheumatism Research Centre (DRFZ), Berlin, Germany; [12]Berlin Center for Advanced Therapies (BECAT), Charité Universitätsmedizin Berlin, Berlin, Germany; Contact: sarah.hochmann@pmu.ac.at

Objective
Critical-size bone fractures remain a global challenge. Rational selection of functional engineered cell transplants would advance bone regeneration towards precision medicine. We compared clinically relevant stromal cells from adult human bone marrow (BM), white adipose tissue (WAT) and umbilical cord (UC) to mature chondrocytes (CH) and skin fibroblasts (FB) for gene expression signature, 3D cartilage organoidogenesis, epigenomic landscape and in vivo fracture healing.

Results
Comprehensive gene expression meta-analysis revealed significant over-representation of skeletal-related genes in BM and CH, correlating with cartilage formation. Relevant osteochondral transcription factors were expressed in all stromal populations, indicating additional molecular players being decisive during endochondral bone regeneration. We found an underlying epigenetic landscape pre-determining bone regeneration. Transcription factor binding sites of common transcription factor families including Runt and bZIP were selectively accessible in enhancers and promoters of ossification-related genes in BM. Complete regeneration of critical size femur defects in a humanized mouse model was observed only with prebuild human BM-derived scaffold-free cartilage organoid transplants.

Conclusions
Results suggest an epigenetically pre-determined differentiation potential facilitating common transcription factors to evoke distinct transcriptional programs, in BMC particularly for skeletal differentiation. BMSC-derived cartilage disc transplantation demonstrates translation into a novel skeletal regeneration strategy.

PARACELSUS MEDIZINISCHE PRIVATUNIVERSITÄT

Klinikum Nürnberg
wir sind für Sie da!

Stem Cell Apheresis: Accuracy of the prediction of the stem cell yield using pre-apheresis CD34⁺ cell count.

Authors: Hornung M., Schaefer-Eckart K., Wendelin K., Dressler, S., Kerache F., Knop S., Gaertner J.

Bone Marrow Transplantation Unit Nuremberg, Department of Oncology and Hematology, Paracelsus Medical University Nuremberg

INTRODUCTION

Accurate prediction of the stem cell yield is essential for planning and executing of the PBSC leucapheresis procedure. Calculation based on pre-apheresis peripheral CD34+ cell count usually shows a good correlation between predicted and actually collected cell count, however slight underestimation and overestimation occurs.

METHODS

We calculated the predicted CD34⁺ yield with the following method[1]:

$$\textbf{Predicted CD34}^{+}\ \textit{per kg Patient Weight} = \frac{\textit{Benchmark CE}^{*} \times \textit{Processed Blood Volume} \times \textit{CD34 Count Donor}}{\textit{Patients Weight in kg} \times 10.000\ (\textit{Metric Conversion Factor})}$$

(*Benchmark CE = collection efficiency coefficient, center specific)

Data were retrospectively analyzed and divided into 3 subgroups, based on their accuracy of the prediction of the calculated CD34⁺ yield compared with the actually collected CD34⁺ count. The results of the 3 subgroups were underestimated (UE, 15% below predicted CD34⁺ yield), overestimated (OE, 15% above predicted CD34⁺ yield) and good estimation (GE, within +/- 15%) were compared with an ANOVA analysis. Additionally, multiple clinical and laboratory data were evaluated. We also investigated possible factors affecting the stem cell mobilizing capacity (table 1).

OBJECTIVES

- Evaluation of the predictive accuracy of the expected number of CD34⁺ cells collection using our formula.
- Identification of factors influencing the accuracy leading to overestimation, underestimation or good estimation.
- Identification of factors influencing the G-CSF dependent mobilization capacity of CD34⁺ cells.

RESULTS

We investigated 607 G-CSF mobilized apheresis (569 donors) procedures during the years 2019 – 2020. The mean value of prediction coefficient (PC) for all apheresis procedures was **1.06**. The Spearman's correlation coefficient (r) between the calculated and actually collected CD34⁺ cells per kg bodyweight recipient was 0.9126 (P<0.01), which indicates a very reliable prediction over this 2 years.

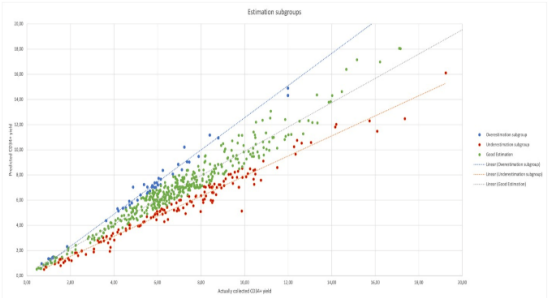

Graph 1: Correlation of predicted and actually collected CD34⁺ cells divided into the 3 subgroups

RESULTS

Most of the collections (66%) showed a very good correlation between predicted and finally collected stem cell count. The OE subgroup contained only 49 (8%) apheresis procedures and the UE subgroup consisted of 155 (26%) procedures (Graph 1).

The mean prediction coefficient of the OE subgroup was 0.81 and of the UE subgroup 1.29 .

The analysis of clinical and laboratory data revealed in the UE subgroup a significant lower CD34⁺ per µl pre-apheresis count, as well as a trend to lower ferritin levels. The underestimation leads to slightly higher than estimated results, so frequently we nevertheless collected a more than sufficient product.

To identify factors influencing the ability to mobilize stem cells we evaluated clinical and laboratory data (table 1) at the time of the initial donor evaluation.

In the statistical analysis for the mobilization capacity only the WBC count, the platelets, the gender (male) and the BMI at time of donor evaluation showed positive, significant correlation.

Mobilizing Capacity		
WBC	Significant	$p = 1.52 \times 10^{-6}$
Platelets	Significant	p = 0.00398
Gender (male)	Significant	p = 0.03037
BMI	Significant	p = 0.01640
Age, Hb, Hkt, MCV, MCH, hepatic steatosis, splenomegaly, WBC, iron, bilirubin, GOT, GPT and ferritin	Non-significant	

Table 1: Overview of the factors influencing mobilizing capacity
BMI = body mass index, Hb = hemoglobin, Hkt = hematokrit, GOT = glutamate-oxalacetate-transaminase, GPT = glutamate-pyruvate-transaminase, LDH = lactate dehydrogenase, MCH = mean corpuscular haemoglobin, MCV = mean corpuscular volume, WBC = white blood cells

CONCLUSION

- Our method of calculating the stem cell yield is highly predictive of the number of CD34⁺ cells actually collected, making planning and adjusting of the apheresis procedure very reliable.
- For donors with low pre-apheresis CD34⁺ count and who are critical to meet the threshold for a successful apheresis, the calculation tends to underestimate the CD34⁺ yield which leads to a better than calculated collection. On the contrary, the clinical more adverse overestimation occurred predominately in the range of more than sufficient apheresis.
- For clinical practice, in case the donors estimated stem cell yield is just below the threshold for a successful collection, we maximize the processed blood volume using higher inlet flow rates and longer procedure time. On the other hand, in the event of a more than sufficient stem cell yield calculation, reducing the procedure time turned out to be safe and reliable.
- Concerning mobilizing capacity, donors with high WBC, high platelets, male gender, and high BMI at the time of the initial donor evaluation showed better mobilization of peripheral stem cells. Accordingly, women with low BMI are at risk for low mobilization.

[1] Pierelli et al., Vox Sanguinis (2006)91:126-34.

Stem Cell Apheresis: Accuracy of the Prediction of the Stem Cell Yield using Pre-Apheresis CD34+ Cell Count

Maximilian Hornung[1], Kerstin Schaefer-Eckart[1], Knut Wendelin[1], Sabine Dressler[1], Francoise Kerache[1], Stefan Knop[1], Johannes Gaertner[1]

[1]Department of Bone Marrow Transplantation, Paracelsus Medical University, Nuremberg, Germany; Contact: maximilian.hornung@stud.pmu.ac.at

Objective
Evaluation of the predictive accuracy of the expected number of CD34+ cells collection using our formula.
Identification of factors influencing the accuracy leading to overestimation, underestimation or good estimation.
Identification of factors influencing the G-CSF dependent mobilization capacity of CD34+ cells.

Methods
We calculated the predicted CD34+ yield with the following method[1]:
Predicted CD34+x10^6/kg = (benchmark collection efficacy x processed blood volume x peripheral CD34+ count per µl) / (patient's weight x metric conversion factor).
Data were retrospectively analyzed and divided into 3 subgroups, based on their accuracy of the calculated CD34+ yield compared with the actually collected CD34+ count. The results of the 3 subgroups which were underestimated (UE, 15% below predicted CD34+ yield), overestimated (OE, 15% above predicted CD34+ yield) and good estimation (GE, within +/- 15%) were compared with an ANOVA analysis. Additionally, multiple clinical and laboratory data were evaluated.

Results
We investigated 607 apheresis (569 donors) procedures during the years 2019-2020. The mean value of the prediction coefficient for all apheresis procedures was 1.06. The Spearman´s correlation coefficient (r) between calculated and actually collected CD34+ cells per kg bodyweight recipient was 0.9126 ($p< 0.01$), which indicates a very reliable prediction over this 2 years. Most of the collections (66%) showed a very good correlation between predicted and finally collected stem cell count. The OE subgroup consisted of only 8% apheresis procedures and the UE subgroup of only 26%. The mean prediction coefficient of the UE was 1.29 and of the OE subgroup 0.81. The analysis of clinical and laboratory data revealed a significantly lower CD34+/µl pre apheresis count in the UE group, as well as a trend to lower ferritin blood levels. The underestimation leads to slightly higher results than estimated, so these collections resulted in more than sufficient products.

Conclusions
Our method of calculating the stem cell yield is highly predictive of the number of CD34+ cells actually collected, making planning and adjusting of the apheresis procedure very reliable. For donors with low pre apheresis CD34+ count and who are critical to meet the threshold for a successful apheresis, the calculation tends to underestimate the CD34+ yield which leads to a better than calculated collection. On the contrary, the clinical more adverse overestimation occurred predominately in the range of more than sufficient apheresis. For clinical practice, in case the donors estimated stem cell yield is just below the threshold for a successful collection, we maximize the processed blood flow volume using higher inlet flow rates and longer procedure times. On the other hand, in the event of a more than sufficient stem cell yield calculation, reducing the procedure time turned out to be safe and reliable.

References
1. Pierelli et al., Vox Sanguinis (2006)91:126-34.

Health data democratization in Austria: Patients' perspective

R Hussein[1], A Stainer-Hochgatterer[1], J Niebauer[1,2] , T Palfinger[3], and R Kaisler[3]
1: Ludwig Boltzmann Institute for Digital Health and Prevention, Salzburg, Austria, 2: Institute of Sports Medicine, Prevention and Rehabilitation, Paracelsus Medical University, Salzburg, Austria, 3: Ludwig Boltzmann Gesellschaft (LBG), LBG Open Innovation in Science Center, Vienna, Austria

OBJECTIVE

During the last decade, mobile health (mHealth) has played an essential role in realizing participatory medicine, in which the patients' voice is vital for their healthcare management (1). This necessitates the integration of mHealth data (patient-generated health data) and the National Electronic Health Record (ELGA in Austria). To achieve this connected health model, data sharing is a prerequisite (2). In Europe, there is a high potential and willingness to have better citizens' access to and sharing of health data reported through the Digital Health in Europe project (3). Accordingly, we organized a workshop in April 2021 with patients living with chronic diseases to discuss health data democratization, ownership, and sharing in Austria.

METHODS

We conducted an online co-creation 3-hours workshop with 9 patients, 6 digital health stakeholders, and a representative from ELGA. Before the workshop, we sent background material and videos on ELGA, General Data Protection Regulation (GDPR) to set the participants' backgrounds. The workshop started with a presentation on the status quo of health data management in Austria.

This was followed by the co-creation of content in small groups (4-5 participants; open space method, each 20 min rotate) facilitated by a moderator. The groups discussed three topics by answering guided questions for each topic:

- Topic 1: Definition of health data
- Topic 2: Needs and access to health data
- Topic 3: Motivation and incentives for sharing health data

The workshop ended with the facilitators' presentations on each topic, collecting open questions, and prioritizing/disagreement of proposed solutions (utilizing the Padlet digital notice board for each topic).

TOPIC 1: DEFINITION OF HEALTH DATA

Question: Which health data would you like to share with researchers and medical professionals via the ELGA system (heart rate, blood pressure, blood sugar level, etc.)? Which personal devices would be suitable?

TOPIC 2: NEEDS AND ACCESS TO HEALTH DATA

Question: Which conditions need to be fulfilled to share my health data? (e.g., options about the use of my health data, restriction/limitations of access to my health data, etc.)

TOPIC 3: MOTIVATION AND INCENTIVES FOR SHARING HEALTH DATA

Question: Which kind of incentives do you expect of sharing your data for research and medical professionals?

- Workshop topics and guided questions

WORKSHOP LEARNING OBJECTIVES

- Learn about the status quo of health data management in Austria
- Learn about reasons to share health data with science
- Learn about the types of health data, ownership, and their legal rights
- Define which type of data they would like to share under which conditions and circumstances
- Address their preferences and needs regarding the health data's access and ownership
- Address their motivation and possible incentives to share their health data

RESULTS

We analyzed the 3 Padlet boards to conclude the main findings and recommendations. Participants showed their willingness to share health data for clinical and research purposes, provided that concerns on data privacy, fear of discrimination, or abuse of commercial benefits are resolved. They also showed great interest in having more transparent and enhanced communication with ELGA services

- Part of the Padlet board for health data

Concerns about sharing health data

Factors enabling willingness to share health data

RECOMMENDATIONS

- A new model for data altruism, including a data-sharing incentive framework, is highly recommended.

CONCLUSIONS

Connected health has created opportunities for realizing preventive and personalized health care services. Citizens' empowerment and engagement in managing their healthcare will be a crucial game-changer for future medicine.

REFERENCES

1. Woods SS, Evans NC, Frisbee KL. Integrating patient voices into health information for self-care and patient-clinician partnerships: Veterans Affairs design recommendations for patient-generated data applications. J Am Med Inform Assoc. 2016 May;23(3):491-5. doi: 10.1093/jamia/ocv109. Epub 2016 Feb 5. PMID: 26911810.

2. Karampela M, Ouhbi S, Isomursu M Connected Health User Willingness to Share Personal Health Data: Questionnaire Study J Med Internet Res 2019;21(11):e14537 URL: https://www.jmir.org/2019/11/e14537. DOI: 10.2196/14537

3. Digital Health Europe Project – DigitalHealthEurope [Internet]. DigitalHealthEurope. [cited 2022 Apr 1]. Available from: https://digitalhealtheurope.eu/.

Corresponding author: Rada Hussein, PhD, FIAHSI | Mail: rada.Hussein@dhp.lbg.ac.at

Health data democratization in Austria: Patients' perspective

Rada Hussein[1], Andreas Stainer-Hochgatterer[1], Josef Niebauer[1,2], Thomas Palfinger[3], Raphaela Kaisler[3]

[1]Ludwig Boltzmann Institute for Digital Health and Prevention, Salzburg, Austria; [2]Institute of Sports Medicine, Prevention and Rehabilitation, Paracelsus Medical University, Salzburg, Austria; [3]Ludwig Boltzmann Gesellschaft (LBG), LBG Open Innovation in Science Center, Vienna, Austria; Contact: rada.hussein@dhp.lbg.ac.at

Objective
During the last decade, mobile health (mHealth) has played an essential role in realizing participatory medicine, in which the patients' voice is vital for their healthcare management (1). This necessitates the integration of mHealth data (patient-generated health data) and the National Electronic Health Record (ELGA in Austria). To achieve this connected health model, data sharing is a prerequisite (2). In Europe, there is a high potential and willingness to have better citizens' access to and sharing of health data reported through the Digital Health in Europe project (3). Accordingly, we organized a workshop in April 2021 with patients living with chronic diseases to discuss health data democratization, ownership, and sharing in Austria.

Methods
We conducted an online co-creation 3-hours workshop with 9 patients, 6 digital health stakeholders, and a representative from ELGA. Before the workshop, we sent background material and videos on ELGA, General Data Protection Regulation (GDPR) to set the participants' backgrounds. The workshop started with a presentation on the status quo of health data management in Austria.
This was followed by the co-creation of content in small groups (4-5 participants; open space method, each 20 min rotate) facilitated by a moderator. The groups discussed three topics by answering three guided questions for each topic: *Topic 1: Definition of health data Topic 2: Needs and access to health data Topic 3: Motivation and incentives for sharing health data*
The workshop ended with the facilitators' presentations on each topic, collecting open questions, and prioritizing/disagreement of proposed solutions (utilizing Padlet digital notice board for each topic).
After the workshop, the 3 Padlet boards were analyzed to conclude the main findings and recommendations.

Results
Participants showed their willingness to share health data for clinical and research purposes, provided that concerns on data privacy, fear of discrimination or abuse of commercial benefits are resolved. They also showed great interest in having more transparent and enhanced communication with ELGA services. A new model for data altruism, including data sharing incentive, is highly recommended.

Conclusions
Connected health has created opportunities for realizing preventive and personalized health care services. Citizens' empowerment and engagement in managing their healthcare will be a crucial game-changer for future medicine.

References
1. Woods SS, Evans NC, Frisbee KL. Integrating patient voices into health information for self-care and patient-clinician partnerships: Veterans Affairs design recommendations for patient-generated data applications. J Am Med Inform Assoc. 2016 May;23(3):491-5.
2. Karampela M, Ouhbi S, Isomursu M Connected Health User Willingness to Share Personal Health Data: Questionnaire Study J Med Internet Res 2019;21(11):e14537.
3. Digital Health Europe Project – DigitalHealthEurope [Internet]. DigitalHealthEurope. [cited 2022 Apr 1]. Available from: https://digitalhealtheurope.eu/.

Larks are more conscientiousness

The six main facets of conscientiousness

- Competence
- Orderliness
- Sense of duty
- Achievement striving
- Self-discipline
- Prudence

Methods & Design

- *n* = 1231 for Pearson Correlation
- To figure out the chronotype the Composite scale of morningness (CSM) with an α=.86 was performed
- To figure out the personality dimensions, the Big five inventory (BFI-10) with an α=.78 – α=.90
- Secondary variables, age groups (10-17) and (18-47)

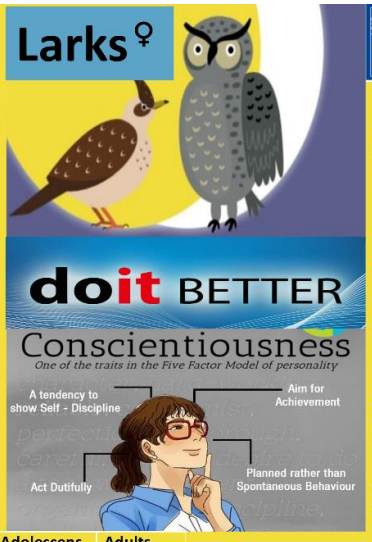

Results

		CSM score	Male	Female	Adolescens (10-17 y)	Adults (18-47 y)
Extraversion	n	1231	576	649	.029	305
	r	.007	-.052	.071	920	-.034
Agreeableness	n	1229	574	649	918	305
	r	.130	.094	.132	.105	.040
Conscientiousness	n	1229	574	649	919	304
	r	.336	.342	.412	.370	.289
Neuroticism	n	1229	575	648	918	305
	r	.016	-.043	-.079	-.073	-.012
Openness	n	1229	575	648	918	305
	r	.020	-.007	.070	.038	.007

Conlusion

Conscientiousness correlated positively and according to Cohen moderate with chronotype morningsuitability. Conscientiousness thus stood out significant (according to the Fisher´s z-transformation of all coefficients) from all other facets of conscientiousness in relation to morningsuitability. The second outcome is, that women achieved a higher coefficient than men. These results are the first conclusions of the PhD thesis and will be examined and validated during the studies in order to create a profiling for shift workers.

PARACELSUS MEDIZINISCHE PRIVATUNIVERSITÄT

Presenter:
Maik P. Jaskolka
PhD Candidate
Lecturer for quantitative methods

References/Credits

1. Randler, C. (2008). Morningness–eveningness, sleep–wake variables and big five personality factors. *Personality and Individual Differences, 45*(2), 191–196. https://doi.org/10.1016/j.paid.2008.03.007

2. Costa, P. McCrae, R. & Dye, D. (1991). Facet Scales for Agreeableness and Conscientiousness: A Revision of the NEO Personality Inventory. *Personality and Individual Differences, 12*(9), 887-898. https://www.researchgate.net/deref/http%3A%2F%2Fdx.doi.org%2F10.1016%2F0191-8869(91)90177-D

Prof. Dr. Lenče Miloševa: Faculty for Medical Sciences University Goce Delcev Stip. North Macedonia
Prof. Dr. Eleonore Soei-Winkels: FOM Düsseldorf
Prof. Dr. med. MHBA Kneginja Richter: Outclinic for Sleep Medicine, University Clinic for Psychiatry and Psychotherapy PMU Nuremberg, Technische Hochschule, Nuremberg

Larks are more conscientiousness

Maik P. Jaskolka[1], Lenče Miloševa[2], Eleonore Soei-Winkels[3], Kneginja Richter[4]

[1]Paracelsus Medical University, Nuremberg, Germany; [2]Faculty for Medical Sciences University Goce Delcev Stip. North Macedonia; [3]FOM Hochschule für Oekonomie & Management, Düsseldorf; [4]Outclinic for Sleep Medicine, University Clinic for Psychiatry and Psychotherapy PMU Nuremberg, Faculty for Medical Sciences University Goce Delcev Stip. North Macedonia, Technische Hochschule, Nuremberg; Contact: maik.jaskolka@stud.pmu.ac.at

Objective
The aim of this study was to find out whether there is a connection between the chronotype and various sleep-wake variables and the "Big Five" (super factors of personality). The "Big Five" are defined as follows: extraversion, neuroticism, openness, agreeableness and conscientiousness.

Methods
Sample A total of 1231 participants took part in this voluntary study. There were 652 female participants and 579 male participants, divided into two age groups, age group 10-17 and age group 18-47. The mean age was (*MW* = 15.76) with a standard deviation of (*SD* = 4.83).
Measurement instruments Composite Scale of Morningness (CSM; Smith, Reilly, & Midkiff, 1989) was used to determine the chronotype. The Cronbach's alpha coefficient of the CSM for the present sample was α=.86 (internal consistency), which demonstrates a very high reliability. To measure the "Big Five", the short version of the "Big Five" Inventory by Rammstedt and John (2007) was used. The Cronbach's alpha coefficients of the five different scales range between α=.78 - α=.90, which reflects good to very good reliability. The correlation between morning sleepiness and personality was calculated using a zero-order Pearson product-moment correlation and controlled for age using a first-order partial correlation. In addition, men and women and adolescents/adults were considered separately.

Results
The main finding of this study was that morningsuitability correlated with conscientiousness $r(1229)=.336$, $p<.001$. The women's group scored $r(647)=.412$, $p<.001$ and the men's group scored $r(.574)=.342$, $p<.001$. A correlation was also found between morningsuitability and agreeableness $r(1229)=.130$, $p<.001$.

Conclusions
The study showed that there is an effect between morningsuitability and conscientiousness, the correlation coefficient of $r=.336$ means according to Cohen that there is a medium effect. Low effects of $r=.1$-$r=.3$ according to Cohen have no relevance in psychological research, for this reason the correlation between morningsuitability and the other super factors of personality with an effect of $r=.020$-$r=.130$ is not taken into account. The women's group with an $r=.412$, scored better than the men's group with an $r=.342$, but according to the Fisher z-transformation this result is not significant ($z=-1.42$, $p=.078$). All other super factors of personality are significantly different from the super factor conscientiousness in terms of morningsuitability according to Fisher's z-transformation.

References
1. Randler, C. (2008). Morningness–eveningness, sleep–wake variables and big five personality factors. Personality and Individual Differences, 45(2), 191–196. https://doi.org/10.1016/j.paid.2008.03.007
2. Costa, P. McCrae, R. & Dye, D. (1991). Facet Scales for Agreeableness and Conscientiousness: A Revision of the NEO Personality Inventory. Personality and Individual Differences, 12(9), 887-898. https://www.researchgate.net/deref/http%3A%2F%2Fdx.doi.org%2F10.1016%2F0191-8869(91)90177-D

Factors influencing the SARS-CoV-2 spike-protein specific IgG antibody response

Tanja Karl[1], Tanja Stiboller[1], Gabriele Dobrovoljski[2], Gertie J. Oostingh[1]

[1] Department of Biomedical Sciences, Salzburg University of Applied Sciences, Puch/Salzburg, Austria
[2] Department of Paediatrics, Paracelsus Medical University, Salzburg, Austria

Introduction

Due to the ongoing severe acute respiratory syndrome coronavirus 2 (SARS-CoV-2) pandemic, many questions concerning the antibody response after vaccination and infection occurred. The aim of this study is, to investigate which factors (e.g., age, body-mass-index (BMI), gender, primary disease or type of vaccine) influence the height of the SARS-CoV-2-specific IgG antibody levels after vaccination, infection or a combination of both.

Methods

A single venous blood sample (serum, 3 ml) was taken from 558 adult volunteers with an average age of 40 years. All participants were either vaccinated and/or recovered from COVID-19 infection. A questionnaire was handed out including anthropometric data, pre-existing conditions and chronic diseases to assess the health status of the participants. The dates of the SARS-CoV-2-vaccinations and information on Covid-19 Infections were also obtained. SARS-CoV-2 spike-protein-specific IgG was then analyzed with an automated chemiluminescence immunoassay by using the VITROS® Anti-SARS-CoV-2 IgG method. Results are displayed in binding-antibody-units (BAU) per ml.

Figure 1 venous blood sampling

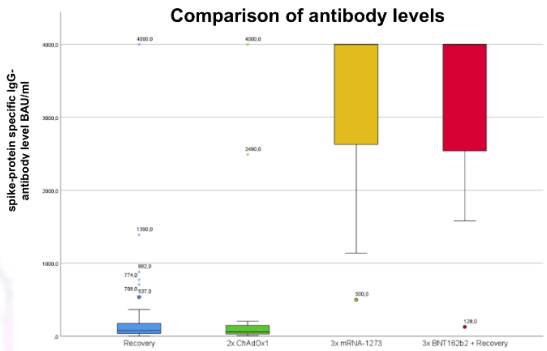

Figure 1 Box-plot diagram with the most significant differences in antibody levels between the different groups.Participants recovered from COVID-19 (n=57) or vaccinated with 2x ChAdOx1 (n=23) show overall low antibody levels. Higher antibody levels can be seen in participants vaccinated with 3x mRNA-1273 (n=26) or 3x BNT162b2 and additional recovery (n=15).

Figure 3 loading the VITROS carousel with samples

Current results

Regarding the different types of COVID-19 vaccines, the highest mean IgG antibody levels were observed in participants vaccinated with 3x mRNA-1273 (Spikevax) or 3x BNT162b2 (Comirnaty) with additional recovery. Low mean antibody levels can be seen in recovered participants and in those, who received 2x ChAdOx1 (Vaxzevria). So far, correlation analysis between antibody level and BMI, age or gender did not show a significant correlation between these parameters.

Discussion & Outlook

As expected, 98.4% of the participants were positive for SARS-CoV-2 spike-protein-specific IgG-antibodies, whereby a difference can be detected depending on the vaccines used and the fact whether a SARS-CoV-2 infection took place. The research on this topic is still ongoing. Further participants are currently recruited with the aim of including 2,000 participants to improve the strength of the obtained data.

This study was approved by the local ethics committee and is registered in the BASG registry.

Factors influencing the SARS-CoV-2 spike-protein specific IgG antibody response

Tanja Karl[1], Tanja Stiboller[1], Gabriele Dobrovoljski[2], Gertie J. Oostingh[1]

[1]Department of Biomedical Sciences, Salzburg University of Applied Sciences, Puch/Salzburg, Austria; [2]Department of Paediatrics, Paracelsus Medical University, Salzburg, Austria; Contact: tanja.karl@fh-salzburg.ac.at

Objective

Due to the ongoing severe acute respiratory syndrome corona virus 2 (SARS-CoV-2) pandemic, many questions concerning the antibody response after vaccination and infection occurred. The aim of this study is, to investigate which factors (e.g. age, body-mass-index (BMI), gender, primary disease or type of vaccine) influence the height of the SARS-CoV-2 spike-protein-specific IgG antibody level. In contrast to SARS-CoV-2-specific IgA and IgM, IgG shows stable concentrations for at least 8 months (1). The concentration of IgG antibodies binding specifically to the spike-protein correlates with the amount neutralizing antibodies in patient samples (2). These spike-protein-specific antibodies can not only be found after a natural infection but also after vaccination with COVID-vaccines (3).

Methods

A single venous blood sample (serum, 3 ml) was taken from 558 adult volunteers with an average age of 40 years. All participants are either vaccinated and/or recovered from COVID-19. A questionnaire was handed out including anthropometric data, pre-existing conditions and chronic diseases to assess the health status of the participants. The dates of the SARS-CoV-2-vaccinations and information on Covid-19 Infections were also obtained. SARS-CoV-2 spike-protein-specific IgG was then analyzed with an automated chemiluminescence immunoassay by using the VITROS® Anti-SARS-CoV-2 IgG detection method. Results are presented in binding-antibody-units (BAU) per ml. This study was approved by the local ethics committee and is registered in the BASG-registry

Results

Regarding the different types of COVID-19 vaccines, the highest mean IgG antibody levels are observed in participants vaccinated with 3x mRNA-1273 (Spikevax) or 3x BNT162b2 (Comirnaty) with additional recovery. Low mean antibody levels can be seen in recovered participants and in those, who received 2x ChAdOx1 (Vaxzevria). Correlation analysis between antibody level and BMI, age or gender did not show significant effects between those parameters.

Conclusions

As expected, 98.4 % of the participants were positive for SARS-CoV-2 spike-protein-specific IgG-antibodies. Interestingly, differences in antibody levels between the different groups of participants, divided according to the received vaccines or natural infection, can be noticed. Nevertheless, the research about this topic is still ongoing. Further participants will be recruited during the next months to reach a final amount of 2,000 participants to improve the strength of the obtained data.

References

1. Cohen KW, et al., 2021. Longitudinal analysis shows durable and broad immune memory after SARS-CoV-2 infection with persisting antibody responses and memory B and T cells. Cell Reports Medicine 2:100354.
2. Legros V, et al., 2021. A longitudinal study of SARS-CoV-2-infected patients reveals a high correlation between neutralizing antibodies and COVID-19 severity. Cellular & Molecular Immunology 18:318-327.
3. Bongiovanni M, et al. 2021. Evaluation of the immune response to COVID-19 vaccine mRNA BNT162b2 and correlation with previous COVID-19 infection. Journal of Clinical Virology 143:104962.

In silico investigation of fadrozole isomer selectivity to cortisol synthase (CYP11B1) and aldosterone synthase (CYP11B2)

Jakub Kollar, Evelyn Hafele, Daniela Schuster
Paracelsus Medical University, Institute of Pharmacy, Department of Pharmaceutical and Medicinal Chemistry

1. Introduction and aims

Fadrozole (fig. 1), a drug approved in Japan to treat breast cancer, is a known inhibitor of aromatase (estrogen synthase, CYP19A1). It also binds to other targets such as cortisol synthase (CYP11B1) and aldosterone synthase (CYP11B2), inhibiting their enzymatic activity. Therefore, its effects can be detrimental due to inhibition of aldosterone or cortisol production. Interestingly, its effect seems to be stereospecific. R-fadrozole is known to inhibit CYP11B2, but not CYP11B1 and aromatase. S-fadrozole on the other hand is known to inhibit CYP11B1 and aromatase, but not CYP11B2.

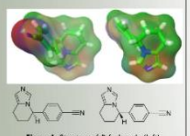

Figure 1. Structure of R-fadrozole (left) and S-fadrozole (right).

In this work, we set out to explore why S-fadrozole preferably inhibits CYP11B1 enzyme and R-fadrozole CYP11B2 enzyme.

CYP11B1 and CYP11B2 each consist of 503 amino acids. Their primary structures show 93 % sequence identity. Interestingly, non-identical amino acids are localized outside of the binding pocket [1]. Although the ligand binding pocket is lined with identical amino acids, the following residues adopt different 3D conformations: Phe231, Phe381, Phe487, Ile488, Trp116, Trp260, and Ala313 [1]. To visualize the differences in the binding site of CYP11B1 and CYP11B2 and the corresponding binding modes of R- and S-fadrozole, alignment of the active site of these enzymes is depicted in fig. 2.
An overlay of the only available crystal structure of CYP11B1 (PDB ID 6M7X – co-crystallized with S-fadrozole) with three crystal structures of CYP11B2 (PDB IDs 4FDH, 4DVQ and 6XZ9, co-crystallized with R-fadrozole, natural ligand deoxycorticosterone, and an inhibitor, respectively) shows that Phe231 and Phe487 adopt the same conformation in all CYP11B2 complexes regardless of the ligand present, while having a different conformation in CYP11B1 (fig. 3).

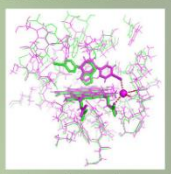

Figure 2. Alignment of the crystal structures of the CYP11B2 complexed with R-fadrozole (green) and CYP11B1 complexed with S-fadrozole (magenta). The enzymes binding pocket is similar, however, spans in opposite directions defined by R- and S-fadrozole. CYP11B1 contains
one crystallographic water molecule in the active site (magenta sphere) hydrogen bonding to cyano group of S-fadrozole, heme group and twice to Glu383 backbone.

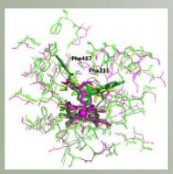

Figure 3. Comparison of the binding cavities of the CYP11B1 enzyme co-crystallized with S-fadrozole (magenta) with three crystal structures of CYP11B2 enzyme co-crystallized with R-fadrozole (green), natural ligand deoxycorticosterone (light green) and an inhibitor (dark green).
Regardless of the ligand bound in CYP11B2 active site, Phe231 and Phe487 adopt the same conformation that is different from the conformation in CYP11B1.

2. Workflow and methods

Protein structures retrieval
Crystal structures of CYP11B1 co-crystallized with S-fadrozole and CYP11B2 co-crystallized with R-fadrozole were retrieved from PDB database [2] under PDB IDs 6M7X [1] and 4FDH [3], respectively.

Docking
The docking was carried out using the GOLD software package [4]. Ligands were generated in 2D and converted into 3D structures using OMEGA [5]. The developed and optimized docking workflow used following settings: ChemPLP score, no template, binding pocket definition within 6 Å from the ligand, genetic algorithm search efficiency of 100%. Ten poses were generated for each docked ligand and the most frequently occurring pose further processed and also shown on the figures herein. The generated docking workflow was subsequently theoretically verified using redocking and crossdocking.
Flexible docking applied the same settings as previously described, except the binding pocket was defined within 9 Å from the ligand. The residues known to adopt different conformations were set flexible (Ile488, Phe231, Phe381, Phe487, Trp116, Trp260, Ala313) [1].

Molecular dynamics (MD)
MD study was performed on four protein ligand complexes. R-fadrozole complexed with CYP11B2 enzyme, S-fadrozole with CYP11B2, R-fadrozole with CYP11B1, and S-fadrozole with CYP11B1. The four complexes were solvated with explicit water molecules forming at least 14 Å layer around the complex. Sodium chloride concentration was set to 0.145 M to account for physiological conditions. Solvated complex was subsequently minimized. The MD study using NVT ensemble at 300 K lasting 2 ns was performed on the four complexes in periodic boundary conditions. The complex was first solvated, minimized and the production phase itself was preceded by heating and equilibration phases. Positional harmonic constraints were applied on iron atom and the four porphyrin nitrogen atoms involved in its coordination to minimize their influence on fadrozole binding in all three MD phases.

3. Results

CYP11B2

Binding site alignment
To address the differences in the binding pockets between CYP11B1 and CYP11B2, binding pockets including the surfaces of the two enzymes were aligned (fig. 4). Comparison of the shape and size of the binding pockets does not directly explain lower potency of S-fadrozole toward CYP11B2 since its binding pocket has appropriate size to accommodate S-fadrozole as well. To provide more insights into the interaction of R- and S-fadrozole with CYP11B2, docking was performed.

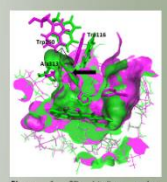

Figure 4. 3D binding pocket comparison of CYP11B2 (green) and CYP11B1 (magenta). CYP11B1 binding pocket is clearly smaller due to spatial arrangement of Trp116, Trp260 and Ala 313 side chains.

Docking
The developed workflow placed R-fadrozole in CYP11B2 enzyme similarly to its co-crystallized pose. However, no plausible docking pose coordinating the iron atom was found for S-fadrozole in CYP11B2 binding pocket (fig. 5) indicating energetically more favourable binding of R-fadrozole than S-fadrozole in CYP11B2.
Furthermore, flexible docking into CYP11B2 of both fadrozole isomers was performed. As opposed to rigid docking, flexible docking workflow generated an S-fadrozole pose in CYP11B2 coordinating the iron atom (fig. 6), pointing at the necessity of special rearrangement of amino acid side chains in order to accommodate the other fadrozole enantiomer and at the same time indicating CYP11B2 inhibition by S-fadrozole, however to a lower extent than seen by R-fadrozole.

CYP11B1

Binding site alignment
Despite CYP11B1 and CYP11B2 enzymes sharing identical amino acids in their binding pockets, several amino acids adopt different conformers. Especially noteworthy are Trp116, Trp260 and Ala313 that are positioned closer to each other in CYP11B1 and further apart in CYP11B2 [1], thus making CYP11B1 binding pocket smaller in that region (fig. 4). This provides a plausible explanation why R-fadrozole fits into CYP11B2 while preventing it to fit in CYP11B1.

Docking
Both R- and S-fadrozole were docked into CYP11B1 binding pocket using the docking workflow developed. While S-fadrozole docks in the same way as it is found co-crystallized in its crystal structure 6M7X, docking of R-fadrozole did not lead to any pose with feasible coordination geometry of the iron atom (fig. 7). A flipped geometry was observed where R-fadrozole coordinated iron atom with the cyano group. Flexible docking workflow did not generate any pose with plausible iron atom coordination geometry for R-fadrozole either. Both rigid as well as flexible docking therefore indicated lower binding affinity of R-fadrozole compared to S-fadrozole towards CYP11B1.

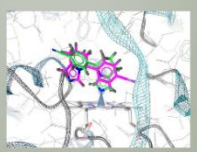

Figure 5. Docking pose of S-fadrozole (magenta) obtained from rigid docking compared to co-crystallized R-fadrozole (green) in CYP11B2.

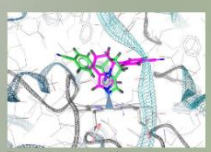

Figure 6. Docking pose of S-fadrozole (magenta) generated using docking with flexible side chains compared to co-crystallized R-fadrozole (green) in CYP11B2.

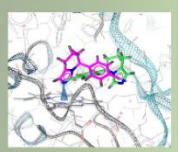

Figure 7. Docking pose of R-fadrozole (green) in CYP11B1 using rigid docking compared to the co-crystallized CYP11B1 ligand S-fadrozole (magenta).

Molecular Dynamics
MD of CYP11B2 complexes with R- and S-fadrozole shows R-fadrozole coordinating the porphyrin iron atom consistently throughout the whole MD simulation. S-fadrozole, however, moved farther away from the porphyrin ring at the earliest stages of the dynamics, indicating its lower binding affinity towards CYP11B2 (fig. 8).

Molecular Dynamics
MD trajectory of CYP11B1 complexes with R- and S-fadrozole shows S-fadrozole rather stable coordinating the porphyrin iron atom consistently for the first 650 ps of the simulation. Afterwards, however, a significant shift can be observed where S-fadrozole shifts further away from the porphyrin iron. R-fadrozole moved farther away from the porphyrin ring almost the beginning of the dynamics indicating its lower binding affinity towards CYP11B1 (fig. 8).

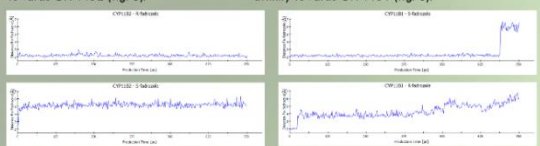

Figure 8. MD trajectory of R- and S-fadrozole in the binding pockets of both CYP11B2 and CYP11B1. The distance between iron atom and its coordinating nitrogen atom of fadrozole is displayed. For better visibility of the S-fadrozole displacement in the early phase of the dynamics, only the first 750 ps are shown.

4. Conclusion

- The binding pocket of CYP11B1 is apparently smaller than that of CYP11B2 to accommodate R-fadrozole energetically favourably
- CYP11B2 may form a complex with R-fadrozole as well as S-fadrozole, however, the docking pose of S-fadrozole seems to be energetically less probable
- MD study confirmed preferential binding of R-fadrozole toward CYP11B2 and binding S-fadrozole toward CYP11B1

5. References

1. Brixius-Anderko, S. and Scott, E. E. (2019). *The Journal of biological chemistry*, 294(2), pp. 453–460.
2. Berman, H. M. et al. (2000). *Nucleic acids research*, 28(1), pp. 235–242.
3. Strushkevich, N. et al. (2013). *Molecular Endocrinology*, 27(2), pp. 315–324.
4. GOLD – Protein Ligand Docking Software. Jones G, Willett P, Glen RC, Leach AR, Taylor RJ Mol Biol 1997. 267: 727-748.
5. Hawkins et al., 2010; OMEGA 4.1.2.0: OpenEye Scientific Software, Santa Fe, NM. http://www.eyesopen.com].

In silico investigation of fadrozole isomer selectivity to cortisol synthase (CYP11B1) and aldosterone synthase (CYP11B2)

Jakub Kollar, Evelyn Hafele, Daniela Schuster

[1]Department of Pharmaceutical and Medicinal Chemistry, Institute of Pharmacy, Paracelsus Medical University, Salzburg, Austria; Contact: jakub.kollar@pmu.ac.at

Objective
Fadrozole, a drug approved in Japan to treat breast cancer, is a known inhibitor of aromatase. It also binds to other targets such as cortisol synthase (CYP11B1) and aldosterone synthase (CYP11B2), inhibiting their enzymatic activity. Its effects are stereospecific, R-fadrozole is known to inhibit CYP11B2, but not CYP11B1 and aromatase. S-fadrozole on the other hand is known to inhibit CYP11B1 and aromatase, but not CYP11B2. Herein, we focused on shedding light in isoform selectivity explanation of fadrozole isomers towards CYP11B1 and CYP11B2.

Methods
Crystal structures of CYP11B1 co-crystallized with S-fadrozole and CYP11B2 co-crystallized with R-fadrozole were retrieved from PDB database under PDB IDs 6M7X and 4FDH, respectively.
Docking of both fadrozole isomers into binding pockets of CYP11B1 and CYP11B2 was carried out using the GOLD software package. Docking workflow was developed and subsequently theoretically verified using redocking and crossdocking. Ten poses were generated for each docked ligand and the most frequently occurring pose further processed. Flexible docking into both enzymes was performed as well.
Molecular dynamics study (MD) was performed on the four studied systems: R-fadrozole complexed with CYP11B2 enzyme, S-fadrozole with CYP11B2, R-fadrozole with CYP11B1, and S-fadrozole with CYP11B1. The four complexes were solvated in explicit water. Sodium chloride concentration was set to 0.145 M to account for physiological conditions. Solvated complex was subsequently minimized and the MD study performed using NVT ensemble at 300 K lasting 2 ns in periodic boundary conditions. Positional harmonic constraints were applied on iron atom and the four porphyrin nitrogen atoms involved in its coordination to minimize their influence on fadrozole binding in all three MD phases.

Results
Binding pockets of CYP11B1 and CYP11B2 are lined with identical amino acids. Alignment of the binding sites showed the fadrozole enantiomers span in opposite directions within the binding pocket of the two enzymes, coordinating porphyrin ring with their imidazole nitrogen atom. However, amino acids Trp116, Trp260, and Ala313 adopt different rotamers, rendering CYP11B1 binding pocket smaller and therefore prevent strong binding of R-fadrozole to this enzyme. Docking and molecular dynamics confirmed the expected lower binding affinity of R-fadrozole compared to S-fadrozole.
The size of the CYP11B2 binding pocket is sufficient to accommodate both fadrozole enantiomers. Nevertheless, both docking as well as molecular dynamics indicated energetically less favorable binding of S-fadrozole.

Conclusions
The binding pocket of CYP11B1 is smaller than that of CYP11B2 and therefore not able to accommodate R-fadrozole energetically as favourably as it does S-fadrozole that points in the opposite direction within the binding pocket. CYP11B2 provides enough space to accommodate both fadrozole isomers, however, docking and molecular dynamics simulation both indicate the interaction with R-fadrozole as energetically more favourable. This is due to an interplay between interactions of all amino acids in the binding pocket and fdrozole isomers.

Cysteinyl leukotriene receptor 1 is a potent regulator of the endosomal-lysosomal system in ARPE-19 cells

Andreas Koller, Susanne Maria Brunner, Julia Preishuber-Pflügl, Christian Runge, Anja-Maria Ladek, Herbert Anton Reitsamer & Andrea Trost

Research Program for Experimental Ophthalmology, Department of Ophthalmology and Optometry, University Hospital of the Paracelsus Medical University

Objective

The endosomal-lysosomal system (ELS) is central for cell homeostasis and comprises the functions and dynamics of particular organelles including endosomes, lysosomes and autophagosomes. In previous studies, we found that the cysteinyl leukotriene receptor 1 (CysLTR1) regulates autophagy in the retinal pigment epithelial cell line ARPE-19 under basal cellular conditions but modulating mechanism are unknown. Thus, a broader analysis of CysLTR1 inhibition-induced effects on the ELS subserves to identify the role of CysLTR1 in autophagy regulation.

Methods

Polarized ARPE-19 cells were treated with the CysLTR1 antagonist Zafirlukast (ZTK) for 1-6 hours in absence and presence of lysosomal inhibitors. In consideration of basal autophagic activity, the impact of CysLTR1 inhibition on the ELS was analyzed by immunofluorescence microscopy and western blot analysis. The following markers were used to analyze ELS regulation: LAMP1 (late endosomes/lysosomes), EEA1 (early endosomes) LysoTracker (endosomes/lysosomes), pHrodo green-labeled EGF (endocytosis) and LC3-II (autophagy).

Results

- CysLTR1 inhibition reduced LAMP1 (Fig. 1), EEA1 (data not shown) and LysoTracker (Fig. 2) particles count and size independent of basal autophagic activity.
- Serum starvation abolished the effect of ZTK on LAMP1 particle count and size (data not shown).
- Furthermore, CysLTR1 inhibition reduced the endocytosis of EGF (Fig. 3).

Conclusions

The role of CysLTR1 in inflammation and cell stress response has been extensively studied, these current data provide new insights in basal activity of CysLTR1 as endocytic regulator and the impact on downstream processes like autophagy. Autophagy induction by ZTK depleted the lysosomal pool but additionally, CysLTR1 inhibition diminished lysosomal biogenesis. Both observed effects were caused by a reduced endocytic capacity and internalization of EGF and its receptor, an important autophagy inhibitor. Serum starvation abolished the effect of ZTK on lysosome consumption and biogenesis, which identifies the endocytic regulation by CysLTR1 as important autophagy-modulatory mechanism.

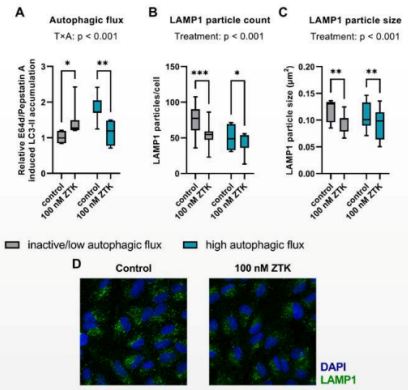

Figure 1. (A) Relative E64d/Pepstatin A-induced LC3-II accumulation and LAMP1 particle (B) count and (C) size in polarized ARPE-19 cells left untreated or treated with 100 nM ZTK for 2 hours, separated in inactive/low and high autophagic flux. (D) Representative immunofluorescence images of labeled LAMP1 in polarized ARPE-19 cells left untreated or treated with 100 nM ZTK for 2 hours. n = 7.

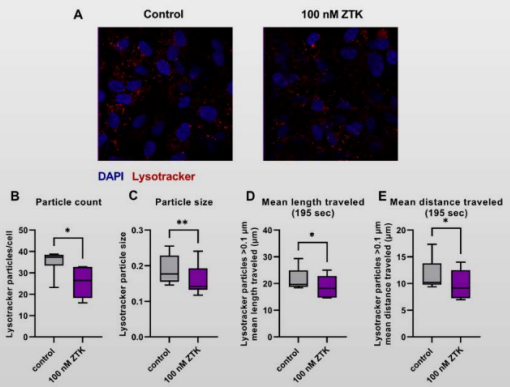

Figure 2. Analysis of LysoTracker-positive particles in polarized ARPE-19 cells. (A) Representative IF images of LysoTracker-positive organelles in polarized ARPE-19 cells left untreated or treated with 100 nM ZTK for 30-60 minutes. Corresponding LysoTracker particle (B) count, (C) size, (D) mean length traveled and (E) mean distance traveled (in µm, analyzed particle size: 0.1 – 17 µm²). n = 6.

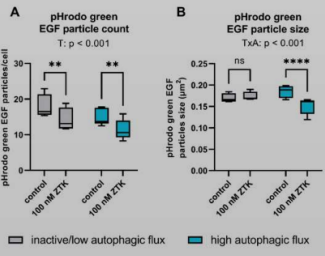

Figure 3. Analysis of pHrodo™ Green-positive EGF particles in polarized ARPE-19 cells. pHrodo green EGF particle (A) count and (B) size in polarized ARPE-19 cells left untreated or treated with 100 nM ZTK for 25 minutes separated in inactive/low and high autophagic flux. n = 4-5.

Cysteinyl leukotriene receptor 1 is a potent regulator of the endosomal-lysosomal system in ARPE-19 cells

Andreas Koller[1], Susanne Maria Brunner[1], Julia Preishuber-Pflügl[1], Christian Runge[1], Anja-Maria Ladek[1], Herbert Anton Reitsamer[1], Andrea Trost[1]

[1]Research Program for Experimental Ophthalmology, Department of Ophthalmology and Optometry, University Hospital of the Paracelsus Medical University, Salzburg, Austria; Contact: a.koller@salk.at

Objective
The endosomal-lysosomal system (ELS) is central for cell homeostasis and comprises the functions and dynamics of particular organelles including endosomes, lysosomes and autophagosomes. In previous studies, we found that the cysteinyl leukotriene receptor 1 (CysLTR1), an inflammatory and cell stress receptor, regulates autophagy in the retinal pigment epithelial cell line ARPE-19 under basal cellular conditions. However, it is unknown by which mechanism CysLTR1 regulates autophagy. Thus, a broader analysis of CysLTR1 inhibition-induced effects on the ELS subserves to identify the role of CysLTR1 in cell homeostasis and autophagy regulation.

Methods
Polarized ARPE-19 cells were used to study the role of CysLTR1 in ELS regulation. Cells were treated with the CysLTR1 antagonist Zafirlukast (100 nM) for 1-6 hours in absence and presence of lysosomal inhibitors. In consideration of basal autophagic activity, the impact of CysLTR1 inhibition on the ELS was analyzed by immunofluorescence microscopy (including live-cell imaging) and western blot analysis. The following markers were used to analyze ELS regulation: LAMP1 (late endosomes and lysosomes), EEA1 (early endosomes), LysoTracker (early-, late-endosomes and lysosomes), pHrodo green-labeled EGF (endocytosis) and LC3-II (autophagy).

Results
CysLTR1 inhibition reduced LAMP1 and LysoTracker particles count and size independent of basal autophagic activity. Serum starvation abolished the effect of Zafirlukast on LAMP1 particle count and size. Furthermore, CysLTR1 inhibition reduced the endocytosis of EGF.

Conclusions
The role of CysLTR1 in inflammation and cell stress response has been exceedingly studied but their involvement in the endosomal-lysosomal pathway is largely unknown. These current data provide new insights in basal activity of CysLTR1 as endocytic regulator and the subsequent impact on downstream processes like autophagy. Autophagy induction in ARPE-19 cells by Zafirlukast depleted the lysosomal pool but additionally, CysLTR1 inhibition diminished lysosomal biogenesis. Both observed effects were caused by a reduced endocytic capacity and internalization of EGF and its receptor, an important autophagy inhibitor. Serum starvation abolished the effect of Zafirlukast on lysosome consumption and biogenesis, which identifies the endocytic regulation by CysLTR1 as important autophagy-modulatory mechanism.

Retinal pericyte density declines with age, which is ameliorated by Montelukast

Anja-Maria Ladek[1,2], Julia Preishuber-Pflügl[1], Andreas Koller[3], Susanne Brunner[1], Christian Runge[1,2], Herbert A. Reitsamer[2,3,4], Andrea Trost[1]

[1]Research Program for Experimental Ophthalmology and Glaucoma Research, Department of Ophthalmology and Optometry, University Hospital of the Paracelsus Medical University Salzburg, Austria
[2]Department of Ophthalmology and Optometry, SALK, University Hospital of the Paracelsus Medical University Salzburg, Austria
[3]Director of the Research Program for Experimental Ophthalmology and Glaucoma Research
contact: a.ladek@salk.at

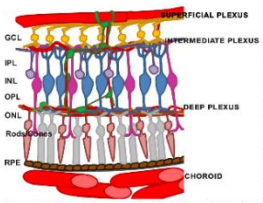

Figure 1: Schematic cross section of the retina with trilaminar inrraretinal plexus. Retinal pericytes are shown in green. GCL-ganglion cell layer, IPL- inner plexiform layer, INL-inner nuclear layer, OPL-outer plexiform layer, ONL- outer nuclear layer, RPE- retinal pigment epithelium

Objective

The retina has one of the highest oxygen and metabolic demands of any organ. The choroid supplies the photoreceptor-layer across the retinal pigment epithelium (RPE), while the other five retinal layers are perfused by the three-layered intraretinal capillary plexus (Figure 1). Here, the capillary tonus, the blood retina barrier as well as early immune and injury responses are strongly influenced by retinal pericyte (PC) activity[1]. PCs wrap around endothelial cell tubes essentially gap-free, sharing one vessel basement membrane and closely communicate with neuronal and glial cells to form a neurovascular unit in CNS tissue [1]. PC are essential for retinal homeostasis and are lost in neovasculartory retinal diseases, such as diabetic retinopathy, which can lead to blindness if untreated.

Montelukast (MTK), a leukotriene receptor antagonist and licensed antiasthmatic, has been decribed to ameliorate symptoms of CNS aging[2] and benefits hypoxic injuries in-vivo[3] and in-vitro[4]. Further, patients who have been chronically treated with MTK have reduced odds of developing diabetic retinopathy[5] and wet age-related macular degeneration[6], both age-related neovascular diseases.

This leads to the two hypothesis: Retinal PC number decreases with healthy age and MTK administration ameliorates age-related PC loss.

Methods

This pilot study was approved by the local comittee for animal use and conforms to the ARVO guidelines for ethical animal use in vision research. Twelve healthy, geriatric 19 month old CD1 mice (7 male, 5 female) were randomly devided into treatment and vehicle groups of equal gender distribution. 10 mg/kg MTK or vehicle (Veh) was administered 5 days a week for 6 weeks in form of buccal-adherent films (IntelGenx). Geriatric mouse frailty was assessed daily to ensure health and minimize cases of sudden death and individuals falling below a score- threshhold were sacrificed early. Three male and three female young adult (2-month-old) mouse retinas from our tissuebank were used as young controls. Wholemounts were immunostained with vessel basement membrane marker Collagen IV (Millipore) and Pericyte marker NG2 (Millipore) using a standard protocol.

For documentation and analysis, the retina was devided into three zones (central, medial and periphery) and within each zone three images were taken for each plexus depth. Microcapillary-length was traced by hand using an ImageJ plugin (NeuronJ) and NG2 positive PC somas located on the traced microcapillaries were counted. Statistical Analysis was performed in GraphPad-Prism 9 using one way ANOVA.

Results

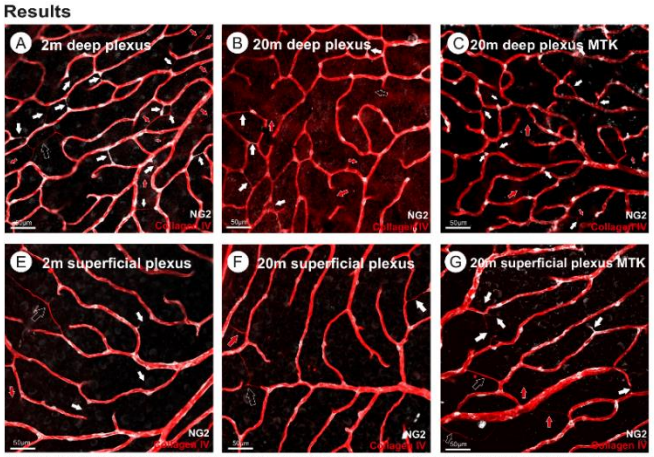

Figure 2: Representative images of deep and superficial peripheral plexus within the different groups (A-C, E-G). Bar graphs of PC density of the three groups in the respective plexus depths(D,H).

The number of PCs (NG2, white) per capillary length (Collagen IV, red) was significantly lower in geriatric mice in all retinal capillary zones and depths compared to young mice (D,H). 6 weeks of MTK treatment significantly increased retinal PC density compared to untreated geriatric mice, but remained lower than the PC density of young mice. Capillary beds of young and old mice, regardless of treatment status, exhibited PC tunneling nanotubes (white arrows), cell free collagen tubes ‚ghost vessels' (clear arrows) and short intercapillary collagen bridges (red arrows), no significant difference of these findings between groups could be observed at this sample size as the magnification and choice of z-axis was often limiting visualisation (A-C; E-F).

Conclusion

Retinal PC density decreases with age, a phenomenon which can be ameliorated by 6 weeks of MTK administration. With this relatively short treatment window, the effect of MTK likely stems from a combination of increased PC survival and proliferation/differentiation. Further, no direct functional assumptions can be made. Potential pathologic features of geriatric capillaries which could be influenced by MTK are outlined in Figure 3. It is further unclear whether the loss of PCs is causal to these features or vice versa. These questions will be investigated in a future project using geriatric PC reporter mice and in-vivo and ex-vivo assessments.

Cell- free vascular collagen tubes are often referred to as ghost vessels and are considered purely pathologic signs by clinicians. In this study, all groups exhibited acellular microvessels with similar frequencies. This might represent a translational language barrier from microbiological to clinical research since the ‚ghost vessels' considered here and in similar histologic literature are too small to be imaged by clinician funduscopy, who consider ‚ghost vessels' to be located in the larger arterioles or venules of the superficial plexus. These main branch ‚ghost vessels' were not observed in any of the mice. NG2 positive PC tunneling nanotubes have been described to be highly functional in neurovascular coupling across single capillaries[8] and will also be further investigated.

In the future, MTK currently a licensed antiasthmatic, might be repurposed as oral preventive therapy of wet- age related macular degeneration or diabetic retinopathy due to its ability to improve vascular PC coverage.

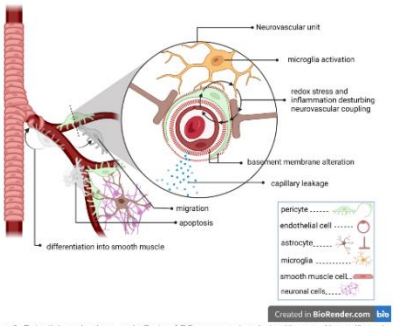

Figure 3: Potential mechanisms and effects of PC coverage loss in healthy age: Noxae like sub-threshold hypoxia or hyper-/hypoglycemia cause redox stress leading to vascular stiffening and constriction as well as neurovascular dysfunction and inflammation in a vicious cycle[7]. The literature describes PCs in physiologic homeostasis to be capable of controlling blood retina barrier tightness, capillary blood flow, glucose uptake, extracellular matrix modelling and angiogenesis[7], all of which are impaired in the geriatric capillary phenotype. Created with BioRender.com.

Citations
1) Trost A. et al. (2016) DOI: 10.3389/fncal.2016.00020; 2) Marschallinger J. et al. (2015) DOI: 10.1038/ncomms9466; 3) Saad M.A. (2015) DOI 10.1007/s11064-014-1478-9; 4) Zhou L. et al. (2018) https://doi.org/10.1007/s10787-019-00611-7
5) Pham B. et al (2021) Oral montelukast is associated with decreased offs of diabetic retinopathy, ARVO 2021 Poster 6) Karaca I. et al. (2021) Association of oral montelukast with reduced offs of developing neovascular age related macular degeneration. ARVO 2021 Poster
7) El Assar M. et al. (2013) DOI: 10.1016/j.freeradbiomed.2013.07.003; 8) Luis Alarcon-Martinez (2020) https://doi.org/10.1038/s41586-020-2589-x

Retinal pericyte density declines with age, which is ameliorated by Montelukast

Anja-Maria Ladek[1,2], Julia Preishuber-Pflügl[1], Andreas Koller[1], Susanne Brunner[1], Christian Runge[1,2], Herbert A. Reitsamer[1,2,3], Andrea Trost[1]

[1]Research Program for Experimental Ophthalmology and Glaucoma Research, Department of Ophthalmology and Optometry, University Hospital of the Paracelsus Medical University Salzburg, Austria; [2]Department of Ophthalmology and Optometry, SALK, University Hospital of the Paracelsus Medical University, Salzburg, Austria; [3]Director of the Research Program for Experimental Ophthalmology and Glaucoma Research; Contact: a.ladek@salk.at

Objective
Hardly any research has explored the consequence of health aging on the homeostasis of the retinal microcirculation. Since retinal pericytes (PCs) are often dysfunctional in age-related retinal diseases like Glaucoma, diabetic retinopathy (DR) or age-related macular degeneration (AMD) one aim of this study was to explore the retinal PC status of healthy geriatric mice. The leukotriene receptor antagonist Montelukast (MTK), a licensed antiasthmatic drug, has been described to be beneficial for the outcome or onset of age- related diseases such as stroke, DR or AMD. Therefore, the second part of this project aimed to investigate the effect of 6-week MTK administration in healthy geriatric mice on the retinal microcirculation.

Methods
Twelve healthy geriatric CD1 mice (7 male, 5 female, 19–month-old) were randomly divided into treatment and vehicle groups of equal gender distribution and orally treated 5 days a week with 10 mg/kg MTK or vehicle for 6 weeks. Three male and three female untreated young CD1 mouse retinas (2-month-old) were used as young controls. All retinas were labeled using a standard immunofluorescence protocol and capillary length and PC soma number were investigated using Image J plugins in nine retinal locations per mouse. Statistical analysis was performed using GraphPad Prism 9.0 and one-way ANOVA.

Results
PC number per capillary length was significantly lower in both MTK and vehicle treated geriatric mice compared to young mice of the same strain ($p=0.0177$ MTK, $p<0.0001$ veh in deep retinal plexus). 6 week MTK administration in geriatric mice increased PC number per capillary length significantly in all retinal zones and capillary plexus depths compared to the vehicle treated control group ($p=0.0002$ in deep, $p<0.0001$ in intermediate and $p<0.0001$ in superficial plexus). The prevalence of PC tunnelling nanotubes, intercapillary collagen bridges and cell free collagen tubes, often referred to as “ghost vessels”, in the capillary beds of all groups and genders did not significantly differ at this sample size.

Conclusions
Healthy aging leads to a loss of retinal PC density, possible causes could include degeneration, de-differentiation, apoptosis and migration. This age-related PC loss is ameliorated after 6 weeks of MTK treatment and with this relatively short treatment window, multiple downstream pathways of action of MTK might be causal to the observed effect. Among MTKs described downstream pathways of action are inhibition of inflammation, beneficial extracellular matrix remodelling and induction of pro-survival translation factors as well as vascular CYP2C8 inhibition. Although PCs express CysLTR1 receptor (MTKs main receptor) it is unclear if PC are directly benefitting from MTK in terms of survival and proliferation, or if their improved numbers are a more passive result of prior stabilisation of the neurovascular niche. These questions will be investigated in a future project using geriatric PC reporter mice and in-vivo and ex-vivo assessments. In the future, MTK, currently a licensed antiasthmatic, might be repurposed as oral preventive therapy of wet-age related macular degeneration or diabetic retinopathy due to its ability to improve vascular PC coverage.

Leveraging immune memory against measles virus as an anti-tumor strategy in a pre-clinical model of aggressive squamous cell carcinoma

VM Leb-Reichl[1,§], M Kienzl[1,§], A Kaufmann[1], A Stöcklinger[2], B Tockner[1], S Kitzmüller[1], N Zaborsky[3], M Steiner[3], G Brachtl[4], L Trattner[1], P Kreideweiss[5], C Reinsch[5], S Panzner[5], R Greil[3], D Strunk[4], J Bauer[1], IK Gratz[2], C Guttmann-Gruber[1], J Piñón Hofbauer[1,§]

[1]EB House Austria, Research Program for Molecular Therapy of Genodermatoses, Department of Dermatology and Allergology, University Hospital of the Paracelsus Medical University Salzburg, Salzburg, Austria; [2]Department of Biosciences, University of Salzburg, Salzburg, Austria; [3]Salzburg Cancer Research Institute-Laboratory for Immunological and Molecular Cancer Research, University Hospital of the Paracelsus Medical University Salzburg, Salzburg, Austria; [4]Experimental and Clinical Cell Therapy Institute, Spinal Cord Injury & Tissue Regeneration Center, Paracelsus Medical University Salzburg, Salzburg, Austria; [5]Lipocalyx GmbH, Halle, Germany; [§]equal contributors

BACKGROUND

The suboptimal design of current therapeutic cancer vaccines, together with the need to overcome immunosuppressive tolerance mechanisms, has hampered the clinical success of cancer vaccination in the treatment of various solid tumors. Most cancer vaccines target 'self' antigens which are subject to tolerance mechanisms designed to prevent autoimmunity. An alternate approach is to harness the pre-existing immunity in the general population against common childhood pathogens as an anti-tumor weapon by expressing the cognate epitope in tumor cells. To provide proof-of-principle, we established a prime-boost vaccination protocol that relied on delivery of a DNA-based vaccine to the dendritic cell –rich region of the skin and included known CD4+ T helper- and CD8+ cytotoxic T lymphocyte (CTL)-epitopes derived from measles virus (MeV). The immune response against the viral antigen was confirmed via IFN-gamma secretion, *in vivo* CTL-mediated killing, and *in vitro* T cell proliferation assays. Finally, we used this model to investigate the impact of harnessing immune memory in controlling the engraftment and outgrowth of syngeneic squamous carcinoma cells (SCC) in tumor challenge experiments.

RESULTS I. Vaccination induced robust CTL immunity in mice

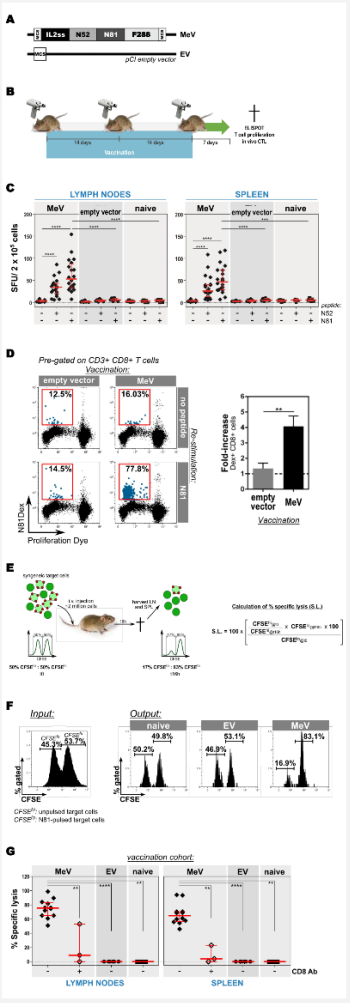

(A) Measles virus (MeV) DNA plasmid vaccine, encoding the IL2 signal sequence (IL2ss), H-2k[d]-restricted CTL epitopes (N52 and N81), and a promiscous T helper epitope (F288), or an empty vector (EV) control plasmid are coated onto gold beads and delivered into the dermis via gene gun.

(B) Mice were immunized a total of 3 times with 14 days between vaccinations. The quality of the immune response generated was evaluated in **IFNg ELISPOT**, **T cell proliferation**, and ***in vivo* CTL assays** 7 days after the last vaccination.

(C) We observed significantly more IFNg spot-forming units in splenic and lymph node preparations isolated from MeV-vaccinated mice in ELISPOT assays, especially when restimulated with the cognate epitope N81.

(D) Using a custom synthesized dextramer consisting of the N81 epitope complexed to H-2k[d] MHC Class I molecules, we identified a N81-specific CD8+ T cell population that could be specifically expanded upon restimulation with N81 peptide-pulsed splenocytes.

(E) For ***in vivo* CTL assays**, syngeneic splenocytes were isolated from naïve mice and labeled with CFSE at two different intensities. The CFSE^{low} fraction was pulsed with N81 peptide and mixed at a 1:1 ratio with unpulsed CFSE^{high} cells. Up to 2 x 10^6 cells of these cells (input cells) were injected via the tail vein into MeV-vaccinated or control recipients. After 16h the mice were sacrificed and single cell suspensions of the spleens and lymph nodes were prepared and analysed for the presence of CFSE-labeled cells via flow cytometry. Specific lysis was calculated based on the loss of the N81-pulsed CFSE^{low} fraction with respect to the unpulsed CFSE^{high} fraction.

(F – G) We observed up to 80% specific lysis of N81-pulsed target cells in the lymph nodes and spleens of MeV-vaccinated mice. In contrast, control mice showed no specific lysis of target cells. Importantly, this killing activity was markedly reduced when immunized mice were injected with an anti-CD8a blocking antibody 24h prior to transfer of the CFSE-labeled target cells.

RESULTS II. Anti-tumor responses in MeV-vaccinated mice

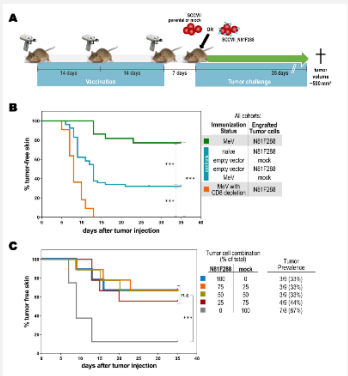

(A) We challenged MeV-vaccinated mice with congenic tumor cells that were engineered to stably express the cognate epitope (N81+). Tumor cells were injected intradermally 7 days after the last immunization. Mice were then monitored for tumor development for up to 35 days.

(B) 68% of mice in the control cohorts (*i.e.* no match in MV immunity status and N81 expression on tumor) succumbed to tumor development with a median onset of 13 days. In contrast, only 23% of MeV-vaccinated mice developed a tumor, while the remaining 77% stayed tumor-free. This protection was abrogated when vaccinated recipients were injected with anti-CD8a blocking antibodies.

(C) We investigated the level of epitope expression within the tumor bulk that is necessary to achieve significant protection by mixing N81-expressing (N81$^+$) and N81-non-expressing (N81$^-$) tumor cells at various ratios prior to injection in mice. MeV-vaccinated mice injected with 100% N81$^+$ tumor cells developed tumors with a prevalence of 87.5% in a median period of 9 days. When a fraction of the tumor cells expressed N81, prevalence of tumor development was approximately 35% (*P* <0.0001). No significant differences in the level of protection was observed whether the N81$^+$ cells represented 25% or 100% of the bulk population.

RESULTS III. In vivo tumor therapy

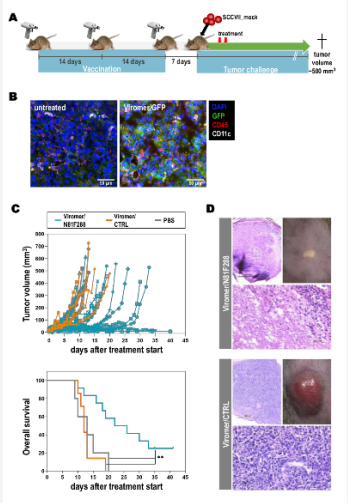

(A) To demonstrate the feasibility of this strategy in a therapeutic setting, MeV-vaccinated mice were engrafted with syngeneic N81-negative SCC cells and developing tumors (<40 mm^3) were treated with intratumoral injections (up to 2 injections, 4 days apart) of IN VIVO Viromer® (Lipocalyx GmBH) complexed with IVT-mRNA encoding the cognate epitope (Viromer/N81F288). Treatment with either PBS or Viromer® complexed with a non-coding RNA (Viromer/CTRL) served as treatment controls. Previous experiments with a GFP-mRNA had demonstrated the suitability of the Viromer as an in vivo transfection agent **(B)**.

(C) Growth of tumors treated with Viromer/N81F288 was significantly reduced, resulting in a significant increase in overall survival of the mice compared with Viromer/CTRL- and PBS-treated cohorts (Log-rank Mantel-Cox test, *p*=0.0079 and 0.0029, respectively).

(D) In 3 of the 12 mice in this cohort (25%), tumor outgrowth was completely inhibited and at the end of the study, H&E staining revealed that the remaining mass consisted of epidermal (keratin) cysts.

CONCLUSIONS

Together with continuing advances in nanoparticle-based delivery technologies, the mRNA-based intratumoral strategy for repurposing of a pre-existing viral immunity as outlined here represents a viable alternative that can meaningfully complement current cancer immune-therapies, including personalized cancer vaccine and checkpoint inhibitor blockade.

ACKNOWLEDGEMENTS:
This work is funded by **DEBRA Austria**, the **Paracelsus Medical University Research Fund** (E-14/20/105-PIN)

EB House Austria, Department of Dermatology, University Hospital of the Paracelsus Medical University Salzburg
✉ Victoria Leb-Reichl, v.reichl@salk.at

Leveraging immune memory against measles virus as an anti-tumor strategy in a pre-clinical model of aggressive squamous cell carcinoma

Victoria Leb-Reichl[1, 6], Melanie Kienzl[1, 6], Anna Kaufmann[1], Angelika Stöcklinger[2], Birgit Tockner[1], Sophie Kitzmüller[1], Nadja Zaborsky[3], Markus Steiner[3], Gabriele Brachtl[4], Lisa Trattner[1], Patrick Kreideweiss[5], Christian Reinsch[5], Steffen Panzner[5], Richard Greil[3], Dirk Strunk[4], Johann W Bauer[1], Iris Gratz[1, 2], Christina Guttmann-Gruber[1], Josefina Piñón Hofbauer[1]

[1]EB House Austria, Research Program for the Molecular Therapy of Genodermatoses, Department of Dermatology and Allergology, University Hospital of the Paracelsus Medical University Salzburg, Salzburg, Austria; [2]Department of Biosciences, Paris Lodron University of Salzburg, Salzburg, Austria; [3]Salzburg Cancer Research Institute-Laboratory for Immunological and Molecular Cancer Research, University Hospital of the Paracelsus Medical University Salzburg, Salzburg, Austria; [4]Experimental and Clinical Cell Therapy Institute, Spinal Cord Injury & Tissue Regeneration Center, Paracelsus Medical University Salzburg, Salzburg, Austria; [5]Lipocalyx GmbH, Halle, Germany; [6]contributed equally; Contact: v.reichl@salk.at

Objective
Viral antigens are among the strongest elicitors of immune responses. A significant proportion of the human population already carries pre-existing immunity against several childhood viruses, which could potentially be leveraged to fight cancer. We sought to provide proof-of-concept in mouse models that a pre-existing measles virus (MeV) immunity can be redirected to inhibit tumor growth by directly forcing expression of cognate antigens in the tumor.

Methods
We designed DNA vaccines against known MeV cytotoxic and helper T epitopes, and administered these intradermally to mice that were subsequently challenged with syngeneic squamous cancer cells engineered to either express the cognate antigens or not. Alternatively, established wild-type tumors in vaccinated animals were treated intratumorally with in vitro-transcribed mRNA encoding the cognate epitopes.

Results
Vaccination generated MeV cytotoxic T lymphocyte (CTL) immunity in mice as demonstrated by enhanced IFNg production, antigen-specific T cell proliferation, and CTL-mediated specific killing of antigen-pulsed target cells. When challenged with syngeneic tumor cells engineered to express the cognate antigens, 77% of MeV-vaccinated mice rejected the tumor versus 21% in control cohorts. Antitumor responses were largely dependent on the presence of CD8+ cells.
Significant protection was observed even when only 25% of the tumor bulk expressed cognate antigens. We therefore tested the strategy therapeutically, allowing tumors to develop in vaccinated mice before intratumoral injection with Viromer® nanoparticles complexed with mRNA encoding MeV antigens. Treatment significantly enhanced overall survival compared to controls, including complete tumor regression in 25% of mice.

Conclusions
Our results indicate that redirecting pre-existing viral immunity to fight cancer is a viable alternative that could complement current cancer immune-therapies including personalized cancer vaccines and checkpoint inhibitor blockade.

Acknowledgements
This project is funded by the PMU-FFF (E-14/20/105-PIN), DEBRA Austria, and BWT Austria GmBH

Atrial Fibrillation Recognition with Detection of Preceding Inter-Atrial Block before and after Cardiac Surgery

Spela Leiler[1], André Bauer[2], Eva Hrovat[3], Theodor Fischlein[1,4], Jurij Matija Kalisnik[1]

[1]Department of Cardiac Surgery, Paracelsus Medical University, Nuremberg, Germany, [2]Department of Computer Sciences, University of Würzburg, Germany, [3] Department of Cardiovascular Surgery, University Medical Centre Ljubljana, Slovenia, [4]Paracelsus Medical University, Nuremberg, Germany
Contact: jurij.kalisnik@klinikum-nuernberg.de

Background

- **Postoperative atrial fibrillation (PoAF):**
  - occurs in more than one third of patients after cardiac surgery
  - is vastly underdiagnosed
  - is related to severe short- and long-term complications such as stroke, heart failure, increased morbidity and mortality

Inter-atrial block (IAB), characterized by a delay of inter-atrial conduction, defined electrocardiographically by a P wave > 120 ms has been related to increased risk of new onset atrial fibrillation[1]. However, little is known about the P wave characteristics with regard to development of PoAF.

Objectives

- To identify ECG morphological changes of the P wave that predispose to **PoAF.**

Methods

- Prospective evaluation of 117 patients undergoing elective coronary artery bypass grafting, aortic valve replacement, or both at University Medical Centre Ljubljana, Slovenia between December 2018 and January 2020.
- P wave shape and IAB from 20-minute high-resolution pre- and postoperative ECG recordings were determined on day before surgery and on the 2nd or the 3rd postoperative day. Standard statistical methods were used to compare demographics, comorbidities, pre- and postoperative ECG parameters between PoAF group and sinus rhythm group (controls).

Results

- PoAF was detected in 22 (19%) patients.

Clinical Parameters

	Control Group (n=95)	PoAF Group (n=22)	p-value
Demographics and Clinical History			
Gender (male, %)	67 (70.5)	12 (54.6)	0.234
Age	67.0 [60.0-73.0]	78.0 [73.0-81.8]	**<0.001**
BMI (kg/m²)	27.9 (4.1)	28.0 (4.7)	0.941
EuroScore II	1.5 [0.9-2.3]	2.1 [1.3-2.8]	**0.038**
AH (%)	1.0 [1.0-1.0]	1.0 [1.0-1.0]	0.067
Creatinine preop.	82.0 [70.3-94.8]	80.5 [65.5-88.8]	0.356
LV-EF< 55% (%)	6 (6.3)	4 (18.2)	0.159
NYHA III or IV	2.00 [2.00-3.00]	2.00 [2.00-2.00]	0.855
Intraoperative Data			
CABG (%)	32 (33.7)	2 (9.1)	**0.044**
AVR (%)	39 (41.1)	9 (40.9)	1.000
CABG +AVR (%)	11 (11.6)	10 (45.5)	**<0.001**
CPB dur. (min)	92.9 (31.6)	99.6 (35.9)	0.438
ACT (min)	68.00 [53.3-89.0]	74.00 [60.0-89.0]	0.403
Postoperative Data			
RBC transfused	0.0 [0.0-2.8]	2.5 [1.0-5.0]	**0.002**
FFP transfused	0.0 [0.0-2.8]	2.5 [1.0-5.0]	**0.072**
TC transfused	000 [0.0-0.0]	0.0 [0.0-0.0]	**0.409**
c-Troponin peak (ng/ml)	4.3 [2.9-9.1]	4.3 [2.2-9.8]	**0.919**
CRP peak (mg/l)	81.5 [44.5-162.3]	87.0 [67.0-132.8]	**0.585**
WBC peak(10⁹/l)	14.50 [12.2-17.7]	16.7 [14.9-19.6]	**0.409**
CSA-AKI	8 (8.4)	4 (18.2)	**0.078**
Creatinine peak(µmol/l)	88.0 [73.5-106.0]	101.0 [72.5-115.3]	**0.764**

[a] Data are presented as median [interquartile range], mean (standard deviation), or n (%),
[b] BMI: body mass index; EuroScore II: mortality scoring system for cardiac surgery patients; AH: arterial hypertension; preop: preoperatively; LV-EF: left ventricular ejection fraction (Simpson); NYHA : New York Heart Classification score; WBC: white blood cell levels; CABG: coronary-arterial bypass graft: AVR: aortic valve replacement; CPB: cardiopulmonary bypass; ACT: aorta cross clamp time; RBC: red blood cells concentrate FFP: fresh frozen plasma concentrate; TC: thrombocyte concentrate; CRP: C-reactive protein; CSA-AKI: cardiac surgery associated acute kidney injury

Table 1 | Preoperative, intraoperative and postoperative clinical parameters

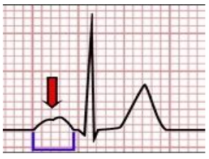

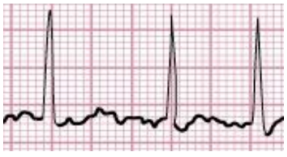

Figure 1 | Partial inter-atrial block Figure 2 | Atrial Fibrillation

Electrocardiographic Parameters

	Control Group (n=95)	PoAF Group (n=22)	p-value
P wave dur. preop. (ms)	112.0 [103.0-123.5]	120.0 [102.5-129.5]	0.418
P wave dur. postop. (ms)	102.0 [96.0-114.0]	120.00 [94.00-128.8]	0.075
P wave dur. (postop.-preop.)(ms)	-8.0 [-18.0-0.0]	0.5 [-18.8-9.0]	0.252
Normal P wave shape preop. (%)	65 (68.2)	15 (68.2)	1.000
Bimodal P wave shape preop. (%)	12 (12.6)	3 (13.6)	1.000
Biphasic P wave shape preop. (%)	15 (15.8)	4 (18.2)	1.000
PQ Interval preop. (ms)	172.0±[148.0-186.0]	162.0±[140.0-180.0]	0.146
PQ Interval postop. (ms)	154.0±[135.0-176.0]	144.0±[135.5.0-164.5]	0.266
PQ (postop.-preop.) (ms)	-10.0 [-27.0--2.0]	-9.0 [-22.5-3.5]	0.653
IAB preop. (%)	23 (24.21)	7 (31.82)	0.642
Intermittent IAB preop. (%)	2 (2.11)	3 (13.64)	0.068
Advanced IAB preop. (%)	18 (19.0)	2 (9.1)	0.428
IAB postop. (%)	25 (26.3)	12 (54.5)	**0.021**
Partial IAB postop. (%)	10 (10.5)	4 (18.2)	0.527
Intermittent IAB postop. (%)	4 (4.2)	4 (18.2)	0.061
Advanced IAB postop. (%)	9 (9.5)	4 (18.2)	0.427
Normal P wave shape postop. (%)	74 (77.9)	13 (59.1)	0.121
Bimodal P wave shape postop. (%)	9 (9.5)	3 (13.6)	0.849
Biphasic P wave shape postop. (%)	9 (9.5)	6 (27.3)	0.058
IAB preop. and postop. (%).	20 (21.1)	9 (40.9)	0.095

[a] Data are presented as median [interquartile range], or mean (standard deviation)
[b] preop.: preoperatively; postop.: postoperatively; dur.: duration; IAB: inter-atrial block

Table 2 | Preoperative and postoperative ECG parameters

Conclusions

- Higher age, EuroScore II, arterial hypertension, combined surgery and red blood cell transfusion were related to higher rates of PoAF while coronary arterial bypass grafting was related to lower incidence of PoAF.
- Postoperative IAB of any type was associated with higher rates of PoAF.

References

[1]Tse G, Wong CW, Gong M, Wong WT, Bazoukis G, Wong SH, Li G, Wu WKK, Tse LA, Lampropoulos K, Xia Y, Liu T, Baranchuk A; International Health Informatics Study (IHIS) Network. Predictive value of inter-atrial block for new onset or recurrent atrial fibrillation: A systematic review and meta-analysis. Int J Cardiol. 2018 Jan 1;250:152-156. doi: 10.1016/j.ijcard.2017.09.176. Epub 2017 Oct 3. PMID: 29017777.

Atrial Fibrillation Recognition with Detection of Preceding Inter-Atrial Block before and after Cardiac Surgery

Spela Leiler[1], André Bauer[2], Eva Hrovat[3], Theodor Fischlein[1,4], Jurij Matija Kalisnik[1]

[1]Department of Cardiac Surgery, Paracelsus Medical University, Nuremberg, Germany; [2]Department of Computer Sciences, University of Würzburg, Germany; [3]Department of Cardiovascular Surgery, University Medical Centre Ljubljana, Slovenia; [4]Paracelsus Medical University, Nuremberg, Germany; Contact: spela.leiler@klinikum-nuernberg.de

Objective
Postoperative atrial fibrillation (PoAF) occurs in more than one third of patients after cardiac surgery. It is a vastly underdiagnosed arrhythmia due to its short term and asymptomatic nature. PoAF is related to severe short- and long-term complications such as stroke, heart failure, increased morbidity and mortality. Inter-atrial block (IAB), characterized by a delay of inter-atrial conduction, defined electrocardiographically by a P wave duration > 120 ms has been related to higher incidence of new onset atrial fibrillation. However, little is known about the P wave characteristics with regard to development of PoAF. The aim of this study was to identify electrocardiographic (ECG) morphological changes of the P wave that predispose to PoAF.

Methods
117 patients undergoing elective coronary artery bypass grafting, aortic valve replacement, or both at University Medical Centre Ljubljana, Slovenia between December 2018 and January 2020 were prospectively evaluated. P wave shape and IAB from 20-minute high-resolution pre- and postoperative ECG recordings were determined on day before surgery, on the 2nd and/or on the 3rd postoperative day. Standard statistical methods were used to compare demographics, comorbidities, pre- and postoperative ECG parameters between PoAF and sinus rhythm group.

Results
PoAF was detected in 22 (19%) patients. Patients in the PoAF group were significantly older (78.0 [73.0-81.8] vs. 67.0 [60.0-73.0], p=<0.001) and had higher EuroScore II (2.1 [1.3-2.8] vs.1.5 [0.9-2.3], p=0.038).The incidence of PoAF was lower in patients who underwent coronary arterial bypass grafting (9.1% vs. 33.7%, p= 0.044). Patients who developed PoAF received more red blood cell concentrates (2.5 [1.0-5.0] vs. 0.0 [0.0-2.8], p=0.002). Patients with postoperative IAB had a higher incidence of PoAF (54.5% vs. 26.3%, p= 0.021).

Conclusions
Higher age, EuroScore II, arterial hypertension, combined surgery, and red blood cell transfusion were related to higher incidence of PoAF. Postoperative IAB of any type was associated with higher rates of PoAF.

The chromatin regulators DAXX, CENP-A and HJURP in thymic epithelial tumors: an immunohistochemical analysis

Georgia Levidou[1, 2], Konstantinos Palamaris[2], Georgios Andreadakis[2], Christos Masaoutis[2], Dimitra Rontogianni[2], Stamatios Theocharis[2]

1.Department of Pathology, Paracelsus Medical University, 90419 Nuremberg, Germany

2. First Department of Pathology, National and Kapodistrian University of Athens, 15772 Athens, Greece.

Objective

Recent advances have demonstrated the role of chromatin regulators, including histone variants and histone chaperones in cancer initiation and progression. In this context it has been demonstrated that the histone chaperone holliday junction recognition protein (HJURP), responsible for depositing histone variant centromere protein (CENP-A) at the centromere is upregulated in several malignancies. A similar significant role has been attributed to chaperone DAXX, which seems to be responsible for the ectopic localization of CENP-A.

Methods and Materials

The expression of DAXX, CENP-A and HJURP was examined immunohistochemically in 95 archival tissue specimens from patients with thymic epithelial tumors (TETs), retrieved from two major hospitals in Athens, Greece, for whom clinical information was available.
An immunoreactivity score (H-score), based on the percentage of positive cells multiplied by the staining intensity was created.
Statistical analysis was performed using STATA 10.0 for Windows.

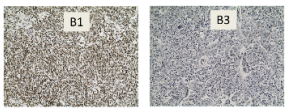

Figure 1. DAXX expression in a type B1 and a Type B3 TET.

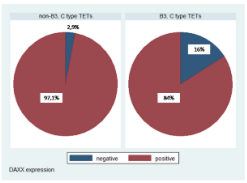

Figure 2. Positivity rate of DAXX in epithelial cells according to the WHO histological subtype. The lymphocyte-poor thymic epithelial tumors (TETs), namely B3 and C are more frequently negative for DAXX in comparison to the rest TETs (p=0,043).

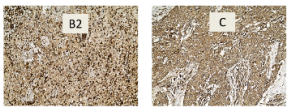

Figure 3. CENP-A expression in a type B2 and a Type C TET.

Results

- **DAXX expression** in epithelial cells was observed in 93,6% of the cases (Figure 1).
- The lymphocyte poor B3 and C-type TETs were more frequently negative for DAXX (p=0,043, Figure 2).

- **CENP-A expression** in epithelial cells was both cytoplasmic (90%) and nuclear (39,8%) (Figure 3).
- B3 and C TETs were more frequently positive for nuclear CENP-A (p=0,008) and showed a higher cytoplasmic and nuclear CENP-A H-score (p=0,007 and p=0,002 respectively, Figure 4A, 4B).
- Higher nuclear CENP-A H-score was associated with advanced Masaoka–Koga stage (p=0,048, Figure 4C).
- The presence of cytoplasmic CENP-A expression was correlated with a favorable overall survival (log-rank test, p=0,035, Figure 4D).

- **HJURP expression** was mainly nuclear in epithelial cells (99%) with 69% of the cases showing also a cytoplasmic immunopositivity (Figure 5).
- B3 and C were more frequently positive for cytoplasmic HJUPR (p=0,022, Figure 6A) and showed a higher cytoplasmic HJURP H-score (p<0,001, Figure 6B).
- The presence of cytoplasmic HJURP expression was correlated advanced Masaoka-Koga stage (p<0,001, Figure 6C).

- There were significant associations between the examined molecules; cytoplasmic HJURP H-score was positively associated with nuclear and cytoplasmic CENP-A H-score (R=0.34, p<0.001 and R=0,25, p=0,016 respectively) and negatively with DAXX H-score (R=-0.21, p=0.043).

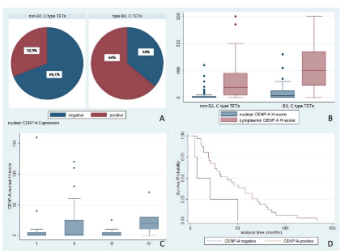

Figure 4. ((A) Positivity rate of nuclear CENP-A in epithelial cells according to the WHO subtype. B3 and C type TETs are more frequently positive for nuclear CENP-A (B) Schematic representation of the associations between CENP-A H-score and WHO subtype. B3 and C type TETs show higher cytoplasmic and nuclear CENP-A H-score. (C) H-score expression according to Masaoka-Koga stage. Stage IV TETs show a higher CENP-A H-score. (D) Kaplan-Meier survival rates according to cytoplasmic CENP-A positivity. The presence of CENP-A immunopositivity was correlated with a favorable overall survival in non-type C TETs

Table 1. Expression of DAXX, CENP-A and HJURP in TETs

	Positivity rate	H-score, median	H-score, range
Epithelial cells			
DAXX	93,6%	90	0-300
CENP-A cytoplasmic expression	90%	50	0-300
CENP-A nuclear expression	39,8%	0	0-160
HJURP cytoplasmic expression	69%	35	0-300
HJURP nuclear expression	99%	120	0-300
Lymphoid cells			
DAXX	95,7%	200	0-300
CENP-A cytoplasmic expression	98,6%	140	0-300
HJURP nuclear expression	98,3%	235	0-300

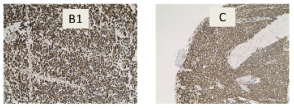

Figure 5. HJURP expression in a type B1 and a Type C TET

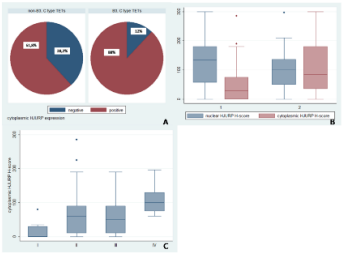

Figure 6. (A) Positivity rate of cytoplasmic HJURP in epithelial cells according to the WHO histological subtype. B3 and C type TETs are more frequently positive for cytoplasmic HJURP (B) Schematic representation of the associations between HJURP H-score and WHO subtype. B3 and C type TETs show higher cytoplasmic HJURP H-score. (C) H-score expression according to Masaoka-Koga stage. Stage IV TETs show a higher HJURP H-score when compared to the other categories.

Conclusions

Our results suggest an interaction between the centromeric histone variant CENP-A and the dedicated CenH3 chaperone HJURP in TETs, being both overexpressed in lymphocyte poor B3 and C-type TETs and both correlated with a more advanced Masaoka-Koga stage. Moreover, our study confirmed the presence of a cytoplasmic immunolocalization of CENP-A, previously attributed to a loss of specific motifs in its amino-terminus, whereas it suggested a possible favorable prognostic value of this specific immunostaining pattern.

Contact

PD Dr. Georgia Levidou
Department of Pathology
Paracelsus Medical University
90419 Nuremberg
Email: georgia.levidou@klinikum-nuernberg.de

References

1. Sitbon D, Podsypanina K, Yadav T, Almouzni G. Shaping Chromatin in the Nucleus: The Bricks and the Architects. Cold Spring Harb Symp Quant Biol. 2017;82:1-14.
2. Verrelle P, Meseure D, Berger F, et al. CENP-A Subnuclear Localization Pattern as Marker Predicting Curability by Chemoradiation Therapy for Locally Advanced Head and Neck Cancer Patients. Cancers (Basel). 2021
3. Lacoste N, Woolfe A, Tachiwana H, et al. Mislocalization of the centromeric histone variant CenH3/CENP-A in human cells depends on the chaperone DAXX. Mol Cell. 2014 Feb 20;53(4):631-44.
4. Montes de Oca R, Gurard-Levin ZA, Berger F, et al. The histone chaperone HJURP is a new independent prognostic marker for luminal A breast carcinoma. Mol Oncol. 2015 Mar;9(3):657-74.
5. Jing R, Xi J, Leng Y, Chen W, et al. Motifs in the amino-terminus of CENP-A are required for its accumulation within the nucleus and at the centromere. Oncotarget. 2017
6. Arimura Y, Shirayama K, Horikoshi N, et al. Crystal structure and stable property of the cancer-associated heterotypic nucleosome containing CENP-A and H3.3. Sci Rep. 2014

The chromatin regulators DAXX, CENP-A and HJURP in thymic epithelial tumors: an immunohistochemical analysis

Georgia Levidou[1,2], Konstantinos Palamaris[2], Georgios Andreadakis[2], Christos Masaoutis[2], Dimitra Rontogianni[2], Stamatios Theocharis[2]

[1]Department of Pathology, Paracelsus Medical University, 90419 Nuremberg, Germany; [2]First Department of Pathology, National and Kapodistrian University of Athens, 15772 Athens, Greece.; Contact: georgia.levidou@klinikum-nuernberg.de

Objective
Recent advances have demonstrated the role of chromatin regulators, including histone variants and histone chaperones in cancer initiation and progression. In this context it has been demonstrated that the histone chaperone holliday junction recognition protein (HJURP), responsible for depositing histone variant centromere protein (CENP-A) at the centromere is upregulated in several malignancies. A similar significant role has been attributed to chaperone DAXX, which seems to be responsible for the ectopic localization of CENP-A.

Methods
The expression of DAXX, CENP-A and HJURP was examined immunohistochemically in 95 archival tissue specimens from patients with thymic epithelial tumors (TETs), retrieved from two major hospitals in Athens, Greece, for whom clinical information was available.

Results
DAXX expression in epithelial cells was observed in 93,6% of the cases, whereas the lymphocyte poor B3 and C-type TETs were more frequently negative for DAXX (p=0,043). CENP-A expression in epithelial cells was both cytoplasmic (90%) and nuclear (39,8%). B3 and C TETs were more frequently positive for nuclear CENP-A (p=0,008) and showed a higher cytoplasmic and nuclear CENP-A H-score (p=0,007 and p=0,002 respectively). Higher nuclear CENP-A H-score was associated with advanced Masaoka–Koga stage (p=0,048). The presence of cytoplasmic CENP-A expression was correlated with a favorable overall survival (log-rank test, p=0,035). Moreover, HJURP expression was mainly nuclear in epithelial cells (99%) with 69% of the cases showing also a cytoplasmic immunopositivity. B3 and C were more frequently positive for cytoplasmic HJUPR (p=0,022) and showed a higher cytoplasmic HJURP H-score (p<0,001). The presence of cytoplasmic HJURP expression was correlated advanced Masaoka-Koga stage (p<0,001). There were significant associations between the examined molecules; cytoplasmic HJURP H-score was positively associated with nuclear and cytoplasmic CENP-A H-score (R=0.34, p<0.001 and R=0,25, p=0,016 respectively) and negatively with DAXX H-score (R=-0.21, p=0.043).

Conclusions
Our results suggest an interaction between the centromeric histone variant CENP-A and the dedicated CenH3 chaperone HJURP in TETs, being both overexpressed in lymphocyte poor B3 and C-type TETs and both correlated with a more advanced Masaoka-Koga stage. Moreover, our study confirmed the presence of a cytoplasmic immunolocalization of CENP-A, previously attributed to a loss of specific motifs in its amino-terminus, whereas it suggested a possible favorable prognostic value of this specific immunostaining pattern.

References
1. Sitbon D, et al., Shaping Chromatin in the Nucleus: The Bricks and the Architects. CSHSQB. 2017.
2. Verrelle P, et al. CENP-A Subnuclear Localization Pattern as Marker Predicting Curability by Chemoradiation Therapy for Locally Advanced Head and Neck Cancer Patients. Cancers (Basel). 2021
3. Jing R, et al. Motifs in the amino-terminus of CENP-A are required for its accumulation within the nucleus and at the centromere. Oncotarget. 2017

A perfect match: combining non-invasive brain stimulation techniques – a case report

Christiane Licht [1] Thomas Stöckl [1] Axel Ruttmann [1] Kneginja Richter [1, 2] Thomas Hillemacher [1]

1 Department of Psychiatry and Psychotherapy, Paracelsus Medical University Clinic, Nuremberg, Germany

2 Technical University of Nuremberg Georg Simon Ohm, Nuremberg, Germany

Klinikum Nürnberg

Introduction

Electroconvulsive therapy (ECT) is a safe and effective treatment method for severe and persistent depression, suicidality and schizophrenia[1]. For augmentation of therapeutic seizures during the treatment, several procedures with varying degrees of success, including hyperventilation and the use of remifentanil or ketamine, have been reported[1].

However, there have only been a handful of case reports on the possible role of repetitive transcranial magnetic stimulation (rTMS) as a support method for ECT[2]. The idea of combining rTMS and ECT in this way allows for addressing fundamental issues in ECT optimization.

We present the case of a 37-year-old female patient with paranoid schizophrenia demonstrates the feasibility of lowering the seizure threshold and therefore inducing a rapid remission using a combined approach of ECT and rTMS.

Case Report

- 37-year-old female patient with paranoid schizophrenia existing for round about 25 years
- pronounced negative symptoms with severe suicidality
- after no response to treatment with six ECT-sessions (bitemporal) with maximized energy (200%) an augmentative application of inhibitory rTMS of left Supplementary Motor Area (SMA) was additionally applied to ECT
- Starting from ECT session six and up to session fifteen, the protocol was intensified to everyday application due to the patient's negative symptoms
- 1 Hz, pulse width 25 ms, 25 series of 40 pulses each, at 30% of the motor stimulus threshold

Combination of ECT and rTMS

Conclusion and Outlook

- After the fifth with rTMS combined ECT-session the patient showed remission of suicidality, recovery of eye contact and mood stabilization
- Efficacy of ECT could be increased due to the combination with inhibitory rTMS in the left SMA
- This case demonstrated the feasibility of combining non-invasive brain stimulation techniques
- rTMS could support patients with long-term ECT treatment to control their negative symptoms
- Further research on the efficacy of such combinations are needed to underline the advantage of different techniques in combination

References

1 Nishikawa, K., & Yamakage, M. (2015). Reconsideration of augmentation strategies in electroconvulsive therapy

2 Albrecht, J. et al. (2019). Lowering the seizure threshold in electroconvulsive therapy using transcranial magnetic stimulation

PARACELSUS MEDIZINISCHE PRIVATUNIVERSITÄT

A perfect match: combining non-invasive brain stimulation techniques – a case report

Christiane Licht[1], Thomas Stöckl[1], Axel Ruttmann[1], Kneginja Richter[1,2], Thomas Hillemacher[1]

[1]Department of Psychiatry and Psychotherapy, Paracelsus Medical University, Nuremberg, Germany; [2]Technical University of Nuremberg Georg Simon Ohm, Nuremberg, Germany; Contact: christiane.licht@gmx.de

Objective

Electroconvulsive therapy (ECT) is a safe and effective treatment method for severe and persistent depression, suicidality and schizophrenia1. For augmentation of therapeutic seizures during the treatment, several procedures with varying degrees of success, including hyperventilation and the use of remifentanil or ketamine, have been reported1. However, there have only been a handful of case reports on the possible role of repetitive transcranial magnetic stimulation (rTMS) as a support method for ECT2. The idea of combining rTMS and ECT in this way allows for addressing fundamental issues in ECT optimization. We present the case of a 37-year-old female patient with paranoid schizophrenia demonstrating the feasibility of lowering the seizure threshold and therefore inducing a rapid remission using a combined approach of ECT and rTMS.

Methods

Case report

• 37-year-old female patient with paranoid schizophrenia existing for round about 25 years
• pronounced negative symptoms with severe suicidality
• after no response to treatment with six ECT-sessions (bitemporal) with maximized energy (200%) an augmentative application of inhibitory rTMS of left Supplementary Motor Area (SMA) was additionally applied to ECT
• Starting from ECT session six and up to session fifteen, the protocol was intensified to everyday application due to the patient's negative symptoms
• 1 Hz, pulse width 25 ms, 25 series of 40 pulses each, at 30% of the motor stimulus threshold

Results

After the fifth with rTMS combined ECT-session the patient showed remission of suicidality, recovery of eye contact and mood stabilization

Conclusions

• Efficacy of ECT could be increased due to the combination with inhibitory rTMS in the left SMA
• This case demonstrated the feasibility of combining non-invasive brain stimulation techniques
• rTMS could support patients with long-term ECT treatment to control their negative symptoms
• Further research on the efficacy of such combinations are needed to underline the advantage of different techniques in combination

References

1. Nishikawa, K., & Yamakage, M. (2015). Reconsideration of augmentation strategies in electroconvulsive therapy
2. Albrecht, J. et al. (2019). Lowering the seizure threshold in electroconvulsive therapy using transcranial magnetic stimulation

1. Aktuelle Fachinformation CABOMETYX®. 2. Choueiri TK et al. N Engl J Med. 2021;384(9):829–841. 3. Motzer RJ et al. Lancet Oncol. 2022;23(7):888–898. 4. Powles T et al. on behalf of the ESMO Guidelines Committee. Ann Oncol.2021;32(12):1511–1519. 5. Ljungberg B et al. EAU Guidelines. Edn. presented at the EAU Annual Congress Amsterdam 2022. ISBN 978-94-92671-16-5; Bedke J et al. Eur Urol. 2021;80(4):393–397. 6. National Comprehensive Cancer Network (NCCN) Clinical Practice Guidelines in Oncology: Kidney Cancer. Version: 4.2022. 7. Bergmann L et al. Onkopedia Leitlinien: Nierenzellkarzinom (Hypernephrom), ICD-10: C64, Mai 2022. 8. Leitlinienprogramm Onkologie (Deutsche Krebsgesellschaft, Deutsche Krebshilfe, AWMF): S3-Leitlinie Diagnostik, Therapie und Nachsorge des Nierenzellkarzinoms, Langversion 3.0, November 2021. 9. Choueiri TK et al. Lancet Oncol. 2016;17(7):917–927. 10. Choueiri TK et al. Eur J Cancer. 2018;94:115–125. 11. Motzer RJ et al. Br J Cancer. 2018;118(9):1176–1178.

CABOMETYX® 20 mg Filmtabletten, CABOMETYX® 40 mg Filmtabletten, CABOMETYX® 60 mg Filmtabletten
Wirkstoff: Cabozantinib-L-malat. **Zusammensetzung:** Jede Filmtablette enthält Cabozantinib-L-malat entsprechend 20 mg/40 mg/60 mg Cabozantinib. Sonstige Bestandteile: *Tablettenkern:* mikrokristalline Cellulose, Lactose, Hyprolose, Croscarmellose-Natrium, hochdisperses Siliciumdioxid, Magnesiumstearat. *Filmüberzug:* Hypromellose 2910, Titandioxid (E171), Triacetin, Eisen(III)-hydroxid-oxid x H_2O (E172). Sonstiger Bestandteil mit bekannter Wirkung: 15,54 mg/31,07 mg/46,61 mg Lactose. **Wirkstof gruppe:** antineoplastisches Mittel, Proteinkinase-Inhibitor. **Anwendungsgebiete:** Nierenzellkarzinom (*renal cell carcinoma*, RCC): CABOMETYX ist als Monotherapie indiziert für die Behandlung des fortgeschrittenen Nierenzellkarzinoms (RCC) - bei nicht vorbehandelten Erwachsenen mit mittlerem oder hohem Risiko - bei Erwachsenen nach vorangegangener zielgerichteter Therapie gegen VEGF (vaskulärer endothelialer Wachstumsfaktor). CABOMETYX ist in Kombination mit Nivolumab für die Erstlinienbehandlung des fortgeschrittenen Nierenzellkarzinoms bei Erwachsenen indiziert. Leberzellkarzinom (*hepatocellular carcinoma*, HCC): CABOMETYX ist indiziert als Monotherapie für die Behandlung des Leberzellkarzinoms (HCC) bei Erwachsenen, die zuvor mit Sorafenib behandelt wurden. Differenziertes Schilddrüsenkarzinom (*differentiated thyroid carcinoma*, DTC): CABOMETYX ist als Monotherapie für die Behandlung von Erwachsenen mit lokal fortgeschrittenem oder metastasiertem differenziertem Schilddrüsenkarzinom (DTC) indiziert, die refraktär gegenüber Radiojod (RAI) sind oder dafür nicht in Frage kommen und bei denen während oder nach einer vorherigen systemischen Therapie eine Progression aufgetreten ist. **Gegenanzeigen:** Überempfindlichkeit gegen den Wirkstoff oder einen der sonstigen Bestandteile. **Nebenwirkungen:** Sehr häufig – *Monotherapie:* abdominale Schmerzen, Asthenie, Hämorrhagie, periphere Ödeme, Schleimhautentzündung, Schmerzen in den Extremitäten, Hypoalbuminämie. – *Mono- und Kombitherapie:* Anämie, Appetitabnahme, Diarrhö, Dysgeusie, Dyspepsie, Dysphonie, Dyspnoe, Erbrechen, Fatigue, Gewichtsabnahme, Hautausschlag, Husten, Hypertonie, Hypothyreose, Kopfschmerzen, Obstipation, palmar-plantares Erythrodysästhesie-Syndrom, Schwindel, Stomatitis, Übelkeit, ALT und AST erhöht, Hypokaliämie, Hypomagnesiämie, Thrombozytopenie. – *Kombitherapie:* Arthralgie, Bauchschmerzen, Hyperthyreose, Infekt der oberen Atemwege, Muskelkrämpfe, Muskuloskelettale Schmerzen, Neutropenie, Ödeme, Pruritus, Pyrexie, Hyperglykämie, Hyperkaliämie, Hyperkalzämie, Hypermagnesiämie, Hypernatriämie, Hypoglykämie, Hypokalzämie, Hyponatriämie, Hypophosphatämie, Leukopenie, Lymphopenie, Proteinurie, erhöht: Alkalische Phosphatase, Amylase, Gesamtbilirubin, Kreatinin, Lipase. Häufig – *Monotherapie:* Abszess, akneähnliche Dermatitis, Arthralgie, Dysphagie, Fisteln, gastrointestinale Perforation, gastroösophageale Refluxkrankheit, Glossodynie, hepatische Enzephalopathie, Hyperkeratose, Lymphopenie, Muskelkrämpfe, Neutropenie, Proteinurie, Pruritus, Anstieg des Amylase-, ALP-, Gamma-GT-, Lipase-, Kreatinin-Serumspiegel, Hyperbilirubinämie, Hyperglykämie, Hyperkaliämie, Hypoglykämie, Hypokalzämie, Hyponatriämie, Hypophosphatämie, Wundheilungsstörungen. – *Mono- und Kombitherapie:* Alopezie, Änderung der Haarfarbe, Dehydratation, Erythem, Pankreatitis, Hämorrhoiden, Lungenembolie, Mundtrockenheit, periphere Neuropathie, Schmerzen im Mund, arterielle Thrombose, venöse Thrombose, Tinnitus, trockene Haut, Anstieg Cholesterin-Serumspiegel, Hypertriglyzeridämie. – *Kombitherapie:* akute Nierenschädigung, Arthritis, Colitis, Eosinophilie, Epistaxis, Gastritis, Hepatitis, Nebenniereninsuffizienz, Nierenversagen, Pleuraerguss, Pneumonie, Pneumonitis, Schmerzen, Tachykardie, Thoraxschmerzen, trockenes Auge, Überempfindlichkeit (einschließlich anaphylaktischer Reaktion), verschwommenes Sehen, Vorhofflimmern. Gelegentlich – *Monotherapie:* Schlaganfall, hypertensive Krise, cholestatische Hepatitis, Krämpfe. – *Mono- und Kombitherapie:* Kieferosteonekrose. – *Kombitherapie:* Autoimmune Enzephalitis, Fisteln, Glossodynie, Guillain-Barré Syndrom, Hypophysitis, infusionsbedingte Überempfindlichkeitsreaktion, Myasthenisches Syndrom, Myokarditis, Myopathie, Nephritis, Perforation des Dünndarms, Psoriasis, Thyreoiditis, Urtikaria, Uveitis. Häufigkeit nicht bekannt – *Monotherapie:* Herzinfarkt, Aneurysmen und Arteriendissektion, posteriores reversibles Enzephalopathie-Syndrom (PRES). Enthält Lactose. Die Informationen zu Warnhinweisen und Vorsichtsmaßnahmen für die Anwendung, Wechselwirkungen mit anderen Arzneimitteln und sonstige Wechselwirkungen sowie Schwangerschaft und Stillzeit entnehmen Sie bitte der Fachinformation. **Verschreibungspflichtig** (DE) / **Rezept- und apothekenpflichtig** (AT); Ipsen Pharma, F-92100 Boulogne-Billancourt; Örtlicher Vertreter: Ipsen Pharma GmbH; Stand der Information: 04/2022; Zulassungsnummern: EU/1/16/1136/002, EU/1/16/1136/004, EU/1/16/1136/006

CBZ-DE-000954 06/2022

IPSEN Innovation for patient care

Jede einzigartige Aorta ansprechen

Entwicklung von Technologien um den unterschiedlichen Patientenanatomien zu entsprechen. Unsere Lösungen reichen von chirurgisch über endovaskulär bis hin zu hybriden und ergänzen die präzise Technik jedes Chirurgen.

TERUMO
Aortic

Is repetitive Transcranial Magnetic Stimulation (rTMS) a new alternative for psychomotor slowing? – a case report

Christiane Licht [1] Thomas Stöckl [1] Axel Ruttmann [1] Kneginja Richter [1, 2] Thomas Hillemacher [1]

1 Department of Psychiatry and Psychotherapy, Paracelsus Medical University Clinic, Nuremberg, Germany

2 Technical University of Nuremberg Georg Simon Ohm, Nuremberg, Germany

Klinikum Nürnberg

Introduction

Major Depressive Disorder (MDD) is one of the most common psychological diseases with significant potential morbidity and mortality. It is a substantive clinical problem complicated by the failure of about 30% of the patients to respond to standard medication treatments[1]. Recent studies of the last two years show a successful utilization of repetitive Transcranial Magnetic Stimulation (rTMS) to treat especially psychomotor slowing by an inhibitory stimulation of the **S**upplementary **M**otor **A**rea (SMA). [2,3]

This study shows the case of a 79-year-old female patient with treatment resistant depression and severe psychomotor slowing who remitted under a short time of rTMS.

Case Report

- 79-year-old female patient with treatment resistant depression
- Severe psychomotor slowing with stupor, mutism and fixed gaze
- 1 Hz, pulse width 25 ms, 25 series of 40 pulses each, at 110% of the motor stimulus threshold

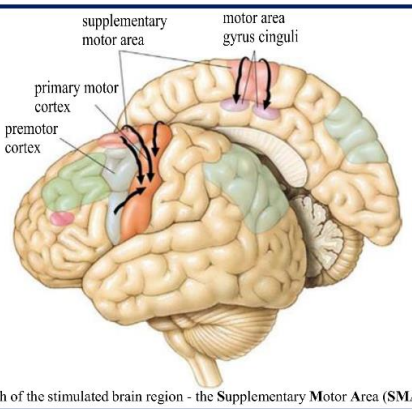

Scetch of the stimulated brain region - the **S**upplementary **M**otor **A**rea **(SMA)** [3]

Exemplary treatment of a patient by means of rTMS butterfly coil.

References

1 Fava, M. (2003). Diagnosis and definition of treatment-resistant depression. *Biological psychiatry*, *53*(8), 649-659.

2 Hansbauer, M. *et al.* rTMS and tDCS for the treatment of catatonia : A systematic review. *Schizophr. Res.* (2020) doi:10.1016/j.schres.2020.05.028.

3 Walther, S. *et al.* Inhibitory Repetitive Transcranial Magnetic Stimulation to Treat Psychomotor Slowing: A Transdiagnostic, Mechanism-Based Randomized Double-Blind Controlled Trial. *Schizophr. Bull. Open* 1, (2020).

Conclusion and Outlook

- After only fifteen rTMS sessions the patient showed partial remission with recovery of speech and eye contact
- rTMS might be a novel procedure to treat psychomotor slowing in also in treatment resistant depression
- Targeted inhibitory rTMS in SMA exclusively compensated for psychomotor slowing for a pronounced motor component opposite to other treatment regions
- rTMS could support patients with long-term ECT treatment to control their depressivesymptoms
- Further clinical trials of patient's are needed to underline the advantage of the technique and to compare it to ECT

PARACELSUS MEDIZINISCHE PRIVATUNIVERSITÄT

Is repetitive Transcranial Magnetic Stimulation (rTMS) a new alternative for psychomotor slowing? – a case report

Christiane Licht[1], Thomas Stöckl[1], Axel Ruttmann[1], Kneginja Richter[1,2], Thomas Hillemacher[1]

[1]Department of Psychiatry and Psychotherapy, Paracelsus Medical University, Nuremberg, Germany; [2]Technical University of Nuremberg Georg Simon Ohm, Nuremberg, Germany; Contact: christiane.licht@gmx.de

Objective
Major Depressive Disorder (MDD) is one of the most common psychological diseases with significant potential morbidity and mortality. It is a substantive clinical problem complicated by the failure of about 30% of the patients to respond to standard medication treatments1. Recent studies of the last two years show a successful utilization of repetitive Transcranial Magnetic Stimulation (rTMS) to treat especially psychomotor slowing by an inhibitory stimulation of the Supplementary Motor Area (SMA). 2,3 This study shows the case of a 79-year-old female patient with treatment resistant depression and severe psychomotor slowing who remitted under a short time of rTMS

Methods
Case Report: 79-year-old female patient with treatment resistant depression
• Severe psychomotor slowing with stupor, mutism and fixed gaze
• 1 Hz, pulse width 25 ms, 25 series of 40 pulses each, at 110% of the motor stimulus threshold

Results
After only fifteen rTMS sessions the patient showed partial remission with recovery of speech and eye contact.

Conclusions
• rTMS might be a novel procedure to treat psychomotor slowing in also in treatment resistant depression.
• Targeted inhibitory rTMS in SMA exclusively compensated for psychomotor slowing for a pronounced motor component opposite to other treatment regions.
• rTMS could support patients with long-term ECT treatment to control their depressive symptoms.
• Further clinical trials of patient's are needed to underline the advantage of the technique and to compare it to ECT.

References
1. Fava, M. (2003). Diagnosis and definition of treatment-resistant depression. Biological psychiatry, 53(8), 649-659.
2. Hansbauer, M. et al. rTMS and tDCS for the treatment of catatonia : A systematic review. Schizophr. Res. (2020) doi:10.1016/j.schres.2020.05.028
3. Walther, S. et al. Inhibitory Repetitive Transcranial Magnetic Stimulation to Treat Psychomotor Slowing: A Transdiagnostic, Mechanism-Based Randomized Double-Blind Controlled Trial. Schizophr. Bull. Open 1, (2020).

Efficacy and Limitations of the Embolization of the middle meningeal artery in chronic subdural hematoma

Wirksamkeit und Limitationen der Embolisation der A. meningea media bei einem chronischen Subduralhämatom

Liebert A., Voit-Hoehne H.-L., Ritter L., Eibl T., Hammer A., Steiner H.-H.

Objective:
The aim of the study is to investigate the efficacy and limitations of the embolization of the middle meningeal artery (MMA) in chronic subdural hematomas (cSDH).

Methods:
We retrospectively analyzed patients who underwent embolization of the MMA for the treatment of cSDH from Aug. 2019 to Oct. 2021. The data acquisition included the age of the patients, the radiological appearance (volume, midline shift and Nakaguchi classification), intake of antithrombotic agents and whether it was a recurrent or a primary cSDH. Abnormalities of the MMA and the applied embolic agents were noted.
Statistical analysis was performed with a significance level two-sided p-value of ≤ .05.

Results:
Thirty patients with 34 cSDHs underwent embolization. The mean age was 77.5 years (SD=7.6). Seventeen cSDHs were primary and 17 were recurrent or embolized adjuvant to surgery.
According to the Nakaguchi classification, 15 cSDHs appeared homogenous, 6 laminar and 13 trabecular.
Thirteen MMAs were embolized with Onyx, 6 with PHIL, 14 with Squid and one MMA with Onyx and Squid.
Three patients scheduled for embolization possessed a rare variant of the MMA with an origin from the ophthalmic artery, which generally restricts embolization.
The mean volume was 71.1 ml (SD=33) prior to embolization and 35 ml (SD=8.5) in the last follow up (p<.001) (Fig. 1).
Six cSDHs did not regress in size in the last follow up CT-scan. This leads to an efficacy of 82%. Three of them needed surgery due to worsening of symptoms.
The presence of a contralateral hematoma demonstrated a higher risk of failure of treatment (p=.021).
There was no influence of age (p=.302), pre-interventional volume (p=.635), midline shift (p=.174), history of trauma (p=.327), recurrence (p=.175), the radiological type, presence of new motor deficit (p=.565) or the embolic agent on the radiological outcome.
Three mild complications and one severe complication, permanent visual deficit, occurred.

Conclusion:
The embolization of the MMA represents an effective therapy for primary and recurrent cSDHs with an efficacy of 82% in this study. The pre-interventional volume does not seem to influence the outcome whereas the presence of bilateral cSDHs influences it negatively. Ophthalmic origin of the MMA is another limitation of this treatment.
Multicenter prospective randomized controlled trials are necessary to prove efficacy and limitations of the treatment in larger patient cohorts.

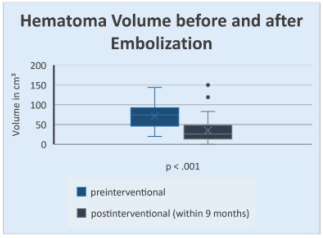

Fig. 1: Hematoma volumes pre- and postinterventional

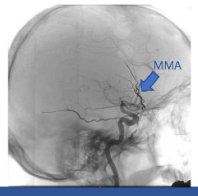

Fig. 2: Angiogram demonstrating MMA, which supplies most of the dura mater and the outer hematoma membrane

Paracelsus Medizinische Privatuniversität | Universitätsklinik für Neurochirurgie | Klinikum Nürnberg | Adrian Liebert | adrian.liebert@klinikum-nuernberg.de

Efficacy and Limitations of the Embolization of the middle meningeal artery in chronic subdural hematoma

Adrian Liebert[1], Heinz-Leonhard Voit-Hoehne[2], Leonard Ritter[1], Thomas Eibl[1], Alexander Hammer[1], Hans-Herbert Steiner[1]

[1]Department of Neurosurgery, Paracelsus Medical University, Nuremberg, Germany; [2]Department of Neuroradiology, Paracelsus Medical University, Nuremberg, Germany; Contact: adrian.liebert@stud.pmu.ac.at

Objective
The aim of the study is to investigate the efficacy and limitations of the embolization of the middle meningeal artery (MMA) in chronic subdural hematomas (cSDH).

Methods
We retrospectively analyzed patients who underwent embolization of the MMA for the treatment of cSDH from Aug. 2019 to Oct. 2021. The data acquisition included the age of the patients, the radiological appearance (volume, midline shift and Nakaguchi classification), intake of antithrombotic agents and whether it was a recurrent or a primary cSDH. Abnormalities of the MMA and the applied embolic agents were noted.
Statistical analysis was performed with a significance level two-sided p-value of ≤ .05.

Results
Thirty patients with 34 cSDHs underwent embolization. The mean age was 77.5 years (SD=7.6). Seventeen cSDHs were primary and 17 were recurrent or embolized adjuvant to surgery.
According to the Nakaguchi classification, 15 cSDHs appeared homogenous, 6 laminar and 13 trabecular.
Thirteen MMAs were embolized with Onyx, 6 with PHIL, 14 with Squid and one MMA with Onyx and Squid.
Three patients scheduled for embolization possessed a rare variant of the MMA with an origin from the ophthalmic artery, which generally restricts embolization.
The mean volume was 71.1 ml (SD=33) prior to embolization and 35 ml (SD=8.5) in the last follow up (p<.001).
Six cSDHs did not regress in size in the last follow up CT-scan. This leads to an efficacy of 82%. Three of them needed surgery due to worsening of symptoms.
The presence of a contralateral hematoma demonstrated a higher risk of failure of treatment (p=.021).
There was no influence of age (p=.302), pre-interventional volume (p=.635), midline shift (p=.174), history of trauma (p=.327), recurrence (p=.175), the radiological type, presence of new motor deficit (p=.565) or the embolic agent on the radiological outcome.
Three mild complications and one severe complication, permanent visual deficit, occurred.

Conclusions
The embolization of the MMA represents an effective therapy for primary and recurrent cSDHs with an efficacy of 82% in this study. The pre-interventional volume does not seem to influence the outcome whereas the presence of bilateral cSDHs influences it negatively. Ophthalmic origin of the MMA is another limitation of this treatment.
Multicenter prospective randomized controlled trials are necessary to prove efficacy and limitations of the treatment in larger patient cohorts.

PARACELSUS MEDIZINISCHE PRIVATUNIVERSITÄT

Klinikum Nürnberg
wir sind für Sie da!

Messungen der Körperzusammensetzung von Frühgeborenen zur Ernährungssteuerung im klinischen Alltag

L. Lücke (1,2), C. Fusch (1), K. Knab (1), S. Schäfer (1), J. Zimmermann (1), A. Szakacs-Fusch (1), N. Rochow (1)

(1) Universitätskinderklinik Nürnberg, (2) Universität Duisburg-Essen

EINLEITUNG

- Gewicht, Länge und Kopfumfang sind Parameter des klinischen Alltags, erlauben jedoch keine Abschätzung der Körperzusammensetzung (BC).
- Die für die Routine zugelassene Airdisplacement-Plethysmographie (ADP) ist der Goldstandard für die Messung der BC bei Frühgeborenen (FG) und Reifgeborenen ohne Atemunterstützung.
- Die Bioelektrische Impedanz (BIA) ist ein im Erwachsenenalter gängiges Verfahren zur KPZ-Messung und neuere Geräte sind auch für FG erhältlich.

- Ziel dieser Qualitätssicherungsinitiative (QI) ist:
  1) den Arbeitsaufwand für wöchentliche Messung der BC bei FG zu analysieren,
  2) die Anwendbarkeit der ADP bei FG in verschiedenen Altersgruppen (SSW) zu beurteilen,
  3) die BC mit aktuellen Referenz-Perzentilkurven zu vergleichen und
  4) die BC der BIA und der ADP zu vergleichen.

METHODE

- Dieses QI-Projekt wurde von Jan. bis Sept. 2021 an der Univ. Kinderklinik Nürnberg durchgeführt.
- Wöchentliche ADP-Daten (PeaPod®, Cosmed, USA) klinisch stabiler Säuglinge ohne Atemunterstützung wurden retrospektiv analysiert.
- In einer Subgruppe wurden BIA-Daten (BioScan touch i8 – nano, Maltron, UK) aus der ersten Lebenswoche täglich und danach wöchentlich analysiert. (Abb.1)
- Individuelle Trajektorien für Fettmasse (FM%), Fettmasse (FM) und fettfreie Masse (FFM) bei FG wurden mit R berechnet und basierend auf in der Literatur vorliegenden BC-Referenzkurven interpretiert.

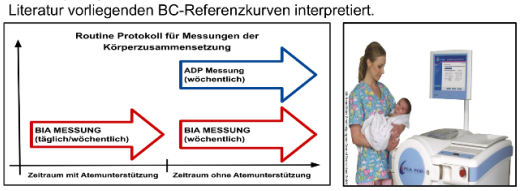

Abb. 1: *Routine Protokoll für BC Messsungen*

ERGEBNISSE

- Zur Verfügung standen 386 Tests von 168 FG. ADP Tests waren bei FG <28 SSW im Vergleich zu FG >32 SSW in signifikant späterer Lebenswoche möglich. Der mögliche stationäre Zeitraum für ADP Messungen war bei FG <28 SSW am längsten. Messungen erfolgten erst zu einem späteren postmenstruellen Alter (Abb. 2).

Schwangerschaftswoche bei Geburt	<28	28-31+6/7	32-36+6/7	Gesamt
Anzahl an Kindern	13	40	115	168
Lebenswoche bei ersten Test	11	5	1	2.5
Postmenstruelles Alter bei ersten Test (Wo)	37	35	35	35,5
Anzahl an Test vor Entlassung	3	2	1,5	2

Abb. 2: *ADP-Messungen in klinischer Routine je SSW bei Geburt*

- Der Zeitaufwand pro ADP betrug 7 min. Die 11 (7-15) wöchentlichen ADP Messungen ergaben eine Arbeitszeit am Testtag von 77 (49-105) min für je jeweils einen Bediener (Kalibrierung, LVP Test) und zwei Pflegepersonal (an- und ausziehen, wiegen). Eine BIA dauerte 3 min mit lediglich einem Personal.
- Die individuellen FM und FFM Trajektorien gemessen mit der ADP verlaufen parallel zu den Referenzkurven (Abb. 3). Die zeitgleichen BIA und ADP Messungen zeigten Differenzen (FM of 60 ±130 g, FFM of 70 ± 140 g and FM% of 2 ± 4 %) (Abb. 3). Die BIA hatte ein kleineres 95% Konfidenzintervall der FM% (10-11%) im Vergleich zur LVP (11,5-13,5%).

ERGEBNISSE

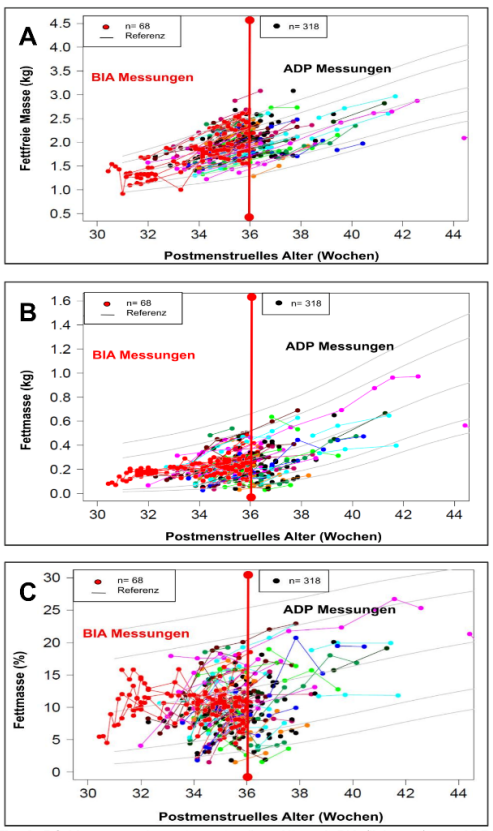

Fig. 2: *BC Messungen je postmenstruellem Alter mit BIA (links, rot) und ADP (rechts, unterschiedliche Farbe je Individuum)*
Graph A: FFM; Graph B: FM; Graph C: FM%

DISKUSSION

- ADP und BIA wurden erfolgreich, mit vertretbarem Arbeitsaufwand in die klinische Routine integriert.
- LVP Messungen erfordern klinische Stabilität ohne Atemunterstützung, welche bei FG <28 SSW relativ spät während des klinischen Aufenthaltes erreicht wird und so das Outcome widerspiegelt, aber wenig Spielraum für frühe Ernährungsintervention in Krankenhaus erlaubt.
- Die parallelen BC Trajetorien zu den Referenzperzentilen weisen darauf hin, dass die untersuchte Kohorte einen ähnlichen klinischen Verlauf wie die Referenzkohorte hat. Die BIA hat Potential BC Messungen über den gesamten Krankenhausaufenthalt zu ermöglichen. Die Validität der BIA Messungen bei FG muss in zukünftigen Studien geprüft werden.
- Die etablierte Routine ermöglicht uns die BC-Entwicklung von Frühgeborenen zu evaluieren. Sie eröffnet Möglichkeiten für weitere Studien und individuelle Ernährungsanpassungen bei Frühgeborenen.

Christoph Fusch, MD, PhD, Pediatrics, Paracelsus Medical University, christoph.fusch@klinikum-nuernberg.de

Messungen der Körperzusammensetzung von Frühgeborenen zur Ernährungssteuerung im klinischen Alltag

Lennart Lücke[1,2], Christoph Fusch[1], Katja Knab[1], Stefan Schäfer[1], Jasper Zimmermann[1], Adel Szakacs-Fusch[1], Niels Rochow[1]

[1]Kinderklinik der Paracelsus Medizinischen Universität Nürnberg, Deutschland; [2]Universität Duisburg-Essen; Contact: lennart.luecke@stud.uni-due.de

Objective
Zur Ernährungssteuerung sind Gewicht, Länge und Kopfumfang Parameter des klinischen Alltags, erlauben jedoch keine Abschätzung der Körperzusammensetzung (Body composition (BC)). Die für die Routine zugelassene Airdisplacement plethysmography (ADP) ist der Goldstandard für die Messung der BC bei Frühgeborenen (FG) und Reifgeborenen ohne Atemunterstützung. Die Bioelektrische Impedanz (BIA) ist ein im Erwachsenenalter gängiges Verfahren zur BC-Messung und neuere Geräte sind auch für FG erhältlich. Ziel dieser Qualitätssicherungsinitiative (QI) ist: 1) den Arbeitsaufwand für wöchentliche Messung der BC bei FG zu analysieren, 2) die Anwendbarkeit der ADP bei FG in verschiedenen Altersgruppen (SSW) zu beurteilen, 3) die BC mit aktuellen Referenz-Perzentilkurven zu vergleichen und 4) die BC der BIA und der ADP zu vergleichen.

Methods
Dieses QI-Projekt wurde von Jan. bis Sept. 2021 an der Univ. Kinderklinik Nürnberg durchgeführt. Wöchentliche ADP-Daten (PeaPod®, Cosmed, USA) klinisch stabiler Säuglinge ohne Atemunterstützung wurden analysiert. In einer Subgruppe wurden BIA-Daten (BioScan touch i8 – nano, Maltron, UK) aus der ersten Lebenswoche täglich und danach wöchentlich analysiert. Individuelle Trajektorien für Fettmasse (FM%), Fettmasse (FM) und fettfreie Masse (FFM) bei FG wurden mit R berechnet.

Results
Zur Verfügung standen 386 Tests von 168 FG. ADP Test waren bei FG <28 SSW im Vergleich zu FG >32 SSW in signifikant späterer Lebenswoche möglich (Abb. 1). Der mögliche stationäre Zeitraum für ADP Messungen war bei FG <28 SSW am längsten, Messungen erfolgten erst zu einem späteren postmenstruellen Alter (Abb. 1). Der Zeitaufwand pro ADP betrug 7 min. Die 11 (7-15) wöchentlichen ADP Messungen ergaben eine Arbeitszeit am Testtag von 77 (49-105) min für jeweils einen Bedienenden (Kalibrierung, ADP Test) und zwei Pflegepersonal (an- und ausziehen, wiegen). Eine BIA dauerte 3 min mit lediglich einer Study Nurse. Die individuellen FM und FFM Trajektorien gemessen mit der ADP verlaufen parallel zu den Referenzkurven. Die zeitgleichen BIA und ADP Messungen zeigten Differenzen (FM: 14±70g, FM%: 5±3%, FFM: 11±70g) (Abb. 2). Die BIA hatte ein kleineres 95% Konfidenzintervall der FM% (10-11%) im Vergleich zur ADP (11,5-13,5%).

Conclusions
ADP und BIA wurden erfolgreich, mit vertretbarem Arbeitsaufwand in die klinische Routine integriert. ADP Messungen erfordern klinische Stabilität ohne Atemunterstützung, welche bei FG <28 SSW relativ spät während des klinischen Aufenthaltes erreicht wird und so das Outcome widerspiegelt, aber wenig Spielraum für frühe Ernährungsintervention im Krankenhaus erlaubt. Die parallelen BC Trajektorien zu den Referenzperzentilen weisen darauf hin, dass die untersuchte Kohorte einen ähnlichen klinischen Verlauf wie die Referenzkohorte hat. Die BIA hat Potential BC Messungen über den gesamten Krankenhausaufenthalt zu ermöglichen. Die Validität der BC Messungen bei FG muss in zukünftigen Studien geprüft werden.

PARACELSUS MEDIZINISCHE PRIVATUNIVERSITÄT

Klinikum Nürnberg
wir sind für Sie da!

Analyse der Reproduzierbarkeit von Messungen der Körperzusammensetzung anhand der Luftverdrängungsplethysmographie bei Frühgeborenen

L. Lücke (1,2), C. Fusch (1), K. Knab (1), A. Szakacs-Fusch (1), S. Schäfer (1), J. Zimmermann (1), N. Rochow (1)

(1) Universitätskinderklinik Nürnberg, (2) Universität Duisburg-Essen

EINLEITUNG

- Daten zur Körperzusammensetzung (Body composition (BC)) können wichtige Informationen zum Ernährungszustand von Früh- und Reifgeborenen (FR) liefern.
- In der NICU des Klinikums Nürnberg wird die BC in der klinischen Routine mit der Airdisplacement-Plethysmographie (ADP) gemessen. ADP misst die Körperdichte über Körpervolumen (KV) und Körpergewicht (KG) und kann bei klinisch stabilen FR ohne Atemunterstützung eingesetzt werden. ADP wurde in mehreren Studien für FR validiert. Die Datenlage zur Reproduzierbarkeit der ADP bei Probanden mit niedrigem KG, postnatalen Alter (PNA) und prozentualem Fettanteil ist jedoch unklar.
- Ziel dieser Qualitätssicherungsinitiative (QS) ist es, die Reproduzierbarkeit der ADP anhand von Test/Re-Test Analyse in der klinischen Routine bei FR zu evaluieren.

METHODEN

- Messung der BC mit PeaPod® (Cosmed, Italien) wurden im Studienzeitraum von März bis Juni 2021 durchgeführt.
- Wöchentliche BC-Doppelmessungen wurden bei klinisch stabilen FR ohne Beatmung jeweils dienstags durchgeführt. Die statistische Auswertung erfolgte mit R.



ERGEBNISSE

- Insgesamt wurden 188 Doppelmessungen an 118 FR (n=88 Frühgeborene, n=30 Reifgeborene) durchgeführt.
- Die Studienpopulation umfasste 50 weibliche und 68 männliche FR. Das mittlere KG der Frühgeborenen und Reifgeborenen war 2,2±0,5 bzw. 3,0±0,7 kg (Abb. 1).

	Frühgeborene	Reifgeborene	Gesamt
Anzahl an Kindern (M/W)	88 (50/38)	30 (18/12)	118 (68/50)
Gestationsalter in Wochen	33.0±3.0	39.2±1.5	34.6±3.8
KG am Testtag (kg)	2.2±0.5	3.0±0.7	2.4±0.6
Länge am Testtag (cm)	42±2.4	49.1±3.0	45.7±2.9
PMA am Testtag (Wochen)	35.9±1.8	39.9±1.5	36.6±2.3
Postnatales Alter am Testtag (Wochen)	3.6±4.1	0.8±0.9	3.1±3.9

Abb. 1: *PeaPod Messungen in klinischer Routine je Frühgeborene und Reifgeborene*

- Die mittlere Differenz von KV und KG waren 5,6±12 mL und -2,5±5g und war im Bland-Altmann Diagramm über den gemessenen Gewichtsbereich konstant.
- Die Abweichung für FFM betrug 56 g (2,5% bezogen auf den Mittelwert der Daten) und die Korrelationsanalyse ergab für FFM ein R^2=0.973 (slope 0.984, intercept 0.05).
- Die entsprechenden Daten für FM sind 54 g (18.0%) und R^2=0.828 (slope 0.859; intercept 0,023).
- Die absolute Abweichung für FFM bei einem PNA von <4 und >12 Wochen waren mit 54±62g und 46±34g vergleichbar. Für FFM/KG zeigt sich eine Abweichung von 23±27g/kg und 16±12g/kg für Messungen bei einem PNA von jeweils <4 und >12 Wochen (Abb. 2)
- FFM/KG zeigte eine Abweichung in den KG-Gruppen >1 und >3kg ist 26±26g/kg und 11±10g/kg (Abb. 2).

ERGEBNISSE

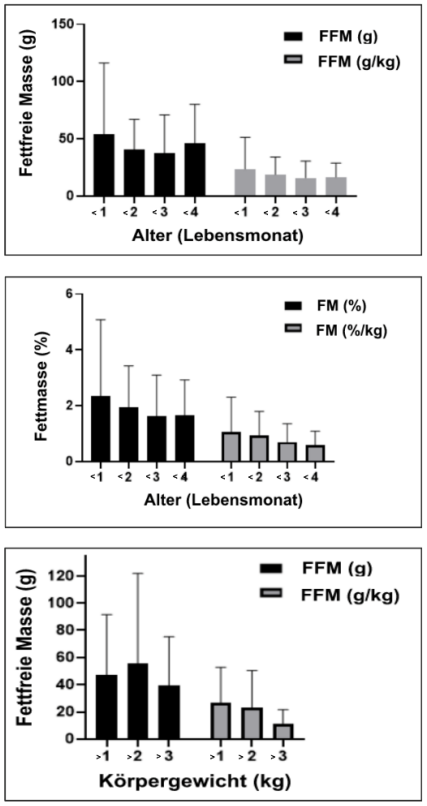

Abb. 2: *Absolute Abweichung zwischen ADP Messungen je Alter (A, B; Lebensmonaten) und Körpergewicht (C; kg); Graph A und C: FFM und FFM/kg; Graph B: FM(%) und FM(%)/kg*

DISKUSSION

- Unsere Analyse zeigt, dass der absolute Messfehler der ADP über den Bereich von 1,4 bis 4,5 kg KG fast konstant war.
- Somit nimmt der relative Fehler der Messung der BC mit der ADP mit zunehmendem KG und Lebensalter ab (Abb.2). Der mittlere Fehler für die FFM (56 g) entspricht bei einem 2000g schweren FG einer Unsicherheit in der Größenordnung von 4 Tagen FFM-Wachstum (i.e. 80% von 15g/kg/d Gewichtszunahme).
- Durch die verbesserten neonatalen Outcomes können leichtere FR früher gemessen werden. Für die klinische Anwendung der ADP zur individuellen Ernährungssteuerung sehen wir für kleinere Patienten noch Optimierungspotential dieser Messmethode.

Christoph Fusch, MD, PhD, Pediatrics, Paracelsus Medical University, christoph.fusch@klinikum-nuernberg.de

Analyse der Reproduzierbarkeit von Messungen der Körperzusammensetzung anhand der Luftverdrängungsplethysmographie bei Frühgeborenen

Lennart Lücke[1,2], Christoph Fusch[1], Katja Knab[1], Adel Szakacs-Fusch[1], Stefan Schäfer[1], Jasper Zimmermann[1], Niels Rochow[1]

[1]Kinderklinik der Paracelsus Medizinischen Universität Nürnberg, Deutschland; [2]Universität Duisburg-Essen; Contact: lennart.luecke@stud.uni-due.de

Objective
Daten zur Körperzusammensetzung (Body composition (BC)) können wichtige Informationen zum Ernährungszustand von Früh- und Reifgeborenen (FR) liefern. In Zukunft könnten diese Daten auch zur Ernährungssteuerung beitragen. In der NICU des Klinikums Nürnberg wird die BC in der klinischen Routine mit der Airdisplacement-Plethysmographie (ADP) gemessen. ADP misst die Körperdichte über Körpervolumen (KV) und Körpergewicht (KG) und kann bei klinisch stabilen FR ohne Atemunterstützung eingesetzt werden. ADP wurde in mehreren Studien für FR validiert. Die Datenlage zur Reproduzierbarkeit der ADP bei Probanden mit niedrigem KG, postnatalen Alter (PNA) und prozentualem Fettanteil ist jedoch unklar. Ziel dieser Qualitätssicherungsinitiative (QS) ist es, die Reproduzierbarkeit der ADP anhand von Test/Re-Test Analyse in der klinischen Routine bei FR zu evaluieren.

Methods
Messung der BC mit PeaPod® (Cosmed, Italien) im Studienzeitraum von März bis Juni 2021. Wöchentliche BC-Doppelmessungen wurden bei klinisch stabilen FR ohne Beatmung jeweils dienstags durchgeführt. Die statistische Auswertung erfolgte mit R.

Results
Insgesamt wurden 188 Doppelmessungen an 118 FR (n=88 Frühgeborene, n=30 Reifgeborene) durchgeführt. Die Studienpopulation umfasste 50 weibliche und 68 männliche FR. Das mittlere KG der Frühgeborenen und Reifgeborenen war 2,2±0,5 bzw. 3,0±0,7 kg (Abb. 1). Die mittlere Differenz von KV und KG waren 9,2 mL (0,4%) und 3,8 g (0,15%) und war im Bland-Altmann Diagramm über den gemessenen Gewichtsbereich konstant. Die Abweichung für FFM betrug 56 g (2,5% bezogen auf den Mittelwert der Daten) und die Korrelationsanalyse ergab für FFM ein R^2=0.973 (slope 0.984, intercept 0.05). Die entsprechenden Daten für FM sind 54 g (18.0%) und R^2=0.828 (slope 0.859; intercept 0,023). Die absolute Abweichung für FFM bei einem PNA von <4 und >12 Wochen waren mit 54±62g und 46±34g vergleichbar. Für FFM/KG zeigt sich eine Abweichung von 23±27g/kg und 16±12g/kg für Messungen bei einem PNA von jeweils <4 und >12 Wochen (Abb. 2). FFM/KG zeigte eine Abweichung in den KG-Gruppen >1 und >3kg ist 26±26g/kg und 11±10g/kg (Abb. 2).

Conclusions
Unsere Analyse zeigt, dass der absolute Messfehler der ADP über den Bereich von 1,4 bis 4,5 kg KG fast konstant war. Dadurch nimmt der relative Fehler der Messung der BC mit der ADP mit zunehmendem Körpergewicht und Lebensalter ab (Abb.2). Der mittlere Fehler für die FFM (56 g) entspricht bei einem 2000g schweren FG einer Unsicherheit in der Größenordnung von 2 Tagen FFM-Wachstum (i.e. 80% von 15g/kg/d Gewichtszunahme). Ähnliche Messfehler sind bereits in der Literatur berichtet.
Durch die verbesserten neonatalen Outcomes können mittlerweile leichtere FR als früher gemessen werden. Für die klinische Anwendung der PNA zur individuellen Ernährungssteuerung sehen wir für kleinere Patienten noch Optimierungspotential dieser Messmethode.

AML-derived extracellular vesicles convey immunomodulatory potential

N. Maeding[1], H.-M. Binder[1], B. Vári [1], A. Raninger[1], M. Wolf [1], T. Heuser[2], A. Obermayr[3], G. Brachtl[1], K. Schallmoser[4], D. Strunk [1]

[1] Experimental and Clinical Cell Therapy Institute (ExCT), Spinal Cord Injury and Tissue Regeneration Center Salzburg (SCI-TreCS), Paracelsus Medical University, Salzburg, Austria
[2] Vienna Biocenter Core Facilities, Medical University, Vienna, Austria
[3] Department of Cell Biology, Biomedical Ultrastructure Research Group, University of Salzburg, Salzburg, Austria
[4] Department of Transfusion Medicine, Paracelsus Medical Private University, Salzburg, Austria

nicole.maeding@pmu.ac.at

INTRODUCTION

Acute myeloid leukemia (AML) is the most common form of adult leukemia with an incidence of 4.3 per 100.000 inhabitants in the US. Although 80-85% of patients show complete remission after initial treatment with anthracycline and cytarabine, the overall outcome remains poor. According to the National Cancer Institute of the US, only 29.7% of people diagnosed with AML survive five or more years. AML is a genetically heterogeneous cancer of the myeloid blood cell lineage exhibiting defective control of its proliferation, differentiation and maturation. It arises from a single transformed cell and is maintained by a small population of leukemia initiating cells (LICs). These LICs are hypothesized to instruct their niche directly or by secreting soluble factors and/or extracellular vesicles (EVs) to become permissive resulting in enhanced leukemia progression and relapse. The mechanisms, however, of niche formation and immune evasion remain poorly understood and are subject to ongoing studies.

HYPOTHESIS

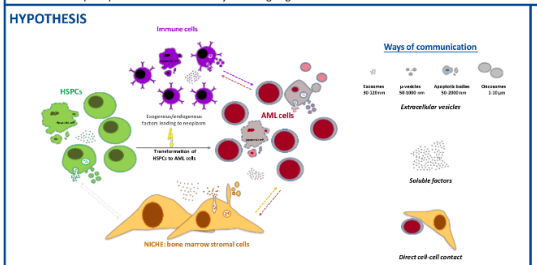

Figure 1: AML cells communicate bi-directionally with their niche and the immune system in various ways, including exchange of cell-derived material and/or information through direct cell-cell contact, extracellular vesicles and other secreted factors. We hypothesize that AML cells instruct their bone marrow niche primarily via EVs to become permissive, resulting in enhanced malignancy progression and relapse risk. Additionally, AML was suggested to suppress the anti-tumor immune response

METHODS

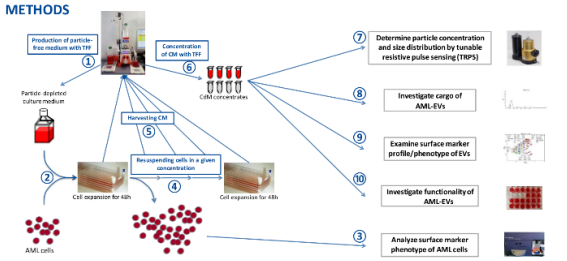

Figure 2: AML cells were grown in particle-depleted medium to exclude serum-derived particles and enable the characterisation of cell-derived particles. Since the cell lines used reached confluency within 48 hours, cells were reseeded every 2 days at optimal density and conditioned media (CM) were pooled from several harvests. After collecting, concentrating and washing the CM with buffered saline solution, we performed in depth characterization of the AML-derived EVs concerning their cargo, surface marker profile and functionality.

QUANTITY & SIZE OF AML-EVs

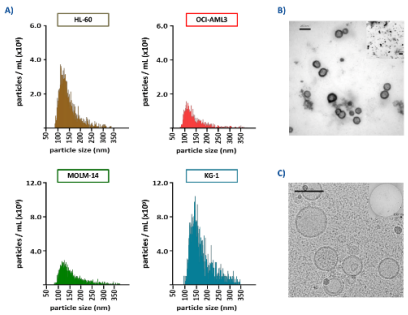

Figure 3: *A)* Size distribution and concentrations of AML-derived particles measured by TRPS *B)* Transmission electron microscopy of MOLM-14 EVs *C)* Cryogenic electron microscopy of MOLM-14 EVs

FUNCTION (IMMUNE RESPONSE & OSTEOGENESIS MODULATION)

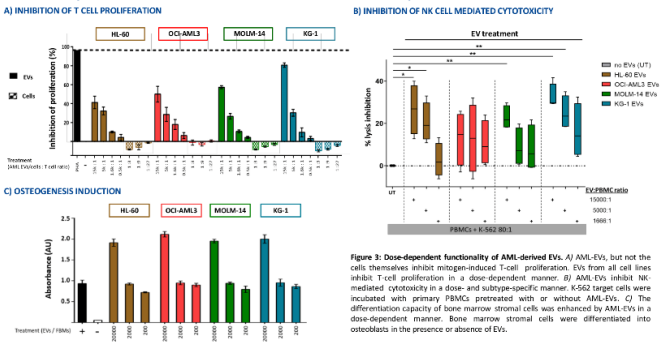

Figure 3: Dose-dependent functionality of AML-derived EVs. *A)* AML-EVs, but not the cells themselves inhibit mitogen-induced T-cell proliferation. EVs from all cell lines inhibit T-cell proliferation in a dose-dependent manner. *B)* AML-EVs inhibit NK-mediated cytotoxicity in a dose- and subtype-specific manner. K-562 target cells were incubated with primary PBMCs pretreated with or without AML-EVs. *C)* The differentiation capacity of bone marrow stromal cells was enhanced by AML-EVs in a dose-dependent manner. Bone marrow stromal cells were differentiated into osteoblasts in the presence or absence of EVs.

IMMUNE PHENOTYPE OF AML CELL LINES

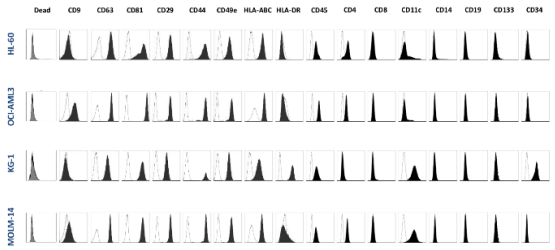

Figure 5: The surface marker phenotype of four AML cell lines was analyzed by flow cytometry. We investigated various markers related to haematopoiesis (CD45, CD4, CD8, CD11c, CD14, CD19) and antigen presentation (HLA-ABC, HLA-DR), the leukemia-related marker CD133 and the hematopoietic stem/progenitor cell marker CD34. Black histograms depict the respective antibody stain, white histograms are the corresponding isotype controls.

AML-EV SURFACE MARKER PROFILING

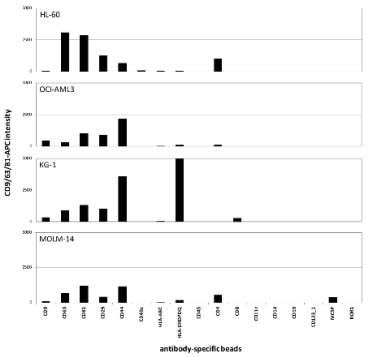

Figure 6: Immune phenotype of AML-EVs. Investigating the surface marker phenotype of EVs with MACS Plex® multiplex bead- based flow cytometry showed high expression levels of classical tetraspanins (CD81, CD63, CD9) as well as intercellular matrix interaction and adhesion proteins such as integrin β1 (CD29) and the hyaluron receptor CD44. Differential expression among the AML cell line derived EVs was observed for the MHC class I and II markers (HLA-ABC and HLA-DRDPDQ, respectively), melanoma-associated chondroitin sulphate proteoglycan (MCSP) and Receptor Tyrosine Kinase Like Orphan Receptor 1 (ROR1). The hematopoietic markers observed on cells were represented in most cases on EV surfaces (CD4, CD8, CD14). Interestingly, CD45, a marker of lymphocytes and CD11c, a marker of dendritic cells were exclusively expressed on cells, not on EVs.

RNA CARGO OF AML-DERIVED EVs

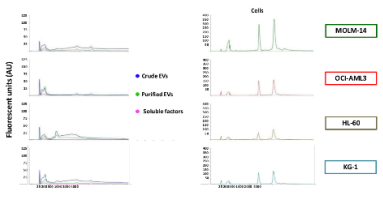

Figure 7: AML-EV preparations contain small RNA species as well as longer RNA molecules, including ribosomal RNA. Further investigations are needed to determine which molecules are inside the EVs and which ones are outside (associated with the EV corona), but protected.

SUMMARY

- Acute myeloid leukemia (AML) cells secrete extracellular vesicles (EVs) and soluble factors into their environment. EV containing conditioned medium can be purified by tangential flow filtration (TFF) to enrich particles in a given size and separate EVs from soluble factors.
- AML-derived EVs, but not the cells exhibit immune modulation capacity in a dose-dependent manner. AML-EVs inhibit NK cell mediated cytotoxicity as well as T cell proliferation. Furhtermore, they induce supra-optimum osteogenic differentiation.
- AML EVs display EV-specific surface markers including canonical tetraspanins, extracellular matrix interaction molecules and integrins. The composition and expression levels of the detected surface markers reflected their AML cell line origin.
- The immune phenotype of the different AML cell lines shows only limited variability.
- AML-EVs contain high levels of small RNA species. Longer RNA molecules, including ribosomal RNAs show lower abundance compared to total the RNA profile of the cells, however they are still present in the EV preparations.

ACKNOWLEDGEMENTS

This work is part of a project that has received funding from the Cancer Cluster Salzburg (CCS).

AML-derived extracellular vesicles convey immunomodulatory potential

Nicole Maeding[1], Heide-Marie Binder[1], Balasz Vári[1], Anna Raninger[1], Martin Wolf[1], Thomas Heuser[2], Astrid Obermayr[3], Gabriele Brachtl[1], Katharina Schallmoser[4], Dirk Strunk[1]

[1]Experimental and Clinical Cell Therapy Institute (ExCT), Spinal Cord Injury and Tissue Regeneration Center Salzburg (SCI-TreCS), Paracelsus Medical University, Salzburg, Austria; [2]Vienna Biocenter Core Facilities, Medical University, Vienna, Austria; [3]Department of Cell Biology, Biomedical Ultrastructure Research Group, University of Salzburg, Salzburg, Austria; [4]Department of Transfusion Medicine, Paracelsus Medical Private University, Salzburg, Austria; Contact: nicole.maeding@pmu.ac.at

Objective
Acute myeloid leukemia (AML) is a genetically heterogeneous adult leukemia with an incidence of 4.3 per 100.000 inhabitants in the US and a poor 5-year survival rate of 29.7%. Extracellular vesicles (EVs) are enriched in AML patients and contribute to disease progression by inducing a leukemia-permissive niche. AML-EVs were also found to promote migration and invasion of AML cells, chemoresistance and quiescence of hematopoietic stem cells. We and others have previously observed immunomodulatory functions of different hematopoietic and non-hematopoietic cell-derived EVs. We therefore asked if AML-EVs can directly target immune cell functions.

Methods
AML cell lines HL-60, KG-1, OCI-AML3 and MOLM-14 were cultured in particle-free medium under large-scale culture conditions to obtain conditioned medium. AML-EVs were purified and enriched using two sequential rounds of tangential flow filtration (TFF). EVs were characterized by electron microscopy, western blotting and bead-based flow cytometry, confirming the double-membrane morphology, purity and identity. Purified AML-EVs were used as active agent in assays interrogating immune modulation during T cell proliferation and NK cell-dependent cytotoxicity.

Results
Purified AML-EVs showed a significant dose-dependent inhibition of PHA-stimulated T cell proliferation that was not observed with AML cells or the isolated soluble factors. Furthermore, AML-derived EVs reduced NK cell-mediated lysis of K-562 target cells in a calcein release assay in a dose-dependent manner. In addition, osteogenic differentiation capacity of bone marrow stromal cells was increased by AML-EVs. Analysis of EV surface marker expression by MACSPlex for EVs and flow cytometry for AML cells showed a comparable pattern reflecting the AML cell origin. In contrast to AML cells, AML-EVs showed only miniscule levels of HLA-ABC (MHC I) which would be necessary for presentation of altered self. RNA cargo analysis of AML-EVs revealed small RNA species (e.g. miRNAs) as well as longer RNA molecules, albeit to a lesser extent.

Conclusions
We show that AML-EVs, but not AML cells or their secreted soluble factors, inhibit T cell proliferation and NK cell functionality while enhancing osteogenic differentiation capacity of bone marrow stroma. These effects could contribute to the creation of a leukemia-permissive niche and immune escape of AML mediated by their EVs. The underlying molecular mechanisms, however, need further investigation.

PARACELSUS MEDIZINISCHE PRIVATUNIVERSITÄT

Universitätsklinikum Erlangen

Sleep as a random walk
A super-statistical analysis of EEG sleep data

Gefördert durch DFG Deutsche Forschungsgemeinschaft

Claus Metzner[1], Achim Schilling[1], Maximilian Traxdorf[2], Holger Schulze[1], Patrick Krauss[1,#]

[1] Neurowissenschaftliches Forschungslabor, Hals-Nasen-Ohren Klinik, Universitätsklinikum Erlangen
[2] Klinik für Hals-Nasen-Ohrenheilkunde, Universitätsklinik der Paracelsus Medizinischen Privatuniversität, Klinikum Nürnberg / Standort Nord
[#] patrick.krauss@uk-erlangen.de

Abstract

Objective: In clinical practice, human sleep is classified into stages, each associated with different levels of muscular activity and marked by characteristic patterns in the EEG signals. It is however unclear whether this subdivision into discrete stages with sharply defined boundaries is truly reflecting the dynamics of human sleep.
Methods: We consider one-channel EEG signals as heterogeneous random walks: stochastic processes controlled by hyper-parameters that are themselves time-dependent. Next, we perform a super-statistical analysis by computing 'hyper-parameters', such as the standard deviation, kurtosis and skewness of the raw signal distributions, within subsequent 30-second epochs. Based on the hyper-parameters, we finally perform a pairwise similarity analysis between the different sleep stages, using a novel quantitative measure for the separability of data clusters in multi-dimensional spaces.
Results: We demonstrate the heterogeneity of the random process underlying human sleep by showing that each sleep stage has a characteristic distribution and temporal correlation function of the raw EEG signals. Furthermore, it turns out that also the hyper-parameters have characteristic, sleep-stage-dependent distributions, which can be exploited for a simple Bayesian sleep stage detection. Moreover, we find that the hyper-parameters are not piece-wise constant, as the traditional hypnograms would suggest, but show rising or falling trends within and across sleep stages, pointing to an underlying continuous rather than subdivided process that controls human sleep
Conclusions: In this work, we treat the signal as a non-stationary, heterogeneous random walk, generated by a stochastic system with parameters that change over time, depending on the physiological state of the subject. In particular, this random walk has different statistical properties in each of the five sleep stages, and these differences can be exploited for a simple automated Bayesian sleep stage detection. In contrast to sleep stage detectors based on deep neural networks which suffer from the *black box problem*, our Bayesian approach is completely transparent and explainable, as the features used to distinguish between sleep stages (i.e. the distributions of hyper-parameters) are explicit. Once these hyper-parameter distributions are extracted from the raw data and included into the likelihood, the Bayesian detector can immediately be applied without any training or further optimization. In contrast, most deep learning applications require extensive training and are *data hungry*.

Sleep-stage-dependent distributions of selected hyper-parameters

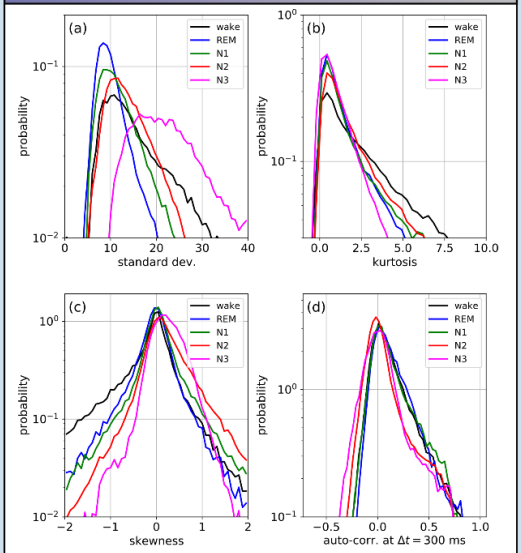

Probability density distributions of hyper-parameters extracted from the raw EEG data. **a:** Standard deviation STD. **b:** Kurtosis KUR. **c:** Skewness SKE. **d:** Auto-correlation at lag-time 300 ms, denoted as CDT.

Temporal evolution of hyper-parameters

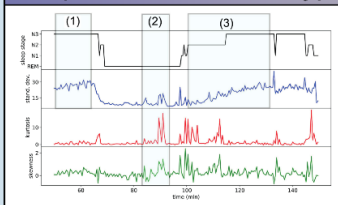

Typical features in the temporal behavior of hyper-parameters, such as consistent trends (1) and extreme fluctuations (2) within an ongoing sleep stage, as well as trends that extend across sleep stages (3).

Bayesian sleep-stage classification

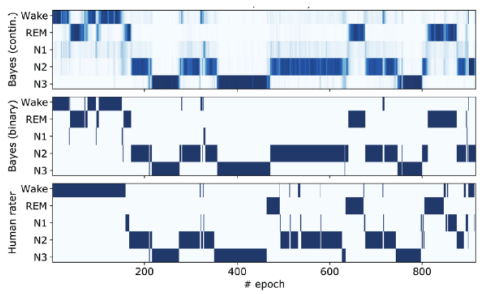

Examples of automated Bayesian sleep stage classification. The upper hypnogram shows, for each 30-second epoch, the posterior probabilities of the sleep stages, with larger color density corresponding to larger probability. The middle hypnogram shows only the predicted sleep stage with maximum posterior probability. The lower hypnogram is the ground truth, provided by the specialist human rater. The accuracy defined as the ratio of correct sleep stage predictions is 0.77

Mutual 'distances' between sleep-stages

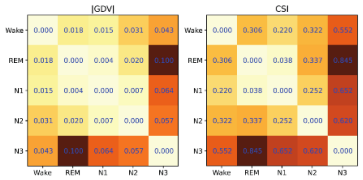

Mutual 'distance' between EGG data from different sleep-stages, evaluated in the embedding space of the three hyper-parameters STD, KUR and SKE. The left distance matrix shows the magnitude of the General Discrimination Value (GDV), the right matrix shows the Cluster Separation Index (CSI). In both measures, the minimum distance is found between REM and N1, whereas the maximum distance is between REM and N3.

Reference and Funding

Metzner, C., Schilling, A., Traxdorf, M., Schulze, H., & Krauss, P. (2021).
Sleep as a random walk: a super-statistical analysis of EEG data across sleep stages.
Communications Biology, 4(1), 1-11.

Funded by DFG Grants:
TR 1793/2-1 to Maximilian Traxdorf
SCHU 1272/16-1 to Holger Schulze

Sleep as a random walk - A super-statistical analysis of EEG sleep data

Claus Metzner[1], Achim Schilling[1], Maximilian Traxdorf[2], Holger Schulze[1], Patrick Krauss[1]

[1]University Hospital Erlangen; [2]Universitätsklinik der Paracelsus Medizinischen Privatuniversität; Contact: patrick.krauss@uk-erlangen.de

Objective
In clinical practice, human sleep is classified into stages, each associated with different levels of muscular activity and marked by characteristic patterns in the EEG signals. It is however unclear whether this subdivision into discrete stages with sharply defined boundaries is truly reflecting the dynamics of human sleep.

Methods
We consider one-channel EEG signals as heterogeneous random walks: stochastic processes controlled by hyper-parameters that are themselves time-dependent. Next, we perform a super-statistical analysis by computing 'hyper-parameters', such as the standard deviation, kurtosis and skewness of the raw signal distributions, within subsequent 30-second epochs. Based on the hyper-parameters, we finally perform a pairwise similarity analysis between the different sleep stages, using a novel quantitative measure for the separability of data clusters in multi-dimensional spaces.

Results
We demonstrate the heterogeneity of the random process underlying human sleep by showing that each sleep stage has a characteristic distribution and temporal correlation function of the raw EEG signals. Furthermore, it turns out that also the hyper-parameters have characteristic, sleep-stage-dependent distributions, which can be exploited for a simple Bayesian sleep stage detection. Moreover, we find that the hyper-parameters are not piece-wise constant, as the traditional hypnograms would suggest, but show rising or falling trends within and across sleep stages, pointing to an underlying continuous rather than subdivided process that controls human sleep.

Conclusions
In this work, we treat the signal as a non-stationary, heterogeneous random walk, generated by a stochastic system with parameters that change over time, depending on the physiological state of the subject. In particular, this random walk has different statistical properties in each of the five sleep- (or, more precisely, vigilance-) stages, and these differences can be exploited for a simple automated Bayesian sleep stage detection. In contrast to sleep stage detectors based on deep neural networks which suffer from the “black box problem”, our Bayesian approach is completely transparent and explainable, as the features used to distinguish between sleep stages (i.e. the distributions of hyper-parameters) are explicit. Once these hyper-parameter distributions are extracted from the raw data and included into the likelihood, the Bayesian detector can immediately be applied without any training or further optimization. In contrast, most deep learning applications require extensive training and are “data hungry”.

References
1. Metzner, C., Schilling, A., Traxdorf, M., Schulze, H., & Krauss, P. (2021). Sleep as a random walk: a super-statistical analysis of EEG data across sleep stages. Communications Biology, 4(1), 1-11.

Entwicklung eines standardisierten Protokolls zur Messung von Validität und Reliabilität kommerziell erhältlicher optischer Herzfrequenzsensoren

Michael Neudorfer[1], Stefan Tino Kulnik[2], Barbara Mayr[1,2], Josef Niebauer[1,2], Bernhard Reich[1], Jan Smeddinck[2], Gunnar Treff[1,2], Mahdi Sareban[1,2]

[1]Universitätsinstitut für präventive und rehabilitative Sportmedizin, Paracelsus Medizinische Privatuniversität Salzburg
[2]Ludwig Boltzmann Institut für digitale Gesundheit und Prävention

Hintergrund

- Körperliche Inaktivität ist einer der entscheidenden, veränderbaren Risikofaktoren für Herz-Kreislauf-Erkrankungen
- WHO-Empfehlung für körperliche Aktivität: 150-300 min/Woche mit moderater bis hoher Intensität
- Fragebogen-basierte Aktivitätserfassung (= Subjektive Einschätzung) von körperlicher Aktivität ist mit Fehlern von Aktivitätsumfang und -intensität verbunden
- Optische, kommerziell erhältliche Herzfrequenzsensoren versprechen kontinuierliche und objektive Messung der Herzfrequenz und Aktivität

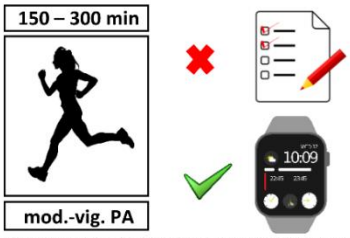

Abbildung 1: Fragebogen vs. Wearable zur Erhebung körperlicher Aktivität

Forschungslücke

Studien zur Messgenauigkeit derartiger Sensoren sind ebenso unterschiedlich, wie die zugrundeliegenden Studienprotokolle.

Ziel

- Entwickeln eines suffizienten und praktikablen Validierungsprotokolls für kommerziell erhältliche optische Herzfrequenzsensoren
- Integration von Labor- und Alltagsbedingungen
- Vergleich mit Gold-Standard: medizinisches Mehrkanal-EKG

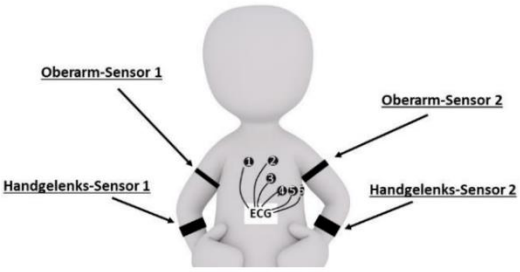

Abbildung 2: Wearable-Platzierung

Auswahlkriterien Wearable

- Akkulaufzeit: > 24 Stunden
- Interner Speicher: > 24 Stunden
- Sekundenweise Aufzeichnung der Herzfrequenz
- Zugriff auf die Rohdaten möglich

Methodik

- Initiale Literaturrecherche zu existierenden Standards für Validierungsprotokolle optischer Herzfrequenzsensoren (MEDLINE via PubMed).
- Zusätzlich wurden die Literaturverzeichnisse relevanter Artikel nach grauer Literatur durchsucht.

Ergebnisse

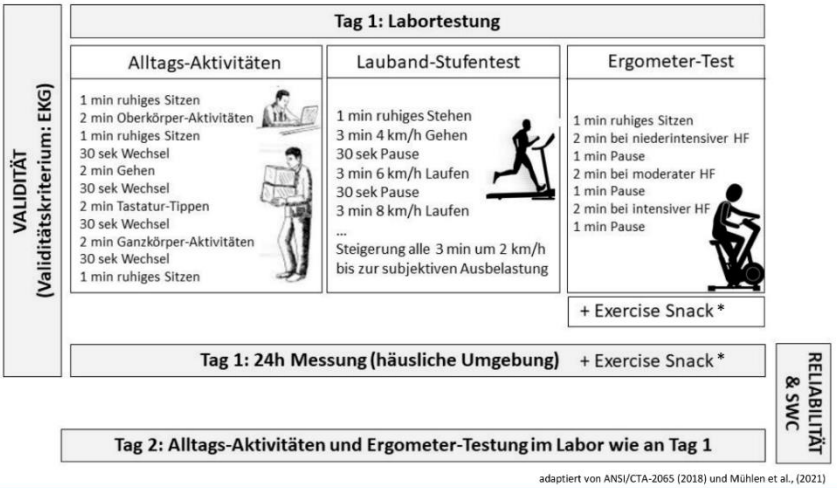

adaptiert von ANSI/CTA-2065 (2018) und Mühlen et al., (2021)

* Kurze intensive Belastung (z.B.: Treppenlauf)

Kontakt: Michael Neudorfer, MSc, MEd
Email: m.neudorfer@salk.at

Entwicklung eines standardisierten Protokolls zur Messung von Validität und Reliabilität kommerziell erhältlicher optischer Herzfrequenzsensoren

Michael Neudorfer[1], Stefan Tino Kulnik[2], Barbara Mayr[1,2], Josef Niebauer[1,2], Bernhard Reich[1], Jan Smeddinck[2], Gunnar Treff[1,2], Mahdi Sareban[1,2]

[1]Universitätsinstitut für präventive und rehabilitative Sportmedizin, Paracelsus Medizinische Privatuniversität Salzburg; [2]Ludwig Boltzmann Institut für digitale Gesundheit und Prävention; Contact: m.neudorfer@salk.at

Objective
Körperliche Inaktivität ist einer der entscheidenden, veränderbaren Risikofaktoren für Herz-Kreislauf-Erkrankungen. Die Weltgesundheitsorganisation empfiehlt pro Woche 150-300 min moderate, beziehungsweise 75-150 min intensive körperliche Aktivität oder eine entsprechende Kombination dieser Vorgaben. Die Beurteilung der körperlichen Aktivität erfolgt häufig auf Basis von Fragebögen. Confounder dieser Methode sind Fehleinschätzungen, Verzerrungen der Erinnerung oder soziale Erwünschtheit. Tragbare optische Herzfrequenzsensoren (Wearables) sind eine Möglichkeit, um die Dauer und Intensität körperlicher Aktivität objektiv und kontinuierlich zu erfassen. Studien zur Messgenauigkeit derartiger Sensoren sind ebenso unterschiedlich, wie die zugrundeliegenden Studienprotokolle.
Ziel dieser Studie ist, ein suffizientes und praktikables Validierungsprotokoll für kommerziell erhältliche optische Herzfrequenzsensoren unter Labor- und Alltagsbedingungen zu entwickeln. Als Referenzmethode soll ein medizinisch zugelassenes Mehrkanal-Elektrokardiogramm (EKG) dienen.

Methods
Initiale Literaturrecherche zu existierenden Standards für Validierungsprotokolle optischer Herzfrequenzsensoren (MEDLINE via PubMed). Zusätzlich wurden die Literaturverzeichnisse relevanter Artikel nach grauer Literatur durchsucht.

Results
Das nun vorgeschlagene Protokoll beinhaltet (i) verschiedene standardisierte Alltagsaktivitäten (z.B. simulierte Computer- oder Hausarbeit), (ii) Gehen und Laufen auf dem Laufband bei verschiedenen Geschwindigkeiten, (iii) subjektive Maximalbelastung zur Bestimmung der maximalen Herzfrequenz, (iv) Radfahren auf dem Ergometer bei drei submaximalen Intensitäten. Darauf folgen (v) eine 24-h Messung der Alltagsaktivitäten in häuslicher Umgebung und (vi) die Wiederholung der simulierten Alltagsaktivitäten und der Radergometerbelastung im Labor zur Reliabilitätsbeurteilung.
Analytisch erfolgt der Vergleich zwischen den 1-Hz aufgezeichneten Wearable-Daten und den EKG-Daten. Maße für Validität und Reliabilität sind Two-way mixed effects Intraclass-Correlation-Coefficient (ICC 2,k), Bland-Altman-Plots und Mean Average Percentage Error (MAPE).

Conclusions
Um kommerziell erhältliche optische Herzfrequenzsensoren zu validieren schlagen wir ein Protokoll vor, das standardisierte Labormessungen mit Feldbeobachtungen im Alltag kombiniert und den EKG-Gold-Standard als Referenz nutzt. Der nächste Schritt ist die Anwendung und Evaluierung des Protokolls. Bei entsprechendem Ausgang lassen sich kommende Wearables für die Verwendung in Interventionsstudien zeiteffizient und vergleichbar zu ihren Vorgängern validieren.

ADHERENCE TO MINIMAL EXPERIMENTAL REQUIREMENTS FOR DEFINING EXTRACELLULAR VESICLES AND THEIR FUNCTIONS: A SYSTEMATIC REVIEW

Poupardin Rodolphe[1*], Wolf Martin[*], Strunk Dirk[1]

rodolphe.poupardin@pmu.ac.at

[1] *Experimental and Clinical Cell Therapy Institute (ExCT), Spinal Cord Injury and Tissue Regeneration Center, Paracelsus Medical University, Salzburg, Austria*

BACKGROUND:

- Extracellular vesicles (EVs) are nanometer-sized membrane-enclosed particles secreted via several mechanisms by virtually all cells. They are thought to be loaded with lipids, proteins, and various nucleic acid species of the source cell.
- Nano-sized lipoproteins or protein aggregates have overlapping characteristics with EVs concerning size or density, making proper selection of appropriate EV purification and characterization methods a key to draw concise conclusions (Fig 1).
- Minimal Information for Studies of Extracellular Vesicles (MISEV) [1, 2] guidelines suggest protocols and steps to follow for documenting specific EV-associated functional activities

In this context, we conducted an unbiased review using a text mining approach to assess adherence to MISEV criteria

Fig. 1: Size and density distribution of extracellular vesicles (EVs) and common contaminating particles and their molecular markers. Diagram showing the overlap between different lipoprotein fractions (blue), extracellular vesicles (orange), protein aggregates (blue-grey) and cells (green) in size (x axis; logarithmic) and density (y-axis). In addition, representative molecular markers found to be most used in our analysis and which were recommended in MISEV2018 as universal markers for identification of extracellular vesicles (orange, bold)

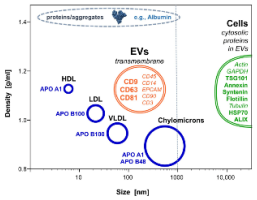

METHODS:

- **Dataset acquisition**: Publications were selected in PubMed using the *RISMed* R package. We searched for manuscripts containing the keywords "extracellular vesicles" or "vesicles" together with "exosomes" in the title or abstract or papers with the major Mesh terms "extracellular vesicles" or "exosomes" (without looking at the child terms (non-explosive search)).
- **Keyword search** using regular expressions (*regex*), only in Material & Methods and Results part to detect methods used for isolation and characterization of EVs. To check for significant trends over time, linear regression analysis was conducted using R. Finally, we investigated whether the quality of identification and characterization of EVs in the manuscripts correlated with the number of citations.

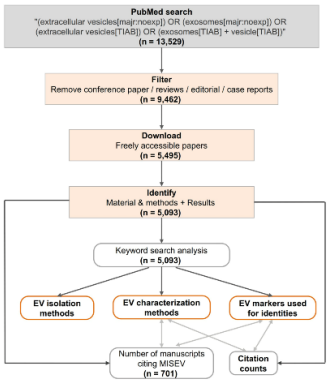

Fig. 2: Dataset selection and approach used to investigate the compliance of the EV field to MISEV guidelines. Research was conducted in PubMed (grey box) and then filtering steps were applied to keep unique records, remove conference / reviews / editorials / case reports. The keyword search was conducted in open access papers where material and methods and/or result sections were found. In parallel, we also extracted citation counts and the list of papers citing MISEV guidelines [1,2] for the 5,093 selected publications.

RESULTS:

The EV field is expanding at a fast pace

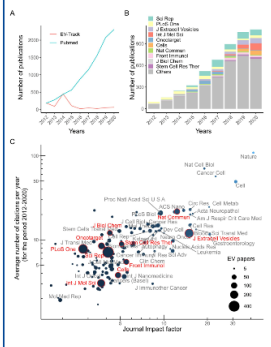

Fig. 3: Overview of the EV publication field growth. (**A**) Steep increase of EV manuscripts. The red line shows the number of EV manuscripts submitted to the EV-track database. (**B**) Bar plot showing the year of publication for the 5,093 selected EV papers. The 10 journals with the highest number of EV related publications (top 10) are shown in different colors as indicated. (**C**) Dot plot showing the relation between journal impact factor and average number of citations for 5,093 selected EV papers between 2012 and 2020. The dot size indicates the number of EV papers found per journal. The top 10 journals identified in Fig. 2B are highlighted in red.

Isolation methods used for EV preparation

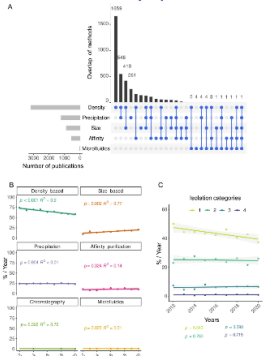

Fig. 4: EV isolation methods. (**A**) The upset plot shows on the left the counts (set size) of the different methods ranked from the most used on the top (density-based isolation) to the least used on the bottom (microfluidics). Intersection size shows the number of publications found for each combination, ranked in descending order. The dot chart corresponding to the upper histogram shows the most used combinations of isolation methods. (**B**) Percentage of papers using the different methods during each year.

Methods used for EV characterization

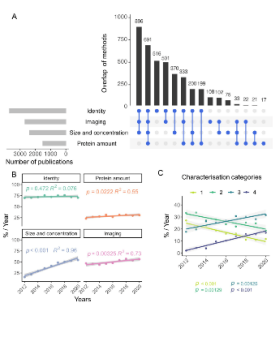

Fig. 5: EV characterization methods. (**A**) The upset plot shows on the left the set size counts of the different methods ranked from the most used on the top (identity) to the least used on the bottom (protein amount). The upper histogram (in descending order) and the dot chart show the most used combinations for characterizing EVs. (**B**) Percentage of papers using the different methods for each year. (**C**) Percentage of EV manuscripts using a combination of characterization methods (identity, protein amount, size and concentration, imaging; color code indicated by legend).

Markers used to check EV purity

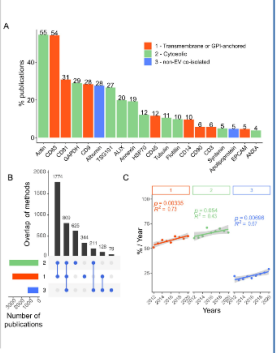

Fig. 6: Analysis of proteins linked to EVs or contaminants. (**A**) Most used marker proteins ordered according to the frequency of use displayed with a color code indicating the category as defined by the MISEV2018 criteria (category 1: **Transmembrane or GPI-anchored** proteins associated to plasma membrane and/or endosomes; category 2: **Cytosolic** proteins recovered in EVs; category 3: Major components of **non-EV co-isolated** structures). (**B**) The upset plot shows on the left the set size counts of the different marker categories (left bars; color code as in A) ranked from the most used on the top to the least on the bottom. The upper histogram (in descending order) and the dot chart show the most used combinations of marker proteins for characterizing EVs. (**C**) Percentage of manuscripts per year using marker proteins from categories 1 - 3 to characterize their EV preparations over the years (2012 - 2020).

Impact of the MISEV guidelines on the EV community

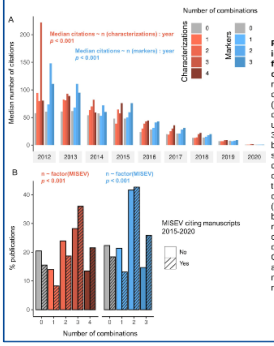

Fig. 7: Impact of EV characterization and identification accuracy on citation frequency plus MISEV-based marker category reporting trends. (**A**) Median number of citations per year for the different combinations of characterization methods (from 0 to 4 characterization categories combined in orange-red) and marker proteins used for EV preparation characterization (0 to 3 marker categories combined (light blue–blue). Linear regression analysis revealed a significant association between the number of characterization categories and median citation numbers ($P = 0.0002$) and between the number of marker categories and median citation numbers ($P = 6.9 \times 10^{-6}$), respectively. (**B**) Percentage of manuscripts citing (dashed bars) or not citing MISEV (non-dashed bars) regarding the number of characterization categories used; red bars) or the different combinations of marker proteins (blue bars). Only manuscripts published between 2015 and 2020 were used for the analysis (701 manuscripts citing MISEV vs 3,878 manuscripts not citing MISEV).

OUTLOOK AND CONCLUSIONS:

- The EV field is prospering at a fast pace leaping from 183 records in 2012 to 2,309 records/year until the end of 2020 (Fig3).

- In this context, we conducted an unbiased review of 5,096 accessible papers published in the EV research field in a broad range of journals between 2012 and 2020 (Fig 2).

- Publications from 810 journals were selected including 205 journals containing at least five EV-related manuscripts. Most manuscripts were found in 'Scientific Reports' (439), 'PLoS One' (284) and 'Journal of Extracellular Vesicles' (JEV; 247) (Fig 3)

- We found that most studies (1,659 / 5,093; 33.2%) used a single density-based isolation technique. The combination of density-based and precipitation methods was the second most frequently applied strategy (548 / 5,093; 10.8% of the manuscripts). (Fig 4)

- In our systematic analysis, we found that the awareness of investigators to better characterize their EV preparations using a combination of several methods was significantly rising. (Fig 5)

- The majority of studies still applied only one method for EV purification with few significant changes over the past years. (Fig 5)

- The three most frequently used markers for category one (**Transmembrane or GPI-anchored proteins)** were tetraspanins CD63, CD81, CD9. Actin, GAPDH and TSG101 were used most frequently for category two (**Cytosolic proteins**), and albumin as well as apolipoproteins for category three (**non-EV co-isolated**). Marker combinations revealed that 34.9% of studies used a combination of category one and two, and 15.9% used the combination of three categories. Finally, a significant increase of testing category one and category three marker determination in EV preparations was evident over time (Fig 6)

- Studies citing the MISEV position statements used significantly more methods for EV characterization and multiple markers to determine EV identity and purity indicating the impact of the guidelines in the EV community. (Fig 7)

- A precise characterization of EV preparations with multiple methods and marker categories also resulted in a significantly higher number of citations. (Fig 7)

REFERENCES

[1] J. Lötvall, et al; JEV. 2014; https://doi.org/10.3402/jev.v3.26913

[2] C. Théry et al; JEV. 2018; https://doi.org/10.1080/20013078.2018.1535750.

Poupardin, R.; Wolf, M.; Strunk, D. Adherence to minimal experimental requirements for defining extracellular vesicles and their functions. Adv. Drug Deliv. Rev.**2021**, 176, 113872

*Rodolphe Poupardin and Martin Wolf contributed equally to this work.

Adherence to minimal experimental requirements for defining extracellular vesicles and their functions: A systematic review

Rodolphe Poupardin[1], Martin Wolf[1], Dirk Strunk[1]

[1]Spinal Cord Injury and Tissue Regeneration Center Salzburg (SCI-TReCS), Cell Therapy Institute, Paracelsus Medical University (PMU), 5020 Salzburg, Austria; Contact: rodolphe.poupardin@pmu.ac.at

Objective
Rigorous measures are required to cope with the advance of extracellular vesicle (EV) research, from 183 studies published in 2012 to 2,309 studies published in 2020. The International Society for Extracellular Vesicles (ISEV) proposed Minimal Information for Studies of Extracellular Vesicles (MISEV) guidelines in 2014, updated in 2018, for assuring and improving EV research quality.

Methods
We performed a systematic review using a text mining approach to assess adherence to MISEV criteria. A keyword search was conducted in 5,093 accessible publications over the period 2012–2020 and analyzed the methodology used for EV isolation and characterization.

Results
We found a significant improvement over the years particularly regarding EV characterization where recent papers used a higher number of methods and EV markers to check for quantity and purity. Interestingly, we also found that EV papers using more methods and EV markers were cited more frequently. Papers citing MISEV criteria were more prone to use a higher number of characterization methods.

Conclusions
We therefore established a concise checklist summarizing MISEV criteria to support EV researchers towards reaching the highest standards in the field.

Cognitive function determined by circadian rhythm disruption and self-reported health, but not decision-reinvestment

BACKGROUND

- Decision-making performance decreases in sleep deprived (SD) individuals (Hansen et al., 2021).
- Sleep deprivation triggers the sympathetic nervous system & hypothalamic-pituitary-adrenal (HPA) axis.
- Overacting sympathetic response increases cortisol secretion, impairs the prefrontal cortex, and slows down reaction time (Arnsten et al., 2015).
- Sympathetic activity is greater in trait related differences of so called decision-reinvesters, that correlate with changes in brain activity in areas that are identical in SD individuals (Mosley et al., 2018).
- This correlation study examined the relationship between cognitive function, sleep patterns, health, and reinvestment.

METHODS

1. 13 male and 8 females football player recorded their sleep with fit-trackers for 7 days.
2. Participants self-reported their a) mental, and physical health (PH) status, b) decision-reinvestment strategy, c) sleep behaviour, and d) stress levels.
3. Athletes then performed a set of cognitive tests to examine e) memory function, f) selective attention, and g) cognitive flexibility; all incl. reaction time (RT).
4. Data was analysed with correlation tests.

© Getty Images

Jasmin Pourhassan, Jane Sarginson, Wolfgang Hitzl, Kneginja Richter

Sleep crucial to win football.

Attention and reaction time in athletes is determined by sleep quality.

Access paper

REFERENCES

Arnsten, A.F., Raskind, M.A., Taylor, F.B. and Connor, D.F. (2015) 'The effects of stress exposure on prefrontal cortex: Translating basic research into successful treatments for post-traumatic stress disorder.' Neurobiology of stress, 1 pp. 89-99.

Hansen, D. A., Satterfield, B. C., Layton, M. E. and Van, D. H. P. A. (2021) 'Sleep deprivation and sleep-onset insomnia are associated with blunted physiological reactivity to stressors.' Military Medicine, 186 pp. 246–252.

Mosley, E., Laborde, S. and Kavanagh, E. (2018) 'Coping related variables, cardiac vagal activity and working memory performance under pressure.' *Acta psychologica, 191*, pp.179-189.

RESULTS

- Awake time & RT, r(12) = 0.66, p = 0.01
- PH & error-rates, r(17) = 0.69, p = 0.00
- PH & decision-reinvestment, r(17) = -0.80, p = 0.00

CONCLUSION

- Athletes with great amount of interrupted sleep were slower in recalling memory. Partial correlation exists when controlling for decision-reinvestment.
- Participants with greater reported physical health had more error-rate in terms of cognitive flexibility.
- Individuals with greater physical health had less tendency to ruminate and reinvest in decisions.

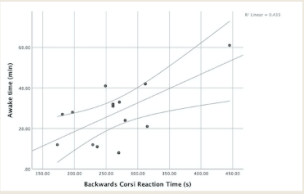

Figure 1: *Relation between Backwards Corsi RT (s) and Awake Time (min). Athletes with little amount of interrupted sleep were faster in recalling memory.*

PARACELSUS MEDIZINISCHE PRIVATUNIVERSITÄT

Presenter:
Jasmin Pourhassan
Sport Scientist
Human Physiologist

Cognitive function determined by circadian rhythm disruption and self-reported health, but not decision-reinvestment

Jasmin Pourhassan[1,2], Jane Sarginson[1], Wolfgang Hitzl[3,4,5], Kneginja Richter[2,6,7]

[1]Faculty of Science and Engineering, Department of Life Sciences, Manchester Metropolitan University, Manchester, United Kingdom; [2]University Clinic for Psychiatry and Psychotherapy, Paracelsus Medical University Nuremberg, Klinikum Nuernberg, Nuremberg, Germany; [3]Department Research and Innovation Management (RIM), Biostatistics and publication of clinical trial studies, Paracelsus Medical University Salzburg, Salzburg, Austria; [4]Department of Ophthalmology and Optometry, Paracelsus Medical University Salzburg, Salzburg, Austria; [5]Research Program Experimental Ophthalmology and Glaucoma Research, Paracelsus Medical University Salzburg, Austria; [6]Faculty for Social Work, Technical University for Applied Sciences, Nuremberg, Germany; [7]Faculty for Medical Sciences, Goce Delcev University, Stip, North Macedonia; Contact: info@jasmin-pourhassan.com

Objective
Decision-making performance is a crucial attribute to athletic performance, and decreases with circadian rhythm disruption (CRD). CRD increases cortisol secretion, and therefore slows down reaction-time. Brain activity in sleep deprived individuals, are identical with those of so-called decision-reinvesters. Decision-reinvestment refers to traits in individuals with greater tendency to ruminate and reinvest in their decisions, with significant decrease in both motor control and cognitive performance. This observational pilot-study examined the relationship between CRD and cognitive function, perceived health, as well as reinvestment strategies. The hypothesis was that individuals with less CRD perceive their health better, and report lower stress levels. And, that better sleepers both perform better and have lower tendency for decision-reinvestment.

Methods
Twenty-one male and female football player recorded their sleep with consumer fit-trackers for 7 days. Participants self-reported their mental and physical health, decision-reinvestment strategy, sleep behaviour, and perceived stress levels. Athletes then performed a set of cognitive tests to examine memory function (Backwards Corsi), selective attention (STROOP), and cognitive flexibility (Wisconsin Card Sorting Test, WCST). Normality was tested with a Shapiro-Wilk test, and analysed with a Pearson's or Spearman's correlation tests.

Results
There was a significant correlation between CRD and Backwards Corsi reaction time, $r = 0.66$, $p = 0.010$. A negative correlation exist in regard of total sleep time and well-being $r = 0.502$, $p = 0.029$, as well as pain scores and Backwards Corsi scores $r = -0.57$, $p = 0.11$. Physical health correlated with error-rates in the WCST, $r = 0.69$, $p = <0.001$. Also, physical health negatively correlated with reinvestment, $r = -0.80$, $p = <0.001$.

Conclusions
Athletes with greater CRD (awake) time were slower in recalling memory, and those with greater pain scores had lower memory function. Participants with greater reported physical health had more error-rates in the WCST; indicating that cognitive flexibility was greater in individuals with worse (lower scores) perceived health. Wellbeing was determined by total sleep-time. And, individuals with lower physical health scores however had greater tendency to ruminate and reinvest in decisions, suggesting a relationship between physical health and reinvestment.

PARACELSUS MEDIZINISCHE PRIVATUNIVERSITÄT

Klinikum Nürnberg
wir sind für Sie da!

Verträglichkeit von Fortifiern aus gefriergetrockneter Frauenmilch zur Anreicherung der Ernährung von Frühgeborenen ab 31 Schwangerschaftswochen

I. Prothmann, N. Rochow, K. Knab, S. Schäfer, J. Zimmermann, A. Szakacs-Fusch, C. Fusch

Klinik für Neugeborene, Kinder und Jugendliche, Paracelsus Medizinische Privatuniversität

EINLEITUNG

- Muttermilch (MM) ist die empfohlene Nahrung für Frühgeborene.
- Um den erhöhten Bedarf an Nährstoffen der FG im Vergleich zu Reifgeborenen zu decken, muss MM mit Eiweiß, Energie, Vitaminen und Mineralien fortifiziert werden.
- In den meisten kommerziellen Fortifiern verwendetes Kuhmilch-Protein erhöht das Risiko für Nekrotisierende Enterokolitis bei FG.
- Ein Fortifier aus humaner Milch könnte dies verringern. Seit kurzem ist gefriergetrocknetes Frauenmilchpulver als Nahrungsergänzungsmittel erhältlich.
- Dessen Einsatz erhöht die Protein- und Energiezufuhr, könnte aber überschüssige Kalorien durch den hohen Fettgehalt zuführen (wünschenswerte Extrazufuhr bei 1,4 g Protein pro 100 ml: 1,0 g Fett und 2,0 g Carbs, tatsächliche Zufuhr 4 g Fett und 6 g Carbs), was den Einsatz eher für reifere Frühgeborene nahelegt.
- Das Ziel dieser Qualitätssicherungsinitiative (QI) ist die Untersuchung der Nährstoffzufuhr, des Wachstums und der Verträglichkeit der Muttermilchfortifizierung mit dem neuen Produkt basierend auf Frauenmilch im Vergleich mit einem kuhmilchbasierten Fortifier (historische Kohorte).

METHODE

- QI-Projekt an der Neonatologie, des Klinikum Nürnberg mit FG ≥ 31 SSW
- Interventionsgruppe (IG): MM angereichert ab enteraler Zufuhr von 120 ml/kg/d mit lyophilisierter Muttermilch (AS50, Ammeva, Werder). Schrittweise Steigerung der Dosis auf 4,8 g/100 ml und zusätzliche Supplementierung mit Vitaminen und Ca-Glycerophosphat.
- Wachstum, Körperzusammensetzung (PeaPod), klinische Laborparameter, Ca, P im Urin, Nahrungsverträglichkeit und Zusammensetzung der Muttermilch (MIRIS, Schweden) wurden analysiert (Tab. 1)
- Historische Kontrollgruppe (KG): Standardfortifizierung (FMS, Nutricia, Friedrichsdorf) wurde aus einem gleichlangen Zeitraum unmittelbar vor Beginn der Intervention durch Matched-Pair (Geburtsgewicht (GG) ± 100g, SSW ± 1 Wo) rekrutiert. In der KG waren Daten zum Wachstum und Nahrungsverträglichkeit vorhanden. Die Analyse erfolgte mit R.

Erhebung	MM-Analyse (täglich)	Fortifier Dosis g/100ml	Blutentnahme		Urin (Kalzium, Phosphat, Kreatinin)	Gewicht (täglich)	Kopf-umfang/ Länge	Körper-zusammen-setzung	Energie-umsatz
			Blutzucker	Harnstoff, Triglyzeride					
Einschleichen Tag 1	x	1,6	x			x			
Einschleichen Tag 2	x	3,2	x			x			
Volldosis Tag 3	x	4,8	x			x		x	x
Tag 7	x	4,8	x	x	x	x	x	x	x
Tag 14	x	4,8	x	x	x	x	x	x	x
Mit 36 Wochen oder zur Entlassung (wenn vor 36 Wochen)	x	4,8	x	x	x	x	x	x	x

Tab 1: Messschema für die Datenerfassung in der Interventionsgruppe

ERGEBNISSE

- In dem QI-Projekt wurden n=64 FG (pro Gruppe n=32) eingeschlossen.
- Die Patientencharakteristika und Outcome waren zwischen den Gruppen nicht unterschiedlich (Tab 2).
- In IG erhielten die FG eine Flüssigkeitszufuhr von 157 ± 8 ml/kg/d und gemeinsam mit der Muttermilchanalyse ergab sich eine tatsächliche Zufuhr von 14,0 ± 0,9 g/kg/d CHO, 3,3 ± 0,4 g/kg/d Protein, 7,4 ± 1,1 g/kg/d Fett und 136 ± 12 kcal/kg/d Energie.
- Keine signifikanten Unterschiede für die Nahrungsverträglichkeit zwischen den Gruppen wurden gefunden.
- Die Blutparameter in der IG waren für Harnstoff 21 ± 12 mg/dl, Triglyzeride 10 5± 36 mg/dl und Blutzucker 86 ± 19 mg/dl im Normbereich.
- Mit einem postmenstruellen Alter (PMA) von 36 Wochen war die Fettmasse 290 ± 110 g (12 ± 3%) und fettfreie Masse 2050 ± 240 g.
- Das Entlassgewicht war in beiden Gruppen nicht unterschiedlich.

ERGEBNISSE

Tab. 2: Patientencharakteristika und Outcome Daten

	Intervention (n=32)	Kontrolle (n=32)
Geburt		
Gestationsalter (Wochen)	32,8 ± 1.0	33,0 ± 1.2
Geburtsgewicht (g)	1900 ± 380	1840 ± 370
Länge (cm)	43,3 ± 2.6	43 ± 3,0
Kopfumfang (cm)	30,5 ± 1,5	30,6 ± 1,3
Geburtsgewichtsperzentile	48 ± 28	44 ± 23
Enterale Ernährung		
Enterale Zufuhr 120 ml/kg/d (Ltg.)	5,0 ± 1,3	5,2 ± 1,5
Start Fortifier (Ltg.)	6,8 ± 1,8	6,8 ± 2,7
Entlassung		
Aufenthaltsdauer (Tage)	27 ± 7	27 ± 10
Postmenstruelles Alter (Wochen)	36,5 ± 0.9	36,6 ± 1.2
Gewicht (g)	2500 ± 380	2490 ± 360
Gewichtsperzentile	30 ± 24	26 ± 18
Länge (cm)	46,5 ± 2.5	47,1 ± 2.3
Kopfumfang (cm)	32,5 ± 1,4	32,5 ± 1,5

Ltg. - Lebenstag

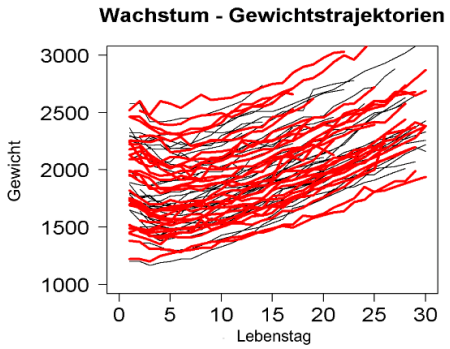

Abb. 2: Vergleich der Wachstumskurven (Intervention - dicke rote Linien, Kontrolle - dünne schwarze Linien)

DISKUSSION

- Die Fortifizierung mit gefriergetrockneter Frauenmilch wird von FG ≥ 31 SSW gut vertragen und das Wachstum ist ähnlich wie mit kuhmilchbasierten Fortifiern.
- Die Körperzusammensetzung mit einem PMA von 36 Wochen war in dem erwarteten Bereich für reifere FG.
- Um den ernährungsphysiologischen Bedürfnissen von FG (< 1,5 kg) besser zu entsprechen, müsste dieser Fortifier hinsichtlich der Mengen an Makronährstoffen und deren Quotienten (höheres Verhältnis von Protein zu Energie) angepasst werden.
- Multizenter-Studien sind nötig, um die Ergebnisse an einer größeren Kohorte zu validieren.

Prof. Dr. med. Christoph Fusch, Paracelsus Medizinische Privatuniversität, christoph.fusch@klinikum-nuernberg.de

Verträglichkeit von Fortifiern aus gefriergetrockneter Frauenmilch zur Anreicherung der Ernährung von Frühgeborenen ab 31 Schwangerschaftswochen

Isabell Prothmann[1]

[1]Paracelsus Medical University, Nuremberg, Germany; Contact: isabell.prothmann@stud.pmu.ac.at

Objective
Muttermilch (MM) ist die empfohlene Nahrung für Frühgeborene (FG). Um deren im Vergleich zu Reifgeborenen erhöhten Nährstoffbedarf zu decken, muss MM mit Eiweiß, Energie und Mineralien fortifiziert werden. Das in den meisten kommerziellen Fortifiern verwendete Kuhmilch-Protein erhöht das Risiko für Nekrotisierende Enterokolitis bei FG. Ein Fortifier aus humaner Milch könnte dies verringern. Seit kurzem ist gefriergetrocknetes Frauenmilchpulver als Nahrungsergänzungsmittel erhältlich. Dessen Einsatz erhöht die Protein- und Energiezufuhr, könnte aber überschüssige Kalorien durch den hohen Fettgehalt zuführen (wünschenswerte Extrazufuhr bei 1,4 g Protein pro 100 ml: 1,0 g Fett und 2,0 g CHO, tatsächliche Zufuhr 4 g Fett u 6 g CHO), was den Einsatz eher für reifere Frühgeborene nahelegt. Ziel dieser Anwendungsbeobachtung ist, Verträglichkeit und Sicherheit dieses Fortifiers zu untersuchen und Wachstum und Metabolismus mit einer historischen Gruppe zu vergleichen.

Methods
Anwendungsbeobachtung (Neonatologie, Klinikum Nürnberg), FG >= 31 SSW; Interventionsgruppe (IG): MM angereichert ab enteraler Zufuhr von 120 ml/kg/d mit 4,8 g/100ml lyophilisierter Muttermilch (AS50, Ammeva, Werder) angereichert. Zusätzlich wurden Vitamine und Ca-Glycerophosphat supplementiert. Wachstum, Körperzusammensetzung (PeaPod), klinische Laborparameter, Ca, P im Urin, Nahrungsverträglichkeit und Zusammensetzung der Muttermilch (MIRIS, Schweden) wurden analysiert. Historische Kontrollgruppe (KG): Standardfortifizierung (FMS, Nutricia, Friedrichsdorf) wurde aus einem gleichlangen Zeitraum unmittelbar vor Beginn der Intervention durch Matched-Pairs (Geburtsgewicht (GG) ±100g, SSW ±1 Wo) rekrutiert. In der KG waren Daten zum Wachstum und Nahrungsverträglichkeit vorhanden. Die Analyse erfolgte mit R.

Results
64 FG, Patientencharakteristika und Outcome waren zwischen den Gruppen nicht verschieden. In IG erhielten die FG eine Flüssigkeitszufuhr von 157±8ml/kg/d und gemeinsam mit der Muttermilchanalyse ergab sich eine tatsächliche Zufuhr von 14,0±0,9 g/kg/d CHO, 3,3±0,4g/kg/d Protein, 7,4±1,1g/kg/d Fett und136±12 kcal/kg/d Energie.
Keine signifikanten Unterschiede für die Nahrungsverträglichkeit zwischen den Gruppen. Harnstoff in KG 21±12 mg/dl, Triglyzeride 105±36 mg/dl, Blutzucker 86±19 mg/dl. Mit 36 Wochen (PMA) war die Fettmasse 290±110g (12 ± 3%) und fettfreie Masse 2050 ± 240 g). Das Entlassgewicht war in beiden Gruppen gleich.

Conclusions
Die Fortifizierung mit gefriergetrockneter Frauenmilch wird von FG >= 31 SSW gut vertragen und das Wachstum ist ähnlich wie mit kuhmilchbasierten Fortifiern. Um den ernährungsphysiologischen Bedürfnissen von VLBW-Frühgeborenen besser zu entsprechen, müsste dieser Fortifier hinsichtlich der Mengen an Makronährstoffen und deren Ratios (höheres Verhältnis von Protein zu Energie) angepasst werden. Multizenter-Studien sind nötig, umdie Ergebnisse an einer größeren Kohorte zu validieren.

Dysfunction of Kir2.1 channels in the aging neuroglia

Alessia Remigante[1], Sara Spinelli[1], Rossana Morabito[1], Angela Marino[1], Antonio Sarikas[2], Michael Pusch[3] and Silvia Dossena[2]

[1]Department of Chemical, Biological, Pharmaceutical and Environmental Sciences, University of Messina, Italy
[2]Institute of Pharmacology and Toxicology, Paracelsus Medical University, Salzburg, Austria
[3]Biophysics Institute, National Research Council, Genoa, Italy

OBJECTIVE

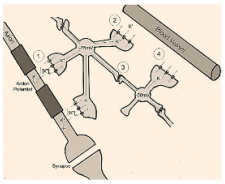

Figure 1. Model of K^+ spatial buffering. Potassium released during action potential propagation is taken up by astrocytes processes at nodes of Ranvier and synapses via strongly rectifying Kir channels, i.e. homomeric Kir2.1 channels, heteromeric Kir4.1/2.1 and Kir4.1/Kir5.1 channels. Potassium is extruded from glia at sites of low K^+ activity via weakly rectifying Kir4.1 homomeric channels. Taken from (3).

Epilepsy is a chronic disease of the brain and its prevalence increases with age. Strikingly, about 50% of all epilepsy cases diagnosed in elderly patients (>65 years) are idiopathic (1). Metabolic changes, including the production of reactive oxygen species, may contribute to epilepsy development (2). The neuronal glia plays a crucial role in epilepsy by controlling neuronal hyperexcitability. One of the key roles of glial cells is the spatial buffering of extracellular K^+ ions that are released by excited neurons and transported through glial inwardly rectifying potassium (Kir) channels from extracellular regions of high K^+ to those of low K^+ to inhibit epileptogenesis (**Figure 1**) (3). However, whether Kir channels can be the target of oxidative stress during aging is not known. Among experimental oxidative stress-related aging models, exposure to D-galactose (D-gal) is considered the most similar to natural aging (4). In the present study, we investigated the effect of D-gal-induced aging on Kir channel function in glioblastoma U87-MG cells.

RESULTS

Screening of all 15 known isoforms of Kir channels by RT-qPCR revealed that the predominant transcript expressed in U87-MG cells corresponds to the Kir2.1 channel (**Figure 2**). Among other Kir channels known to be expressed in neuronal glia, Kir4.1 was 26-fold less expressed and other Kir members, such as Kir5.1, were virtually absent. Additionally, exposure of cells to 10 µM ML-133, a specific inhibitor of Kir2.1, induced a decrease of inwardly rectifying K^+ currents in U-87MG cells (**Figure 3 A**), thus confirming RT-qPCR results. Conversely, application of 10 µM VU013, a specific inhibitor of Kir4.1, failed to inhibit the potassium current in U-87MG cells (**Figure 3 B**).

Figure 2. Kir transcript expression in U87-MG cells. One µg total RNA from three independent subcultures was reverse transcribed and probed for expression of the transcripts of all 15 known Kir isoforms by qPCR on the RotorGene (QIAGENE) platform. Human whole kidney, frontal cortex and thyroid served as positive controls.

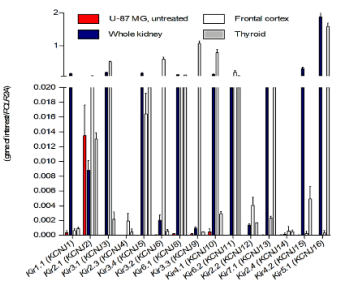

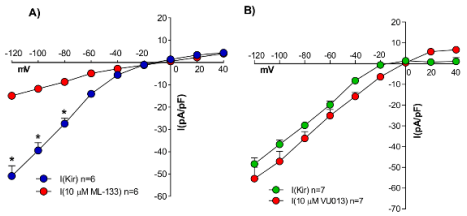

Figure 3. ML-133 reduced, while VU013 did not affect the Ba^{2+}-sensitive K^+ conductance in U87-MG cells. The whole cell inwardly rectifying Ba^{2+}-sensitive K^+ current was studied in U87-MG cells endogenously expressing Kir2.1. The voltage protocol consisted of voltage steps from -120 to 40 mV in 20 mV increments from a holding potential of -60mV. The duration of the voltage steps was 400 ms. **A**) Exposure to ML-133 inhibited the K^+ current, while **B**) VU013 was ineffective. * p<0.05, unpaired Student's t-test. (n) refers to the number of cells.

METHODS

RT-qPCR was utilized to identify the isoform(s) of Kir channels expressed in glioblastoma U87-MG cells. In addition, cell viability and oxidative stress following exposure of cells for 24 hours to 30 or 100 mM D-Galactose (D-Gal) have been assessed by the MTT colorimetric assay and estimation of thiobarbituric acid reactive substances (TBARS) levels –a marker of lipid peroxidation– as well as total sulfhydryl (-SH) groups, respectively. The membrane K^+ conductance was measured by the patch-clamp technique in whole-cell configuration. As Kir channels are sensitive to Ba^{2+}, all currents have been subtracted of the Ba^{2+}-insensitive component. Moreover, to confirm the role of Kir2.1, ML-133, a specific inhibitor, was used in patch clamp technique. To obtain equal osmolarity, equimolar amounts of mannitol were used as the control for D-Gal.

RESULTS

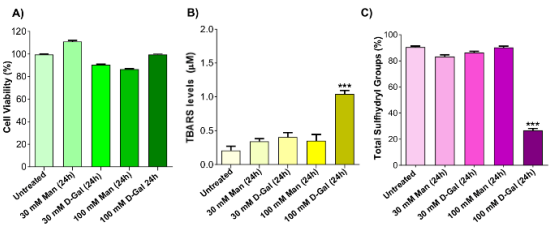

Figure 4. *In vitro* effects of increasing concentrations of D-Gal (30 and 100 mM) for 24 hours. **A**) Cell viability (MTT assay), **B**) thiobarbituric acid reactive substance (TBARS) and **C**) total sulfhydryl groups. ***p<0.001 versus control, 30 mM D-Gal, 30-100 mM Mannitol, as determined by one way ANOVA followed by Bonferroni's post hoc test (n=3).

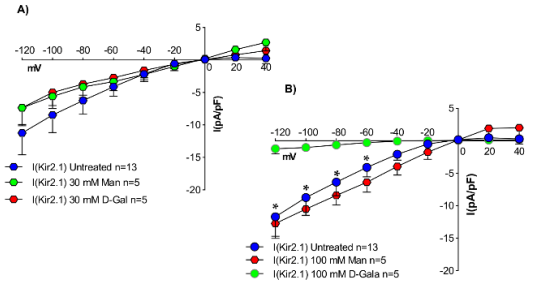

Figure 5. D-gal inhibits Kir2.1 channel function. The voltage protocol consisted of voltage steps from -120 to 40 mV in 20 mV increments from a holding potential of -60 mV. The duration of the voltage steps was 400 ms. **A**) Treatment with 30 mM D-Gal for 24 hours did not suppress the Kir2.1current **B**) Treatment with 100 mM D-Gal for 24 hours suppressed the Kir2.1current. Kir2.1 currents were isolated from the total currents by subtracting currents measured in the same cell after application of 1 mM $BaCl_2$, an efficient blocker of Kir2.1. * p<0.05, unpaired Student's t-test. (n) refers to the number of cells.

CONCLUSIONS

-These findings reveal a novel Kir2.1 channel modulation that is likely to occur in oxidative stress.

-We suggest that inhibition of Kir2.1 in neuronal glia may alter the extracellular K^+ buffering and contribute to oxidative stress-related neuronal hyperexcitabilty and epileptogenesis during aging.

REFERENCES

1. Beghi E, Giussani G. Aging and the Epidemiology of Epilepsy. Neuroepidemiology. 2018;51(3-4):216-223.
2. Pereira MD, Ksiazek K, Menezes R. Oxidative stress in neurodegenerative diseases and ageing. Oxid Med Cell Longev. 2012;2012:796360. Hibino H, Inanobe A, Furutani K, Murakami S, Findlay I, Kurachi Y. Inwardly rectifying potassium channels: their structure, function, and physiological roles. Physiol Rev. 2010 Jan;90(1):291-366.
3. Butt AM, Kalsi A. Inwardly rectifying potassium channels (Kir) in central nervous system glia: a special role for Kir4.1 in glial functions. J Cell Mol Med. 2006 Jan-Mar;10(1):33-44.
4. Azman KF, Zakaria R. D-Galactose-induced accelerated aging model: an overview. Biogerontology. 2019 Dec;20(6):763-782.

Dysfunction of Kir2.1 channels in the aging neuroglia

Alessia Remigante[1], Sara Spinelli[1], Rossana Morabito[1], Angela Marino[1], Antonio Sarikas[2], Michael Pusch[3], Silvia Dossena[2]

[1]Department of Chemical, Biological, Pharmaceutical and Environmental Sciences, University of Messina, Italy.; [2]Institute of Pharmacology and Toxicology, Paracelsus Medical University, Salzburg, Austria.; [3]Biophysics Institute, National Research Council, Genoa, Italy.; Contact: aremigante@unime.it

Objective

Oxidative stress (OS) has a main role in the pathogenesis of central nervous system disorders (1). In this regard, epilepsy is a highly prevalent serious brain disease and
its prevalence increases with age. Strikingly, about 50% of all epilepsy cases diagnosed in elderly patients (>65 years) are idiopathic (2). Metabolic changes, including the production of reactive oxygen species (ROS), are regarded to as possible mechanism involved in epileptogenesis. The neuronal glia plays a crucial role in epilepsy by controlling neuronal hyperexcitability. One of the key roles of glial cells is the spatial buffering of extracellular K^+ ions that are released by excited neurons and transported through glial inwardly rectifying potassium (Kir) channels from extracellular regions of high K^+ to those of low K^+ to inhibit epileptogenesis (3). Among experimental OS-related aging models, long-term (24 hours) exposure to D-Galactose (D-Gal) is considered the most similar to natural aging. In the present study, we investigated the effect of D-Gal-induced aging on Kir channel activity in glioblastoma U87-MG cells.

Methods

RT-qPCR was utilized to identify the isoform(s) of Kir channels expressed in U87-MG cells. In addition, cell viability and OS following exposure of cells for 24 hours to 30 and 100 mM D-Gal have been assessed by the MTT colorimetric assay and estimation of thiobarbituric acid reactive substances (TBARS levels), as well as membrane total sulfhydryl (-SH) groups, respectively. The membrane K^+ conductance was measured by the patch-clamp technique. As Kir channels are sensitive to Ba^{2+}, all currents have been subtracted of the Ba^{2+} insensitive component. To confirm the functional role of the involved Kir channel, different inhibitors (ML-133 and VU013) were used in the patch clamp technique. In addition, to obtain equal osmolarity, equimolar amounts of Mannitol (Man) were used as the control for D-Gal.

Results

Screening of all fifteen Kir isoforms revealed that the predominant transcript corresponds to Kir2.1, with minor contribution of Kir4.1. D-Gal (30 and 100 mM) had no obvious cytotoxicity, but 100 mM D-Gal strongly promoted OS, namely increased lipoperoxidation levels and decreased the membrane protein sulfhydryl group abundance. Interestingly, D-Gal exposure was associated with a decrease of inwardly rectifying K^+ currents sensitive to ML-133, a specific inhibitor of Kir2.1 channels. Importantly, 30 mM D-Gal and 30 or 100 mM Man failed to elicit OS and, accordingly, had no significant effect on the Ba^{2+}-sensitive K^+ current.

Conclusions

Our findings reveal a novel Kir2.1 channel modulation that is likely to occur in OS. We suggest that inhibition of Kir2.1 channels in glia cells may alter extracellular K^+ buffering and contribute to OS-related neuronal hyperexcitability and epileptogenesis during aging.

References

1. DOI: 10.1155/2012/796360
2. DOI: 10.1159/000493484
3. PMID: 20086079

Genetic determinants of deafness and Enlarged Vestibular Aqueduct in Austria

Sebastian Roesch[1], Emanuele Bernardinelli[2], Arnoldas Matulevicius[2], Antonio Sarikas[2], Gerd Rasp[1], Silvia Dossena[2]

[1]Department of Otorhinolaryngology, Paracelsus Medical University, Salzburg, Austria
[2]Institute of Pharmacology and Toxicology, Paracelsus Medical University, Salzburg, Austria

Background and Objectives

- Hearing loss affects at least 1 in 1000 newborns, is a major cause of disability in children, and the most common sensorial deficit in humans
- In developed countries, at least 60% of cases of hearing loss are of genetic origin and are frequently associated with inner ear malformations
- The most commonly detected inner ear malformation is the Enlarged Vestibular Aqueduct (EVA) (**Figure 1**)
- Genes that have been linked to EVA are *SLC26A4*/pendrin, *GJB2*, *FOXI1*, *KCNJ10*, and *POU3F4*
- In Caucasian cohorts, approximately 25% of cases of non-syndromic EVA are linked to biallelic mutations in *SLC26A4* gene
- Approximately 25% of patients have a non-diagnostic genotype represented by monoallelic mutations in the *SLC26A4* gene
- A large fraction of patients (50%) remain undiagnosed, thus providing a strong imperative to further explore the etiology of this condition

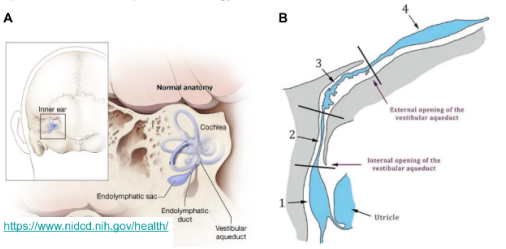

Figure 1. A, Anatomy of the inner ear. Vestibular aqueducts are narrow, bony canals that travel from the inner ear to deep inside the skull. **B, Schematic drawing of the vestibular aqueduct and the endolymphatic duct and sac.** The vestibular aqueduct (grey) is delimited by its medial (internal) and external apertures. The endolymphatic duct and sac (blue) are membranous structures that lie within the vestibular aqueduct and comprise the sinus (1), the isthmus (2), a rugose (3), and a smooth portion (4). Black lines indicate the limits between the different portions of the endolymphatic duct and sac. Taken from [1].

Methods

- A cohort of 33 subjects referring to the Otorhinolaryngology Department of the Salzburg general hospital for hearing loss were recruited between 2014 and 2022 (17 females and 16 males aged between 5 and 63 years; average age 32 years)
- For all patients, imaging studies of the inner ear by computer tomography (CT) of the temporal bones were performed. EVA was defined as an enlargement of the vestibular aqueduct ≥1.5 mm midway between the endolymphatic sac and the vestibule (**Figure 2**)
- Patient whole blood was collected from all patient via venipuncture after informed consent. Total genomic DNA (gDNA) was purified from ~350 µL blood with the EZ1 DNA Blood 350 µL kit (Qiagen, Hilden, Germany) using the EZ1 Advanced XL platform (Qiagen)
- The entire coding region and intron-exons boundaries of *SLC26A4*, *GJB2*, *FOXI1*, *KCNJ10*, and *POU3F4* were amplified by end-point PCR and Sanger sequenced
- To discriminate between pathogenic and non-pathogenic *SLC26A4* sequence alterations, the corresponding protein variants were characterized in cell-based assays to determine their expression levels and ion transport activity as formerly described [2,3].
- The presence of the newly discovered Caucasian EVA (CEVA) haplotype [4] was verified with the rhAmp™ SNP Genotyping assay (Integrated DNA Technologies)

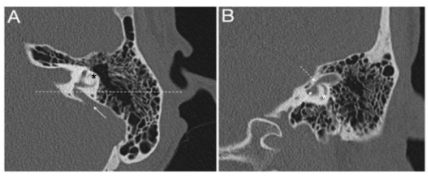

Figure 2. Computed tomography of the left temporal bone of a 12-year-old female patient with bilateral EVA and congenital moderate to profound hearing loss. A, axial plane; the arrow indicates the Enlarged Vestibular Aqueduct; *, lateral semicircular canal; the dotted line is the plane of section B. **B,** coronal plane; the continuous arrow indicates the Enlarged Vestibular Aqueduct; the dotted arrow is the isthmus of the enlarged vestibular aqueduct; *, posterior semicircular canal. The patient harbors biallelic pathogenic variants (c.1301C > A; p.A434D and c.1730T > C; p.V577A) in the *SLC26A4* gene. Taken from [1].

Results

					CEVA haplotype										
					1	2	3	4	5	6	7	8	9	10	11	12
Patient #	Patient ID	Mutated gene	Protein variant		rs117714350	rs150942317	rs17424561	rs79579403	rs17425867	rs117413959	rs17349280	rs117336523	rs80149210	rs8649298	rs199667576	rs199915614
1	119	?														n.a.
2	267	FOXI1	p.Y152X	p.Y152X												n.a.
3	271	SLC26A4	p.A434D	p.V577A												n.a.
4	272	?														n.a.
5	278	?								n.a.						n.a.
6	305	?														n.a.
7	307	GJB2	p.G12VfsX13	p.G12VfsX13												n.a.
8	308	FOXI1	p.Y152X	p.Y152X												n.a.
9	358	SLC26A4	p.M21V	WT												n.a.
10	359	?														n.a.
11	395	?														n.a.
12	421	GJB2	p.G12VfsX13	p.G12VfsX13												n.a.
13	568	?														n.a.
14	569	POU3F4	p.S74Afs*8	-												n.a.
15	610	?							n.a.							n.a.
16	616	SLC26A4	p.Y115D	WT												
17	622	?														n.a.
18	632	?														n.a.
19	653	SLC26A4	p.G740V	WT												
20	654	SLC26A4	p.L597S	WT												
21	657	?														n.a.
22	659	SLC26A4	p.I136N	p.A864V												
23	660	SLC26A4	p.Q101R	p.R409H												n.a.
24	663	?							n.a.							n.a.
25	666	?				n.a.										n.a.
26	667	POU3F4	p.C327X	-												n.a.
27	669	?														n.a.
28	670	SLC26A4	p.R185T	p.N248Kfs*41												n.a.
29	671	SLC26A4	splice donor	WT												
30	672	?			n.a.								n.a.			
31	678	?														
32	679	?				n.a.										
33	680	?														

Table 1. Genotype of patients of the Salzburg EVA cohort.
? indicates an undetermined feature. n.a., not assessed.

Pathogenic variant
Benign variant
Monoallelic variant
Biallelic variant

- Hearing loss and EVA in this cohort are associated with biallelic pathogenic variants in the *SLC26A4* (n=4/33, 12% of patients) and *FOXI1* (n=2/33, 6% of patients) genes and monoallelic X-linked pathogenic variants in the *POU3F4* gene (n=2/33, 6% of patients) (**Table 1**)
- Non-pathogenic variants in the *SLC26A4* gene were found in 2/33 patients (6%)
- Three/33 patients (9%) showed monoallelic pathogenic variants in the *SLC26A4* gene, which is a non-diagnostic phenotype
- Probably coincidental biallelic pathogenic variants in the *GJB2* gene were also detected in 2/33 patients (6%)
- The 12 SNPs of the Caucasian EVA haplotype were found in 5/33 patients (15%); of these, 2/33 patients (6%) harbor monoallelic pathogenic variants in the *SLC26A4* gene and one (3%) harbors a monoallelic non-pathogenic variant in the *SLC26A4* gene

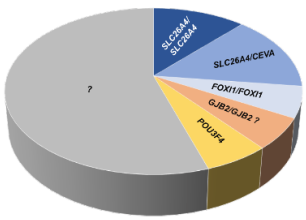

Figure 3. Approximate proportion of genetic determinants (first allele/second allele) of hearing loss and EVA in the Salzburg cohort. CEVA, Caucasian Enlarged Vestibular Aqueduct haplotype; ? indicates a controversial finding or undetermined feature.

Conclusions and Outlook

- Biallelic pathogenic variants in the *SLC26A4* and *FOXI1* genes and monoallelic X-linked pathogenic variants in the *POU3F4* gene explain EVA and hearing loss in 24% of patients in this cohort (**Figure 3**)
- The Caucasian EVA haplotype with or without pathogenic variants in the *SLC26A4* gene may account for EVA and hearing loss in 15% of patients
- The remaining patients (n=18/33, 55%) miss the identification of the genetic cause of their condition. This is in line with other Caucasian cohorts
- **Further studies are needed to establish the impact of the CEVA haplotype on a molecular and functional level**
- **Next-generations sequencing technologies, including Whole Exome Sequencing, will be essential to reach a conclusive genetic diagnosis of deafness in patients who are negative for the known causative genes**

References

1. Roesch, S.; Rasp, G.; Sarikas, A.; Dossena, S. Genetic Determinants of Non-Syndromic Enlarged Vestibular Aqueduct: A Review. Audiol. Res. 2021, 11:423-442
2. De Moraes, V.C.S.; Bernardinelli, E.; ... Dossena, S. Reduction of cellular expression levels is a common feature of functionally affected pendrin (SLC26A4) protein variants. Mol Med. 2016, 22:41-53
3. Roesch, S.; Bernardinelli, E.; ... Dossena, S. Functional testing of SLC26A4 variants-clinical and molecular analysis of a cohort with enlarged vestibular aqueduct from Austria. Int J Mol Sci. 2018, 19(1):209
4. Chattaraj, P., Munjal T.; Honda, K.; Rendtorff, N.D.; Ratay, J.S.; Muskett, J.A.; Risso, D.S.; Roux, I.; Gertz, E.M.; Schäffer, A.A.; Friedman, T.B.; Morell, R.J.; Tranebjærg, L.; Griffith, A.J. A common SLC26A4-linked haplotype underlying non-syndromic hearing loss with enlargement of the vestibular aqueduct. J Med Genet. 2017, 54(10):665-673.

Genetic determinants of deafness and Enlarged Vestibular Aqueduct in Austria

Sebastian Roesch[1], Emanuele Bernardinelli[2], Arnoldas Matulevicius[2], Antonio Sarikas[2], Gerd Rasp[1], Silvia Dossena[2]

[1]Department of Otorhinolaryngology, Paracelsus Medical University, Salzburg, Austria; [2]Institute of Pharmacology and Toxicology, Paracelsus Medical University, Salzburg, Austria; Contact: silvia.dossena@pmu.ac.at

Objective
Hearing loss affects at least 1 in 1000 newborns, is a major cause of disability in children and the most common sensorial deficit in humans. In developed countries, at least 60% of cases of hearing loss are of genetic origin and are frequently associated with inner ear malformations, of which the most commonly detected is the Enlarged Vestibular Aqueduct (EVA). Genes that have been linked to EVA are *SLC26A4*/pendrin, *GJB2*, *FOXI1*, *KCNJ10* and *POU3F4*. In Caucasian cohorts, a large fraction of patients (50%) remain undiagnosed, thus providing a strong imperative to further explore the etiology of this condition.

Methods
A cohort of 33 subjects referring to the Otorhinolaryngology Department of the Salzburg general hospital for hearing loss were recruited between 2014 and 2022 (17 females and 16 males aged between 5 and 63 years; average age 32 years). For all patients, imaging studies of the inner ear by computer tomography (CT) of the temporal bones were performed. The entire coding region and intron-exons boundaries of *SLC26A4*, *GJB2*, *FOXI1*, *KCNJ10*, and *POU3F4* were amplified by end-point PCR and Sanger sequenced. To discriminate between pathogenic and non-pathogenic *SLC26A4* sequence alterations, the corresponding protein variants were characterized in cell-based assays to determine their expression levels and ion transport activity. The presence of the newly discovered Caucasian EVA (CEVA) haplotype was verified with the rhAmp™ SNP Genotyping assay (Integrated DNA Technologies).

Results
Hearing loss and EVA in this cohort are associated with biallelic pathogenic variants in the *SLC26A4* (n=4/33, 12% of patients) and *FOXI1* (n=2/33, 6% of patients) genes and monoallelic X-linked pathogenic variants in the *POU3F4* gene (n=2/33, 6% of patients). Non-pathogenic variants in the *SLC26A4* gene were found in 2/33 patients (6%). Three/33 patients (9%) showed monoallelic pathogenic variants in the *SLC26A4* gene, which is a non-diagnostic phenotype. Probably coincidental biallelic pathogenic variants in the *GJB2* gene were also detected in 2/33 patients (6%). The 12 SNPs of the Caucasian EVA haplotype were found in 5/33 patients (15%); of these, 2/33 patients (6%) harbor monoallelic pathogenic variants in the *SLC26A4* gene and one (3%) harbors a monoallelic non-pathogenic variant in the *SLC26A4* gene.

Conclusions
Biallelic pathogenic variants in the *SLC26A4* and *FOXI1* genes and monoallelic X-linked pathogenic variants in the *POU3F4* gene explain EVA and hearing loss in 24% of patients in this cohort. The Caucasian EVA haplotype with or without pathogenic variants in the *SLC26A4* gene may account for EVA and hearing loss in 15% of patients. The remaining patients (n=18/33, 55%) miss the identification of the genetic cause of their condition. Further studies are needed to establish the impact of the CEVA haplotype on a molecular and functional level; next-generations sequencing technologies will be essential to reach a conclusive genetic diagnosis of deafness in patients who are negative for the known causative genes.

Global, regional, and national trends of Spinal Injuries 1990-2019: findings from the Global Burden of Diseases (GBD) study 2019

Dr. Mahdi Safdarian, Prof. Eugen Trinka

Department of Neurology, Christian Doppler Klinik, Paracelsus Medical University

Keywords: spinal injuries, incidence, prevalence, years lived with disability

Introduction

Spinal injuries contribute to a major burden of disabilities causing health loss due to premature mortality and residual disability. While spinal injuries are a public health issue, no comprehensive report on their global temporal, spatial and demographic patterns has not been published. We aimed to measure the global, regional, and national incidence, prevalence, and years lived with disability (YLDs) of spinal injuries from 1990 to 2019 using data from the Global Burden of Diseases, Injuries, and Risk Factors Study.

Methods

Data on incidence, prevalence, and YLDs of spinal injuries were derived systematically from the GBD 2019 study. Using the framework of GBD 2019, we provide numbers and age-standardized rate changes with 95% uncertainty intervals (UIs) for incidence, prevalence, and YLDs of spinal injuries at neck level and below neck level globally and for 21 GBD regions and 204 countries and territories, among all age groups and both sexes from 1990 to 2019. We tried to detect and report meaningful trends based on location, age and gender.

Results

Globally, there were 20.6 million (95% UI: 18.9–23.6) individuals with spinal injuries in 2019. The incidence number of spinal injuries was 909,000 cases (95% UI: 706,952–1,156,409) with an estimated 6.2 million (95% UI: 4.4–8.1) YLDs. There was a significant 81.5% [95% UI: 74.2 to 87.1], 52.7% [95% UI: 30.3 to 69.8] and 65.4% [95% UI: 56.3 to 76.0] increase in the global prevalence, incidence and YLDs numbers of spinal injuries respectively from 1990 to 2019. However, global age-standardised incidence, prevalence and YLDs rates per 100,000 population for spinal injuries, showed slighter changes of 5.8% (95% UI: 2.6–9.5), -6.1% (-17.2–1.5) and -1.5 % (-5.5–3.2) from 1990 to 2019, respectively. There were great geographical variations in the age-standardised rates of spinal Injuries in 2019, in addition to changes from 1990. The incidence increases with age and remains higher than 50,000 cases from 20 to 84 years with two peaks at 30-34 and 50-54 years. The prevalence and YLDs charts; however, show similar patterns, as they both have one peak around 45-59, and 50-54 years, respectively. Globally, the numbers of incidence, prevalence and YLDs have been always more in males from 1990 to 2019 and this difference remains almost stagnant for all the three indexes during this period with a slight increase for both sexes during this period. “Spinal cord lesions at neck level” was more common in comparison to “spinal cord lesions below neck level” in all incidence, prevalence and specially YLDs values.

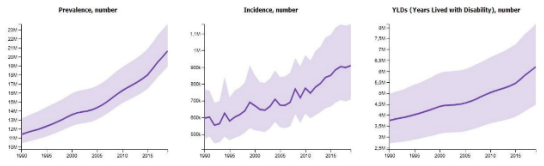

Figure 1. Global numbers of prevalence, incidence and YLDs for spinal injuries from 1990 to 2019 from all causes for both sexes and all ages. 95% uncertainty intervals are shown in bright purple.

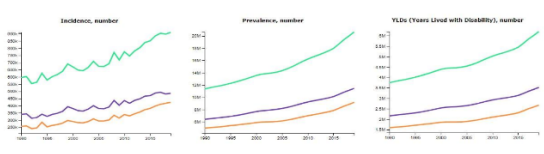

Figure 2. Global numbers of incidence, prevalence and YLDs for Spinal Injuries from all causes and for all ages in 1990 and 2019 for two sexes. (95% UI are not shown in order to avoid confusion).

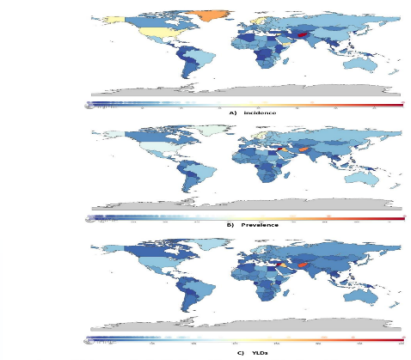

Figure 2.Global age-standardised incidence (A), prevalence (B) and YLDs (C) rates per 100,000 population for spinal injuries in 2019 from all causes and for both sexes.

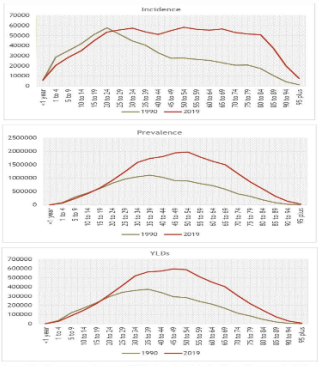

Figure 3. Global numbers of incidence, prevalence and YLDs for spinal injuries from all causes in 1990 and 2019 according to age groups. (95% UIs are not shown in order to avoid confusion but are available in table 3)

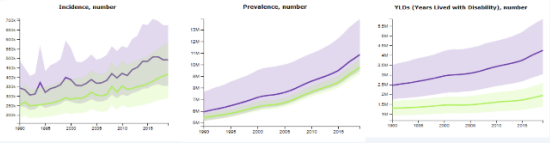

Figure 5. Global incidence, prevalence and YLDs for spinal injuries from 1990 to 2019 from all causes and for both sexes and all ages according to the level of injury

Conclusion

Epidemiology of spinal injuries tend to shift toward older ages and the number of affected population is increasing worldwide. While age-standardised rates of incidence, prevalence, and YLDs for spinal injuries changed slightly, absolute counts increased substantially from 1990. There is also a wide geographical heterogeneity in demographic, spatial and temporal patterns of spinal injuries, both at national and regional level, which should be considered by the local injury-prevention decision makers to reduce the overall burden of spinal injuries.

References

1.Hartkopp A, Brønnum-Hansen H, Seidenschnur AM, Biering-Sørensen F. Survival and cause of death after traumatic spinal cord injury. A long-term epidemiological survey from Denmark. Spinal cord. 1997;35(2):76-85.
2.Thietje R, Pouw MH, Schulz AP, Kienast B, Hirschfeld S. Mortality in patients with traumatic spinal cord injury: descriptive analysis of 62 deceased subjects. The journal of spinal cord medicine. 2011;34(5):482-7.
3.van den Berg ME, Castellote JM, de Pedro-Cuesta J, Mahillo-Fernandez I. Survival after spinal cord injury: a systematic review. Journal of neurotrauma. 2010;27(8):1517-28.

Contact

Mahdi Safdarian, MD Phone: +43 681 81 629 217 Email: m.safdarian@salk.com

Global, regional, and national trends of Spinal Injuries 1990-2019: findings from the Global Burden of Diseases (GBD) study 2019

Mahdi Safdarian[1]

[1]Department of Neurology, Christian Doppler Klinik, Paracelsus Medical University, Salzburg, Austria.; Contact: m.safdarian@salk.at

Objective
Spinal injuries contribute to a major burden of disabilities causing health loss due to premature mortality and residual disability. While spinal injuries are a public health issue, no comprehensive report on their global temporal, spatial and demographic patterns has not been published. We aimed to measure the global, regional, and national incidence, prevalence, and years lived with disability (YLDs) of spinal injuries from 1990 to 2019 using data from the Global Burden of Diseases, Injuries, and Risk Factors Study.

Methods
Data on incidence, prevalence, and YLDs of spinal injuries were derived systematically from the GBD 2019 study. Using the framework of GBD 2019, we provide numbers and age-standardized rate changes with 95% uncertainty intervals (UIs) for incidence, prevalence, and YLDs of spinal injuries at neck level and below neck level globally and for 21 GBD regions and 204 countries and territories, among all age groups and both sexes from 1990 to 2019. We tried to detect and report meaningful trends based on location, age and gender.

Results
Globally, there were 20.6 million (95% UI: 18.9–23.6) individuals with spinal injuries in 2019. The incidence number of spinal injuries was 909,000 cases (95% UI: 706,952–1,156,409) with an estimated 6.2 million (95% UI: 4.4–8.1) YLDs. There was a significant 81.5% [95% UI: 74.2 to 87.1], 52.7% [95% UI: 30.3 to 69.8] and 65.4% [95% UI: 56.3 to 76.0] increase in the global prevalence, incidence and YLDs numbers of spinal injuries respectively from 1990 to 2019. However, global age-standardised incidence, prevalence and YLDs rates per 100,000 population for spinal injuries, showed slighter changes of 5.8% (95% UI: 2.6–9.5), -6.1% (-17.2–1.5) and -1.5 % (-5.5–3.2) from 1990 to 2019, respectively. There were great geographical variations in the age-standardised rates of spinal Injuries in 2019, in addition to changes from 1990. The incidence increases with age and remains higher than 50,000 cases from 20 to 84 years with two peaks at 30-34 and 50-54 years. The prevalence and YLDs charts; however, show similar patterns, as they both have one peak around 45-59, and 50-54 years, respectively. Globally, the numbers of incidence, prevalence and YLDs have been always more in males from 1990 to 2019 and this difference remains almost stagnant for all the three indexes during this period with a slight increase for both sexes during this period. “Spinal cord lesions at neck level” was more common in comparison to “spinal cord lesions below neck level” in all incidence, prevalence and specially YLDs values.

Conclusions
Epidemiology of spinal injuries tend to shift toward older ages and the number of affected population is increasing worldwide. While age-standardised rates of incidence, prevalence, and YLDs for spinal injuries changed slightly, absolute counts increased substantially from 1990. There is also a wide geographical heterogeneity in demographic, spatial and temporal patterns of spinal injuries, both at national and regional level, which should be considered by the local injury-prevention decision makers to reduce the overall burden of spinal injuries.

References
1. Hartkopp A, et al. Survival and cause of death after traumatic spinal cord injury A long term epidemiological survey from Denmark Spinal cord 1997 35 2 76 85

Ethical Decision-Making Confidence Scale (EDMCS) for Nurse Leaders: Psychometric Evaluation

Firuzan Sari Kundt[1], Patrick Kutschar[1], Lorri Birkholz[2], Margitta Beil-Hildebrand[1]

[1]Institute of Nursing Science and Practice, Paracelsus Medical University Salzburg, Austria

[2]Chatham University School of Nursing, Pittsburgh, PA, USA

Background: Ethical decision-making confidence develops from clinical expertise and is a core competency for nurse leaders. To date, no tool exists to measure confidence levels in nurse leaders based upon an ethical decision-making framework.

Aim: The objective of this research was to compare ethical decision-making among nurse leaders in the U.S. and three German-speaking countries in Europe by developing and testing a newly constructed Ethical Decision-Making Confidence (EDMC) scale.

Methods: The cross-sectional survey included 18 theory-derived questions on ethical decision-making confidence which were used to develop the scale. Ethical approval was given by the IRB Board of a U.S. university. Participation in the survey implied voluntary consent.
Participants were a convenience sample of nurse leaders from the U.S. (n=91) and three German-speaking countries (n=225) in Europe who self-identified as holding a leadership position.
As for statistical analyses, a principal component analysis (PCA) applying an oblique (promax) rotation method was carried out for total sample and separately by country. After examination of item correlation matrices, scree plot and Kaiser Eigenvalue criteria (>1.0) were used to extract the optimal number of components.

Results: The scale's a) item structure dimensionality and b) subscale reliability were analyzed and c) compared between nurse leaders from all German-speaking countries and the U.S.

a) Item structure dimensionality
- In total sample, PCA showed high between-item correlations of the 18 items and identified a two-factor solution, cumulatively explaining 58.23% of total variance, and factor loadings ranging from 0.536-0.889 were observed
- Subsample (U.S. vs. German-speaking countries) analysis revealed that three items differed in terms of their component alignment, and thus, were excluded
- Finally, a 15-item bi-dimensional EDMC scale yielding a skill-related (9-item) and a behavior-related (6-item) confidence dimension was identified

b) Subscale reliability
- Mean index variables were computed for the two subscales
- Subscale means and internal consistency (Cronbach α) were analyzed for the total and the subsamples
- EDMC subscales showed good-to-excellent internal consistency ranging between 0.851 and 0.938
- Corrected item-scale correlation and Cronbach α if item deleted further indicated that all items correlated well with total item average and deletion of certain items would not lead to any increase of internal consistency, respectively

c) Comparison of EDMC between nurse leaders by countries
- Overall, U.S. nurse leaders rated their skill-related (Δ=0.38, p<0.001, CI 95% 0.22-0.48) as well as their behavior-related (Δ=0.40, p<0.001, 0.23-0.58) ethical decision-making confidence significantly higher than their European counterparts

Reliability and Statistical Comparisons by Country

EDMC subscale	AT-DE-CH	U.S.A.	Total
Skill-related confidence dimension – 1 (very low) to 5 (very high)			
Cronbach α	0.884	0.938	0.908
x̄ (SD), Ra	3.42 (0.6), 1.7-5.0	3.80 (0.7), 2.2-5.0	3.53 (0.6), 1.8-5.0
T, p, CI 95% of mean difference	5.02, <0.001, 0.22-0.48		
Behavior-related confidence dimension – 1 (very low) to 5 (very high)			
Cronbach α	0.851	0.911	0.874
x̄ (SD), Ra	3.15 (0.7), 1.0-5.0	3.55 (0.7), 2.0-5.0	3.3 (0.8), 1.0-5.0
T, p (df), CI 95% of mean difference	4.51, <0.001, 0.23-0.58		

Notes: x̄ Mean, SD Standard Deviation, Ra Range, α alpha (internal consistency), T Student T-Test, p significance level, df degrees of freedom, CI 95% confidence interval; AT Austria, DE Germany, CH Switzerland

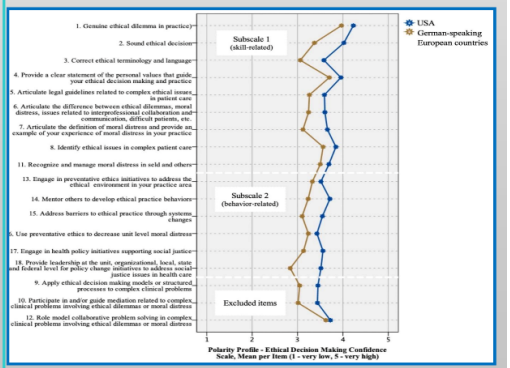

Discussion/Conclusion: This newly developed scale is an effective tool for measuring ethical decision-making confidence in nurse leaders. An overarching factor structure was identified, which is shared by the samples of nurse leaders. The promising results of this study should be replicated to ensure validity and reliability of the EDMC scale measuring skill-related and behavior-related concepts and include nurse leaders from various cultural, social, and demographic groups.

Literature:
[1] Birkholz L, Kutschar P, Kundt FS & Beil-Hildebrand M. (2022) Ethical decision-making confidence scale for nurse leaders: Psychometric evaluation. Nursing Ethics. 1:9697330211065847. Epub ahead of print. DOI: 10.1177/09697330211065847. PMID: 35230887.

Ethical Decision-Making Confidence Scale (EDMCS) for Nurse Leaders: Psychometric Evaluation

Firuzan Sari Kundt[1], Patrick Kutschar[1], Lorri Birkholz[2], Margitta Beil-Hildebrand[1]

[1]Institute of Nursing Science and Practice, Paracelsus Medical University, Salzburg, Austria; [2]Chatham University School of Nursing, Pittsburgh, PA, USA; Contact: firuzan.sari@pmu.ac.at

Objective
Ethical decision-making confidence develops from clinical expertise and is a core competency for nurse leaders. No tool exists to measure confidence levels in nurse leaders based upon an ethical decision-making framework.
The objective of this research was to compare ethical decision-making among nurse leaders in the U.S. and three German-speaking countries in Europe by developing and testing a newly constructed Ethical Decision-Making Confidence (EDMC) scale.

Methods
The cross-sectional survey included 18 theory-derived questions on ethical decision-making confidence which were used to develop the scale. Participants are a convenience sample of nurse leaders from the U.S. and three German-speaking countries in Europe who self-identified as holding a leadership position. Ethical approval was given by the IRB Board of a U.S. university. Participation in the survey implied voluntary consent.

Results
The scale's item structure dimensionality and subscale's reliability were analyzed and compared between nurse leaders from all four countries. A principal component analysis (PCA) produced a 15-item bi-dimensional EDMC scale yielding a skill-related (9-item) and a behavior-related (6-item) confidence dimension. EDMC subscales showed good-to-excellent internal consistency. In both subscales, U.S. nurse leaders rated their mean EDMC score higher than their German-speaking counterparts in Europe.

Conclusions
This exploratory study is the first of its kind to focus on nurse leaders' confidence regarding ethical decision-making in an international context. An overarching factor structure was identified, which is shared by the two samples of nurse leaders and to examine (sub)scales' psychometric properties.
This newly developed scale is an effective tool for measuring ethical decision-making confidence in nurse leaders from a variety of backgrounds. The promising results of this study should be replicated to ensure validity and reliability of the EDMC scale measuring skill-related and behavior-related concepts.

UNIKLINIKUMSALZBURG

Comparison of high tone therapy and transcutaneous electrical nerve stimulation therapy in chemotherapy-induced polyneuropathy (CIPN)

Robert Sassmann[1]; Dagmar Schaffler-Schaden[2]; Florian Rieder[1]; Tim Johansson[2]; Simon Peter Gampenrieder[3,4,5]; Gabriel Rinnerthaler[3,4,5]; Katrin Lampl[1]; Richard Greil[3,4,5]; Maria Flamm[2]; Josef Niebauer[1,6]

1 Institute of Physical Medicine and Rehabilitation, Paracelsus Medical University Salzburg, Austria; 2 Institute of General Practice, Family Medicine and Preventive Medicine, Paracelsus Medical University Salzburg, Austria; 3 Department of Internal Medicine III with Haematology, Medical Oncology, Haemostaseology, Infectiology and Rheumatology, Oncologic Center, Paracelsus Medical University Salzburg, Salzburg, Austria; 4 Salzburg Cancer Research Institute (SCRI) - Laboratory for Immunological and Molecular Cancer Research (LIMCR) and Center for Clinical Cancer and Immunology Trials (CCCIT), Salzburg, Austria; 5 Cancer Cluster Salzburg, Salzburg, Austria; 6 Institute of Sports Medicine, Prevention and Rehabilitation, Paracelsus Medical University Salzburg, Austria.

Introduction

Chemotherapy-induced peripheral neuropathy (CIPN) is a worldwide concern in patients receiving neurotoxic agents. There is no evidence-based treatment available so far (1).

The aim of this randomized control trial was to determine the efficacy of home based HTEMS therapy in CIPN patients compared to transcutaneous electrical nerve stimulation (TENS).

Methods

Male and female cancer patients with clinical relevant CIPN 4 to 24 weeks after ending of neurotoxic chemotherapy (platinum or taxane) were randomized to HTEMS or TENS therapy. Primary and secondary outcomes were measured at baseline (T0) and after 8 weeks of therapy (T1).

Primary outcome: EORTC-QLQ-CIPN 20 questionnaire.

Secondary outcomes: clinical examination, classification of CINP after CTCAE and the EORTC QLQ-C30 questionnaire.

Interventions were performed at least 5 days a week, for 30 minutes at home.

Results

51 patients were included in the study, one patient was lost to follow-up. 25 patients supplied with HTEMS and 25 patients supplied with TENS were analysed per intention to treat for the primary endpoint. 42 patients (HTEMS n=22, TENS n=20) were analysed per protocol for secondary outcomes. 8 patients did not fulfil compliance criteria.

Primary outcome: Improvements of the sensory and motor scale in both groups (HTEMS p<.001and p=.003; TENS p=.004 and p=.003). **(Fig. 1 and 2)**

Secondary outcomes: Improvements in the classification of CIPN after CTCAE (grade 1=mild to 4= life-threatening) in both groups from 2 to 1 in the HTEMS (p=.012) and 3 to 1 in the TENS (p=.004) group. **(Fig. 3)**

Improvements in EORTC QLQ-C30 in quality of life (+8.7%, p=.018) and physical functioning (+7.9%, p=.006) in the HTEMS group, and pain (-17.5%, p=.039) in the TENS group.

No between group differences in any variable or further changes in other parameters.

Conclusion

This randomized controlled trial addressed a worldwide significant problem in many cancer patients - CIPN. We showed that both modes of electrical stimulation were successful in improving relevant limitations in daily life. However, with this design, it is not possible to estimate the influence of spontaneous improvements over time.

References

Hou S et al. Treatment of chemotherapy-induced peripheral neuropathy: systematic review and recommendations. Pain Physician 2018

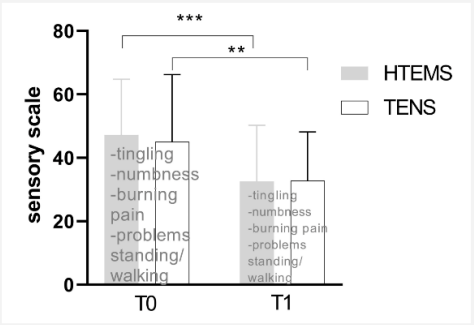

FIG.1 Changes in EORTC-QLQ-CIPN 20 sensory scale before (T0) and after (T1) interventions in the HTEMS and TENS groups. Significant within group changes ***p<.001; **p<.01. Values are presented as means + SD.

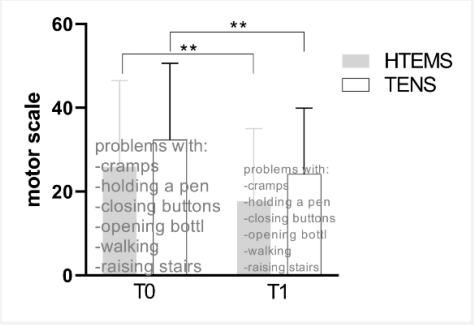

FIG.2 Changes in EORTC-QLQ-CIPN 20 motor scale before (T0) and after (T1) interventions in the HTEMS and TENS groups. Significant within group changes **p<.01. Values are presented as means + SD.

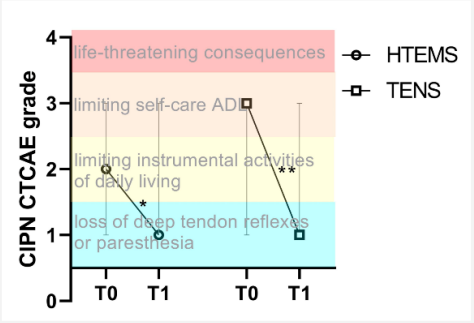

FIG.3 Changes in CINP CTCAE classification before (T0) and after (T1) interventions in the HTEMS and TENS groups. Significant within group changes **p<.01; *p<.05. Values are presented as median.

Contact: Institute of Physical Medicine and Rehabilitation, Paracelsus Medical University Salzburg, Austria
Mag. Robert Sassmann, r.sassmann@salk.at

Comparison of high tone therapy and transcutaneous electrical nerve stimulation therapy in chemotherapy-induced polyneuropathy

Robert Sassmann[1], Dagmar Schaffler-Schaden[2], Florian Rieder[1], Tim Johansson[2], Simon Peter Gampenrieder[3,4,5], Gabriel Rinnerthaler[3,4,5], Katrin Lampl[1], Richard Greil[3,4,5], Maria Flamm[2], Josef Niebauer[1,6]

[1]Institute of Physical Medicine and Rehabilitation, Paracelsus Medical University Salzburg, Austria; [2]Institute of General Practice, Family Medicine and Preventive Medicine, Paracelsus Medical University Salzburg, Austria; [3]Department of Internal Medicine III with Haematology, Medical Oncology, Haemostaseology, Infectiology and Rheumatology, Oncologic Center, Paracelsus Medical University Salzburg, Salzburg, Austria; [4]Salzburg Cancer Research Institute (SCRI) - Laboratory for Immunological and Molecular Cancer Research (LIMCR) and Center for Clinical Cancer and Immunology Trials (CCCIT), Salzburg, Austria; [5]Cancer Cluster Salzburg, Salzburg, Austria; [6]Institute of Sports Medicine, Prevention and Rehabilitation, Paracelsus Medical University Salzburg, Austria; Contact: r.sassmann@salk.at

Objective
Chemotherapy-induced peripheral neuropathy (CIPN) is a worldwide concern in patients receiving neurotoxic agents for cancer therapy. Unfortunately, there is no evidence-based treatment available so far (1). High tone external muscle stimulation (HTEMS) is a promising therapeutic approach to alleviate symptoms of CIPN in diabetic peripheral neuropathic patients. Therefore, the primary objective of this randomized control trial was to determine the efficacy of home based HTEMS therapy in CIPN patients compared to transcutaneous electrical nerve stimulation (TENS).

Methods
Male and female cancer patients with clinical relevant CIPN 4 to 24 weeks after ending of neurotoxic chemotherapy (platinum or taxane) were randomized to HTEMS or TENS therapy. Primary and secondary outcomes were measured at baseline and after 8 weeks of therapy. The primary outcome were changes in the patient-reported EORTC-QLQ-CIPN 20 questionnaire. Secondary outcomes included clinical examinations, a classification of CINP after CTCAE and the EORTC QLQ-C30 questionnaire. Both electrical interventions were performed at least 5 days a week, for 30 minutes at home.

Results
Fifty-one patients were included in the study, one patient was lost to follow-up. Twenty-five patients supplied with HTEMS and 25 patients supplied with TENS were analysed per intention to treat for the primary endpoint. Forty-two patients (HTEMS n=22, TENS n=20) were analysed per protocol for secondary outcomes because 8 patients did not fulfil the minimal usage criteria of 1200 minutes electrical therapy. The primary outcome questionnaire improved for the sensory and motor scales in both groups (HTEMS p<.001, p=.003; TENS p=.004, p=.003). Also the classification of CIPN after CTCAE (grade 1=mild to 4= life-threatening) improved in both groups from 2 to 1 in the HTEMS (p=.012) and 3 to 1 in the TENS (p=.004) groups. The EORTC C30 showed significant improvements in quality of life (+8.7%, p=.018) and physical functioning (+7.9%, p=.006) in the HTEMS group, and pain (-17.5%, p=.039) in the TENS group, only. There were no between group differences in any variable or further changes in other parameters.

Conclusions
This randomized controlled trial addressed a worldwide significant problem in many cancer patients - CIPN. We showed that both modes of electrical stimulations were successful in improving relevant limitations in daily life. However, with this design, it is not possible to estimate the influence of spontaneous improvements over time.

References
1. Hou S. et al. Treatment of chemotherapy-induced peripheral neuropathy: systematic review and recommendations. Pain Physician, 2018

DO PRO- AND ANTIANGIOGENIC EFFECTS OF TENDON CELLS DEPEND ON OXYGEN AVAILABILITY?

Judit K. Schachinger[1,2], Herbert Tempfer[1,2], Christine Lehner[1,2] and Andreas Traweger[1,2]

[1]Institute of Tendon and Bone Regeneration, Paracelsus Medical Private University, 5020 Salzburg, Austria;
[2]Austrian Cluster for Tissue Regeneration, Vienna, Austria

Austrian Cluster for Tissue Regeneration

PARACELSUS MEDIZINISCHE PRIVATUNIVERSITÄT

Tendons are hierarchically organized connective tissues that anatomically link muscle to bone and enable efficient energy transmission from muscle to the skeleton [1,2]. Healthy tendons harbor few cells, are rich in extracellular matrix (ECM) and have a low blood vessel density [3]. Injured tendons, however, are characterized by an excessive deposition of ECM, an increase in cell number and excessive blood vessel ingrowth. It is assumed that pro- and antiangiogenic factors are well balanced in healthy tendon, maintaining low vascularization, whereas this balance is lost in overused or injured tendon. Additionally, hypoxia inducible factor 1 alpha (HIF1-a) is supposed to be a crucial player in terms of oxygen regulation and blood supply. But, this mechanism remains poorly understood in healthy and overused tendons. [4,5].

OBJECTIVE

- To analyze potential oxygen- dependent pro- and antiangiogenic mechanisms exerted by tendon cells with a focus on HIF1-a (hypoxia inducible factor 1a).

METHODS

- Human semitendinosus tendon derived stem/ progenitor cells (TDSPCs) and human adipose tissue derived stem cells (ADSCs) were cultured under normoxic (19% O_2) and hypoxic conditions (5% O_2). Cell supernatants were tested in a human umbilical vein endothelial cell (HUVEC) based tube formation assay, allowing to assess their impact on angiogenesis- related cellular mechanisms. ADSCs were used as a control group to validate the model, since they are known to induce angiogenesis [6]. (Figure 1)

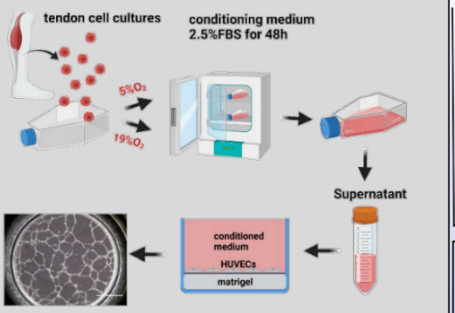

Figure 1: Workflow of culturing cells under two different O_2 concentrations in order to collect the supernatant for tube formation analysis.

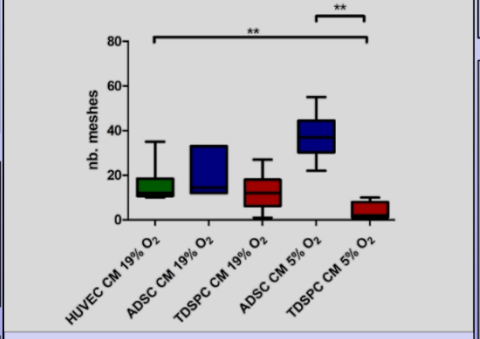

Figure 2: Quantification of HUVEC tube formation assay reveals that tendon stem/progenitor cell (TDSPC) derived conditioned medium (CM) cultivated at 5% O_2 significantly reduces the number of meshes, compared to proangiogenic adipose derived stem cell (ADSC) derived conditioned medium.

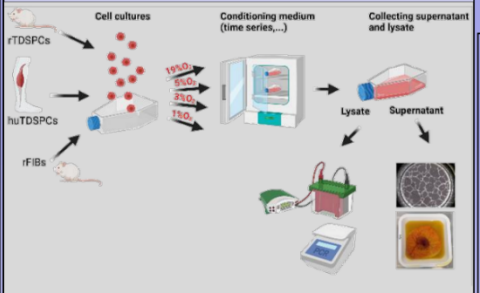

Figure 3: Workflow of culturing cells under different O_2 concentrations in order to make lysates for HIF1-a analysis by Westsern Blot.

- Human and rat tendon cells and dermal fibroblasts cultured under different O_2 concentrations, are analysed by Western Blot regarding HIF1-a and other angiogenesis related factors. Additionally, the HET-CAM (hen's egg test – chorion allantoic membrane) assay is established for the analysis of pro-and antiangiogenic effects of tendon cells. (Figure 3)

PRELIMINARY RESULTS

- TDSPCs conditioned medium (CM) generated at 5% O_2 significantly decreased the number of formed tubes compared to ADSC CM (5% O_2) and TDSPCs CM 19% O_2 (p=0.005). (Figure 2)

CONCLUSION & OUTLOOK

With this work we show that cultured tendon cells exert antiangiogenic mechanisms mediated by soluble factors. In future work, these factors will be further examined by mass spectrometry and mRNA sequencing. Moreover, potential changes of the balance between pro- and antiangiogenic factors will be examined by in vitro and ex vivo model of tendon disease.

The HET-CAM assay will be established for examining the anti-angiogenic effect of tendon cells on the blood vessel network.

REFERENCES

[1] Kirkendall DT., Scand J Med Sci Sports 1997: 7: 62-66

[2] Pufe et al., Scand J Med Sci Sports, 2005, 15, 211-22

[3] Kannus. P. Scand J Med Sci Sports; 2000 10: 312-20.

[4] Tempfer and Traweger, Front Physiol. 2015 Nov 18;6:330.

[5] Olmedo-Suàrez M.Á. Micromachines(Basel), 2020, 11(5), 475

[6] Efimenko et al., Tsitologiia, 52, 144-54

CONTACT

judit.schachinger@pmu.ac.at

Do pro and antiangiogenic factors effects of tendon cells depend on oxygen availability?

Judit Schachinger[1,2], Herbert Tempfer[1,2], Christine Lehner[1,2], Andreas Traweger[1,2]

[1]Institute of Tendon and bone Regeneration, Paracelsus Medical Private University, Salzburg, Austria; [2]Austrian Cluster for Tissue Regeneration, Vienna, Austria; Contact: judit.schachinger@pmu.ac.at

Objective

Tendons are hierarchically organized connective tissues that anatomically link muscle to bone and enable efficient energy transmission from muscle to the skeleton [1,2]. Healthy tendons harbor few cells, are rich in extracellular matrix (ECM) and have a low blood vessel density [3]. Injured tendons, however, are characterized by an excessive deposition of ECM, an increase in cell number and excessive blood vessel ingrowth. It is assumed that pro- and antiangiogenic factors are well balanced in healthy tendon, maintaining low vascularization, whereas this balance is lost in overused or injured tendon. Additionally, hypoxia inducible factor 1 alpha (HIF1-a) is supposed to be a crucial player in terms of oxygen regulation and blood supply. But, this mechanism remains poorly understood in healthy and overused tendons. [4,5].
The objective is to analyze potential oxygen- dependent pro- and antiangiogenic mechanisms exerted by tendon cells with a focus on HIF1-a (hypoxia inducible factor 1a).

Methods

Human semitendinosus tendon derived stem/ progenitor cells (TDSPCs) and human adipose tissue derived stem cells (ADSCs) were cultured under normoxic (19% O2) and hypoxic conditions (5% O2). Cell supernatants were tested in a human umbilical vein endothelial cell (HUVEC) based tube formation assay, allowing to assess their impact on angiogenesis- related cellular mechanisms. ADSCs were used as a control group to validate the model, since they are known to induce angiogenesis [6]. (Figure 1)
Human and rat tendon cells and dermal fibroblasts cultured under different O2 concentrations, are analysed by Western Blot regarding HIF1-a and other angiogenesis related factors. Additionally, the HET-CAM (hen‘s egg test – chorion allantoic membrane) assay is established for the analysis of pro-and antiangiogenic effects of tendon cells. (Figure 3)

Results

TDSPCs conditioned medium (CM) generated at 5% O2 significantly decreased the number of formed tubes compared to ADSC CM (5% O2) and TDSPCs CM 19% O2 ($p=0.005$). (Figure 2)

Conclusions

With this work we show that cultured tendon cells exert antiangiogenic mechanisms mediated by soluble factors. In future work, these factors will be further examined by mass spectrometry and mRNA sequencing. Moreover, potential changes of the balance between pro- and antiangiogenic factors will be examined by in vitro and ex vivo model of tendon disease.
The HET-CAM assay will be established for examining the anti-angiogenic effect of tendon cells on the blood vessel network.

References

1. Kirkendall DT., Scand J Med Sci Sports 1997: 7: 62-66
2. Pufe et al.,. Scand J Med Sci Sports, 2005, 15, 211-22
3. Kannus. P. Scand J Med Sci Sports; 2000 10: 312-20
4. Tempfer and Traweger, Front Physiol. 2015 Nov 18;6:330
5. Olmedo-Suàrez M.À. Micromachines(Basel), 2020, 11(5), 475
6. Efimenko et al., Tsitologiia, 52, 144-54

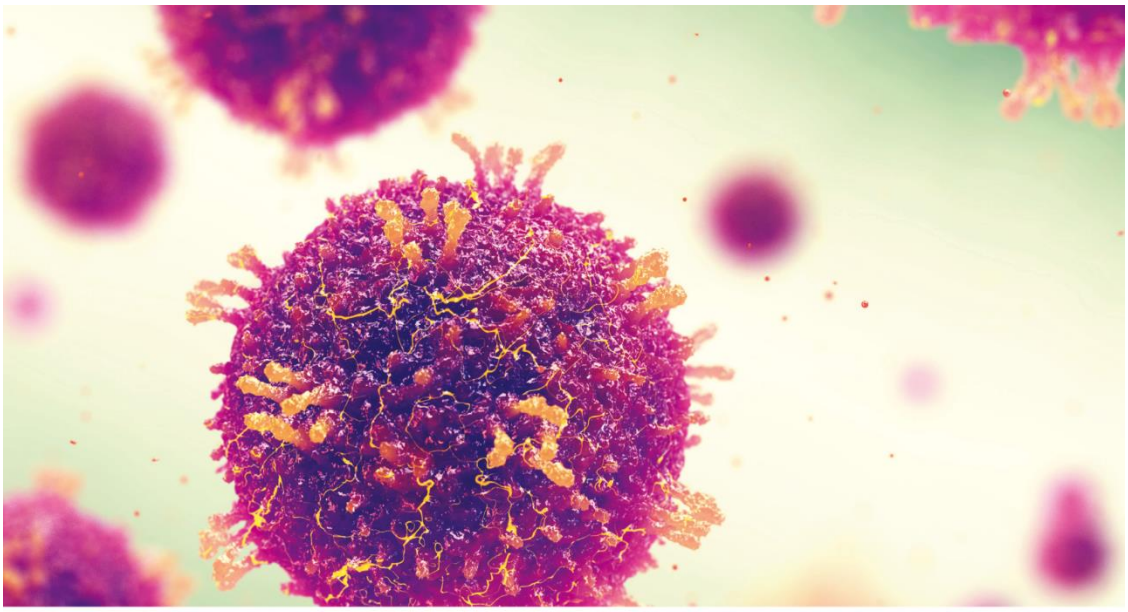

Arbeiten Sie im Bereich Infektionskrankheiten?

Gestatten, wir sind New England Biolabs (NEB) – Ihr starker Partner für Ihre Forschung und Entwicklung.

Viele Wissenschaftler kennen NEB als zuverlässigen Lieferanten von Forschungsreagenzien für die Life-Science-Gemeinschaft. Was Sie aber vielleicht nicht wissen ist, dass wir ein großes Produktportfolio anbieten, das in der Infektionsforschung, der Genomsequenzierung, der Entwicklung von Diagnostika und Therapeutika eingesetzt wird.

Viele unserer Produkte haben die Entwicklung von COVID-19-Diagnostika und -Impfstoffen unterstützt und finden ihren Einsatz auch bei der Erforschung und Diagnostik von Influenza und Malaria.

Wir bieten Ihnen unsere ISO 13485-konformen Reagenzien auch in „GMP-grade" Qualität oder als lyophilisierte bzw. lyo-ready Variante an – bei Bedarf in auf Ihre Bedürfnisse perfekt zugeschnittenen Formaten oder Sonderformulierungen.

- 50 Profitieren Sie von fast 50 Jahren Erfahrung in der Molekularbiologie und Enzymologie.
- Arbeiten Sie mit unserem OEM & Customized Solutions Team zusammen, um die perfekte Lösung für Ihre Bedürfnisse zu finden.
- Profitieren Sie von unseren umfangreichen Produktionsmöglichkeiten.
- Nutzen Sie unsere Produkte in „GMP-grade" Qualität*, lyophilisiert, lyo-ready oder glyzerinfrei.
- Vertrauen Sie für Ihre Vorhaben auf die Leistung unserer zuverlässigen Produkte, abgesichert durch stringente Qualitäts- & regulatorische Maßnahmen.

Interesse geweckt? Dann erfahren Sie mehr unter **www.neb.com/InfectiousDiseases**

NEW ENGLAND BioLabs® GmbH

be INSPIRED
drive DISCOVERY
stay GENUINE

* "GMP-grade" ist eine Bezeichnung, die NEB verwendet, um Reagenzien zu beschreiben, die unter besonders kontrollierten Produktionsbedingungen unter Einhaltung der Vorgaben der Qualitätsmanagementsysteme ISO 9001 und ISO 13485 produziert werden. Es handelt sich dabei aber nicht um aktive pharmazeutische Inhaltsstoffe (APIs). NEB garantiert nicht die Beachtung aller Vorschriften der aktuellen Good Manufacturing Practice (GMP).

PARACELSUS MEDIZINISCHE PRIVATUNIVERSITÄT

Klinikum Nürnberg
wir sind für Sie da!

Analysis of H_V1 proton channel expression in acute leukemias and non-Hodgkin lymphomas compared to healthy control samples by qPCR

Nicole Schneider[1], Christian Derst[2], Anna Bold[3], Heike Gross[3], Elisabeth Holzmann[3], Boris Musset[2]

[1]Paracelsus Medical University, Nuremberg, Germany; Contact: nicole.schneider@stud.pmu.ac.at
[2]Center of Physiology, Pathophysiology and Biophysics, Paracelsus Medical University, Nuremberg, Germany
[3]Department of Hematology and Medical Oncology, Paracelsus Medical University, Nuremberg, Germany

Introduction and Objectives

High expression of the human-voltage gated proton channel (H_V1) significantly correlated with negative prognosis in studies of breast cancer and colorectal cancer cells. Several isoforms of H_V1 are known. A short isoform contributes to the pathogenesis of chronic lymphocytic leukemia. The aim of the study was to detect expression differences of the H_V1 gene (HVCN1) in mononuclear cells of acute leukemias, non-Hodgkin lymphomas and controls, as well as the occurrence of the shorter isoform.

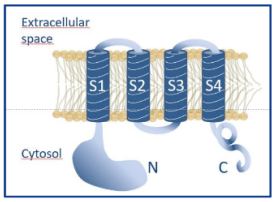

Figure 1. **Architectural model of H_V1-channel.** Kindly provided by Dr. Gustavo Chaves.

Methods

We analysed HVCN1-mRNA expression in 103 blood and 65 bone marrow samples from 33 patients (25 acute myeloid leukemia (AML), five acute lymphatic leukemia (ALL), two multiple myeloma (MM), one B-cell non-Hodgkin lymphoma (NHL)) and 11 non-leukemic individuals. Data were obtained by qPCR using GAPDH as reference gene. The presence of the two isoforms was analysed in 33 samples by RT-PCR.

qPCR

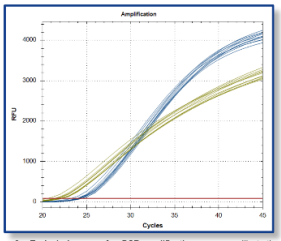

Figure 2. **Typical image of qPCR-amplification curves.** Illustration of fluorescence detection in real-time during a qPCR run. blue: HVCN1 (FAM), yellow: GAPDH (VIC), red line: threshold. Image taken and modified with qPCR analysis software from Biorad.

Transcript variants

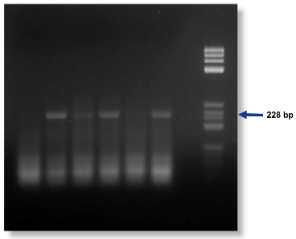

Figure 3. **RT-PCR analysis of expression of H_V1 channel mRNA-transcript variants 1, 2 and 3.** mRNA and protein sequence were derived from NCBI Genbank: NM_001040107.2, NM_032369.4, NM_001256413.2.

Results

The resulting ΔΔCq values demonstrated a wide dispersion as well as significant lower HVCN1 expression in AML (p=4e-08), ALL (p=5.5e-02) and MM (Mean 2+ΔΔCq=0.05) compared to the control group. In contrast, 2.8-fold higher HVCN1 expression was measured in NHL. Direct comparison of sample materials from identical patient showed higher HVCN1 expression in bone marrow samples compared to blood samples. Differentiation between short and long isoforms were not possible by RT-PCR.

Significantly lower HVCN1 expression in blood cancer

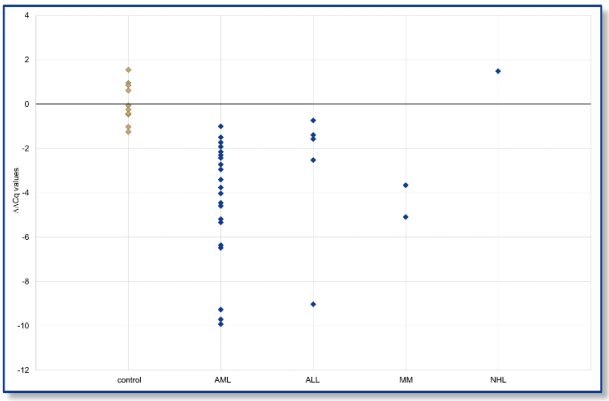

Figure 4. **ΔΔCq-values plotted to control group and diseases. The** mRNA-expression was analysed in control (n=11), AML (n=25), ALL (n=five), MM (n=two) and B-cell NHL (n=one) samples. Lower HVCN1 expression was demonstrated in samples from AML, ALL and MM compared to control group. qPCR-results B-cell NHL showed higher HVCN1 expression than control samples. Use of TaqMan assays for GAPDH (Hs999905_m1) and HVCN1 (Hs01032838_m1) from Applied Biosystems (Waltham, Massachusetts, United States).

Comparison of sample material

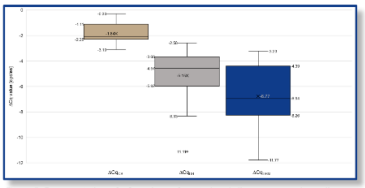

Figure 5. **Representation of ΔCq values of control and disease group depending on sample material.** Comparison showed statistically significant difference of HVCN1 expression between ΔCqCB and ΔCqDB (p=5.5e-06) as well as between ΔCqCB and ΔCqDBM (p=7.8e-07). No difference between ΔCqDB and ΔCqDBM (p=0.36).
Abbrev.: ΔCqCB, ΔCq of blood samples in control group; ΔCqDB, ΔCq of blood samples in disease group; ΔCqDBM, ΔCq of bone marrow samples in disease group.

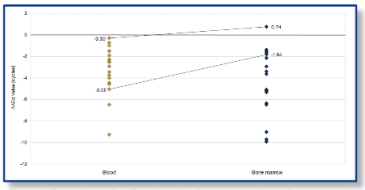

Figure 6. **Comparison of ΔΔCq values in disease group depending on sample material.** No significant difference of HVCN1 expression (ΔCqDB vs. ΔCqDBM: p=0.36). The two lines connect ΔΔCq values of two cases, from which blood and bone marrow samples were tested. The results indicate increased expression of HVCN1 in bone marrow samples. Abbrev.: ΔCqDB, ΔCq of blood samples in disease group; ΔCqDBM, ΔCq of bone marrow samples in disease group.

Comparison with age and sex

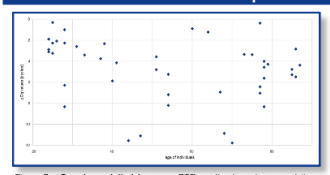

Figure 7. **ΔCq-values plotted by age.** qPCR-results showed no correlation between HVCN1 expression and age of patients (r=-0.24; p > 0.05).

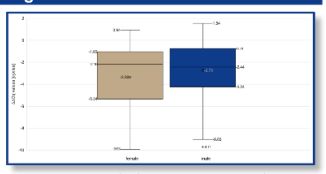

Figure 8. **Representation of ΔΔCq-values depending on sex of individuals.** Comparison of samples from male (n=31) and female (n=13) patients showed no significant difference between HVCN1 expression in these groups (p=0.5237).

Conclusion and Outlook

Wide dispersion confirmed interindividual differences of HVCN1 expression. Lower HVCN1 expression in AML, ALL, and MM is an indicator for lower functional importance of the H_V1 channel in these diseases.

- It is unclear whether cellular expression changes or loss of cell populations with higher HVCN1 expression are responsible.
- Further steps include evaluation of clinical patient data, expansion of the patient cohort and investigation of cell-specific HVCN1 expressions.

Expression differences between sample materials should be further investigated by testing both sample materials from the same patients.

The location of the splice sites at the extreme 5' end complicated the differentiation between the two isoforms.

- The use of isoform-qPCR assays could be examined.
- Confirmation of higher expression of the short isoform would be beneficial for the development of cancer-specific biomarkers.
- Therapeutic options could prevent inhibition of the physiologically relevant long isoform.

Acknowledgement

From the Center of Physiology, Pathophysiology and Biophysics, Paracelsus Medical University, Nuremberg, Germany:

- Univ.-Prof. Dr. Dr. Boris Musset (doctoral supervisor), Dr. Christian Derst (practical supervisor), Dr. Eva Schrader, Dr. Gustavo Chaves, Patricia Romberg.

From the Department of Hematology and Medical Oncology, Paracelsus Medical University, Nuremberg, Germany:

- Prof. Dr. Martin Wilhelm, Dr. Anna Bold, Heike Gross, Elisabeth Holzmann.

Many thanks to all voluntary blood donors.

Key References

1. Wang Y, Li SJ, Wu X, Che Y, Li Q. Clinicopathological and Biological Significance of Human Voltage-gated Proton Channel Hv1 Protein Overexpression in Breast Cancer. J Biol Chem. 2012;287(17):13877-13888. doi:10.1074/jbc.M112.345280
2. Wang Y, Wu X, Li Q, Zhang S, Li SJ. Human voltage-gated proton channel hv1: a new potential biomarker for diagnosis and prognosis of colorectal cancer. *PloS One*. 2013;8(8):e70550. doi:10.1371/journal.pone.0070550
3. Bare DJ, Cherny VV, DeCoursey TE, Abukhdeir AM, Morgan D. Expression and function of voltage gated proton channels (Hv1) in MDA-MB-231 cells. Pizzo SV, ed. PLOS ONE. 2020;15(5):e0227522. doi:10.1371/journal.pone.0227522
4. Hondares E., Brown MA, Musset B, et al. Enhanced activation of an amino-terminally trun-cated isoform of the voltage-gated proton channel HVCN1 enriched in malignant B cells. Proc Natl Acad Sci. 2014;111(50):18078-18083. doi:10.1073/pnas.1411390111

Analysis of Hv1 proton channel expression in acute leukemias and non-Hodgkin lymphomas compared to healthy control samples by qPCR

Nicole Schneider[1], Christian Derst[2], Anna Bold[3], Heike Gross[3], Elisabeth Holzmann[3], Boris Musset[2]

[1]Paracelsus Medical University, Nuremberg, Germany; [2]Center of Physiology, Pathophysiology and Biophysics, Paracelsus Medical University, Nuremberg, Germany; [3]Department of Hematology and Medical Oncology, Paracelsus Medical University, Nuremberg, Germany; Contact: nicole.schneider@stud.pmu.ac.at

Objective
High expression of the human-voltage gated proton channel (H_V1) significantly correlated with negative prognosis in studies of breast cancer and colorectal cancer cells. (1,2,3) Several isoforms of H_V1 are known. (3,4) A short isoform contributes to the pathogenesis of chronic lymphocytic leukemia. (4) The aim of the study was to detect expression differences of the H_V1 gene (HVCN1) in mononuclear cells of acute leukemias, non-Hodgkin lymphomas and controls, as well as the occurrence of the shorter isoform.

Methods
We analysed HVCN1-mRNA expression in 103 blood and 65 bone marrow samples from 33 patients (25 acute myeloid leukemia (AML), five acute lymphatic leukemia (ALL), two multiple myeloma (MM), one B-cell non-Hodgkin lymphoma (NHL)) and 11 non-leukemic individuals. Data were obtained by qPCR using GAPDH as reference gene. The presence of the two isoforms was analysed in 33 samples by RT-PCR.

Results
The resulting $\Delta\Delta$Cq values demonstrated a wide dispersion as well as significant lower HVCN1 expression in AML ($p = 4e\text{-}08$), ALL ($p = 5.5e\text{-}02$) and MM (Mean2+$\Delta\Delta$Cq = 0.05) compared to the control group. In contrast, 2.8-fold higher HVCN1 expression was measured in NHL. Direct comparison of sample materials from identical patient showed higher HVCN1 expression in bone marrow samples compared to blood samples. Differentiation between short and long isoforms were not possible by RT-PCR.

Conclusions
Wide dispersion confirmed interindividual differences of HVCN1 expression. Lower HVCN1 expression in AML, ALL, and MM is an indicator for lower functional importance of the HV1 channel in these diseases. It is unclear whether cellular expression changes or loss of cell populations with higher HVCN1 expression are responsible. Future steps include evaluation of clinical patient data, expansion of the patient cohort and investigation of cell-specific HVCN1 expressions. The location of the splice sites at the extreme 5' end complicated the differentiation between the two isoforms. Confirmation of higher expression of the short isoform would be beneficial for the development of cancer-specific biomarkers. Therapeutic options could prevent inhibition of the physiologically relevant long isoform.

References
1. Wang Y, et al. Clinicopathological and Biological Significance of Human Voltage-gated Proton Channel Hv1 Protein Overexpression in Breast Cancer. J Biol Chem. 2012;287(17):13877-13888.
2. Wang Y, et al. Human voltage-gated proton channel hv1: a new potential biomarker for diagnosis and prognosis of colorectal cancer. PloS One. 2013;8(8):e70550.
3. Bare DJ, et al. Expression and function of voltage gated proton channels (Hv1) in MDA-MB-231 cells. Pizzo SV, ed. PLOS ONE. 2020;15(5):e0227522.
4. Hondares E, et al. Enhanced activation of an amino-terminally trun-cated isoform of the voltage-gated proton channel HVCN1 enriched in malignant B cells. Proc Natl Acad Sci. 2014;111(50):18078-18083.

MOTOR IMAGERY IN DISORDERS OF CONSCIOUSNESS USING FMRI

Laura Schnetzer[1,2,3], Verena Schätzle[2,4], Martin Kronbichler[2,4], Jürgen Bergmann[1,2], Eugen Trinka[1,2,3]

[1]Department of Neurology, Neurological Intensive Care and Neurorehabilitation, Christian Doppler Medical Centre, Paracelsus Medical University, Salzburg, Austria
[2]MRI Research Unit, Neuroscience Institute, Christian Doppler Medical Centre, Paracelsus Medical University, Salzburg, Austria
[3]Karl Landsteiner Institute of Neurorehabilitation and Space Neurology, Salzburg, Austria
[4]Centre for Cognitive Neuroscience and Department of Psychology, University of Salzburg, Salzburg, Austria

Background. Due to numerous complicating environmental and patient-related factors, diagnoses in patients with disorders of consciousness (DOC) are prone to misdiagnosis, especially, if examiners solely rely on clinical testing at patients' bedside [1]. Thus, research in recent years has sought additional approaches to make diagnosis in patients with DOC more reliable. One such approach discussed with great promise in current literature is functional Magnetic Resonance Imaging (fMRI) [2].

Aim. The main objective of this study was to investigate the response rates of patients with DOC in fMRI. Possible inconsistencies in the assessment of behavioural and neuronal correlates of consciousness should be uncovered. Furthermore, the study aimed to determine the indication, reliability and practical utility of fMRI for identifying preserved consciousness in patients with DOC and its use to improve the diagnostic process.

Methods. In line with the approach of Monti et al. (2010) [3], 71 patients with DOC (34 with Unresponsive Wakefulness Syndrome (UWS), 33 in Minimally Conscious State (MCS), 4 recovered according to the Coma Recovery Scale-Revised (CRS-R)) and 27 healthy controls performed a motor imagery task while being scanned with fMRI technique at the Christian Doppler Medical Centre in Salzburg, Austria. Blood-oxygen-level-dependent responses in the supplementary motor area (SMA) were then investigated in a region of interest (ROI) analysis and results were associated with various clinical parameters.

Results. Significant activations in the SMA during the motor imagery task were found in 9 of 71 patients with DOC (12.7%; e.g., Figure 1) compared to 25 of 27 controls (92%; e.g., Figure 2). Of the 9 patients who neuronally responded to the motor imagery task, 3 had been clinically classified as recovered, 5 as MCS and 1 as UWS. All 9 patients who showed significant activations in the SMA had a non-traumatic brain injury.

Conclusions. This study includes one of the largest samples to date of patients with DOC who have been assessed by fMRI for their neuronal responses in a command-following task and thus represents an important extension of research in this area. The high response rate of our control group showed the reliability of the procedure. The proportion of patients who were able to follow the commands were similar to the proportion reported by Monti et al. (2010). Nevertheless, in contrast to their findings, all our patients who showed significant activations in the SMA had a non-traumatic brain injury and most of them were clinically classified with a higher level of consciousness (i.e. MCS or recovered). However, the patient who was clinically diagnosed with UWS and responded with significant activations in the SMA, demonstrates the need for fMRI as an additional diagnostic tool in everyday clinical practice in order to perform more reliable differential diagnostics and find patients whose conscious perception would be missed at the bedside.

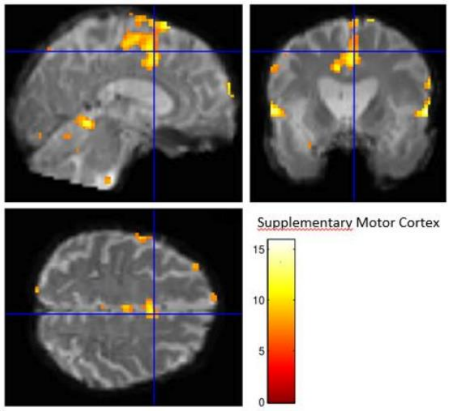

Figure 1. Activity pattern of a patient during motor imagery task

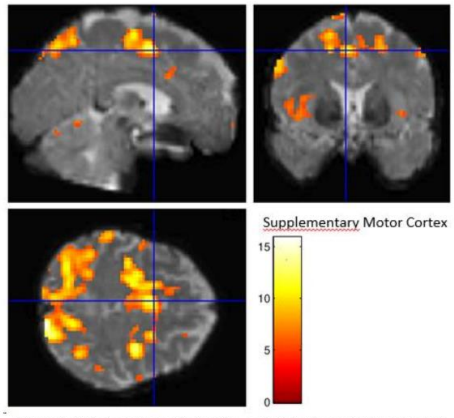

Figure 2. Activity pattern of a healthy control during motor imagery task

Laura Schnetzer has received the Paracelsus Medical University Research and Innovation Fund – PhD Researcher Excellence, grant agreement number 2021-PRE-001-Schnetzer

1. Schnakers C et al., BMC Neurol., 2009. 2. Kondziella D et al. Eur J Neurol, 2020 3. Monti M M et al. New England journal of medicine, 2010

Lesional Differences in Locked-in and Locked-in Plus Syndrome

Laura Schnetzer[1, 2, 3], Mark McCoy[1], Jürgen Steinbacher[4], Alexander Kunz[1, 3], Jürgen Bergmann[1, 2], Martin Kronbichler[2, 5], Eugen Trinka[1, 2, 3]

[1]Department of Neurology, Neurological Intensive Care and Neurorehabilitation, Christian Doppler Medical Centre, Paracelsus Medical University, Salzburg, Austria; [2]MRI Research Unit, Neuroscience Institute, Christian Doppler Medical Centre, Paracelsus Medical University, Salzburg, Austria; [3]Karl Landsteiner Institute of Neurorehabilitation and Space Neurology, Salzburg, Austria; [4]Department of Neuroradiology, Christian Doppler Medical Centre, Paracelsus Medical University Salzburg, Austria; [5]Centre for Cognitive Neuroscience and Department of Psychology, University of Salzburg, Salzburg, Austria; Contact: laura.schnetzer@stud.pmu.ac.at

Objective
The Locked-in Syndrome (LiS) is one of the severest neurological conditions, classically defined as a loss of all voluntary muscle movements except vertical eye movements and blinking motions combined with preserved cognitive abilities. Most cases are caused by the thrombosis of the basilar artery which results in the infarction of the ventral pons. Nevertheless, there are patients whose symptoms involve a dysfunction in consciousness and other cognitive abilities. These patients suffer from the Locked-in Plus Syndrome (LIPS). The main objective of this study was to explore differences between LiS and LIPS patients, focusing on lesion patterns.

Methods
Nine LiS patients were retrospectively identified and assigned to three groups (no major cognitive impairment, disturbances in cognition or consciousness and no consciousness detectable) according to clinical parameters like the Coma Recovery Scale-Revised. MRI scans were segmented semiautomatically using the 3D Slicer software package in order to identify the lesions and calculate different 2D and 3D shape features. With the help of these parameters, differences between the three groups were determined.

Results
Of the nine LiS patients involved, two had no major cognitive impairment, six showed disturbances and one displayed no signs of consciousness at all. A Kruskal-Wallis test including exact methods due to the very small sample size was conducted to examine the differences according to the lesional parameters. Significant differences ($H(2)=4.82$, $p=.048$) between the groups were found concerning the elongation of the lesions.

Conclusions
Lesions of LiS patients are round and confined to the pons, whereas lesions of LIPS patients are more elongated and reach other neighbouring areas as the mesencephalon, thalamus or the ascending reticular activating system. Our findings are in line with other studies which showed cognitive impairments in LiS patients who had lesions that expanded beyond the pons [1,2]. However, as our study sample is very small, more studies are needed to confirm our findings. The differentiation of LiS and LIPS patients is important as the patients need completely different therapies and care. Moreover, LIPS should not be confused with disorders of consciousness like the unresponsive wakefulness syndrome as the pathophysiology and therefore possible future therapeutic approaches differ.

Acknowledgements
Laura Schnetzer has received the Paracelsus Medical University Research and Innovation Fund – PhD Researcher Excellence, grant agreement number 2021-PRE-001-Schnetzer

References
1. Kumral E et al., Acta Neurol Belg, 2021
2. Schnakers C et al., J Neurol, 2008

LESIONAL DIFFERENCES IN LOCKED-IN AND LOCKED-IN PLUS SYNDROME

*Laura Schnetzer[1,2,3], *Mark McCoy[1], *Jürgen Steinbacher[4], Alexander Kunz[1,3], Jürgen Bergmann[1,2], Martin Kronbichler[2,5], Eugen Trinka[1,2,3]

*contributed equally

[1]Department of Neurology, Neurological Intensive Care and Neurorehabilitation, Christian Doppler Medical Centre, Paracelsus Medical University, Salzburg, Austria
[2]MRI Research Unit, Neuroscience Institute, Christian Doppler Medical Centre, Paracelsus Medical University, Salzburg, Austria
[3]Karl Landsteiner Institute of Neurorehabilitation and Space Neurology, Salzburg, Austria
[4]Department of Neuroradiology, Christian Doppler Medical Centre, Paracelsus Medical University Salzburg, Austria
[5]Centre for Cognitive Neuroscience and Department of Psychology, University of Salzburg, Salzburg, Austria

Background. The Locked-in Syndrome (LiS) is one of the severest neurological conditions, classically defined as a loss of all voluntary muscle movements except vertical eye movements and blinking motions combined with preserved cognitive abilities [1]. Most cases are caused by the thrombosis of the basilar artery which results in the infarction of the ventral pons [2]. Nevertheless, there are patients whose symptoms go beyond the ones described and involve a dysfunction in consciousness and other cognitive abilities. These patients suffer from the Locked-in Plus Syndrome (LIPS).

Hypothesis. The main objective of this study was to explore differences between LiS patients with and without impairments of consciousness, focusing on the lesion patterns. We hypothesized that more severely affected patients tend to have lesions that extend further rostral from the pons into the mesencephalon and the thalamus or further dorsal involving the ascending reticular activating system (ARAS).

Methods. Nine LiS patients were retrospectively identified at the Department of Neurology at the Christian Doppler Medical Centre, Salzburg, Austria and assigned to three groups (no major cognitive impairment, disturbances in cognition or consciousness and no consciousness detectable) according to clinical parameters and medical reports like the Coma Recovery Scale-Revised [3]. MRI scans were segmented semiautomatically using the grow from seeds algorithm of 3D Slicer software package in order to identify the lesions and calculate different 2D and 3D shape features [4-6]. With the help of these parameters, differences between the three groups were determined.

Results. Of the nine LiS patients involved, two had no major cognitive impairment, six showed disturbances and one displayed no signs of consciousness at all. A Kruskal-Wallis test including exact methods due to the very small sample size was conducted to examine the differences between the three groups according to the lesional parameters. Significant differences ($H(2)=4.82$, $p=.048$) between the groups were found concerning the elongation of the lesions (see Figure 1 and 2) which describes the relation of the main axis to the smallest axis or in other words how oblong the lesion is.

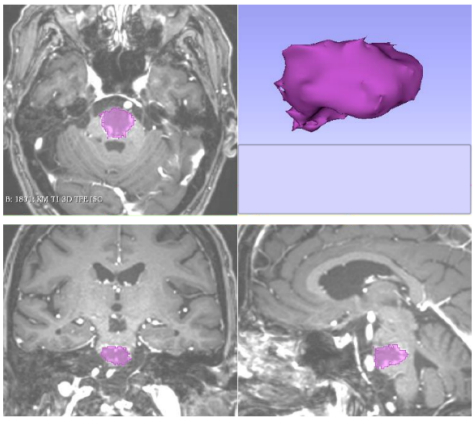

Figure 1. Lesion of a LiS patient

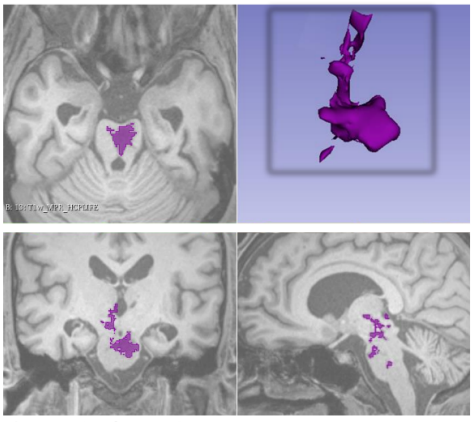

Figure 2. Lesion of a LIPS patient

Conclusion. Our results show that LiS and LIPS are caused by different lesions. Lesions of LiS patients are round and confined to the pons, whereas lesions of LIPS patients are more elongated and reach other neighbouring areas. The occlusion of the paramedian arteries which originate shortly after the bifurcation of the basilar artery (top of the basilar syndrome) result in lesions of the medial and intralaminar thalamic nuclei which play an important role for consciousness and other cognitive functions [7]. Another structure that could be involved is the ARAS, situated in the dorsal brainstem and important for arousal and therefore consciousness [8]. Our findings are in line with other studies which showed cognitive impairments in LiS patients who had lesions that expanded beyond the pons [9,10]. However, as our study sample is very small, more studies are needed to confirm our findings. The differentiation of LiS and LIPS patients is important as the patients need completely different therapies and care. Moreover, LIPS should not be confused with disorders of consciousness like the unresponsive wakefulness syndrome as the pathophysiology and therefore possible future therapeutic approaches differ.

Laura Schnetzer has received the Paracelsus Medical University Research and Innovation Fund – PhD Researcher Excellence, grant agreement number 2021-PRE-001-Schnetzer

1. Plum F and Posner J B, Contemp Neurol Ser, 1972. 2. Patterson J R and Grabois M, Stroke, 1986. 3. Giacino J T et al., Arch Phys Med Rehabil, 2004. 4. Slicer Community, https://www.slicer.org, accessed 2022. 5. Fedorov A et al., Magn Reson Imaging, 2012. 6. van Griethuysen JJM et al., Cancer Res, 2017. 7. Carvalho V and Cruz V T, Porto Biomed J, 2020. 8. Moruzzi G and Magoun H W, Electroencephalogr Clin Neurophysiol, 1949. 9. Kumral E et al., Acta Neurol Belg, 2021. 10. Schnakers C et al., J Neurol, 2008.

Motor Imagery in Disorders of Consciousness using fMRI

Laura Schnetzer[1, 2, 3], Verena Schätzle[2, 4], Martin Kronbichler[2, 4], Jürgen Bergmann[1, 2], Eugen Trinka[1, 2, 3]

[1]Department of Neurology, Neurological Intensive Care and Neurorehabilitation, Christian Doppler Medical Centre, Paracelsus Medical University, Salzburg, Austria; [2]MRI Research Unit, Neuroscience Institute, Christian Doppler Medical Centre, Paracelsus Medical University, Salzburg, Austria; [3]Karl Landsteiner Institute of Neurorehabilitation and Space Neurology, Salzburg, Austria; [4]Centre for Cognitive Neuroscience and Department of Psychology, University of Salzburg, Salzburg, Austria; Contact: laura.schnetzer@stud.pmu.ac.at

Objective

Due to complicating environmental and patient-related factors, diagnoses in patients with disorders of consciousness (DOC) are prone to misdiagnosis, especially, if examiners solely rely on clinical bedside testing. Thus, research has sought additional approaches to make diagnosis of DOC more reliable. One such approach is functional Magnetic Resonance Imaging (fMRI). The main objective of this study was to investigate the response rates of patients with DOC in fMRI. Possible inconsistencies in the assessment of behavioural and neuronal correlates of consciousness should be uncovered. Furthermore, the study aimed to determine the indication, reliability and practical utility of fMRI for identifying preserved consciousness in patients with DOC and its use to improve the diagnostic process.

Methods

In line with the approach of Monti et al. (2010) [1], 71 patients with DOC (34 with Unresponsive Wakefulness Syndrome (UWS), 33 in Minimally Conscious State (MCS), 4 recovered according to the Coma Recovery Scale-Revised (CRS-R)) and 27 healthy controls performed a motor imagery task while being scanned with fMRI technique at the Christian Doppler Medical Centre in Salzburg, Austria. Blood-oxygen-level-dependent responses in the supplementary motor area (SMA) were then investigated in a region of interest (ROI) analysis and results were associated with various clinical parameters.

Results

Significant activations in the SMA during the motor imagery task were found in 9 of 71 patients with DOC (12.7%; e.g., Figure 1) compared to 25 of 27 controls (92%; e.g., Figure 2). Of the 9 patients who neuronally responded to the motor imagery task, 3 had been clinically classified as recovered, 5 as MCS and 1 as UWS. All 9 patients who showed significant activations in the SMA had a non-traumatic brain injury.

Conclusions

This study includes one of the largest samples to date of patients with DOC who have been assessed by fMRI for their neuronal responses in a command-following task. The high response rate of our control group showed the reliability of the procedure. The proportion of patients who were able to follow the commands were similar to the proportion reported by Monti et al. (2010). Nevertheless, in contrast to their findings, all our patients who showed significant activations in the SMA had a non-traumatic brain injury and most of them were clinically classified with a higher level of consciousness (i.e. MCS or recovered). However, the patient who was clinically diagnosed with UWS and responded with significant activations in the SMA, demonstrates the need for fMRI as an additional diagnostic tool in everyday clinical practice in order to perform more reliable differential diagnostics and find patients whose conscious perception would be missed at the bedside.

Acknowledgements

Laura Schnetzer has received the Paracelsus Medical University Research and Innovation Fund – PhD Researcher Excellence, grant agreement number 2021-PRE-001-Schnetzer

References

1. Monti M M et al. New England journal of medicine, 2010

Abstract ID: 316

PAIN PHENOMENON LIPOEDEMA

Nadine Schuessler, Johanna Dellinger, Nadja Nestler,
Institute of Nursing Science and Practice, Paracelsus Medical University Salzburg, Austria

Background

Little is known about lipoedema and its long-term effects[1]. Epidemiologic data are scarce and estimates range from 1 in 72,000 in the United Kingdom[2] to 11% in post-pubertal women and girls in Germany[3]. To date, no therapy has been described that eliminates the cause of the disease, but liposuction may reduce symptoms and improve functioning and mobility[1, 4].

The accumulation of adipose tissue results in symmetrical swellings just above the ankles or wrists (cuff marks), which are characteristic of lipoedema. Although the name suggests swelling caused by body water, the deformity is actually caused by fat cells. Initial onset and exacerbation of symptoms are associated with hormonal changes such as puberty, pregnancy or menopause, although hormonal causes have not yet been proven[1].

Some characteristic symptoms of lipoedema [1, 3, 4]

- nodules to swellings
- uneven skin as well as dimples,
- formation of skin flaps mostly on the lower, less frequently on the upper extremities,
- localized pain,
- tenderness,
- bruising, often without cause.

Research question and objectives

The painful nature of lipoedema and the often prolonged periods of pain place high demands on patient self-management. To obtain an overview of pain patterns and pain-related problems, self-management needs in dealing with pain and other symptoms, a narrative literature review was conducted.

Methods

A five-step process was developed for this review, which is summarized in Table 1 on the right. All types of English- and German-language publications that addressed lipoedema as a main topic or therapeutic strategies for it were included. The search took place from January to April 2021.

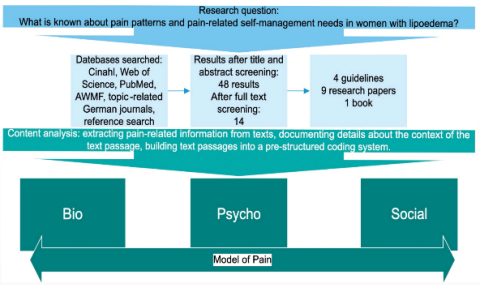

Results from the category "biological"[5]

Primary pain phenomena are localized pain, tenderness, painful tightness and pain from touch and pressure during activities in the swollen areas. Heaviness and pain from even light touch are described[1].

Secondary pain phenomena occur as:

- Joint pain (mostly knee and hip),
- back pain
- pain due to restricted movement and sparing behavior

Results from category "psycho"[5]

There are reports of a high proportion of lipoedema patients also suffering from depression, low self-esteem, self-harming behaviour and eating disorders. Similar to chronic pain, psychological disorders can exacerbate the negative effects of lipoedema.

Results from category "social"[5]

Those affected experience stigmatisation due to the publicly noticeable physical change, which is often mistaken for being overweight. Equally public are failed attempts to lose weight, which in patients with lipoedema has little effect on the deformity of the legs.

Family relationships are described ambivalently: Women of previous generations may also be affected and convey enduring this inheritance as the only solution strategy.

Conclusions

Pain treatment strategies for lipoedema patients must especially take into account the psycho-social concomitants and/or burden and address the interaction between pain, chronification processes, social life and improved well-being. So far, only few offers are available for this in the German-speaking countries. Lipoedema patients can receive support with nutrition and exercise and get information about therapy options. Structured inclusion of pain management, such as raising awareness of the risk of developing chronic pain, should be developed based on patients' needs and investigated for its effectiveness.

This review formed the theoretical basis for an interview study conducted with lipoedema patients in Austria. Based on the literature, a knowledge gap regarding the frequency of pain syndromes and chronic pain was revealed in the patient group. The results also show how important early psychological therapy is for lipoedema patients.

References

1) Wounds UK. (2017). Best Practice Guidelines The management of lipoedema. Wounds UK. download from: www.wounds-uk.com
2) Child, A. H., Gordon, K. D., Sharpe, P., Brice, G., Ostergaard, P., Jeffery, S., & Mortimer, P. S. (2010). Lipedema: An inherited condition. *American Journal of Medical Genetics Part A*, *152A*(4), 970–976. https://doi.org/10.1002/ajmg.a.33313
3) Bertsch, T., & Erbacher, G. (2018). *Lipödem – Mythen und Fakten Teil 1*. https://doi.org/10.12687/PHLEB2411-2-2018
4) Dadras, M., Mallinger, P. J., Corterier, C. C., Theodosiadi, S., & Ghods, M. (2017). Liposuction in the Treatment of Lipedema: A Longitudinal Study. *Archives of Plastic Surgery*, *44*(4), 324–331. https://doi.org/10.5999/aps.2017.44.4.324
5) The complete list of findings can be requested from the first author

Contact: nadine.schuessler@pmu.ac.at

PAIN PHENOMENON LIPOEDEMA

Nadine Schuessler[1], Johanna Delinger[1], Nadja Nestler[1]

[1]Institute of Nursing Science and Practice, Paracelsus Medical University Salzburg; Contact: nadine.schuessler@pmu.ac.at

Objective
Lipoedema is a little-known condition that is often misdiagnosed (1, 3). Lipoedema presents with nodular to swollen areas that can lead to induration, nodular, uneven skin, as well as dimpling and skin flap formation, most commonly on the lower extremities, more rarely on the upper extremities. The accumulation of adipose tissue results in characteristic symmetrical swelling of the extremities, ending above the ankles or wrists (cuff-sign)(1). Primary pain phenomena include localized pain, tenderness, painful tightness, and pain on touch and pressure during activities (1-3)
To get an insight in necessary self-management of pain and symptoms, a narrative review was conducted to identify requirement of self-management for coping with phenomena of pain in lipoedema and associated comorbidities.

Methods
The narrative literature review includes international medical and guideline databases, as well as social media reports from affected persons. Analysis was performed using the content analysis method. Requirements of self-management, coping behaviour as well as individual case descriptions were searched.

Results
48 publications were identified. Guidelines and publications on guidelines accounted for a large proportion. Presentation of results outlines the range of requirements to manage pain with a bio-psycho-social pattern in the synthesis. Limiting spontaneous and pressure pain and secondary pain phenomena such as joint pain and mobility limitations are described. The prevention of chronification of pain in association with lipoedema has not yet been a direct aim in the therapeutic strategy.

Conclusions
Pain treatment strategies for lipoedema patients must especially take into account the psycho-social concomitants and/or burden and address the interaction between pain, chronification processes, social life and improved well-being. So far, only few offers are available for this in the German-speaking countries. Lipoedema patients can receive support with nutrition and exercise and get information about therapy options. Structured inclusion of pain management, such as raising awareness of the risk of developing chronic pain, should be developed based on patients' needs and investigated for its effectiveness.
This review formed the theoretical basis for an interview study conducted with lipoedema patients in Austria. Based on the literature, a knowledge gap regarding the frequency of pain syndromes and chronic pain was revealed in the patient group. The results also show how important early psychological therapy is for lipoedema patients.

References
1. Wounds UK. (2017). Best Practice Guidelines The management of lipoedema. Wounds UK. download from: www.wounds-uk.com
2. Child, A. H., Gordon, K. D., Sharpe, P., Brice, G., Ostergaard, P., Jeffery, S., & Mortimer, P. S. (2010). Lipedema: An inherited condition. American Journal of Medical Genetics Part A, 152A(4), 970–976. https://doi.org/10.1002/ajmg.a.33313
3. Bertsch, T., & Erbacher, G. (2018). Lipödem – Mythen und Fakten Teil 1. https://doi.org/10.12687/PHLEB2411-2-2018

ANTIMICROBIAL AND WOUND HEALING CAPACITIES OF BARK EXTRACTS

Anja Schuster [1], Stefanie Emrich[1], Thomas Schnabel[2,3] and Gertie J. Oostingh[1],

[1] Department of Biomedical Sciences, Salzburg University of Applied Sciences, Puch/Salzburg, Austria
[2] Salzburg University of Applied Science, Department of Forest Products Technology & Timber Constructions
[3] Transilvania University of Brasov, Faculty of Furniture Design and Wood Engineering, Brasov, Romania

INTRODUCTION

The contents of several wood species are known to harbor antimicrobial[1], antiviral[2], anti-inflammatory[3] and wound healing[4] capacities. The aim of this work was, to identify beneficial properties of Austrian larch, birch and beech bark extracts for their potential usage as additives or active ingredients for dermatological applications.

Anti-microbial activity of wood bark extracts

Agar diffusion and broth growth tests were used to study the anti-microbial activity of wood extracts. All tested Gram-positive strains, including MRSA, *C. acnes* and *S. epidermidis,* were susceptible to birch and beech extracts, whereas gram negative *E. coli,* was resistant. Inhibition zones are displayed in Table 1. Results were confirmed using a broth growth test.

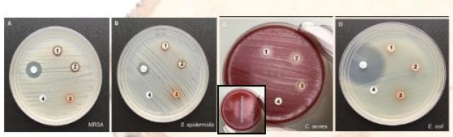

Agar Diffusion Tests. A: MRSA with Vancomycin as positive control, B: S. epidermidis with Penicillin as positive control, C: C. acnes with Benzylpenicillin E-test on extra plate (insert), D: E. coli with Ciprofloxacin as positive control on agar plate. 1 = Birch Extract, 2 = Beech Extract, 3 = Larch Extract, 4 = H_2O (extract solvent/ negative control).

Bacterial strain	Birch	Beech	Larch
MRSA	9.25 (****)	9.25 (****)	0 (ns)
C. acnes	9.75 (****)	10.5 (****)	7.75 (****)
S. epidermidis	7.88 (****)	7.75 (****)	0 (ns)
E. coli	0 (ns)	0 (ns)	0 (ns)

*Statistical analysis of agar diffusion test, inhibition zones are displayed in mm. **** $p < 0.0001$*

Wound-healing effect of wood bark extracts

A scratch assay was used to detect accelerated wound closure in HaCaT cell lines after treatment with wood extracts. Birch and beech extracts at a concentration of 25 µg/ml significantly accelerated the wound closure after 24 h.

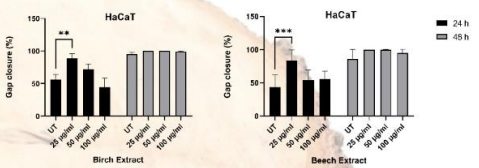

Pro-inflammatory cell signaling

IL-8 expression was measured in cell culture supernatants from native or heat inactivated *C. acnes* stimulated THP-1 and HaCaT cell lines after 24 h extract incubation. In both cell lines, a dose dependent increase in IL-8 expression was seen up to 500 µg/ml and 100 µg/ml of birch and beech extract resp. The decrease at higher extract concentrations correlates with a decreased viability.

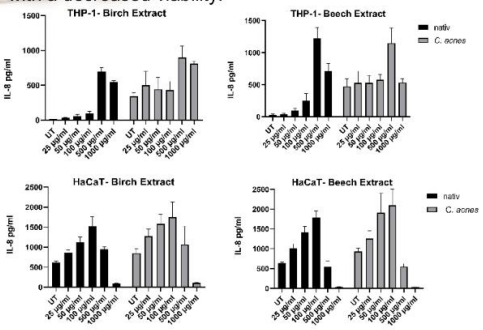

CONCLUSION & OUTLOOK

Our findings show a successful growth inhibition with birch and beech bark extracts of Gram-positive bacteria, involved in skin diseases, like acne. Wound closing using an *in-vitro* scratch assay was shown to be faster with low concentrations of birch and beech extract treatments compared to controls. Whereas beneficial properties of birch components are described in the literature, the very similar effects of beech contents are new. Their combined positive effect in wound-healing and antimicrobial activity has great potential for treatment of various skin diseases. In addition, the use of biomolecules in form of an extract from wood bark, which is often considered as waste or by-product during a variety of industrial processes, enables a sustainable use of natural and renewable products.

[1] Schuster et al., BioResources 2020/ [2] Tienaho et al. Front Bioeng Biotechnol. 2021/ [3] Tuli et al. plants 2021/ [4] Ebeling et al. PLoS One 2014

ANTIMICROBIAL AND WOUND HEALING CAPACITIES OF BARK EXTRACTS

Anja Schuster[1], Stefanie Emrich[1], Thomas Schnabel[2,3], Geja Oostingh[1]

[1]Salzburg University of Applied Science, Biomedical Science,Urstein Süd 1, 5412 Puch/Salzburg, Austria; [2]Salzburg University of Applied Science, Department of Forest Products Technology & Timber Constructions, Markt 136a, 5431 Kuchl, Austria; [3]Transilvania University of Brasov, Faculty of Furniture Design and Wood Engineering, B-dul. Eroilor nr. 29, 500036 Brasov, Romania; Contact: anja.schuster@fh-salzburg.ac.at

Objective
The contents of several wood species are known to harbor antimicrobial (1), antiviral (2), anti-inflammatory (3) and wound healing (4) capacities. The aim of this work was to identify beneficial properties of larch, birch and beech bark extracts in terms of antimicrobial activity and wound-healing capacity as well as immune-modulating properties for the use of these wood extracts as additives or active ingredient for dermatological applications in cosmetics and medicine.

Methods
Anti-bacterial activity was measured using bacterial agar diffusion assay and resazurin-based broth microdilution assay. Test microorganisms included *Cutibacterium acnes*, *Staphylococcus epidermidis*, *MRSA-Staphylococcus aureus subsp. aureus Rosenbach* and *Escherichia coli*. To gain more insight in cellular response to wood extracts, resazurin based viability tests, scratch-assays using cell-free gap from Ibidi and ELISAs for pro-inflammatory protein expression including IL-8 and IL-1β were performed.

Results
Birch and Beech extracts showed strong antimicrobial activities against gram positive bacteria, including *C. acnes*, *S. epidermidis* and *MRSA*. Gram negative bacteria were not inhibited. Wound closure was enhanced at 24h with birch and beech extracts at a concentration of 25 µg/ml compared to controls in the scratch-assays. A dose dependent increase in IL-8 expression was seen after 24h birch and beech exposure in THP-1 and HaCaT cell lines.

Conclusions
Our findings show a successful growth inhibition with birch and beech bark extracts of gram-positive bacteria, involved in skin diseases. The combined positive effect in wound-healing and antimicrobial activity has great potential for treatment of various skin diseases, including acne in future dermal applications. In addition, the use of biomolecules in form of an extract from wood bark, which is often considered as waste or by-product during a variety of industrial processes, enables a sustainable use of natural and renewable products.

References
1. Schuster et al. (2020). Compounds extracted from Larch, Birch bark, Douglas Fir, and Alder Woods with four different solvents: effects on five skin-related microbes. In: BioResources 15: 3368-3381. DOI: 10.15376/biores.15.2.3368-3381
2. Tienaho et al. (2021). Salix spp. Bark Hot Water Extracts Show Antiviral, Antibacterial, and Antioxidant Activities—The Bioactive Properties of 16 Clones In: Front Bioeng Biotechnol. 9: 797939.DOI: 10.3389/fbioe.2021.797939
3. Tuli et al. (2021). Anti-Inflammatory and Anticancer Properties of Birch Bark-Derived Betulin: Recent Developments In: plants 10(12), 2663. DOI: https://doi.org/10.3390/plants10122663
4. Ebeling et al. (2014) From a Traditional Medicinal Plant to a Rational Drug: Understanding the Clinically Proven Wound Healing Efficacy of Birch Bark Extract. PLoS ONE 9(1): e86147. DOI: https://doi.org/10.1371/journal.pone.0086147PLoS One 2014

CAMPUS Pflegewissen | digital | kompakt

Annemarie Strobl[1], Beate Brandauer-Stickler[1], Daniel Braun[2], Patrizia Ebner[1], Jessica Grausgruber[2], Daniel Hausmann[1], Tabea Klausner[1], Alexander Kraus[1], Verena Leinemann[1], Patrick Mülleder[1], Anita Ruf[1], Christine Salzgeber[2], Markus Schwarz[2], Klaus Seidl[1], Johannes Wallner[2], Jürgen Osterbrink[1]

[1]Institut für Pflegewissenschaft und -praxis, Paracelsus Medizinische Privatuniversität, Strubergasse 21, 5020 Salzburg, Österreich; [2]SeneCura Gruppe, Lassallestraße 7a Unit 4, Top 8, 1020 Wien, Österreich; [3]Senevita Gruppe, Worbstrasse 46, CH-3074 Muri b. Bern, Schweiz
Kontakt: annemarie.strobl@pmu.ac.at

ZIELE

Pflegerelevante Wissensbestände nehmen rasant zu und auch Versorgungsstrukturen verändern sich ständig, z.B. Polymorbidität, Einbindung betagter Menschen in die Gesellschaft der Zukunft. Dies erfordert innovative Bildungsmöglichkeiten, damit Pflegekräfte den Anforderungen gerecht werden können. Das Institut für Pflegewissenschaft und -praxis arbeitet daher bereits seit Jahren mit der SeneCura Gruppe und nun auch mit der Senevita Gruppe zusammen. Drei weitere Kooperationen sind in Planung. Das gemeinsame Ziel: Entwicklung von maßgeschneiderten Lernplattformen zur Fort- und Weiterbildung in der Langzeitpflege. Diese Lernplattformen werden »Campus« genannt.

METHODEN

Aufbau und Weiterentwicklung von Campus:

- Installation einer auf das Unternehmen angepassten Lernplattform; Koppelung von Managementsystemen
- Systematische Aufbereitung der Lerninhalte ist orientiert an Leitlinien, gesetzlichen Grundlagen, aktuellen Erkenntnissen aus der Versorgungsforschung und Unternehmensstandards
- Durchführung einer Pilotphase und Roll-out mit standardisierter Datenerhebung zu Usability und inhaltlicher Evaluierung

SCHLUSSFOLGERUNG

Campus bietet maßgeschneiderte, wissenschaftlich fundierte, innovative Bildungsangebote, die sich an den Bedarfen und Bedürfnissen der Kooperationspartner und seinen Mitarbeitenden orientieren. Nach Aktualisierung von bestehenden Lerninhalten und Neuentwicklung von Lernkursen folgen Evaluationsphasen und pflegewissenschaftliche Begleitforschung, um die Versorgungsqualität und lebenslanges Lernen positiv zu beeinflussen.

ERGEBNISSE

Lernen mit Smartphone, Tablet, PC oder Laptop – zu jeder Zeit, an jedem Ort

8000 Nutzer*innen, 27 000 Kursabschlüsse, 30 Lernkurse

Inhalte aktuell in vier Sprachen – drei weitere in Planung

Zum Kursabschluss wird ein personalisiertes Zertifikat verliehen

Im Bachelor *Pflegewissenschaft Online* ist Verkürzung der Studiendauer durch Anrechnungsverfahren möglich

Campus – Pflegewissen von heute für morgen: digital und kompakt

Annemarie Strobl[1], Beate Brandauer-Stickler[1], Daniel Braun[3], Patrizia Ebner[1], Jessica Grausgruber[2], Daniel Hausmann[1], Tabea Klausner[1], Alexander Kraus[1], Verena Leinemann[1], Patrick Mülleder[1], Anita Ruf[3], Christine Salzgeber[3], Markus Schwarz[2], Klaus Seidl[1], Johannes Wallner[2], Jürgen Osterbrink[1]

[1]Institut für Pflegewissenschaft und -praxis, Paracelsus Medizinische Privatuniversität, Strubergasse 21, 5020 Salzburg, Österreich; [2]SeneCura Gruppe, Lassallestraße 7a Unit 4, Top 8, 1020 Wien, Österreich; [3]Senevita Gruppe, Worbstraße 46, 3074 Muri b. Bern, Schweiz; Contact: annemarie.strobl@pmu.ac.at

Objective
Pflegerelevante Wissensbestände nehmen rasant zu und auch Versorgungsstrukturen verändern sich ständig, z.B. Polymorbidität, Einbindung betagter Menschen in die Gesellschaft der Zukunft. Dies erfordert innovative Bildungsmöglichkeiten, damit Pflegekräfte den Anforderungen gerecht werden können. Das Institut für Pflegewissenschaft und -praxis arbeitet daher bereits seit Jahren mit der SeneCura Gruppe und nun auch mit der Senevita Gruppe zusammen. Drei weitere Kooperationen sind in Planung. Das gemeinsame Ziel: Entwicklung von maßgeschneiderten Lernplattformen zur Fort- und Weiterbildung in der Langzeitpflege. Diese online Lernplattformen werden ‚Campus' genannt.

Methods
Aufbau und Weiterentwicklung von Campus:
· Installation einer auf das Unternehmen angepassten Lernplattform; Koppelung von Managementsystemen
· Systematische Aufbereitung der Lerninhalte ist orientiert an Leitlinien, gesetzlichen Grundlagen, aktuellen Erkenntnissen aus der Versorgungsforschung und Unternehmensstandards
· Durchführung einer Pilotphase und Roll-out mit standardisierter Datenerhebung zu Usability und inhaltlicher Evaluierung

Results
Lerninhalte in Campus ermöglichen ein zeit- und ortsungebundenes Lernen via Smartphone, Tablet, PC und Laptop für über 8.000 User*innen und können mit Workshops oder Praxistrainings kombiniert werden. Die Inhalte werden aktuell in vier Sprachen (an Länderspezifika angepasst) veröffentlicht und stehen als interaktive Lernobjekte mit Bild-, Ton-, Text- und Quizsequenzen zur Verfügung. Drei weitere Sprachen sind in Planung. Nach erfolgreicher Absolvierung einer Lernerfolgskontrolle erhalten die User*innen ein personalisiertes Zertifikat. Ca. 27.000 Kursabschlüsse von über 30 Lernkursen wurden bereits verzeichnet. Die onlinebasierten Angebote sind für Pflegekräfte verschiedener beruflicher Qualifikationen abrufbar. Eine Verkürzung der Studiendauer im Bachelorstudiengang Pflegewissenschaft Online am Institut für Pflegewissenschaft und -praxis ist durch ein individuelles Anrechnungsverfahren beruflicher Kompetenzen kombiniert mit Campus möglich.

Conclusions
Campus bietet maßgeschneiderte, wissenschaftlich fundierte, innovative Bildungsangebote, die sich an den Bedarfen und Bedürfnissen der Kooperationspartner und seinen Mitarbeitenden orientieren. Nach Aktualisierung von bestehenden Lerninhalten und Neuentwicklung von Lernkursen folgen Evaluationsphasen und pflegewissenschaftliche Begleitforschung, um die Versorgungsqualität und lebenslanges Lernen positiv zu beeinflussen.

PARACELSUS MEDIZINISCHE PRIVATUNIVERSITÄT

Klinikum Nürnberg
wir sind für Sie da!

Establishment of a fetal MRI method to measure the body composition for the assessment of fetal fat mass and fat-free mass trajectories

David Surmann[1], Niels Rochow[1], Michael Noseworthy[2], Bryon DeFrance[3], Christoph Fusch[1]

[1]Department of Pediatrics, Paracelsus Medical University, Nuremberg;
[2]Department of Pediatrics, [3]Department of Obstetrics and Gynecology, McMaster University, Hamilton

INTRODUCTION

- It is recommended that preterm infants should develop like their healthy fetal counterparts which stay in utero until term age.
- To optimize nutrition, growth references for body composition of healthy fetuses would be needed.
- Available references for body composition (BC) are based on deceased newborns and may not reflect physiological growth.
- Postnatal growth charts based on preterms are no physiological reference.
- A non-invasive method to measure fetal body composition could be fetal MRI (fetMRI). Measurement of the body composition by MRI has been established for adults.
- The aim of this study is to develop a method to measure fetal body composition with MRI.

OBJECTIVES

- To review literature for potential side effects of fetal MRI.
- To validate fetMRI as a method of acquiring body composition in utero.

METHODS

- This validation study measured body composition in 10 subjects scheduled for c-section during the 37 to 40 week of gestation. Data was acquired with 1.5T Siemens Symphony Tim MRI device at McMaster University, Hamilton, Canada.
- FetMRI was performed up to 3 days prior to birth. Up to 3 days postnatally, a full body MRI (pMRI) scan as well as air displacement plethysmography (Peapod) was conducted on the newborn.
- Dixon water suppressed sequences were segmented using 3D Slicer (v4.11) with semi-automatic package 'grow from seeds'.
- Two methods, i) phantom reference approach and ii) subcutan fat referenced (SCF) were used to assess the fat mass.
- i) A calibration phantom (Fig. 3) was developed with 0, 10, 20, 30, 40, 50 and 100% oil dissolved in sodium lauryl sulfate for MRI reference.
- Ii) The intensity of known reference tissue was analyzed: subcutaneous fat and amniotic fluid (fetMRI) and subcutaneous fat and the bladder of the newborn (pMRI)
- Most abundant intensity of subcutaneous fat was set to 100% fat and amniotic fluid / bladder to 0% fat.
- Regression equations for relation between voxel intensity and percent fat mass (FM%) and volume were used to calculate BC.

RESULTS

Literature review:

- We didn't identify studies which could show any harmful long-term effects on the human fetus related to the static magnetic field, pulsed radio frequency or time-varying magnetic gradient fields exposure (N= 1 review, 14 papers).
- Vena cava syndrome is a non-specific complication for MRI that should always be considered in longer examinations. This complication can be prevented by laying the pregnant woman into a left lateral side position.

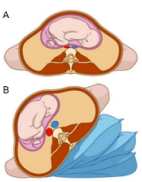

Fig. 1: Vena cava and aorta compression by the fetus (A) and reliefed by tilting (B).

RESULTS

Phantom and development of regression analysis:

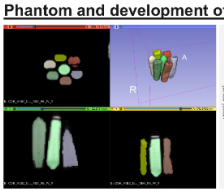

Fig. 2: Screenshot of calibration phantom

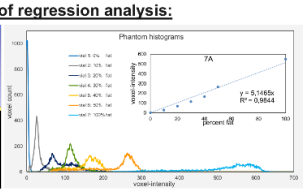

Fig. 3: Histograms gained from phantom segmentation

- N=10 newborns with gestational age 38 ± 2 weeks and birth weight of 3553 ± 360g.
- Repeatability of volume measurement was tested with 10 consecutive measurements of the same baby.

Birth weight estimations:

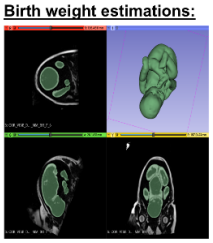

Fig. 4: Segmentation of baby (volume/ histogram)

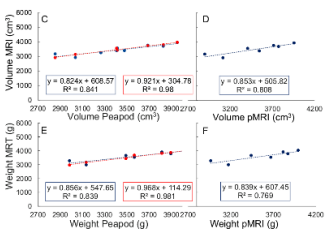

Fig. 5: Blue: fetMRI, red: pMRI, C&E Volume and weight correlation to Peapod, D&F correlation between pMRI & fetMRI

- Weight was calculated through the two compartments with it's specific densities of 0.9007 g/cm3 (fat) and 1.064 g/cm3 (fat free mass).
- Body weight was estimated using fetMRI and highly correlates with the birth weight R2= 0.9.

Evaluation of body composition:

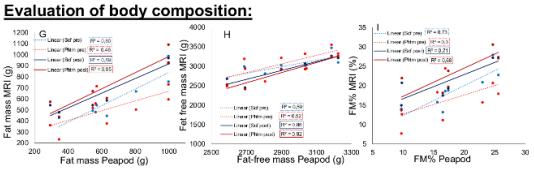

Fig. 6: Blue: SCF, red: Phantom, G: the absolute fat contant, H: absolute fat-free mass, I: FM%

- Average deviation of FM% between fetMRI and Peapod was 2%.
- Phantom fetMRI and Peapod as well as pMRI and Peapod correlate with R2 of 0.3 and 0.68, respectively.
- Subcutan fat referenced (SCF) fetMRI and Peapod correlate as well as SCF pMRI and Peapod with R^2 of 0,73 and 0,71, respectively.

CONCLUSION

- Literature review showed that fetal MRI seems to be save for the human fetus.
- Fetal MRI could be used to assess fetal volume, weight and BC.
- In the future, fetal MRI will be employed to a longitudinal study during pregnancy to establish reference data for fetal body composition.

Christoph Fusch, MD, PhD, Pediatrics, Paracelsus Medical University, christoph.fusch@klinikum-nuernberg.de

Establishment of a fetal MRI method to measure the body composition for the development of fetal fat mass and fat-free mass trajectories

David Surmann[1], Niels Rochow[1], Michael Noseworthy[2], Bryon DeFrance[3], Christoph Fusch[1]

[1]Department of Pediatrics, Paracelsus Medical University, Nuremberg, Germany; [2]Department of Pediatrics, McMaster University, Hamilton, Canada; [3]Department of Obstetrics and Gynecology, McMaster University, Hamilton, Canada; Contact: david.surmann11@googelmail.com

Objective
To understand growth of fetal body composition (BC) during pregnancy, BC ideally shall be longitudinally measured in healthy pregnancies delivering at term. Method of choice will be MRI: it allows non-invasive and direct full body quantitation of compartments (fetMRI). In contrast, serial ultrasound relies on one- or two-dimensional measurements (i.e. assessing bone length, circumferences of body parts or areas) followed by transforming these data into compartment volumes by means of multilinear regression with obviously inbuilt limitations and drawbacks.
MRI body composition has been established for adults. It is the aim of the current study to assess fetal body composition using two approaches for calibration of fat mass. Results of pre- and postnatal measurements are compared also against a second independent method, air displacement plethysmography (ADP). The second aim was to review risk factors of fetMRI to compromise maternal or fetal well being.

Methods
Comparison of fetal and postnatal BC in 9 subjects scheduled for C-section at term. FetMRI scan was performed up to 2 days prior to birth. Up to 3 days postnatally, BC was measured using a full body MRI scan (pMRI; 1.5T Symphony Tim, Siemens; segmentation of Dixon water suppressed sequences using 3D Slicer (v4.11), semi-automatic package 'grow from seeds'). BC was measured using a second, independent method (ADP, PeaPod, Cosmed, Concord,US)).For MRI absolute quantitation was done using (i) a calibration phantom (Fig. 3) with 0, 10, 20, 30, 40, 50 and 100% oil dissolved in sodium lauryl sulfate and (ii) by using subcutaneous fat tissue, urine and amnion fluid as internal reference for 0 and 100% fat calibration points. For (i) regression equations of voxel intensity and %fat were used to calculate BC.

Results
Literature review did not identify studies proving harmful long-term effects on human fetuses related to static magnetic fields, pulsed RF or time-varying magnetic gradient fields exposure (N= 1 review, 14 papers). For positioning of pregnant subjects, a vena cava syndrome should always be avoided by choosing a left lateral side position. In total, 9 infants were analyzed. The soft tissue approach was outperforming the phantom approach when fetal MRI was compared with the peapod. Postnal MRI and peapod were highly correlated (Fig. 6).

Conclusions
The literature review showed fetal MRI seems to be save for a human fetus. Further, our validation study shows that fetal MRI might be used to assess fetal BC. However, there are several options (voxel size, slice thickness, use of similar coils, intensity inhomogeneity correction, position of phantom, short interval between fetal MRI and PeaPod, phantom in size and position in the MRI field) that might to be optimized to improve the measurements. A standard protocol for fetMRI BC should be developed. In the future, fetal MRI will be employed to a longitudinal study during pregnancy to establish reference data for fetal body composition.

Benzylated dihydrochalcones as potent multitarget inhibitors of cancer cell growth

Temml V[1], Huber-Cantonati P[2], Carre A[1], Jordan PM[3], Herzog R[3], Viault G[4] , Seraphin S[4] , Möller G[5], Mähr T[2], Schwitzer F[2], Helesbeux JJ[4], Werz O[3], Pachmayr J[2], Schuster D[1]

[1]Institute of Pharmacy/Pharmaceutical and Medicinal Chemistry, Paracelsus Medical University, Salzburg;
[2]Institute of Pharmacy/Pharmaceutical Biology and Clinical Pharmacy, Paracelsus Medical University, Salzburg;
[3]Department of Pharmaceutical/Medicinal Chemistry, Institute of Pharmacy, Friedrich Schiller University Jena, Jena, Germany.
[4]Univ Angers, SONAS, SFR4207 QUASAV, Angers, France
[5]Institute of Cancer and Diabetes , Helmholtz Zentrum München, Neuherberg, Germany

Introduction

Dihydrochalcones constitute a family of natural polyphenols that are well known for their anti-oxidative abilities. MF-15, a natural benzylated dihydrochalcone contained in *Melodorum fruticosum* Lour. has been found to have wide ranging polypharmacological activity (on 5- and 15-lipoxygenase (LOX), microsomal prostaglandin E2 synthase (mPGES-1), 17-β hydroxysteroid dehydrogenase (17β-HSD5)/prostaglandin F synthase (PGFS), and the androgen and glucocorticoid receptors) leading to pronounced anti-inflammatory and anti-cancer effects [1,2].
Based on this compound, a series of >80 derivatives was synthesized and investigated for their pharmacological and anti-cancer activity.

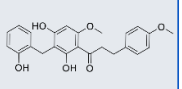

Leaves of *Melodorum fruticosum* and structure of the benzylated dihydrochalcone MF-15

Methods

Compounds were evaluated in enzymatic assays for their inhibitory activity on 17β-HSD5 [2]. Activity on lipid mediator formation was investigated in human M2 macrophages analogous to Kretzer et al [3].
Cancer cell proliferation inhibition was measured in hepatocellular carcinoma cell lines Hep3B.
Docking studies were conducted using GOLD 5.3.

Multitarget Activity of Benzylated Dihydrochalcones

Multitarget Activities of MF-15

Target	Activity
mPGES-1	IC_{50} = 1.8 µM
17β-HSD5	87% inhibition at 10 µM
5-LOX	IC_{50} = 3.4 µM
15-LOX	stimulation
Resolvins	elevated

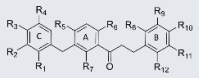

82 synthetic derivatives (C1-C82)

SAR Analysis

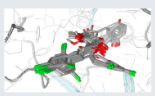

C16 in 17β-HSD5

Influence of active groups on 17β-HSD5 inhibition

Stimulation of 15-LOX Product Formation

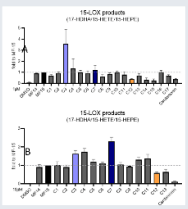

15-LOX stimulation at 10 µM (A) and 1 µM (B)

17β-HSD5 Activity and Anti-proliferative Activity of C16

91.4% inhibition of 17β-HSD5 at 10µM

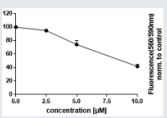

Hep3B hepatocellular carcinoma cell proliferation

Conclusion

Among the derivatives of MF-15, several showed improved pharmacological effects on different targets. C16, which displayed a stronger inhibition of 17β-HSD5 than the parent compound, also showed a more potent effect on hepatocellular carcinoma cell proliferation.
A lipid mediator profiling in human M2 macrophages displayed a strong potential for upregulating of resolvins that counteract inflammation. This effect was most enhanced by compounds C3 and C7.
Docking studies were conducted on several of the involved targets and allowed us to pin down, which modifications are associated with improved activity on a particular target and where structural optimization towards higher bioactivity and selectivity is feasible.
Benzylated dihydrochalcones are prime examples of polypharmacologically active natural product-derived compounds that would usually be disregarded for their promiscuity. However, the potent anti-cancer activities suggest that it is worthwhile to analyze their effects and to treat them as promising lead structures.

References

[1] Kafka et al Cancers 12(8):2092. doi: 10.3390/cancers12082092. .
[2] Mayr et al, International Journal of Molecular Sciences 2020, doi: 10.3390/ijms21197102
[3] Kretzer et ak, Biochemical Pharmacology 195, 114825, 2022, https://doi.org/10.1016/j.bcp.2021.114825

Acknowledgements

FWF Hertha Firnberg Project T942: New ways to counter inflammation Computer aided discovery of multi-target anti-inflammatory natural products

Contact

Veronika.Temml@pmu.ac.at

Benzylated dihydrochalcones as potent multitarget inhibitors of cancer cell growth

Veronika Temml[1], Petra Huber-Cantonati[2], Arthur Carre[1], Paul Mike Jordan[3], Rosa Herzog[3], Guillaume Viault[4], Denis Seraphin[4], Gabriele Möller[5], Theresa Mähr[2], Felix Schwitzer[2], Jean-Jacques Helesbeux[4], Oliver Werz[3], Johanna Pachmayr[2], Daniela Schuster[1]

[1]Institute of Pharmacy/Pharmaceutical and Medicinal Chemistry, Paracelsus Medical University, Salzburg; [2]Institute of Pharmacy/Pharmaceutical Biology and Clinical Pharmacy, Paracelsus Medical University, Salzburg; [3]Department of Pharmaceutical/Medicinal Chemistry, Institute of Pharmacy, Friedrich Schiller University Jena, Jena, Germany; [4]Univ Angers, SONAS, SFR4207 QUASAV, Angers, France; [5]Institute of Cancer and Diabetes , Helmholtz Zentrum München, Neuherberg, Germany; Contact: Veronika.Temml@pmu.ac.at

Objective

Dihydrochalcones constitute a family of naturalpolyphenols that are well known for their anti-oxidative abilities. MF-15, a natural benzylated dihydrochalcone contained in Melodorumfruticosum Lour. has been found to have wideranging polypharmacological activity (on 5- and15-lipoxygenase (LOX), microsomal prostaglandin E2 synthase (mPGES-1), 17-β hydroxysteroid dehydrogenase (17β-HSD5)/prostaglandin Fsynthase (PGFS), and the androgen and glucocorticoid receptors) leading to pronounced anti-inflammatory and anti-cancer effects [1,2].

Based on this compound, a series of >80derivatives was synthesized and investigated for their pharmacological and anti-cancer activity.

Methods

Compounds were evaluated in enzymatic assays for their inhibitory activity on 17β-HSD5 [2].

Activity on lipid mediator formation was investigated in human M2 macrophages analogous to Kretzer et al [3].

Cancer cell proliferation inhibition was measured in hepatocellular carcinoma cell lines Hep3B.

Docking studies were conducted using GOLD 5.3

Results

Among the derivatives of MF-15, several showed improved pharmacological effects on different targets. C16, which displayed a stronger inhibition of 17β-HSD5 than the parent compound, also showed a more potent effect on hepatocellular carcinoma cell proliferation.

A lipid mediator profiling in human M2 macrophages displayed a strong potential for upregulating of resolvins that counteract inflammation. This effect was most enhanced by compounds C3 and C7.

Docking studies were conducted onseveral of the involved targets andallowed us to pin down, which modifications are associated with improved activity on a particular target and where structural optimization towards higher bioactivity and selectivity is feasible.

Conclusions

Benzylated dihydrochalcones are prime examples of polypharmacologically activenatural product-derived compounds that would usually be disregarded for their promiscuity. However, the potent anti-cancer activities suggest that it is worthwhile to analyze their effects and to treat them as promising lead structures.

References

1. Kafka et al Cancers 12(8):2092. doi: 10.3390/cancers12082092.
2. Mayr et al, International Journal of Molecular Sciences 2020 ,doi: 10.3390/ijms21197102
3. Kretzer et ak, Biochemical Pharmacology 195, 114825, 2022, https://doi.org/10.1016/j.bcp.2021.114825

The Superficial Anastomosing Veins of the Human Brain Cortex: A Microneurosurgical Anatomical Study

SO Tomasi, GE Emmanuele Umana, G Scalia, G Raudino, F Graziano, P Palmisciano, SM Priola, PF Cappai, C Capone, PM. Lawrence, CA. Erös, KD. Martin, B Chaurasia, R Maugeri, G Iacopino, V Da Ros, MT. Lawton, CJ. Griessenauer and PA. Winkler

Introduction: In this microneurosurgical and anatomical study, we characterized the superficial anastomosing veins of the human brain cortex in human specimens.

Material and Methods: We used 21 brain preparations fixed in formalin (5%) that showed no pathological changes and came from the autopsy sections. The superficial veins were dissected out of the arachnoid with the aid of a surgical microscope.

Results: We dissected nine female and 12 male brain specimens, with an average age of 71 ± 11 years (range 51–88 years). We classified the superficial veins in five types: (I) the vein of Trolard as the dominat vein; (II) the vein of Labbé as the dominant vein; (III) a dominant sylvian vein group, and the veins of Trolard and Labbé nonexistent or only rudimentary present without contact to the Sylvian vein group; (IV) very weak sylvian veins with the veins of Trolard and Labbé codominant; and V) direct connection of Trolard and Labbé bypassing the Sylvian vein group. The vein of Trolard was dominant (Type I) in 21.4% and the vein of Labbé (Type II) in 16.7%. A dominant sylvian vein group (Type III) was found in 42.9%. Type IV and Type V were found in 14.3 and 4.7% respectively.

Conclusion: No systematic description or numerical distribution of the superior anastomotic vein (V. Trolard) and inferior anastomotic vein (V. Labbé) has been found in the existing literature. This study aimed to fill this gap in current literature and provide data to neurosurgeons for the practical planning of surgical approaches.

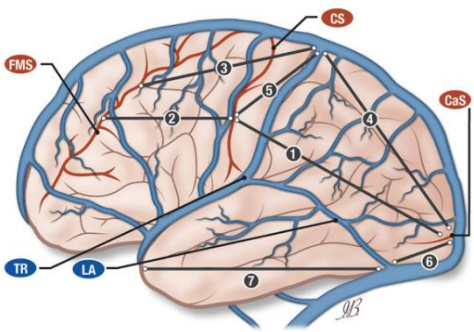

FIGURE 1 | Anatomical illustration of the vein of Trolard (TR) and vein of Labbé (LA) and their relationship with central sulcus (CS), calcarine sulcus, (CAS) and frontomarginal sulcus (FMS). The drawing is illustrating the distances between central sulcus (CS), calcarine sulcus (CAS), and frontomarginal sulcus (FMS). SSS, superior sagittal sinus; CS, central sulcus; CaS, calcarine sulcus; FMS, frontomarginal sulcus; Tr, vein of Trolard; La, vein of Labbé; DTr, distance vein of Trolard-central sulcus.

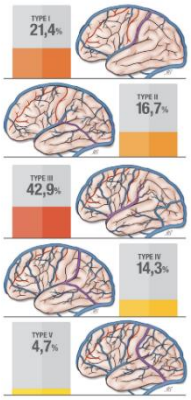

FIGURE 2 | Classification for the superficial anastomosing vein patterns (According to Erös et al.) in the current study.

The Superficial Anastomosing Veins of the Human Brain Cortex: A Microneurosurgical Anatomical Study

Santino Ottavio Tomasi[1], Giuseppe Emmanuele Umana[2], Gianluca Scalia[3], Giuseppe Raudino[4], Francesca Graziano[3], Paolo Palmisciano[2], Stefano M. Priola[5], Pier Francesco Cappai[6], Crescenyo Capone[7], Peter M. Lawrence[8], Christian A. Erös[9], Klaus D. Martin[10], Bipin Chaurasia[11], Rosario Maugeri[12], Gerardo Iacopino[12], Valerio Da Ros[11], Michael T. Lawton[8], Christoph J. Griessenauer[1], Peter A. Winkler[1]

[1]Christian Doppler Clinic, University Hospital Salzburg, Paracelsus Medical University, Salzburg, Austria; [2]Department of Neurosurgery, Cannizzaro Hospital, Catania, Italy; [3]Garibaldi Hospital, Catania, Italy; [4]Humanitas Centro Catanese di Oncologia, Catania, Italy; [5]Division of Neurosurgery Health Sciences North, Northern Ontario School of Medicine, Sudbury, ON, Canada; [6]G. Brotzu Hospital, Cagliari, Italy; [7]Department of Neurosurgery, University Hospital Zürich, Zurich, Switzerland; [8]Department of Neurosurgery, Barrow Neurological Institute (BNI), Phoenix, AZ, United States; [9]Department of Neurosurgery, Städtisches Klinikum Dresden, Dresden, Germany; [10]Neurochirurgie Dresden, Dresden, Germany; [11]Department of Neurosurgery, University of Rome Tor Vergata, Rome, Italy; [12]Department of Neurosurgery, University of Palermo, Palermo, Italy; Contact: s.tomasi@salk.at

Objective
In this microneurosurgical and anatomical study, we characterized the superficial anastomosing veins of the human brain cortex in human specimens.

Methods
We used 21 brain preparations fixed in formalin (5%) that showed no pathological changes and came from the autopsy sections. The superficial veins were dissected out of the arachnoid with the aid of a surgical microscope.

Results
We dissected nine female and 12 male brain specimens, with an average age of 71 ± 11 years (range 51–88 years). We classified the superficial veins in five types: (I) the vein of Trolard as the dominat vein; (II) the vein of Labbé as the dominant vein; (III) a dominant sylvian vein group, and the veins of Trolard and Labbé nonexistent or only rudimentary present without contact to the Sylvian vein group; (IV) very weak sylvian veins with the veins of Trolard and Labbé codominant; and V) direct connection of Trolard and Labbé bypassing the Sylvian vein group. The vein of Trolard was dominant (Type I) in 21.4% and the vein of Labbé (Type II) in 16.7%. A dominant sylvian vein group (Type III) was found in 42.9%. Type IV and Type V were found in 14.3 and 4.7% respectively.

Conclusions
No systematic description or numerical distribution of the superior anastomotic vein (V. Trolard) and inferior anastomotic vein (V. Labbé) has been found in the existing literature. This study aimed to fill this gap in current literature and provide data to neurosurgeons for the practical planning of surgical approaches.

Perforating Arteries of the Lemniscal Trigone: A Microsurgical Neuroanatomic Description

Santino Ottavio Tomasi, Giuseppe Emmanuele Umana, Gianluca Scalia, Roberto Luis Rubio-Rodriguez, Giuseppe Raudino, Julian Rechberger, Philipp Geiger, Bipin Chaurasia, Kaan Yağmurlu, Michael T. Lawton and Peter A. Winkler

Background: The perforating arteries in the dorsolateral zone of the midbrain play a crucial role in the functions of the brain stem. Their damage due to herniation, pathological lesions, or surgery, favored by the narrow tentorial incisura, can lead to hemorrhages or ischemia and subsequently to severe consequences for the patient.

Objective: In literature, not much attention has been directed to the perforating arteries in the lemniscus; in fact, no reports on the perforators of this anatomical region are available. The present study aims to a detailed analysis of the microanatomy and the clinical implications of these perforators, in relation to the parent vessels. We focused on the small vessels that penetrate the midbrain's dorsolateral surface, known as lemniscal trigone, to understand better their microanatomy and their functional importance in the clinical practice during the microsurgical approach to this area.

Methods: Eighty-seven alcohol-fixed cadaveric hemispheres (44 brains) without any pathological lesions provided the material for studying the perforating vessels and their origin around the dorsolateral midbrain using an operating microscope (OPMI 1 FC, Zeiss). Measurements of the perforators' distances, in relation to the parent vessels, were taken using a digital caliper.

Results: An origin from the SCA could be found in 70.11% (61) and from the PCA in 27.58% (24) of the hemispheres. In one hemisphere, an origin from the posterior choroidal artery was found (4.54%). No perforating branches were discovered in 8.04% of specimens (7).

Conclusion: The perforating arteries of the lemniscal trigone stem not only from the superior cerebellar artery (SCA), as described in the few studies available in literature, but also from the posterior cerebral artery (PCA). Therefore, special attention should be paid during surgery to spare those vessels and associated perforators. A comprehensive understanding of the lemniscal trigone's perforating arteries is vital to avoid infarction of the brainstem when treating midbrain tumors or vascular malformations.

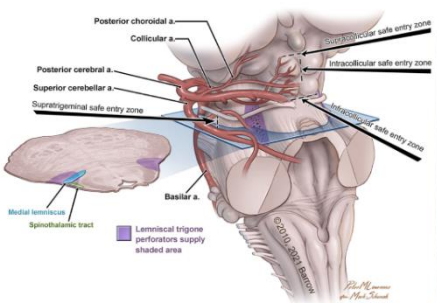

FIGURE 1 | Anatomical illustration of the lemniscal trigone zone. a., artery. Used with permission from Barrow Neurological Institute, Phoenix, Arizona.

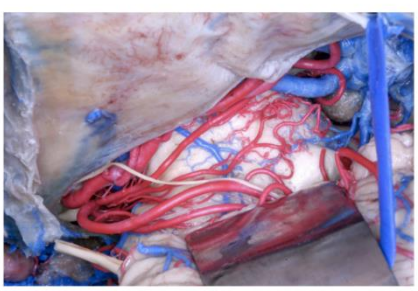

FIGURE 2 | Anatomical picture of the microsurgical dissection of the left lemniscal trigone zone.

Perforating Arteries of the Lemniscal Trigone: A Microsurgical Neuroanatomic Description

Santino Ottavio Tomasi[1,2,3], Giuseppe Emmanuele Umana[4], Gianluca Scalia[5], Roberto Luis Rubio-Rodriguez[6,7,8], Giuseppe Raudino[9], Julian Rechberger[2], Philipp Geiger[2], Bipin Chaurasia[10], Kaan Yağmurlu, Michael T. Lawton[12], Peter A. Winkler[1,2,3]

[1]Department of Neurological Surgery - Christian Doppler Klinik, Salzburg, Austria; [12]Department of Neurosurgery, Barrow Neurological Institute, St. Joseph's Hospital and Medical Center, Phoenix, AZ, United States; [2]Department of Neurosurgery, Paracelsus Medical University Salzburg, Salzburg, Austria; [3]Laboratory for Microsurgical Neuroanatomy - Christian Doppler Klinik, Salzburg, Austria; [4]Department of Neurosurgery, Cannizzaro Hospital, Trauma Center, Gamma Knife Center, Catania, Italy; [5]Neurosurgery Unit, Highly Specialized Hospital and of National Importance "Garibaldi", Catania, Italy; [6]Skull Base and Cerebrovascular Laboratory, University of California, San Francisco, San Francisco, CA, United States; [7]Department of Neurological Surgery, University of California, San Francisco, San Francisco, CA, United States; [8]Department of Otolaryngology - Head and Neck Surgery, University of California, San Francisco, San Francisco, CA, United States; [9]Department of Neurosurgery - Humanitas, Istituto Clinico Catanese, Catania, Italy; [10]Department of Neurosurgery, Neurosurgery Clinic, Birgunj, Nepal; [11]Department of Neurosurgery, University of Virginia, Charlottesville, VA, United States; Contact: s.tomasi@salk.at

Objective
In literature, not much attention has been directed to the perforating arteries in the lemniscus; in fact, no reports on the perforators of this anatomical region are available. The present study aims to a detailed analysis of the microanatomy and the clinical implications of these perforators, in relation to the parent vessels. We focused on the small vessels that penetrate the midbrain's dorsolateral surface, known as lemniscal trigone, to understand better their microanatomy and their functional importance in the clinical practice during the microsurgical approach to this area.

Methods
Eighty-seven alcohol-fixed cadaveric hemispheres (44 brains) without any pathological lesions provided the material for studying the perforating vessels and their origin around the dorsolateral midbrain using an operating microscope (OPMI 1 FC, Zeiss). Measurements of the perforators' distances, in relation to the parent vessels, were taken using a digital caliper.

Results
An origin from the SCA could be found in 70.11% (61) and from the PCA in 27.58% (24) of the hemispheres. In one hemisphere, an origin from the posterior choroidal artery was found (4.54%). No perforating branches were discovered in 8.04% of specimens (7).

Conclusions
The perforating arteries of the lemniscal trigone stem not only from the superior cerebellar artery (SCA), as described in the few studies available in literature, but also from the posterior cerebral artery (PCA). Therefore, special attention should be paid during surgery to spare those vessels and associated perforators. A comprehensive understanding of the lemniscal trigone's perforating arteries is vital to avoid infarction of the brainstem when treating midbrain tumors or vascular malformations.

Reliability of blood gas analysers Radiometer ABL 90 flex and Siemens Rapid Point 500 near sea level and at high altitude

F Treff[1], B Mayer[2], P Schmidt[1], LM Schiefer[1,3], L Schäfer[1], B Mayr[4], KE Swenson[5], ER Swenson[6], J Niebauer[4], JM Steinacker[7], MM Berger[8], M Sareban[4], G Treff[4,7]

1: Department of Anesthesiology, Perioperative and General Critical Care Medicine, Paracelsus Medical University, Salzburg, Austria. **2**: Institute of Epidemiology and Medical Biometry, Ulm University, Germany. **3**: Innovation Salzburg G.m.b.H, Salzburg, Austria. **4**: Institute of Sports Medicine, Prevention and Rehabilitation, Paracelsus Medical University, Salzburg, Austria. **5**: Division of Pulmonary and Critical Care Medicine, Stanford University, Palo Alto, CA, USA. **6**: Pulmonary, Critical Care and Sleep Medicine, VA Puget Sound Health Care System, University of Washington, Seattle, WA, USA. **7**: Division of Sports and Rehabilitation Medicine, University Hospital Ulm, Germany. **8**: Department of Anesthesiology and Intensive Care Medicine, University Hospital Essen, Germany.

INTRODUCTION

Blood gas analyzers ABL 90 flex (RAD) and Siemens Rapid Point 500 (SIE) are used in clinical and scientific settings such as altitude studies.We aimed to evaluate the real-world reliability of RAD vs. SIE in near-sea level (423 m) and high altitude (4,559 m) field test conditions.

DESIGN & METHODS

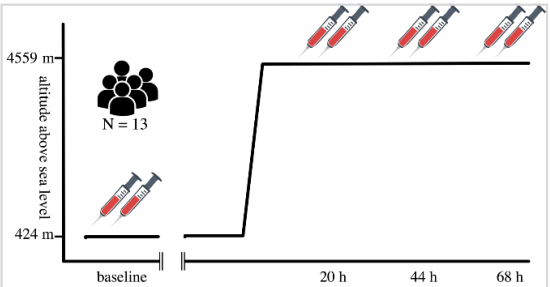

Figure 1: Study design.

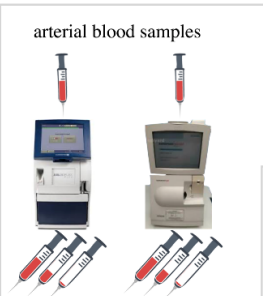

Figure 2: Sample processing

- Two arterial samples per participant at baseline, 20, 44, and 68 h after ascent
- Triplicate analysis in alternating order between devices

Statistics: A mixed model was applied to calculate the intraclass correlation coefficient ICC (3,1) for each device and variable, where condition (i.e. SL vs. HA) was included as fixed effect. Same model was applied to calculate differences CV% from triplicate measurements between conditions and devices.

RESULTS

Table 1: Estimates, (standard errors) and p-values of the linear mixed model (LMM). Data are based on individual coefficients of variation (%CV) of triplicate measurements for selected variables of blood gas analysis conducted with Siemens Rapid Point and Radiometer ABL 90 at 423 m and 4,559 m a.s.l.

Variable	Siemens			Radiometer			Siemens vs. Radiometer	
	423 m asl	4,559 m asl	p	423 m asl	4,559 m asl	p	p@423 m	p@4,559 m
Hb	1.16 (0.54)	1.36 (0.37)	0.763	0.49 (0.54)	0.50 (0.37)	0.985	0.383	0.108
PO_2	5.29 (0.49)	1.36 (0.34)	<0.001	3.79 (0.49)	0.99 (0.34)	<0.001	0.035	0.444
PCO_2	5.11 (0.57)	3.55 (0.43)	0.033	0.43 (0.57)	0.54 (0.39)	0.875	<0.001	<0.001
COHb	28.56 (3.54)	9.52 (2.46)	<0.001	8.98 (3.54)	2.49 (2.42)	0.132	<0.001	0.044
Lac	7.07 (1.56)	6.73 (1.03)	0.828	5.10 (1.56)	3.56 (0.79)	0.276	0.232	0.017
pH	0.06 (0.01)	0.06 (0.01)	0.733	0.03 (0.01)	0.03 (0.01)	0.870	0.104	0.004

The differences in ICC between RAD vs. SIE ranged from Δ0.01 (0.58 vs. 0.57) for pH to Δ0.30 for COHb (0.61 vs. 0.31). All ICCs except for [Lac] were slightly higher in RAD (0.44 – 0.82, poor to good) than in SIE (0.31 – 0.64, poor to moderate). This result is in line with the CVs, which were always lower in RAD and significantly different between devices for PO_2, PCO_2, COHb at 423 m and for PCO_2, COHb, [Lac], and pH at 4,559 m (Tab. 1).

CONCLUSION

Reliability of RAD was superior to SIE at 423 m and 4,559 m. Thus, RAD may be preferred at these altitudes for particular variables like PO_2, PCO_2, or COHb. Differences in reliability for other variables such as pH appear to be negligible.

Corresponding author: Priv.-Doz. Dr. Gunnar Treff | Mail: gunnar.treff@pmu.ac.at

Reliability of blood gas analysers Radiometer ABL 90 flex and Siemens Rapid Point 500 near sea level and at high altitude

Franziska Treff[1], Benjamin Mayer[2], Peter Schmidt[1], Lisa M Schiefer[1,3], Larissa Schäfer[1], Barbara Mayr[4], Kai E Swenson[5], Eric R Swenson[6], Josef Niebauer[4], Jürgen M Steinacker[7], Marc M Berger[8], Mahdi Sareban[4], Gunnar Treff[4,7]

[1]Department of Anesthesiology, Perioperative and General Critical Care Medicine, Paracelsus Medical University, Salzburg, Austria; [2]Institute of Epidemiology and Medical Biometry, Ulm University, Germany.; [3]Innovation Salzburg G.m.b.H, Salzburg, Austria.; [4]Institute of Sports Medicine, Prevention and Rehabilitation, Paracelsus Medical University, Salzburg, Austria.; [5]Division of Pulmonary and Critical Care Medicine, Stanford University, Palo Alto, CA, USA.; [6]Pulmonary, Critical Care and Sleep Medicine, VA Puget Sound Health Care System, University of Washington, Seattle, WA, USA.; [7]Division of Sports and Rehabilitation Medicine, University Hospital Ulm, Germany.; [8]Department of Anesthesiology and Intensive Care Medicine, University Hospital Essen, Germany.; Contact: gunnar.treff@pmu.ac.at

Objective
Blood gas analyzers like Radiometer ABL 90 (RAD) and Siemens Rapid Point 500 (SIE) are frequently used to evaluate changes in blood variables in altitude studies. Since reliability of blood gas analysis is critical for several scientific purposes, we aimed to evaluate the reliability of RAD and SIE in normoxic (423 m) and hypoxic conditions (4,559 m) during a field-based altitude study.

Methods
Two arterial blood samples from 13 subjects were drawn in supine position after 10 min of rest once at 423 m and three times at 4,559 m (20, 44, and 68 h after ascent), using the respective manufacturer recommended syringes and instructions. Afterwards, samples were analyzed in triplicate in an alternating order between RAD and SIE to assess the directly measured variables hemoglobin concentration ([Hb], mg/dl), carboxyhemoglobin (COHb, %), partial pressures of oxygen (pO_2, mmHg) and carbon dioxide (pCO_2, mmHg), Lactate ([Lac], mmol/L), and pH.
A mixed model was used to calculate the intraclass correlation coefficient ICC (3,1) for each device and variable including all measurements. Coefficients of variation (CV) were calculated from triplicate measurements and the mixed model was applied to calculate differences in CV between conditions and between devices.

Results
The differences in ICC between RAD vs. SIE ranged from Δ0.01 (0.58 vs. 0.57) for pH to Δ0.30 for COHb (0.61 vs. 0.31). All ICCs except for [Lac] were slightly higher in RAD (0.44 – 0.82, poor to good) than in SIE (0.31 – 0.64, poor to moderate). This result is in line with the CVs, which were always lower in RAD and significantly different between devices for PO_2, PCO_2, COHb at 423 m and for PCO_2, COHb, [Lac], and pH at 4,559 m.

Conclusions
Reliability of RAD was superior to SIE at 423 m and 4,559 m. Thus, RAD may be preferred at these altitudes for particular variables like PO_2, PCO_2, or COHb. Differences in reliability for other variables such as pH appear to be negligible.

Differentiation between septic and aseptic femoral and tibial shaft non-union: a multicenter clinical study

Katharina Trenkwalder[1],[2], Sandra Erichsen[1],[2], Ferdinand Weisemann[3], Peter Augat[1],[2], Matthias Militz[3], Simon Hackl[2],[3]

[1] Institute for Biomechanics, BG Unfallklinik Murnau, Germany; [2] Institute for Biomechanics, Paracelsus Medical University Salzburg, Austria; [3] Department of Trauma Surgery, BG Unfallklinik Murnau, Germany

BGU Murnau
Berufsgenossenschaftliche Unfallklinik Murnau

Introduction

Non-union is a common complication in facture healing, which pathogenesis is either aseptic or septic. The therapeutic strategy treating aseptic or septic non-unions follows different principles [1-4]. Therefore, an early determination of the underlying genesis is important. However, in practice discrimination can be difficult and low-grade infections often remain undetected with conventional diagnostics [5, 6].

Figure 1: Femoral non-union

The aim of the clinical study is to develop (pre-)surgical diagnostic criteria to improve the differential diagnosis between aseptic and septic non-union. We hypothesize that additional molecular biological, histopathological and laboratory chemical findings will improve the infect diagnosis compared with the current gold standard.

Multicenter study structure

In eight study centers 60 patients with aseptic and 30 with septic femur or tibia shaft non-unions admitted to the hospitals for a revision surgery and 30 control patients with regular healed femoral or tibial shaft fractures undergoing implant removal are included. Laboratory chemical diagnostics, preoperative peripheral blood samples und intraoperative tissue specimens as well as the osteosynthesis material are collected from each patient (Figure 2).

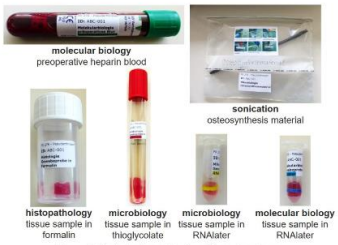

Figure 2: Collected samples for different analyses

BG Unfallklinik Murnau as the main study center is responsible for organization and realization of the multicenter study. The collected specimen are sent overnight together with patient data (demographics, comorbidities, injury) in a provided sample box to the Institute for Biomechanics of the BG Unfallklinik Murnau and Paracelsus Medical University Salzburg. Samples are processed in the biological laboratory on the subsequent day. Histopathological and molecular biological analyses are conducted in collaboration with partners (Figure 3).

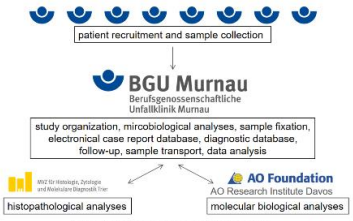

Figure 3: Structure of the multicenter study

One year after study surgery the patient`s individual healing process is assessed in a clinical follow-up.

Material and Methods

Samples are analyzed with different techniques (microbiological, molecular biological, histopathological) for presence of an infection. One tissue sample is processed for conventional microbiological long-term cultivation. Another tissue sample is classified into septic or aseptic non-union according to histopathological criteria. And a third tissue sample is analyzed by PCR for the presence of bacteria. Additional osteosynthesis material is examined for a possible biofilm by sonication with subsequent vacuum filtration for quantification of bacterial load (Figure 4).

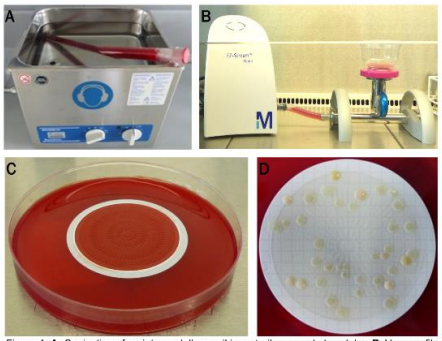

Figure 4: **A:** Sonication of an intramedullary nail in a sterile capped glass tube; **B:** Vacuum filtration of the sonication fluid through membrane filters (0.45 µm pore size); **C:** Membrane filter incubation on Columbia sheep blood agar; **D:** Quantification of colony forming units (cfu)

The differential diagnostic performances in discrimination of septic and aseptic non-union for the different diagnostic methods are determined in relation to the current gold standard, i.e. two positive tissue cultures with the same pathogen.

Plasma and peripheral blood mononuclear cells (PBMC) are isolated from peripheral blood samples via density gradient centrifugation. Pro- and anti-inflammatory cytokines and antimicrobial peptides are analyzed in the plasma and one tissue sample to identify biomarkers for the differentiation between septic and aseptic non-union. Thresholds for biomarkers are determined via receiver operating characteristic.

PBMCs are stimulated with titanium dioxide particles and cells immune response is analyzed via enzyme-linked immunosorbent assay to test for a possible implant intolerance.

Value of the Project

The findings will improve the clinical differential diagnosis in septic and aseptic non-unions. Identification of further diagnostic criteria for the reliable differentiation between aseptic and septic non-union would be of great value for clinical procedures in everyday medical practice. Based on a better differential diagnosis, earlier and more targeted treatment of non-union would be possible according to its genesis. This would result in an improved therapy algorithm, which would lead to a qualitatively better as well as shorter treatment of the affected patients.

In summary, this would allow for further optimization of therapy of aseptic and septic non-unions with the aid of a comprehensive spectrum of appropriate analytical methods.

PARACELSUS MEDIZINISCHE PRIVATUNIVERSITÄT
20 JAHRE

Literature:

[1] Hierholzer et al., J Orthop Surg Res, 2014. 9: p. 86.
[2] Metsemakers et al., J Orthop Trauma, 2020. 34(1): p. 18-29.
[3] Depypere et al., J Orthop Trauma, 2020. 34(1): p. 30-41.
[4] Militz et al., Trauma und Berufskrankheit, 2014. 16(4): p. 444-451.
[5] Hackl et al., Injury, 2021. 52(11): p. 3498-3504.
[6] Dapunt et al., Ther Clin Risk Manag, 2015. 11: p. 1843-52.

Contact:

Mag.[2] rer. nat. Katharina Trenkwalder
E-mail: katharina.trenkwalder@bgu-murnau.de
Phone: +49 8841 48-3069
Fax: +49 8841 48-4573

BG Unfallklinik Murnau
Paracelsus Medizinische Privatuniversität Salzburg
Prof.-Küntscher-Str. 8
82418 Murnau am Staffelsee
www.bg-kliniken.de/unfallklinik-murnau/

Paracelsus virtual Science Get Together 2022

Differentiation between septic and aseptic femoral and tibial shaft non-union: a multicenter clinical study

Katharina Trenkwalder[1,2], Sandra Erichsen[1,2], Ferdinand Weisemann[3], Peter Augat[1,2], Matthias Militz[3], Simon Hackl[2,3]

[1]Institute for Biomechanics, BG Unfallklinik Murnau, Germany; [2]Institute for Biomechanics, Paracelsus Medical University Salzburg, Austria; [3]Department of Trauma Surgery, BG Unfallklinik Murnau, Germany; Contact: katharina.trenkwalder@bgu-murnau.de

Objective

Non-union is a common complication in facture healing, which pathogenesis is either aseptic or septic. The therapeutic strategy treating aseptic or septic non-unions follows different principles [1-4]. Therefore, an early determination of the underlying genesis is important. However, in practice discrimination can be difficult and low-grade infections often remain undetected with conventional diagnostics [5, 6]. The aim of the clinical study is to develop (pre-)surgical diagnostic criteria to improve the differential diagnosis between aseptic and septic non-union. We hypothesize that additional molecular biological, histopathological and laboratory chemical findings will improve the infect diagnosis compared with the current gold standard.

Methods

In eight study centers 60 patients with aseptic and 30 with septic femur or tibia shaft non-unions and 30 control patients with regular healed femoral or tibial shaft fractures are included. Laboratory chemical diagnostics, preoperative peripheral blood samples und intraoperative tissue specimens as well as the osteosynthesis material are collected from each patient. These samples are analyzed with different techniques for presence of an infection. One tissue sample is processed for conventional microbiological long-term cultivation, another is classified into septic or aseptic non-union according to histopathological criteria. A third tissue sample is analyzed by PCR for the presence of bacteria. Osteosynthesis material is examined for a possible biofilm by sonication. The differential diagnostic performances in discrimination of septic and aseptic non-union for the different diagnostic methods are determined in relation to the current gold standard. Plasma and peripheral blood mononuclear cells (PBMC) are isolated from peripheral blood samples. Pro- and anti-inflammatory cytokines and antimicrobial peptides are analyzed in the plasma and one tissue sample to identify biomarkers for the differentiation between septic and aseptic non-union. PBMCs are stimulated with titanium dioxide particles and cells immune response is analyzed to test for a possible implant intolerance.

Conclusions

The findings will improve the clinical differential diagnosis in septic and aseptic non-unions. Identification of further diagnostic criteria for the reliable differentiation between aseptic and septic non-union would be of great value for clinical procedures in everyday medical practice. Based on a better differential diagnosis, earlier and more targeted treatment of non-union would be possible according to its genesis. This would result in an improved therapy algorithm, which would lead to a qualitatively better as well as shorter treatment of the affected patients. In summary, this would allow for further optimization of therapy of aseptic and septic non-unions with the aid of a comprehensive spectrum of appropriate analytical methods.

References

1. Hierholzer et al., J Orthop Surg Res, 2014. 9: p. 88.
2. Metsemakers et al., J Orthop Trauma, 2020. 34(1): p. 18-29.
3. Depypere et al., J Orthop Trauma, 2020. 34(1): p. 30-41.
4. Militz et al., Trauma und Berufskrankheit, 2014. 16(4): p. 444-451.
5. Hackl et al., Injury, 2021. 52(11): p. 3498-3504.
6. Dapunt et al., Ther Clin Risk Manag, 2015. 11: p. 1843-52.

Fate mapping of PDGFRb-tdTomato⁺ cells in wound healing upon optic nerve crush

Andrea Trost, Julia Preishuber-Pflügl, Veronika Altinger, Andreas Koller, Susanne Maria Brunner, Daniela Mayr, Christian Runge, Anja-Maria Ladek and Herbert Anton Reitsamer

Research Program for Experimental Ophthalmology,
Department of Ophthalmology and Optometry,
University Hospital of the Paracelsus Medical University

Objective

Pericytes (PCs), constituents of the microvasculature, are important regulators of vascular development, stabilization, maturation and remodeling of microvessels, therefore, playing a key role in tissue homeostasis, including barrier functions. In addition, they possess an *in vitro* multi-lineage potential, and in line their trans-differentiation potential was reported in *in vivo* studies, raising expectations that endogenous PCs may contribute to wound healing and regeneration. To study the participation of PCs in wound healing following optic nerve crush (ONC), an inducible PC specific fate mapping mouse model was used and the reporter cells were studied at different time points post lesion.

Methods

In the PC specific fate mapping mouse model (PDGFRb-P2A-CreER^{T2}–tdTomato) labeling of cells with an active PDGFRb promotor was induced upon tamoxifen injection (100 mg/kg body weight TAM) at early postnatal time points (P4-P14). Male and female TAM and corn oil (control) induced PDGFRb-tdTom mice (~ 12 weeks of age, n = 34) were subjected to an unilateral ONC of the right eye, leaving the dura intact. 2, 4, 7, 21 days and 8 weeks post lesion, the ON and tdTom⁺ cells were characterized by immunofluorescence microscopy.

Results

TAM induction resulted in tdTom⁺ labeling of vascular (87.8%) and non-vascular cells (12.2%) in the healthy ON (Figure 1). 7 dpl, 21 dpl and 8 weeks pl, 9.9%, 20.8% and 19.8% of DAPI⁺ cells within the lesion were tdTom⁺ (Figure 2). Thereof, 56.6-77.6% revealed no association to CD31⁺ vascular structures, indicating a role distinct from vascular functions (Figure 3). Further, 96.1 % of tdTom+ cells revealed PDGFRb immunoreactivity, but did not express microglia (Iba1) or astrocytic (GFAP) marker (Figure 4).

Conclusions

Using the inducible PDGFRb-P2A-CreER^{T2}-tdTomato transgenic mouse, the entire population of perivascular cells of the ON is labeled, enabling fate mapping of these cells in lesioned tissue. Of note, 10% of tdTom⁺ cells are non-vascular in the healthy ON. Within the lesion, an accumulation of non-vascular tdTom⁺ cells was detected, which strongly indicates that PCs or PC-derived cells participate in wound healing and scar formation/tissue repair in the ON. Therefore, PCs may be a promising target to modulate wound healing and subsequently regenerative approaches.

The work was supported by the the Research Support Fund of the Paracelsus Medical University (PMU-FFF E-19/30/158-ZUR). Contact: a.zurl@salk.at

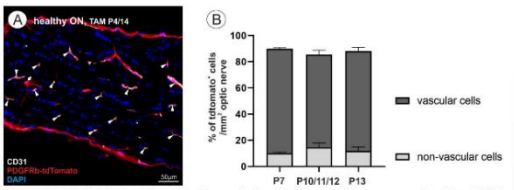

Figure 1: (A) In the healthy ON, the majority of tdTom⁺ cells are associated to CD31⁺ vascular structures (arrowheads), some tdTom⁺ cells reveal no vascular association (arrow). (B) Following early TAM induction between P4 and P14, 87.8% of tdTom⁺ cells are associated to vascular structures, 12.2% show no vascular association.

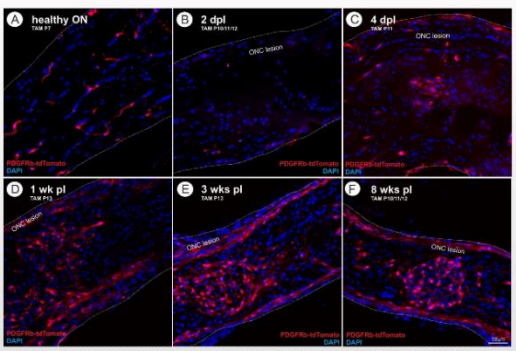

Figure 2: Localization of tdTom⁺ cells in the lesion over time. (A) TdTom⁺ cells in the healthy ON, (B) two days post injury, the lesioned area was nearly cell-free and also devoid of tdTom ⁺ cells, (C) single tdTom⁺ cell clusters were detected 4 dpl, (D) 7 dpl the number of tdTom⁺ cells increased, forming a network like structure in the lesion core. (E) 21 dpl and (F) 8 wks post lesion 21.3% (n = 4) and 22.0% (n = 6) of the DAPI⁺ cells within the lesion were tdTom⁺.

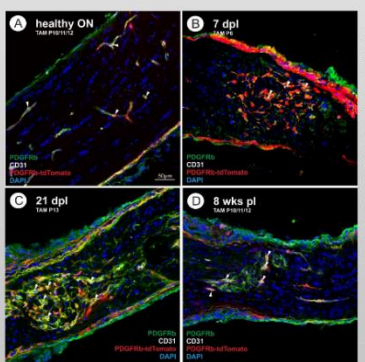

Figure 3: Vascular association of tdTom⁺ cells in the lesion. (A) In the healthy ON the majority of tdTom⁺ cells shows vascular association (arrowheads), (B) 7 dpl, 22.4% of tdTom⁺ cells were associated to vascular structures (n = 6). (C) 21 dpl, 24.9% of tdTom⁺ cells revealed an association to CD31 vascular structures (n = 6), (D) which increased to 43.4% 8 weeks post lesion.

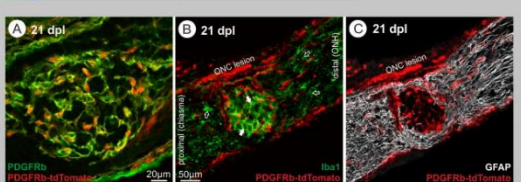

Figure 4: (A) 94.5-98.6% of tdTom+ cells reveal PDGFRb immunoreactivity, but lack (B) Iba1 (microglia) or (C) GFAP (astrocytes) immunreactivity.

Fate mapping of PDGFRb-tdTomato+ cells in _x000B_wound healing upon optic nerve crush

Andrea Trost[1], Julia Preishuber-Pflügl[1], Veronika Altinger[1], Andreas Koller[1], Susanne Maria Brunner[1], Daniela Mayr[1], Christian Runge[1], Anja-Maria Ladek[1], Herbert Anton Reitsamer[1]

[1]Research Program for Experimental Ophthalmology, Department of Ophthalmology and Optometry, University Hospital of the Paracelsus Medical University; Contact: a.zurl@salk.at

Objective
Pericytes (PCs), constituents of the microvasculature, are important regulators of vascular development, stabilization, maturation and remodeling of microvessels, therefore, playing a key role in tissue homeostasis, including barrier functions. In addition, they possess an in vitro multi-lineage potential, and in line their trans-differentiation potential was reported in in vivo studies, raising expectations that endogenous PCs may contribute to wound healing and regeneration. To study the participation of PCs in wound healing following optic nerve crush (ONC), an inducible PC specific fate mapping mouse model was used and the reporter cells were studied at different time points post lesion.

Methods
In the PC specific fate mapping mouse model (PDGFRb-P2A-CreER^{T2}–tdTomato) labeling of cells with an active PDGFRb promotor was induced upon tamoxifen injection (100 mg/kg body weight TAM) at early postnatal time points (P4-P14). Male and female TAM and corn oil (control) induced PDGFRb-tdTom mice (~ 12 weeks of age, n = 34) were subjected to an unilateral ONC of the right eye, leaving the dura intact. 2, 4, 7, 21 days and 8 weeks post lesion, the ON and tdTom+ cells were characterized by immunofluorescence microscopy.

Results
TAM induction resulted in tdTom$^+$ labeling of vascular (87.8%) and non-vascular cells (12.2%) in the healthy ON. 7 dpl, 21 dpl and 8 weeks pl, 9.9%, 20.8% and 19.8% of DAPI$^+$ cells within the lesion were tdTom$^+$. Thereof, 56.6-77.6% revealed no association to CD31$^+$ vascular structures, indicating a role distinct from vascular functions. Further, 96.1 % of tdTom$^+$ cells revealed PDGFRb immunoreactivity, but did not express microglia (Iba1) or astrocytic (GFAP) marker.

Conclusions
Using the inducible PDGFRb-P2A-CreER^{T2}-tdTomato transgenic mouse, the entire population of perivascular cells of the ON is labeled, enabling fate mapping of these cells in lesioned tissue. Of note, 10% of tdTom$^+$ cells are non-vascular in the healthy ON. Within the lesion, an accumulation of non-vascular tdTom$^+$ cells was detected, which strongly indicates that PCs or PC-derived cells participate in wound healing and scar formation/tissue repair in the ON. Therefore, PCs may be a promising target to modulate wound healing and subsequently regenerative approaches.

Acknowledgements
The work was supported by the the Research Support Fund of the Paracelsus Medical University (PMU-FFF E-19/30/158-ZUR).

MRI-BASED SEMI-QUANTITATIVE ASSESSMENT ALLOWS TARGETED SELECTION OF KNEES WITH ACCELERATED QUANTITATIVE CARTILAGE THICKNESS LOSS: DATA FROM THE OAI FNIH BIOMARKER CONSORTIUM

Wolfgang Wirth[1,2,3], Susanne Maschek[1,2], Anna Wisser[1,2], Ali Guermazi[4,5,6], David J. Hunter[7,8], Felix Eckstein[1,2,3], Frank W. Roemer[9,5,6]

[1]Dept. of Imaging & Functional Musculoskeletal Res., Inst. of Anatomy & Cell Biology, Paracelsus Med. Univ., Salzburg, Austria
[2]Chondrometrics GmbH, Freilassing, Germany
[3]Ludwig Boltzmann Inst. for Arthritis and Rehabilitation, Paracelsus Med. Univ., Salzburg, Austria
[4]Dept. of Radiology, VA Boston Healthcare System, Boston, MA
[5]Quantitative Imaging Ctr., Dept. of Radiology, Boston Univ. Sch. of Med., Boston, MA
[6]Boston Imaging Core Lab LLC, Boston, MA
[7]Rheumatology Dept., Royal North Shore Hosp., Sydney, Australia
[8]Inst. of Bone and Joint Res., Kolling Inst., Univ. of Sydney, Sydney, Australia
[9]Dept. of Radiology, Univ. of Erlangen, Erlangen, Germany

Presence of joint space narrowing (JSN) has been observed to be a good predictor for subsequent structural progression, but has also been reported to not only depend on cartilage loss but also on meniscus extrusion and damage. MRI-based MOAKS scores may allow a more specific selection of knees with expected accelerated progression than radiographic selection criteria, as they provide a more comprehensive description of joint tissue damages compared to radiography.

OBJECTIVE

1) To investigate, whether and which MRI-derived tissue features based on MOAKS assessment are predictive for subsequent ipsi-compartmental accelerated cartilage thickness loss.
2) To assess the sensitivity to change for MOAKS and medial JSN strata

METHODS

- 599 of the 600 OAI FNIH study participants (age: 62y, BMI: 31kg/m², 59% female) had baseline MOAKS assessments (grading by expert radiologists) and baseline and 2-year follow-up cartilage thickness measurements in the medial (MFTC) and lateral femorotibial compartment (LFTC) from manual quality-controlled segmentation
- 3 tibial and the central femoral MOAKS subregions (medial and lateral) were used to match the MOAKS regions with weight-bearing MFTC/LFTC cartilage thickness measures (Fig. 1)
- Cartilage thickness change was stratified by absence/presence of ipsi-compartmental baseline cartilage damage (>0), bone marrow lesions (BML, any), meniscus damage (root tear, morphology>1 or extrusion >0), or effusion/synovitis (>0) scores and additionally by MOAKS subscales
- Between-group comparisons performed using ANCOVA (adjusted for age, sex, BMI); Cohen's D used as a measure of effect size

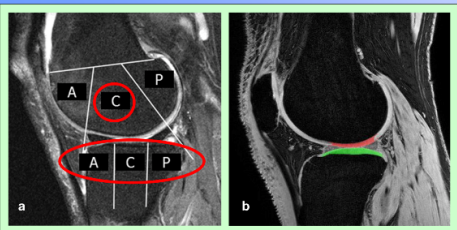

Figure 1: a) MOAKS regions of the lateral femur and tibia. Each 3 tibial and the central femoral subregions (C) were included (marked in red) to match regions of interest for cartilage thickness measurements. b) segmentation of the lateral tibia and weight bearing lateral femur.

Table 1: 2-year change in MFTC cartilage thickness stratified by presence/absence of baseline MOAKS scores

	Absence				Presence				Mean adj. diff				
	N	Mean	SD	SRM	N	Mean	SD	SRM	Mean	95% CI		P-Value	Cohen's D
Cartilage damage (MFTC)	154	-10	121	-0.08	445	-131	222	-0.59	-109	-147	-71	<0.001	-0.60
BMLs (MFTC)	317	-50	164	-0.30	282	-156	236	-0.66	-95	-128	-62	<0.001	-0.53
Meniscus (MFTC)	123	-21	128	-0.17	476	-120	219	-0.55	-88	-129	-47	<0.001	-0.48
Effusion/ Synovitis	121	-61	150	-0.41	478	-109	219	-0.50	-42	-83	-1	0.046	-0.24

Change and SD provided in µm. MFTC: Medial femorotibial compartment; BML: Bone marrow lesions; SD: Standard deviation; 95% CI: 95% confidence intervals; SRM: Standardized response mean (mean change / SD of change)

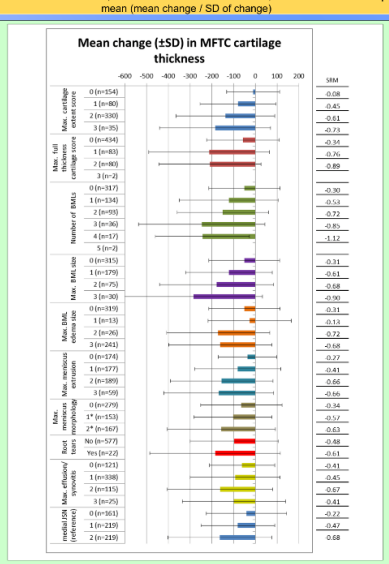

Figure 2: Mean change in MFTC cartilage thickness (in µm) for different medial compartment MOAKS features (*meniscus morphology: 1=any tear, 2=any maceration)

RESULTS

- In the MFTC, presence of cartilage damage, BMLs, meniscus damage/ extrusion, and synovitis/effusion were associated with greater subsequent cartilage thickness loss over 2 years (Table 1).
- The greatest effect size was observed for presence of cartilage damage (Cohen's D:-0.60) followed by presence of BMLs (Cohen's D:-0.53) and presence of meniscus damage/extrusion (Cohen's D: -0.48) (Table 1).
- In the LFTC, presence of joint damage was less pronounced than in the MFTC and only presence of LFTC meniscus damage/extrusion was associated with subsequent LFTC cartilage thickness loss (data not shown).
- For most of the MOAKS features and subscales, MFTC cartilage thickness loss increased with increasing severity of the respective feature. The greatest magnitude of change was observed in knees with large BMLs (grade 3), several BMLs (>2), or full thickness cartilage damage (Fig. 2). The same features also displayed the greatest sensitivity to change (SRM range:-0.85 to -1.12). In comparison, SRMs were -0.47 / -0.68 in knees with medial JSN 1 / 2.
- 67 of the 438 knees with medial JSN 1 or 2 had no medial cartilage damage (MOAKS grade 0.0) & 98 of the 219 knees with medial JSN 2 had no full thickness lesions (MOAKS full thickness = 0).

CONCLUSIONS

- Presence and severity of semi-quantitatively MRI-based joint tissue damage was associated with the magnitude of quantitative cartilage loss.
- MRI-based simplified in only few subregions may therefore allow specific selection (or exclusion) of knees likely (or unlikely) to exhibit high sensitivity to change.
- Selection by MOAKS scores or simplified SQ measures may therefore allow reducing the sample size when compared to JSN grades, that were observed to not necessarily reflect cartilage damage.

CONTACT: wolfgang.wirth@pmu.ac.at

MRI-BASED SEMIQUANTITIAVE CARTILAGE ASSESSMENT (MOAKS) ALLOWS TARGETED SELECTION OF KNEES WITH ACCELERATED QUANTITATIVE CARTILAGE THICKNESS LOSS: DATA FROM THE FNIH BIOMARKER CONSORTIUM

Wolfgang Wirth[1,2], Susanne Maschek[1,2], Anna Wisser[1,2], Ali Guermazi[3,4], David J Hunter[5], Felix Eckstein[1,2], Frank Roemer[3,6]

[1]Department of Imaging and Functional Musculoskeletal Research, Institute of Anatomy and Cell Biology, Paracelsus Medical University, Salzburg, Austria; [2]Chondrometrics GmbH, Freilassing, Germany; [3]Boston Imaging Core Lab, Boston, MA, USA; [4]Department of Radiology, VA Boston Healthcare, Boston, MA, USA; [5]Rheumatology Department, Royal North Shore Hospital and Institute of Bone and Joint Research, Kolling Institute, University of Sydney, Sydney, Australia; [6]Department of Radiology, University of Erlangen, Erlangen, Germany; Contact: wolfgang.wirth@pmu.ac.at

Objective
Structural eligibility in DMOAD trials usually relies on radiographic selection criteria to enrich the study cohort with knees likely to exhibit structural progression. MRI-based MOAKS scores may allow more specific selection of knees with accelerated progression than radiographic criteria as they provide a more comprehensive description of joint damages. The objective of this study was to investigate, whether (and which) MRI-based MOAKS scores are predictive for subsequent accelerated cartilage thickness loss.

Methods
The OAI FNIH study investigated predictors for symptomatic and/or medial radiographic progression. Of the 600 participants, 599 had MOAKS assessments and quantitative cartilage thickness measurements (age: 62y, BMI: 31kg/m², 59% female) at baseline and 2-year follow-up in the medial and lateral femorotibial compartment (MFTC/LFTC). Baseline MOAKS scores were graded by expert radiologists. MFTC and LFTC cartilage thickness change over the subsequent two years was stratified by presence/absence of ipsicompartmental baseline cartilage damage, bone marrow lesion (BML), meniscus damage or extrusion, or effusion/synovitis scores. Changes were additionally stratified by MOAKS cartilage subscales, BML subscales, meniscus subscales, and effusion/synovitis severity. Between-group comparisons were performed using ANCOVA with adjustment for age, sex, and BMI. The standardized response mean (SRM) was used to assess the sensitivity to change, Cohen's D was used as a measure of effect size.

Results
In the MFTC, presence of cartilage damage, BMLs, meniscus damage/extrusion, and synovitis/effusion were associated with greater subsequent cartilage thickness loss over 2 years. The greatest effect size was observed for presence of cartilage damage (Cohen's D: -0.60) followed by presence of BMLs (Cohen's D: -0.53) and presence of meniscus damage/extrusion (Cohen's D: -0.48). In the LFTC, presence of joint damage was less pronounced than in the MFTC and only presence of meniscus damage/extrusion was associated with subsequent LFTC loss (data not shown). For most of the MOAKS features and subscales, MFTC cartilage thickness loss increased with increasing severity of the respective feature. The greatest magnitude of change was observed in knees with large (grade 3) BMLs, several (>2) BMLs, or full thickness cartilage damage. The same features also displayed the greatest sensitivity to change (SRM range: -0.85 to -1.12).

Conclusions
Presence and severity of MRI-based joint tissue damage was associated with the magnitude of cartilage loss and MRI-based scoring systems may therefore allow specific selection of knees more likely to exhibit high sensitivity to change. In addition, MRI-based scoring of joint damage may also allow exclusion of knees, in which a DMOAD is unlikely to be effective (e.g., wide-spread full thickness damage) or in which a treatment with DMOADs is not indicated (e.g., no absence of cartilage damage despite presence of JSN).

ASSOCIATION OF SEMIQUANTITATIVE MRI-BASED MEASURES OF KNEE CARTILAGE WITH INCREASED CARTILAGE LOSS IN KNEES AT ELEVATED RISK OF DEVELOPING OSTEOARTHRITIS - DATA FROM THE OSTEOARTHRITIS INITIATIVE

A. Wisser[1], F. Roemer[3,4,5], S. Maschek[1], F. Eckstein[1,2], A. Guermazi[3,4,6] , W. Wirth[1,2]

[1]Department for Imaging and Functional Musculoskeletal Research, Institute of Anatomy and Cell Biology - Salzburg, Center for Anatomy and Cell Biology, Paracelsus Med. Univ., Salzburg, Austria,
[2]Ludwig Boltzmann Inst. for Arthritis and Rehabilitation, Paracelsus Med. Univ., Salzburg, Austria,
[3]Quantitative Imaging Ctr., Dept. of Radiology, Boston Univ. Sch. of Med., Boston, MA,
[4]Boston Imaging Core Lab LLC, Boston, MA,
[5]Dept. of Radiology, Univ. of Erlangen, Erlangen, Germany,
[6]Dept. of Radiology, VA Boston Healthcare System, Boston, MA

Radiographically normal knees (Kellgren & Lawrence grade (KLG) 0) with radiographic osteoarthritis (ROA, KLG2-4) in the contralateral (CL) knee (idiopathic OA) have been reported to exhibit greater cartilage thinning than KLG0 knees with CL KLG0, in particular in the lateral compartment [1]. KLG0 knees with CL ROA could therefore be of interest for evaluating preventive OA drug effects targeting early, pre-radiographic OA stages. Semi-quantitative (SQ) MRI assessment of different joint tissue pathologies may allow to specifically identify knees at risk of cartilage loss even if no radiographic signs are present.

OBJECTIVES

1. Explore the association between baseline SQ MOAKS cartilage scores and subsequent three-year change in quantitative (Q) cartilage thickness in KLG0 knees with CL ROA.
2. Investigate, whether longitudinal change in cartilage thickness is associated with the severity of baseline MOAKS cartilage scores (i.e. area extent & full thickness damage) in KLG0 knees with CL ROA.

METHODS

- OAI participants with KLG0 in the target knee ('at risk knee') and ROA (KLG ≥ 2), but no trauma history in the CL knee.
- Cartilage in the target knee graded using SQ MOAKS scores (grades: 0.0 to 3.3, see Table 2) in each 3 tibial & 1 central femoral subregions for both the medial and lateral compartment (MFTC / LFTC).
- MFTC and LFTC cartilage thickness was measured from quality-controlled manual segmentations.
- ANCOVA (adjusted for age, sex, BMI) was used to compare changes between knees with max. MOAKS score >0 (MOAKSmax), max. MOAKS extent (MOAKSext), & max. full thickness extent (MOAKSft) vs. knees without MOAKS lesions.

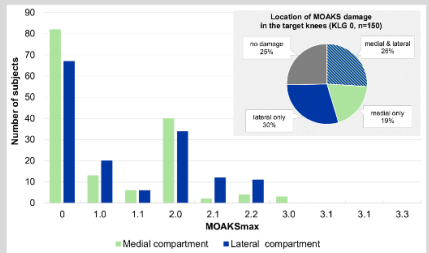

MOAKSmax: combines the maximum MOAKS area extent (1st component) and maximum MOAKS full thickness cartilage damage extent (2nd component) scores.

Figure 1: Maximum MOAKS cartilage scores and affected compartment in the target knee (KLG0) of the 150 subjects.

Table 1: Difference in the 3-year cartilage thickness change [mm] in the target knee (KLG0) between subjects with vs. without MOAKS damage, stratified by maximum MOAKS grade (MOAKSmax)

	Medial compartment			Lateral compartment		
MOAKSmax	Mean differ.	95% CI	P-value*	Mean differ.	95% CI	P-value*
0 (n=82/67)	Reference			Reference		
1.0 (n=13/20)	-0.02	[-0.1, 0.06]	0.67	-0.03	[-0.1, 0.05]	0.44
1.1 (n=6/6)	-0.04	[-0.15, 0.07]	0.48	-0.04	[-0.16, 0.08]	0.53
2.0 (n=40/34)	-0.03	[-0.08, 0.02]	0.28	-0.04	[-0.1, 0.02]	0.23
2.1 (n=2/12)	-0.07	[-0.26, 0.12]	0.47	-0.15	[-0.24, -0.06]	<0.01
2.2 (n=4/11)	-0.06	[-0.19, 0.07]	0.38	-0.11	[-0.2, -0.02]	0.02
3.0 (n=3/-)	-0.01	[-0.17, 0.15]	0.91	-	-	-

None of the subjects had a MOAKSmax of 3.1 or higher

n = medial/lateral values; CI: Confidence Interval; MOAKSmax: combines the maximum MOAKS area extent (1st component) and maximum MOAKS full thickness cartilage damage extent (2nd component) scores; *ANCOVA with adjustment for age, sex, BMI.

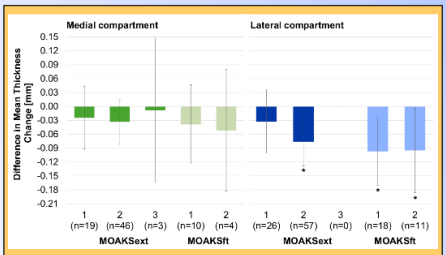

Figure 2: Difference in the 3-year cartilage thickness change in the target knee (KLG0) between subjects with vs. without MOAKS damage stratified by MOAKS subscales: area extent (MOAKSext) & full thickness damage (MOAKSft; *: p<0.05)

Table 2: MRI Osteoarthritis Knee Score (MOAKS) for grading of cartilage damage

	MOAKSmax subcomponents	
Abbreviation	MOAKSext	MOAKSft
Description	Max. MOAKS area extent (partial and full-thickness loss) relative to the size of the subregion	Max. MOAKS full thickness cartilage damage extent relative to the size of the subregion
Digit of max. MOAKS score	1st digit of MOAKSmax	2nd digit of MOAKSmax
Grades	0: none	0: none
	1: <10% of region of cartilage surface area	1: <10% of region of cartilage surface area
	2: 10-75% of region of cartilage surface area	2: 10-75% of region of cartilage surface area
	3: >75% of region of cartilage surface area	3: >75% of region of cartilage surface area

RESULTS

- 150 knees of 150 participants included (age 65±9 years, BMI 28±4 kg/m², 59% female).
- Most knees showed no or low grade MOAKS damage (Fig. 1).
- Across the entire sample, cartilage thickness loss tended to be greater in the LFTC (-0.03± 0.15mm) than in the MFTC (-0.01±0.13mm).
- In knees without MOAKS damage, cartilage thickness remained stable in both the MFTC (0.001±0.118mm) and LFTC (0.002±0.093).
- MFTC cartilage thickness change did not differ for the various MOAKS strata compared to knees without MOAKS lesions (Table 1).
- LFTC cartilage thickness loss was higher in knees with presence of any lateral MOAKS lesion compared to the reference group without lesions (adj. mean diff.: -0.06mm, 95% CI: [-0.11, -0.01]mm). This difference was mainly driven by the 23 knees with MOAKSmax 2.1/2.2 (Table 1).
- Knees with MOAKSext grade 2 & MOAKSft 1&2 showed greater LFTC cartilage loss than knees without MOAKSext /MOAKSft damage (Fig. 2).

CONCLUSIONS

- In this pre-ROA sample, the majority of KLG0 knees showed cartilage damage according to MOAKS grades.
- Presence of baseline MOAKS cartilage damage was associated with ipsi-compartmental cartilage thickness loss over three years in the more severely affected lateral compartment.

The results of this study therefore indicate:

- that cartilage loss can be quantitatively assessed even in knees without radiographic signs of osteoarthritis and
- MOAKS assessments allow to specifically select such knees. Baseline MOAKS cartilage scores may therefore be of help for selecting knees for future cartilage repair trials before ROA is established.

CONTACT: anna.wisser@pmu.ac.at

FUNDING: Bundesministerium für Bildung und Forschung, Germany (01EC1408D)

REFERENCES: [1] Eckstein et al., Osteoarthritis Cartilage 2019, 27(2)

ASSOCIATION OF SEMIQUANTITATIVE MRI-BASED MEASURES OF KNEE CARTILAGE WITH INCREASED CARTILAGE LOSS IN KNEES AT ELEVATED RISK OF DEVELOPING OA – DATA FROM THE OSTEOARTHRITIS INITIATIVE

Anna Wisser[1], Frank Roemer[3,4,5], Susanne Maschek[1], Felix Eckstein[1,2], Ali Guermazi[4,5], Wolfgang Wirth[1,2]

[1]Department for Imaging and Functional Musculoskeletal Research, Institute of Anatomy and Cell Biology - Salzburg, Center for Anatomy and Cell Biology, Paracelsus Medical University, Salzburg, Austria; [2]Ludwig Boltzmann Institute for Arthritis & Rehabilitation, Paracelsus Medical University, Salzburg, Austria; [3]Department of Radiology, University of Erlangen; [4]BICL, Boston, MA, USA; [5]Quantitative Imaging Center (QIC), Department of Radiology, Boston University, Boston, MA, USA; Contact: anna.wisser@stud.pmu.ac.at

Objective
Radiographically normal knees (Kellgren & Lawrence grade (KLG) 0) with radiographic osteoarthritis (ROA; KLG2-4, idiopathic OA) in the contralateral knee have been previously reported to exhibit greater cartilage thinning than KLG0 knees with contralateral KLG0, in particular in the lateral compartment. Semi-quantitative (SQ) MRI-based assessment of different joint tissue pathologies may allow to specifically identify knees at risk of cartilage loss even if no radiographic signs are present. This may be of interest for preventive OA trials. The aim of the current study was to explore the association between baseline semi-quantitative (SQ) cartilage MOAKS scores and the three-year change in quantitative (Q) cartilage thickness in KLG0 knees with contralateral ROA. Further, we wished to explore, whether longitudinal change in cartilage thickness is associated with the severity of baseline MOAKS cartilage scores: area extent and full thickness involvement.

Methods
The analysis was conducted in participants of the Osteoarthritis Initiative cohort study, who had KLG0 in the target knee ('at risk knee') and ROA (KLG ≥ 2) in the contralateral knee. The SQ MOAKS score assesses cartilage using two digits taking into account the area extent and the extent of full thickness loss in the same subregion (grades ranging from 0.0 to 3.3). The maximum MOAKS area extent (MOAKSext, 1st component), the maximum MOAKS full thickness cartilage damage extent (MOAKSft, 2nd component) and the maximum MOAKS cartilage score (MOAKSmax) were determined in each 3 tibial and 1 central femoral MOAKS subregions. Medial/lateral compartment cartilage thickness (MFTC/LFTC) changes over 3 years were stratified by ipsi-compartmental baseline MOAKS scores. Comparisons were performed using ANCOVA adjusted for age, sex, and BMI.

Results
150 knees of 150 participants were included (age 65±9 years (mean±SD), BMI 28±4 kg/m², 59% female). LFTC thickness loss (-0.03±0.15mm) tended to be greater than MFTC loss (-0.01±0.13mm). Grades 1/2/3 of MOAKSext were present as follows: 13%/31%/2% medially, 17%/38%/0% laterally, and for grade 1/2 of MOAKSft: 7%/3% medially, 12%/7% laterally. MFTC cartilage thickness change over three years did not differ for the various MOAKS strata compared to the without-lesion reference. LFTC cartilage thickness loss was higher in knees with presence of any lateral MOAKS lesion (adj. diff.: -0.06mm, 95% CI: [-0.11, -0.01]mm). This difference was mainly driven by the 23 knees with MOAKSmax 2.1/2.2. Knees with MOAKSext of 2 (adj. diff.: -0.08mm, [-0.13, -0.02]mm) and with MOAKSft damage (grade 1: -0.10mm, [-0.17, -0.02]mm; grade 2: -0.10mm, [-0.19, 0.00]mm) also showed greater LFTC loss than MOAKSext/MOAKSft 0 knees. Similar results were observed after adjustment for presence of other MOAKS features.

Conclusions
In this pre-ROA sample, presence of baseline MOAKS cartilage damage was associated with ipsi-compartmental cartilage loss over three years in the more commonly affected lateral compartment. Baseline MOAKS cartilage scores may therefore help select knees with expected subsequent cartilage thickness loss for inclusion in preventive OA trials.

Design of a proangiogenic protein corona around extracellular vesicles

Martin Wolf[1], Rodolphe W Poupardin[1], Patricia Ebner-Peking[1], André Cronemberger Andrade[1], Constantin Blöchl[2], Astrid Obermayer[2], Fausto Gueths Gomes[1,3], Balazs Vari[1], Essi Eminger[1], Heide-Marie Binder[1], Anna M Raninger[1], Sarah Hochmann[1], Gabriele Bracht[1], Andreas Spittler[4], Thomas Heuser[5], Racheli Ofir[6], Christian G Huber[2], Zami Aberman[6], Katharina Schallmoser[3], Hans-Dieter Volk[7], Dirk Strunk[1]

[1]Cell Therapy Institute, Spinal Cord Injury and Tissue Regeneration Center Salzburg (SCI-TReCS), Paracelsus Medical University (PMU), Salzburg, Austria
[2]Dept. of Biosciences, Paris Lodron University Salzburg
[3]Department of Transfusion Medicine and SCI-TReCS, PMU, Salzburg, Austria
[4]Anna Spiegel Center of Translational Research, Medical University, Vienna
[5]Vienna Biocenter Core Facilities, Medical University, Vienna
[6]Pluristem Ltd., Haifa, Israel
[7]BCRT & Institute of Medical Immunology, Charite - Universitätsmedizin Berlin, Germany

martin.wolf@pmu.ac.at

INTRODUCTION

Peripheral artery disease affects >10% of the European elderly population resulting in an increased risk for cardiovascular failures and death. Critical limb ischemia (CLI), as its final stage, often leads to amputation. Allogeneic placental expanded (PLX) stromal cells are currently evaluated in a clinical phase III trial as an advanced CLI therapy. In our study, we aim to identify the mode of action of this novel cell-based treatment. Therefore, we hypothesize that PLX-cell-derived extracellular vesicles (EVs) contribute to PLX-cell effectiveness. This project is part of **PACE "A multicenter phase III study using HLA-unmatched allogeneic placenta-derived stromal cells (PLX-PAD) for the treatment of severe critical limb ischemia accompanied by mechanistic studies".**

HYPOTHESIS

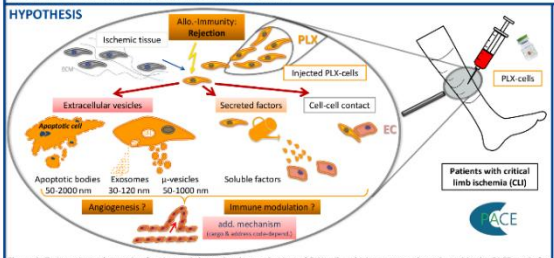

Figure 1: To investigate the mode of action and the molecular mechanism of PLX cells, which are currently evaluated in the PACE study for their application in CLI patients, we aim to investigate whether direct cell-cell contact of PLX cells with endogenous endothelial cells (ECs), secreted soluble factors or EVs facilitate angiogenic potential. We further plan to find out whether signals from the ischemic environment influence this effect.

METHODS

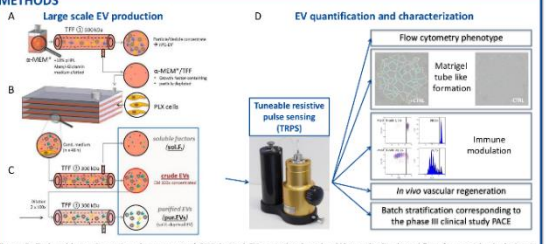

Figure 2: To be able to determine the potency of PLX-derived EVs, we developed a **(A)** standardized workflow for particle depletion in medium supplemented with pooled human platelet lysate (pHPL) via tangential flow filtration (TFF) **(B)** as well as subsequent large scale cell propagation and **(C)** EV purification protocols to separate soluble factors (sol.F.) from crude EVs and purified (puc) EVs. **(D)** The major goal of our project lies in the extensive characterization of EV functions to better understand their role in vascular regeneration.

PRODUCTION AND PHENOTYPE OF PLX EVs

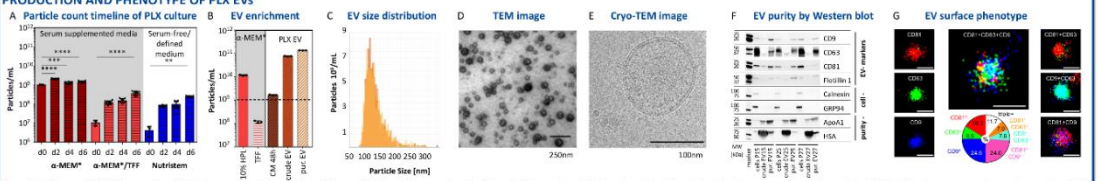

Figure 3: **(A)** To quantify the EV production, PLX cells were cultured in particle containing α-MEM* vs. EV free medium for 6 days. Particles produced by the cells could not be distinguished from the media background in α-MEM* while there was a continuous increase in particle depleted α-MEM* of chemically defined medium. **(B)** Particle numbers measured by TRPS show efficient enrichment of particles during the EV purification process with TFF. **(C)** The size distribution of PLX EV was measured by TRPS. **(D)** Both, negative contrast TEM picture and **(E)** cryo-TEM image show round structures of about 100 nm. The cryo-TEM image in addition shows a characteristic double membrane structure. **(F)** Western blot analysis of EV identity and purity markers according to MISEV 2018 criteria. **(G)** Super-resolution microscopy topology display of tetraspanins CD81 (red), CD63 (green) and CD9 (blue), via single molecule fluorescence of individual EV^{TFF2} (left) and the overall distribution of double and triple marker positive EVs as indicated based on 99,209 EV areas analyzed. Scale bars 100 nm.

PROTEOMIC COMPARISON OF PLX SECRETOME FRACTIONS

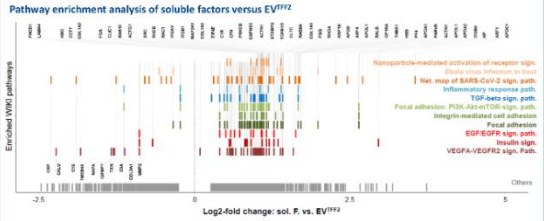

Figure 4: Pathway enrichment analysis for significantly differentially detected proteins (n = 814, adjusted p < 0.05). Enriched proteins (n = 118) and corresponding WIKI pathways highlighted in the same color. Proteins most significantly (absolute log2-fold-change > 1) enriched in soluble factors (bottom left; n = 10) and proteins enriched in the EV^{TFF2} fractions (top; n = 47) shown. Proteins found in several pathways are shown with one bar with different corresponding color codes. The remaining differentially detected proteins are highlighted as grey barcode on the bottom (category "others"; n = 696). Abbreviations: Net., network; path., pathway; sign., signaling.

ANGIOGENIC AND IMMUNE MODULATION POTENTIAL OF PLX CELLS AND PLX-DERIVED EVs

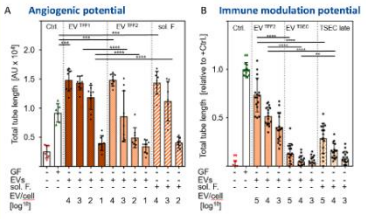

Figure 5: PLX-EVs capture proangiogenic factors. **(A)** Angiogenic potential of different PLX secretome fractions as analyzed by endothelial network formation in a matrigel assay. Total length of the endothelial networks in the presence of PLX-EVs at the indicated EV per endothelial cell ratio is shown (e.g., Log10 [3] = 1000:1). Volumes of soluble factors (sol. F.) added to the assay were calculated accordingly corresponding to EV number as described in the methods section. Results pooled from three independent donors (***p < 0.0002, ****p < 0.0001). **(B)** Separation of EV^{TFF2} from their adjacent proteins by size exclusion chromatography (EV^{SEC}) revealed significant loss of proangiogenic function.

IN VIVO VASCULOGENESIS AND SKIN REGENERATION BY PLX EVs

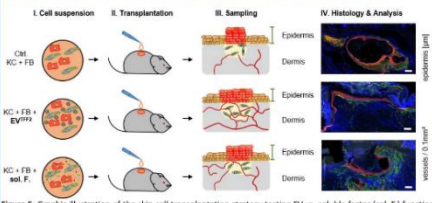

Figure 6: Graphic illustration of the skin cell transplantation strategy testing EV vs. soluble factor (sol. F.) function during in vivo full thickness skin wound regeneration[32]. Keratinocyte + fibroblast (KC + FB) cell suspension grafts, transplanted in the absence or presence of either TFF2-isolated PLX-EVs (+EV^{TFF2}) or sol. F. as described in the methods section (step I + II). Human skin biopsy sampling (III) and representative immunohistochemistry (IV; anti-human CD44, red; anti-human vimentin, green). Histology of day 14 post grafting. Quantification showing significantly increased epidermal thickness[28] in cell grafts in the absence of EVs^{TFF2} in transplants of KC+FB 'cells only' or KC+FB transplanted in the presence of sol.F., compared to control human skin (ctrl). **(O)** Vessel density in grafted dermis. Mean ± SD results (N, O). One-Way-ANOVA, multiple comparison of four biological and three technical replicates (*p < 0.05, ****p < 0.0001).

PROTEIN CORONA VISUALIZATION AND FUNCTIONAL IMPORTANCE

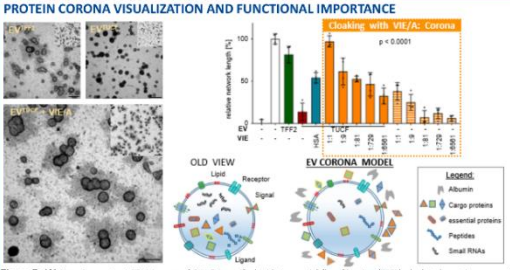

Figure 7: **(A)** Negative contrast TEM images of PLX EVs purified with tangential flow filtration (TFF2), depleted protein corona after TFF followed by ultracentrifugation (TUCF) and with protein corona re-established by defined factors VEGF+ IGF+ EGF in albumin solution (VIE/A). Scale bar 250 nm, small insert showing overview image with scale bar 500 nm. **(B)** Endothelial cell network formation comparing EVs^{TFF2} with ultracentrifuged, i.e., corona-depleted EVs (EV^{TUCF}) and free growth factors and growth factor corona-cloaked EVs. Representative experiment, quadruplicates. **(B)** Dose dependent endothelial cell network formation in the presence (+) or absence (-) of EV^{TUCF} in an 8% human albumin solution containing VEGF, IGF and EGF (VIE/A) (n = 3; individual additional experiments color-coded in red, green, blue, and covering a broader dose range than in (A)). Statistics were calculated using a linear mixed model with treatment as fixed effect and dilution as random effect **(C)** New EV corona model and current/old view on EV

SUMMARY

- Proteomic analysis of PLX cell secretome revealed significant enrichment of proteins associated with angiogenesis, cell movement and negative regulation of immune responses in the EV fraction compared to sol.F..
- PLX EVs show high angiogenic potential *in vitro and in vivo* in a dose-dependant manner. A functional protein corona around PLX EVs is essential for their angiogenic potential.

ACKNOWLEDGEMENTS

This work is part of a project that has received funding from the European Union's Horizon 2020 research and innovation program under grant agreement N°733006
PACE (A multicenter phase III study using HLA-unmatched allogeneic placenta-derived stromal cells (PLX-PAD) for the treatment of severe critical limb ischemia accompanied by mechanistic studies)

Design of a proangiogenic protein corona around extracellular vesicles

Martin Wolf[1], Rodolphe W Poupardin[1], Patricia Ebner-Peking[1], André André Cronemberger Andrade[1], Constantin Blöchl[2], Astrid Obermayer[2], Fausto Gueths Gomes[2], Balazs Vari[1], Nicole Maeding[1], Essi Eminger[1], Heide-Marie Binder[1], Anna M. Raninger[1], Sarah Hochmann[1], Gabriele Brachtl[1], Andreas Spittler[4], Thomas Heuser[5], Racheli Ofir[6], Christian G. Huber[2], Zami Aberman[6], Katharina Schallmoser[3], Hans-Dieter Volk[7], Dirk Strunk[1]

[1]Cell Therapy Institute, Spinal Cord Injury and Tissue Regeneration Center Salzburg (SCI-TReCS), Paracelsus Medical University (PMU), Salzburg, Austria; [2]Department of Biosciences, Paris Lodron University Salzburg, Austria; [3]Department of Transfusion Medicine and SCI-TReCS, PMU, Salzburg, Austria; [4]Core Facility Flow Cytometry and Department of Surgery, Research Laboratories, Medical University of Vienna, Vienna, Austria; [5]Vienna Biocenter Core Facilities, Vienna, Austria; [6]Pluristem Ltd., Haifa, Israel; [7]Berlin Institute of Health at Charité – Universitätsmedizin, BIH Center for Regenerative Therapies (BCRT), Berlin, Germany; Contact: martin.wolf@pmu.ac.at

Objective
Although it is well established that synthetic nanoparticles (NP) acquire a protein corona as soon as they are exposed to biological environments, this phenomenon has not yet been investigated for extracellular vesicles. This protein corona was shown to play an important role in the NP's interaction with cells. To investigate whether such a corona also exists for biological NPs, such as extracellular vesicles (EVs) and how they contribute to their effects on target cells, we purified extracellular vesicles from clinical grade placental derives stromal cells (PLX).

Methods
We used large-scale culture of PLX cells in particle-depleted medium to harvest and purify EVs by tangential flow filtration (TFF). These EVs were extensively characterized according to MISEV criteria by tunable resistive pulse sensing (TRPS), western blot, cryo- and transmission electron microscopy and super resolution microscopy. To remove the natural occurring protein corona from TFF purified EVs we utilized ultracentrifugation and subsequently reestablished the corona by adding defined angiogenic factors identified via proteomic analysis before. The angiogenic potential of different EV preparations with and without protein corona was assessed using endothelial cell network formation on matrigel and in a mouse in vivo wound healing model.

Results
Comparing TFF versus ultracentrifugation purified EV preparations using transmission electron microscopy with negative contrast staining, we could observe corona like structures surrounding EVs from TFF while this structure was absent for ultra-centrifuged EVs and re-appeared after re-establishing the protein corona. In addition, in the in vitro angiogenesis assay the ultra-centrifuged EVs showed significantly reduced network formation compared to TFF EVs, which could be restored by the re-establishment of the protein corona.

Conclusions
With this observation, we provide the first evidence that also extracellular vesicles can carry a protein corona that contributes the functionality of EVs. This finding not only contributes to the basic understanding of EV biology and offers a new model for the mode of action for EVs, it also is important for selecting suitable purification methods. Furthermore, our findings offers new opportunities for designing extracellular vesicle based therapies.

The development of a digital tool for planning physical exercise training during cardiac rehabilitation

Daniela Wurhofer[a], Eva-Maria Strumegger[a,b], Rada Hussein[a], Andreas Stainer-Hochgatterer[a], Josef Niebauer[a,c], and Stefan Tino Kulnik[a]

[a] *Ludwig Boltzmann Institute for Digital Health and Prevention, Salzburg, Austria,*
[b] *Salzburg University of Applied Sciences, Salzburg, Austria*
[c] *University Institute of Sports Medicine, Prevention and Rehabilitation, Paracelsus Medical University, Salzburg, Austria*

Objective

aktivplan

- Physical activity planning tool for heart-healthy physical activity
- Used by health professionals together with their patients
- Joint creation, monitoring and regular review of a personalized, heart-healthy physical activity plan

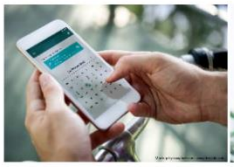

Methods

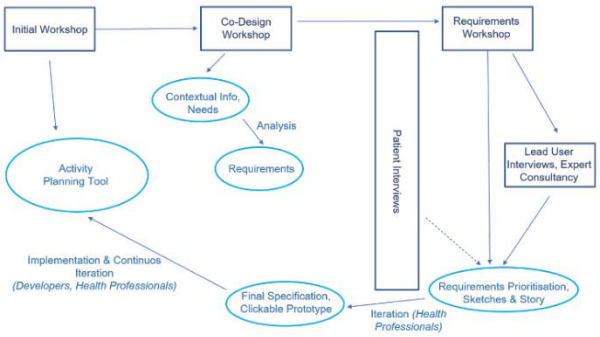

Sketch of **aktiv**plan development according to user-centered design process including activities and outcomes

Exemplary workshop outcomes: detailed information about context, sketches for activity planning

Results

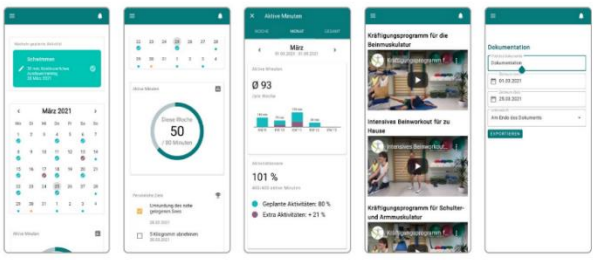

Characteristic functionalities of **aktiv**plan: (1) training plan, (2) active minutes and goals, (3) progress over time, (4) training videos, (5) data export

Overview on features provided by **aktiv**plan

Kontakt: Dr. Daniela Wurhofer
Email: daniela.wurhofer@dhp.lbg.ac.at

The development of a digital tool for planning physical exercise training during cardiac rehabilitation

Daniela Wurhofer[1], Eva-Maria Strumegger[1,2], Rada Hussein[1], Andreas Stainer-Hochgatterer[1], Josef Niebauer[1,3], Stefan Tino Kulnik[1]

[1]Ludwig Boltzmann Institut für digitale Gesundheit und Prävention; [2]Fachhochschule Salzburg; [3]Universitätsinstitut für präventive und rehabilitative Sportmedizin, Paracelsus Medizinische Privatuniversität Salzburg; Contact: daniela.wurhofer@dhp.lbg.ac.at

Objective
The COVID-19-related lockdown in Austria highlighted the need for digital support also for patients with cardiovascular disease (CVD) to assure continued cardiac rehabilitation in a safe and effective manner e.g. at home. Responding to this situation, we developed a prototype for digital training support in cardiac rehabilitation (aktivplan).

Methods
The conceptualization and development of aktivplan was an explorative and iterative process, adopting a user-centered design (UCD) approach (1). In particular, the process consisted of 4 phases: (1) Idea and concept generation; (2) Refinement of idea and concept generation; (3) Technical specifications; (4) Implementation and continuous adaption. During the whole process, the two core user groups for such a digital tool were involved, i.e., rehabilitation professionals and patients.

Results
As a result of a UCD approach, we developed a tool which allows rehabilitation professionals and their patients to jointly set up, monitor, and regularly review a personalized heart-healthy physical activity plan.
Patients are involved and guided by rehabilitation professionals in setting up a personalized physical activity plan. Together with a professional, patients select exercises and activities they enjoy and define personally meaningful goals. Through the app interface, patients can conveniently access their plan on a calendar, log, adjust or add activities, review their performance, and access a library of resources such as exercise videos. At follow-up appointments with their rehabilitation professional, patients can review their documented performance and discuss the plan going forward.
Rehabilitation professionals are supported in providing personalized physical exercise prescription as well as ongoing review and optimization of their patients' performance. Through the web interface, rehabilitation professionals can conveniently view patients' activity logs. Activity logs can be exported and printed, to be filed in medical records, to provide documentation to health insurances, and to be used for joint review and further planning with patients at follow-up appointments.

Conclusions
This work presents the development of a tool which offers a solution for digital support for physical exercise training during cardiac rehabilitation based on a UCD process. After first evaluations of the prototype with both patients and rehabilitation professionals in the field, a larger scale study is planned for the future.

References
1. H. Beyer, and K. Holtzblatt, Contextual Design: Defining Customer-Centered Systems, Morgan Kaufmann Publishers, San Francisco, 1998.

Liste der Einreicher*innen und korrespondierenden Autor*innen

(in alphabetischer Reihenfolge)

- Berufsgenossenschaftliche Unfallklinik Murnau – Lehrkrankenhaus der PMU Salzburg
- Fachhochschule Salzburg
- Friedrich-Alexander-Universität Erlangen-Nürnberg
- Ludwig Boltzmann Institut für digitale Gesundheit und Prävention
- Paracelsus Medizinische Privatuniversität Nürnberg / Klinikum Nürnberg
- Paracelsus Medizinische Privatuniversität Salzburg / Universitätsklinikum Salzburg
- Universität Messina

Verzeichnis aller Autor*innen

(fett gedruckt = Präsentator*in)

#vSGT

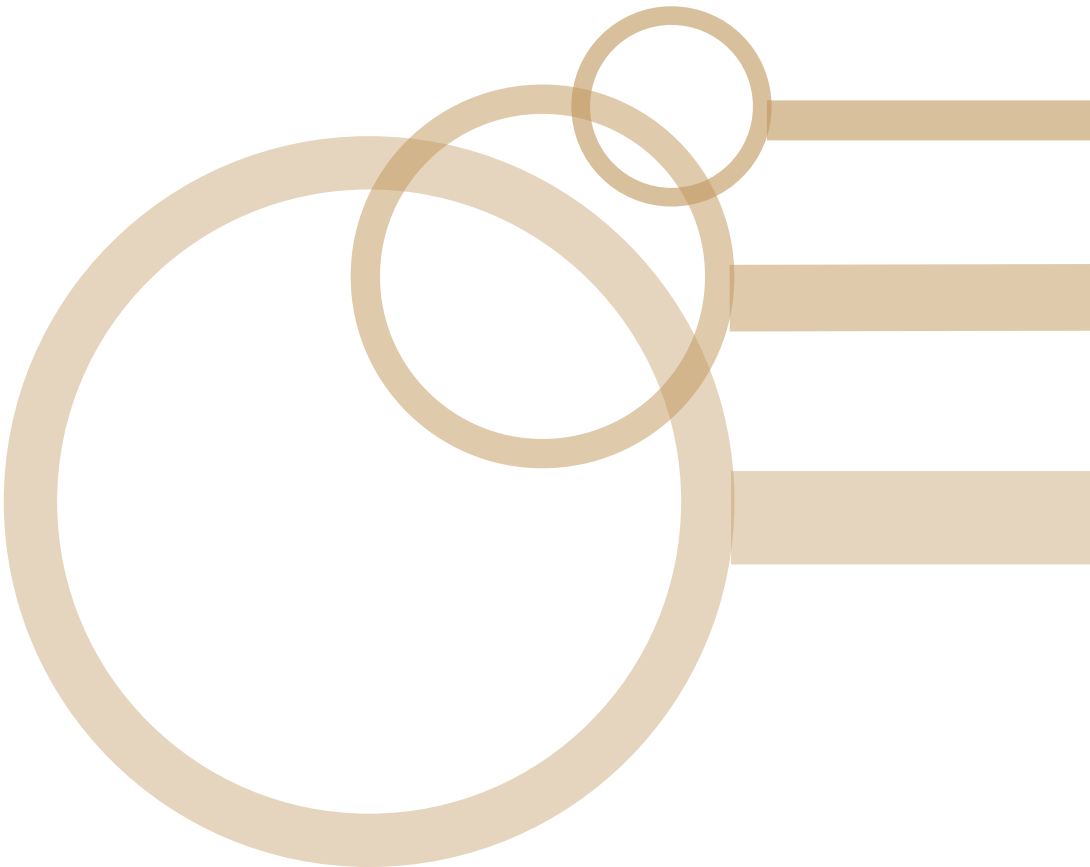

Paracelsus Medizinische Privatuniversität
Forschungsmanagement | Salzburg
Strubergasse 21, 5020 Salzburg, Austria
+43 (0)662 2420-80281
www.pmu.ac.at

ISBN: 978-3-200-08887-0